GRID-SUPPORTIVE CHARGING INFRASTRUCTURE FOR PLUG-IN ELECTRIC VEHICLES

Niels LEEMPUT

Examination Committee:

Prof. dr. ir. Jean Berlamont, chair

Prof. dr. ir. Johan Driesen, supervisor

Prof. dr. ir. Ronnie Belmans

Prof. dr. ir. Chris Tampère

Prof. dr. ir. Sjef Cobben
(Eindhoven University of Technology)

Prof. dr. ir. Andreas Sumper
(Polytechnic University of Catalonia)

Dissertation presented in partial fulfilment of the requirements for the degree of PhD in Engineering Science: Electrical Engineering

November 2015

Voorwoord

In September 2010 begon ik aan mijn doctoraatsonderzoek bij Electa. Op dat moment werden de eerste moderne plug-in elektrische wagens geïntroduceerd, en sindsdien is hun aantal sterk gegroeid. Vanuit dit perspectief wordt de impact van het opladen van plug-in elektrische voertuigen op het elektriciteitsnet steeds belangrijker. Het is een boeiend academisch en persoonlijk pad geweest, dat ik niet alleen heb afgelegd.

Vooreerst bedank ik van harte mijn promotor prof. Johan Driesen om mij de kans te geven om dit onderzoek uit te voeren. Dankzij de verschillende projecten omtrent het opladen van plug-in elektrische wagens heb ik de nodige inzichten verworven om dit doctoraatsonderzoek tot een goed einde te brengen. Bedankt voor de constructieve samenwerking, de steun en het vertrouwen tijdens de vijf afgelopen jaren.

Ik bedank ook graag de andere leden van de begeleidingscommissie en de examencommissie, met name prof. Ronnie Belmans, prof. Chris Tampère, en prof. Sjef Cobben. Dank voor het nalezen, en voor de constructieve en waardevolle suggesties ter verbetering van deze tekst. Ook bedank ik prof. Jean Berlamont om het voorzitterschap van de doctoraatsjury op zich te nemen.

Special thanks goes to prof. Andreas Sumper for being a member of the doctoral committee, and for hosting me at the Polytechnic University of Catalonia, Barcelona, during my mobility stay for the EIT-KIC InnoEnegy PhD School. The academic collaboration and the seven-month stay were a great experience. Moltes gràcies per l'oportunitat, Andreas.

Bedankt aan IWT-Vlaanderen voor de financiële ondersteuning tijdens de laatste vier jaren van mijn onderzoek. Ook bedankt aan de EIT-KIC InnoEnergy PhD School voor de cursussen ter verruiming van mijn inzicht in de energiesector, en voor de financiële ondersteuning die mijn verblijf aan de Polytechnische Universiteit van Catalonië mogelijk heeft gemaakt.

Dank aan de Electa/EnergyVille-collega's voor de goede sfeer tijdens en na het werk! Het was een plezier om samen te werken, maar ook de koffiepauzes, lunches en de activieiten na de werkuren zullen me bijblijven. In het bijzonder bedank ik Juan Van Roy, Frederik Geth en Jeroen Büscher voor de waardevolle samenwerking met betrekking tot plug-in elektrische voertuigen, en voor het verbeteren van mijn doctoraatstekst. Dank aan het de administratieve en technische Electa-medewerkers, om mij te helpen bij de praktische aspecten van mijn onderzoek.

Thanks to the colleagues at the Polytechnic University of Catalonia, for the hospitality and the good atmosphere, both during and after work. Special thanks go to Pol Olivella-Rosell, Guiem Bosch-Llufriu, and Mario Kovačević for the collaboration relating to my doctoral research.

Bedankt aan mijn familie en vrienden voor hun steun en om mij te helpen om alles te relativeren, door het leven naast het onderzoek zo waardevol te maken. Bijzondere dank aan mijn ouders voor hun jarenlange steun en voor alle kansen die ze mij gegeven hebben, om in alle vrijheid mijn eigen keuzes te maken.

Por último, pero no menos importante quiero agradecer a mi novia Scarlett por su apoyo durante los últimos meses de mi investigación de doctorado.

Niels Leemput

Leuven, November 2015

Abstract

The number of plug-in electric vehicles (PEVs) on the road is growing significantly, which allows to reduce the consumption of greenhouse gas emitting fossil fuels, such as gasoline and diesel. This is due to the increased primary energy efficiency of electrically powered vehicles compared to conventional vehicles on the one hand, and the primary fuel flexibility for electricity generation on the other hand. The absence of tailpipe emissions reduces the local concentrations of harmful pollutants, which benefits human health. PEVs are able to charge at every location that offers a suitable grid connection opportunity, e.g., at home and the workplace. The typical long standstill times at these locations and the low average daily driven distances allow low-power charging to fulfill the majority of the mobility needs, thereby keeping the charging infrastructure investments low.

As the number of PEVs on the road increases, the grid impact of PEV charging is observed more widely, e.g., altered grid load profiles, increased peak power, and increased voltage magnitude deviations. Therefore, an extensive amount of research is conducted on coordinated charging strategies that have the objective to mitigate the grid impact of PEV charging. Typically, large-scale coordination mechanisms are being investigated, which require a sufficiently high large-scale PEV penetration rate to be effective. However, due to the clustering of PEV users, high local concentrations may occur prior to a high widespread PEV penetration. Therefore, certain distribution grids will already be impacted in the near-term future. More specifically, the residential low voltage (LV) grid impact may be challenging, due to the simultaneity between PEV charging and residential electricity consumption.

This dissertation investigates several local PEV charging strategies that have the objective to mitigate the distribution grid impact with a minimal amount of external input. Two active power control strategies for PEV charging are assessed separately, and in combination: voltage-dependent charging and standstill time-based charging. The former strategy does not need require any input, as the voltage magnitude is measured anyway within the onboard charger. The latter strategy only requires the next departure time, so that the charging power rating can be reduced as much as possible, while still being fully charged for the next trip.

Besides the abovementioned active power control strategies, reactive power control is also investigated, i.e., reactive power current injections during PEV charging. Certain PEV charger topologies allow for the injection of reactive power flows into

the grid, so this capability could be enabled. The advantage compared to the active power control strategies is that, given an appropriate sizing of the PEV charger, this grid-supportive measure does not impact the user comfort, because the active power flow is not altered. Reactive current injection does not require any external inputs, because it is merely a power factor set point of the onboard PEV charger.

Finally, the distribution grid impact and sizing requirements of fast charging infrastructure is assessed. Opposed to plug-in hybrid electric vehicles (PHEVs), all of the required propulsion energy for battery electric vehicles (BEVs) must be delivered by the onboard battery. Therefore, fast charging is indispensable for long-distance driving, so that recharging does not take excessively long. Because slow and fast charging are complementary charging options, different slow charging strategies are taken into account when the fast charge requirements are assessed. Furthermore, different representative LV grid topologies are taken into account, as well as the medium voltage (MV) grid topology to which the different LV grids and the fast charging infrastructure are connected.

The proposed local active and reactive power control strategies allow to substantially mitigate the distribution grid impact of PEV charging, with limited adaptations compared to their current implementation. The active power control strategies could be implemented on all of the currently used onboard PEV chargers. The reactive power control strategies can be implemented on onboard PEV chargers with a full-bridge active rectifier topologies, as used for several PEVs. The distribution grid impact of the slow charging control strategies is more significant than the presence of fast charging infrastructure. Therefore, it the limited additional distribution grid impact of fast charging infrastructure can even be compensated for by implementing the proposed control strategies for slow charging.

Samenvatting

Het aantal plug-in elektrische voertuigen (PEV's) neemt sterk toe, wat het verbruik van broeikasgas uitstotende fossiele brandstoffen, zoals benzine en diesel, kan verlagen. Dit komt door de hogere primaire energie-efficiëntie, vergeleken met conventionele voertuigen enerzijds, en de brandstof-flexibiliteit voor elektriciteitsproductie anderzijds. De afwezigheid van uitlaatgasemissies vermindert de lokale concentraties van schadelijke stoffen, wat voordelig is voor de volksgezondheid. PEV's zijn in staat om op te laden op elke locatie met een geschikte netaansluiting, bijvoorbeeld thuis en op de werkplek. De typische lange stilstand tijden op deze locaties en de lage gemiddelde dagelijkse gereden afstanden laten toe om de meerderheid van de mobiliteitsbehoeften te voorzien met opladen aan laag vermogen, waardoor de investeringen in laadinfrastructuur laag blijven.

Aangezien het aantal PEV's toeneemt, wordt hun netimpact op steeds vaker waargenomen, bijvoorbeeld aangepaste netbelastingsprofielen, een verhoogd piekvermogen en toegenomen spanningsafwijkingen. Daarom wordt er een uitgebreide hoeveelheid onderzoek uitgevoerd op gecoördineerde oplaadstrategieën, met als doelstelling om de netimpact te beperken. Gewoonlijk worden er grootschalige coördinatiemechanismen onderzocht, waarbij er een voldoende hoge grootschalige PEV-penetratiegraad nodig is om doeltreffend te kunnen functioneren. Vanwege de clustering van PEV-gebruikers kunnen er hoge lokale concentraties optreden voorafgaand aan een grootschalige hoge PEV-penetratiegraad. Daarom zullen distributienetten reeds beïnvloed worden in de nabije toekomst. Meer specifiek, de impact op het laagspanningsnet kan een uitdaging zijn, als gevolg van de gelijktijdigheid tussen het opladen van PEV's en het residentiële elektriciteitsverbruik.

Dit proefschrift onderzoekt verschillende lokale PEV-oplaadstrategieën, die als doelstelling hebben om de impact op distributienetten te verminderen met een minimale hoeveelheid aan externe input. Twee actieve vermogensstrategieën voor het opladen van PEV's worden afzonderlijk en in combinatie beoordeeld: spanningsafhankelijk opladen en stilstand tijd-gebaseerd opladen. De eerste strategie heeft geen input nodig, omdat de netspanning toch wordt gemeten in de PEV-lader. De tweede strategie vereist alleen de volgende vertrektijd, zodat het laadvermogen zoveel mogelijk verminderd kan worden, terwijl de batterij toch volledig is opgeladen voor de volgende rit.

Naast de bovengenoemde actieve vermogensstrategieën, wordt er tevens een reactieve vermogensstrategie onderzocht, waarbij er reactief vermogen in het elektriciteitsnet wordt geïnjecteerd tijdens het opladen. Bepaalde PEV's zijn uitgerust met een ladertopologie die deze functionaliteit toelaat, dus deze mogelijkheid zou bij deze PEV's kunnen geïmplementeerd worden. Het voordeel ten opzichte van de actieve vermogensstrategieën, gegeven de juiste dimensionering van de PEV-lader, is dat deze net-ondersteunende maatregel geen invloed heeft op het comfort van de gebruiker, omdat het actieve laadvermogen niet wordt gewijzigd. Reactieve stroominjectie vereist geen externe input, omdat het slechts een power factor setpoint van de PEV-lader is.

Tenslotte wordt de distributienetimpact en de dimensioneringsvereisten van snellaadinfrastructuur beoordeeld. In tegenstelling tot plug-in hybride elektrische voertuigen (PHEV's), moet alle benodigde aandrijfenergie bij batterij elektrische voertuigen (BEV's) worden geleverd door de batterij. Daarom is snelladen onmisbaar om over lange afstanden te rijden, zodat het opladen niet overdreven lang duurt. Omdat langzaam en snel opladen complementaire oplaadmogelijkheden zijn, wordt er met de verschillende laadstrategieën voor traagladen rekening gehouden bij het beoordelen van de vereisten voor snelladen. Bovendien wordt er met verschillende representatieve topologieën voor laagspanningsnetten rekening gehouden, evenals met een representatieve topologie voor middenspanningsnetten, waarmee de laagspanningsnetten en de snellaadinfrastructuur verbonden zijn.

De voorgestelde lokale oplaadstrategieën voor actief en reactief vermogen laten toe om de distributienetimpact van het opladen van PEV's aanzienlijk te beperken, met beperkte aanpassingen in vergelijking met de huidige implementatie. De actieve vermogensstrategieën kunnen worden geïmplementeerd op alle PEV-laders die tegenwoordig gebruikt worden. De reactieve vermogensstrategieën kunnen worden geïmplementeerd op PEV-laders met een volle brug actieve gelijkrichter topologie, zoals gebruikt wordt in verschillende PEV's. De oplaadstrategieën voor traagladen hebben een grotere distributienetimpact dan de aanwezigheid van snellaadinfrastructuur. Daarom kan de beperkte extra distributienetimpact van snellaadinfrastructuur gecompenseerd worden door de implementatie van de voorgestelde oplaadstrategieën voor traagladen.

List of abbreviations

AC	Alternating Current
BEV	Battery Electric Vehicle
BMS	Battery Management System
CCCV	Constant Current Constant Voltage
CCS	Combined Charging System
DOD	Depth Of Discharge
DSO	Distribution System Operator
DC	Direct Current
ETC	European Transient Cycle
EREV	Extender Range Electric Vehicle
EV	Electric Vehicle
EU	European Union
EVSE	Electric Vehicle Supply Equipment
FTP	Federal Test Procedure
G2V	Grid to Vehicle
GDP	Gross Domestic Product
HEV	Hybrid Electric Vehicle
HWFET	Highway Fuel Economy Driving Schedule
IC-CPD	In-Cable Control and Protecting Device
ICE	Internal Combustion Engine
IEC	International Electrotechnical Commission
LCO	Lithium Cobalt Oxide
LDV	Light-Duty Vehicle
LFP	Lithium Iron (Fe) Phosphate
Li-ion	Lithium-ion
LMO	Lithium Manganese Oxide
LTO	Lithium Titanate Oxide
LV	Low Voltage
MAS	Multi-Agent System
MCB	Miniature Circuit Breaker
MV	Medium Voltage
NCA	Nickel Cobalt Aluminum
NMC	Nickel Manganese Cobalt
NYCC	New York City Cycle
OPP	One Percent Peak
PE	Protective Earth
PEV	Plug-in Electric Vehicle
PF	Power Factor
PHEV	Plug-in Hybrid Electric Vehicle

PM	Particulate Matter
PV	Photovoltaic
PWM	Pulse Width Modulation
RCD	Residual Current Device
RES	Renewable Energy Sources
RRC	Rolling Resistance Coefficient
SOC	State Of Charge
TOU	Time Of Use
TSO	Transmission System Operator
V2G	Vehicle to Grid
VPP	Virtual Power Plant

List of symbols

U^{rat}	Rated voltage magnitude	[V]
$U_{p,i}$	Voltage rms magnitude at phase p and grid connection node i	[V]
ph	Phase index	
i	Grid connection node index	
k	Time step index	
F_i^{VU}	Voltage unbalance factor at grid connection node i	[%]
U_i^P	Positive sequence voltage at grid connection node i	[V]
U_i^N	Negative sequence voltage at grid connection node i	[V]
m	Vehicle mass	[kg]
S	Vehicle front surface	$[\text{m}^2]$
C_x	Drag coefficient	[-]
F_k^a	Air resistance force	[N]
F_k^r	Rolling resistance force	[N]
F_k^i	Inertial resistance force	[N]
F_k^s	Slope resistance force	[N]
P_k^p	Propulsion power	[W]
ρ	Volumetric density of air	$[\text{kg}/\text{m}^3]$
v_k	Vehicle speed at time step k	$[\text{m}/\text{s}]$
g	Gravity constant	$[9.81\ \text{m}/\text{s}^2]$
f_r	Rolling resistance coefficient	[-]
α	Road slope	[rad]
a_k	Acceleration at time step k	$[\text{m}/\text{s}^2]$
$P_{\text{out},k}^{\text{bat}}$	Battery discharging power at time step k	[W]
$P_{\text{in},k}^{\text{bat}}$	Battery charging power at time step k	[W]
$P_{ch,\text{max}}^{\text{bat}}$	Maximum battery charging rate	[W]
e^{rec}	Fraction of regenerative braking	[-]
η^{in}	Power electronic charging efficiency	[-]
η^{out}	Power electronic discharging efficiency	[-]

η_{ch}^{bat}	Battery charging efficiency	[-]
η_{d}^{bat}	Battery discharging efficiency	[-]
η^{m}	Electric motor efficiency at motor mode	[-]
η^{g}	Electric motor efficiency at generator mode	[-]
$E_{ch,k}^{\mathrm{bat}}$	Battery charging energy at time step k	[kWh]
$E_{d,k}^{\mathrm{bat}}$	Battery discharging energy at time step k	[kWh]
$\Delta E_{k}^{\mathrm{bat}}$	Change of battery energy content at time step k	[kWh]
P^{aux}	Auxiliary power	[kW]
SOC_k	State of charge at time step k	[%]
δ^{sd}	Battery self-discharge rate	[%]
$E_{\mathrm{rat}}^{\mathrm{bat}}$	Battery rating	[kWh]
$\Delta E_{\mathrm{cycle}}^{\mathrm{bat}}$	Energy usage during drive cycle	[kWh]
$E_{\mathrm{end}}^{\mathrm{bat}}$	Battery energy content at the end of the drive cycle	[kWh]
$E_{\mathrm{start}}^{\mathrm{bat}}$	Battery energy content at the start of the drive cycle	[kWh]
E^{spec}	Specific power consumption	[kWh/km]
b	Battery capacity parameter	
c	Charging case parameter	
p	Charging power rating parameter	
d^{range}	PEV pure electric range	[km]
d^{cycle}	Distance of the drive cycle	[m]
$E_{\mathrm{eff}}^{\mathrm{bat}}$	Usable battery capacity	[kWh]
P_{k}^{ch}	Grid charging power at time step k	[kW]
P_{k}^{rec}	Regenerative braking losses	[kW]
P_{k}^{g}	Electric motor losses at generator mode	[kW]
P_{k}^{in}	Power electronic charging losses	[kW]
$P_{ch,k}^{bat}$	Battery charging losses	[kW]
P_{k}^{m}	Electric motor losses at motor mode	[kW]
P_{k}^{out}	Power electronic discharging losses	[kW]
$P_{d,k}^{bat}$	Battery discharging losses	[kW]
P_{k}^{sd}	Battery self-discharge losses	[kW]
F^{U}	PHEV utility factor	[%]
F^{B}	Battery utilization factor	[%]
a^{gc}	Grid connection availability	[%]

a^{dc}	Discharging energy availability	[kWh/vehicle]
$a_{\mathrm{fc}}^{\mathrm{dc}}$	Discharging energy availability of fully charged vehicles	[kWh/vehicle]
a^{ch}	Charging energy availability	[kWh/vehicle]
a_{75}^{ch}	Charging energy availability for 75 % of time	[kWh/vehicle]
I_d	Direct current component	[A]
I_q	Quadrature current component	[A]
R	Resistance	[Ω]
X	Reactance	[Ω]
$I^{\max}$	Cable current rating	[A]
Z^{cable}	Specific cable impedance	[Ω/km]
S^{tr}	Transformer apparent power rating	[kVA]
Z^{tr}	Transformer impedance	[Ω]
h	Household index	
H_o	Set of household loads	
e	Electric vehicle index	
$\mathcal{E}_o$	Set of electric vehicle loads	
$U_{ph,i,k}$	Voltage at phase ph, household node i, during time step k	
P_k^c	Charging power for charging case c during time step k	
$\Delta T_k^{\mathrm{dep}}$	Standstill time span until the next trip at time step k	[s]
SOC_k	State of charge during time step k	[%]
n_t	Number of simulation time steps	
ε^V	Voltage error during consecutive iteration steps	[V]
ε^P	Charging power error during consecutive iteration steps	[W]
$S_{\max}^{\mathrm{tr}}$	Highest occurring transformer loading	[kVA]
$S_{ph,k}^{\mathrm{tot}}$	Transformer loading at phase ph during time step k	[kVA]
$P_{ph,k}^{\mathrm{grid}}$	Active grid losses at phase ph during time step k	[kW]
$Q_{ph,k}^{\mathrm{grid}}$	Reactive grid losses at phase ph during time step k	[kVAR]
E^{del}	Delivered energy	[kWh]
E^{grid}	Grid power consumption	[kWh]

$P_{ph,h,k}^{\text{load}}$	Residential load at phase ph, for household h during time step k	[kW]
$P_{ph,e,k}^{\text{ch}}$	Grid charging power at phase ph, for vehicle e during time step k	[kW]
U^{min}	Lowest occurring voltage magnitude	[pu]
F_{max}^{VU}	Highest occurring voltage unbalance factor	[%]
$PF_{h,k}^{load}$	Power factor of household h at time step k	[-]
$P_{k,h}^{\text{load}}$	Residential load of household h at time step k	[kW]
$P^{\text{EOC}}(SOC_k)$	End of charge behavior as a function of the state of charge, at time step k	[kW]
E_k^{bat}	Energy content of the battery at time step k	[kWh]
P_{nom}^{ch}	Charging power rating	[kW]
T_k	Time of day	
ΔT	Simulation time step	[1 min]
r^{ch}	Ratio of reactive to active power during charging	[-]
Q_k^c	Reactive power injection for charging case c during time step k	[kVAR]
I^{ch}	Charging current rating	[A]
S^{ch}	Apparent power rating	[kVA]
$R_{\text{MAX}}^{\text{PEV}}$	Plug-in electric vehicle hosting capacity	[%]

Contents

List of figures

List of tables

1. Introduction

1.1 Context and motivation

Transport accounts for approximately 20 % of the energy usage worldwide, of which about half is used by light duty-vehicles (LDVs) [1]. Because most vehicle make use of an internal combustion engine (ICE) of some kind, e.g., reciprocating engines and jet engines, more than 90 % of the transportation fuels are petroleum based fossil fuels, e.g., gasoline, diesel, and kerosene [1]. As a result, transportation accounts for approximately 25 % of the global CO_2-emissions [1]. Besides this significant amount of energy usage and CO_2-emissions, the ICEs are also a source of pollutant emissions, e.g., particulate matter (PM), NO_X, and SO_2. It is estimated that road transport account for about 50 % of the air pollution impacts and costs in the European Union (EU) [2]-[3], exceeding 3 % of GDP in three quarters of the EU member states [3].

Electrification of LDVs is a manner to reduce the abovementioned negative impacts. The use of grid-supplied electricity as a transportation fuel in plug-in electric vehicles (PEVs), whether being battery electric vehicles (BEVs) or plug-in hybrid electric vehicles (PHEVs), allows to reduce the dependency of the transportation sector on fossil fuels [4]-[5], due to the primary fuel flexibility for electricity generation. Furthermore, the higher primary energy efficiency of electric vehicle propulsion compared to powertrains that are solely equipped with an ICE reduces the energy requirements for the transportation sector [6], as well as the related CO_2-emissions [7]. The absence of tailpipe emissions during pure electric driving reduces local concentrations of pollutant emissions, resulting in a positive impact on public health [8].

PEVs can provide further benefits, as they could adapt their grid electricity consumption pattern, to improve the load factor of the electricity consumption or to follow the variable generation pattern of renewable energy sources (RES) [9]. As a result, the share of RES can be increased at an acceptable cost, without compromising the security of supply of the electricity system [10]-[11]. This synergy of RES and PEVs as a flexible electric load allows for a simultaneous reduction of fossil-fuel dependency in both electricity generation and transport. Furthermore, because electricity is already widely available in a usable form in the built environment, the grid connection can be realized at a reasonable cost.

PEV charging will impact the different levels of the electricity system, depending on their penetration rate at the specific level [12]-[16]. Even though PEV sales are significantly increasing since 2010, their market share is still low [17]. However, similar to residential photovoltaic (PV) installations, local clusters of PEVs will occur soon. As a consequence, the distribution grid will already be impacted by PEV charging in the near-term future [18]-[24]. Therefore, distribution grid impact mitigation of PEV charging is necessary, to obtain a widespread high PEV penetration rate in the medium- to long-term future.

1.2 Scope and objectives

The objective of this dissertation is to analyze how the charging process of PEVs can be altered to mitigate their impact on low voltage (LV, <500 households) and medium voltage (MV, <5000 households) grids. As a result, the PEV hosting capacity of the distribution is increased, which defers distribution grid infrastructure investments. Flemish residential low voltage reference grid topologies, which are delivered by the two Flemish distribution system operators (DSOs), are used throughout this dissertation. The resulting distribution grid impact assessment is also applicable for other European regions, because similar grid topologies occur throughout Europe. Because no vast rural areas occur in Flanders, as there are for example in France, the results should are not to be generalized to such rural areas without further investigation.

The focus is on distributed control strategies, as they are implemented within each PEV separately. These strategies require no communication between the PEV and the grid operator, direct or through a PEV charging aggregator, and a minimal input from the PEV user. These control strategies could be implemented in the short-term future, as they do not require widespread infrastructure adaptations. The investigated control mechanisms should be compatible with widespread coordination approaches that are expected to be implemented in the medium/long term future, when a sufficiently high PEV penetration rate occurs.

Bidirectional charging strategies, often referred to as vehicle-to-grid (V2G), are not specifically considered, as the focus is on strategies that can be implemented in current PEVs. V2G typically requires hardware adaptations to the on-board charger, as most PEVs have a unidirectional charger topology. This might be overcome with an off-board bidirectional charger, but still there is a need for a standardized V2G protocol to take into account PEV and grid parameters.

Opposed to large scale mechanisms for the *coordination* of PEV charging, local *control* mechanisms have not been extensively investigated. More specifically, the

distribution grid impact of such local control strategies is investigated in this dissertation. The goal is to provide local control strategies for PEV charging that could be implemented in the near-term future, to mitigate problems caused by local clusters of PEVs. These control mechanisms make use of the inherent functionality of the power electronic interface between the PEV and the grid, to reduce the grid impact of the PEV charging process. Only when local grid constraints can be addressed effectively, the widespread rollout of PEVs and their required charging infrastructure can be realized.

Even though slow and fast PEV charging influence each other, this has not been extensively investigated in the literature. Therefore, the requirements for both types of charging infrastructure are overestimated, as they both are assumed to supply all of the charging energy. The interdependency between slow and fast charging will be investigated, to assess the additional distribution grid impact of fast charging, taking into account the above mentioned local control mechanisms for slow charging.

The focus in this dissertation is on passenger vehicles, because their usage pattern and specific power consumption is significantly different than for freight vehicles and buses. Furthermore, the charging opportunities and required charging infrastructure will be completely different for these other types of vehicles, and therefore, it requires a study on its own.

1.3 Outline

Chapter 2 gives a brief background on the aspects that influence the PEV charging process. First, the PEV topologies are discussed, in terms of their layout and resulting operational principles. Many different layouts are commercially available, and no convergence towards a single specific layout is expected. However, all of these layouts can support the electrification of a substantial amount of the mobility requirements, given a suitable sizing of the components. The batteries are discussed, as they are a key component in PEVs.

The variety of common lithium-ion (Li-ion) battery cell types is summarized and compared. Because a battery pack consists out of multiple cells, the battery management system (BMS) is discussed. Furthermore, the battery charger topologies are discussed, because the combination of the BMS and the charger determines the charging process. The charging infrastructure is discussed, for which a significant level of standardization is present already. Finally, the distribution grid layout and grid constraints are discussed, as these cannot be ignored when implementing PEV charging infrastructure.

Chapter 3 discusses the vehicle and fleet modeling for PEVs. First, the mobility behavior is modeled, for each individual vehicle and the resulting fleet mobility behavior, respectively. The segmentation of the vehicle fleet is modeled, to take into account the differences between subcompact, midsize, and large vehicles. This segmentation is relevant for a more accurate modeling of the individual energy consumption of each vehicle, taken into account the composition of the Flemish vehicle fleet. The specific power consumption is modeled, for a representative mix of urban, rural, and highway driving, using realistic driving cycles for a detailed assessment of the specific power consumption.

The general parameters, which are similar for the three vehicle categories, are discussed and used to calculate the specific power consumption. A sensitivity analysis is performed on the general parameters, as they significantly influence the results. The resulting fleet power consumption is calculated and discussed. The daily power consumption for the fleet, and the impact of the PEV battery capacity, charging opportunities, and charging power rating on the fleet charging profile are discussed.

Chapter 4 discusses the literature on coordinated charging of PEVs. The literature is structured in term of coordination layers, objectives, methods, and scales. Then, a correlation mapping is conducted to assess in which areas the research is concentrated. In this way, the missing links in the literature can be identified, more specifically in linking the coordination mechanisms to a practical implementation within the distribution grid in the near-term future.

This dissertation will focus on the missing links in the literature, as they are required for a successful implementation of PEV charging infrastructure, which is a prerequisite for the large-scale rollout of PEVs. Local active and reactive power control mechanisms on the interface between the PEV and the grid are identified, as well as individual coordination mechanisms that only require a limited amount of input from the PEV user.

Chapter 5 discusses the LV grid impact of active power control of PEV charging. Two strategies, serving different goals, are assessed separately and in combination. First, the voltage-dependent charging behavior is intended to provide a robust and safe mechanism in case the grid voltage magnitude bounds are exceeded. When the grid is in a disturbed state, the voltage dependent charging behavior avoids the grid going from the disturbed to the critical state, while not interfering in the charging process when the grid is in the normal state.

Second, an individual coordination mechanism is used to limit the grid impact of PEV charging, while only require a minimal amount of input from the PEV user, i.e., the next departure time. Such type of coordination can be used as long as no widespread

coordination mechanisms are implemented, due to the low overall PEV penetration rate, while clusters of PEVs already occur in some LV grids. The coordination mechanism also influences the charging process when the grid is in the normal state, as the goal is to prevent the disturbed state. The combination of both mechanisms is investigated, as coordination and grid-stabilizing mechanisms will co-exist, each with their own objective.

Chapter 6 discusses LV grid impact of reactive power grid injections during PEV charging. Certain charger topologies allow for the injection of reactive power flows into the grid, so this capability could be enabled. The advantage compared to the active power control strategies of Chapter 5 is that this grid-supportive measure does not influence the user comfort, given an appropriate sizing of the charger, as the active power flow is not altered.

The LV grid impact of reactive power support is assessed, in terms of voltage deviations, peak power demand, and grid losses. The impact is discussed for different active power charging strategies, to assess the interdependency between both active and reactive power charging strategies. Furthermore, a sensitivity analysis to the LV grid topology is performed, to assess whether the reactive power control strategies are widely applicable.

Chapter 7 discusses the sizing requirements and the MV/LV grid impact of fast charging infrastructure. Fast charging is indispensable for pure battery electric vehicles, as they have no backup on-board power source for when the slow charging capabilities are insufficient to meet certain mobility requirements. Opposed to fossil fuel stations, fast charging stations are not needed for all charging activities, as there are many slow charging options for PEVs. Therefore, it is of importance to take into account the complementarity between slow and fast charging infrastructure when assessing the sizing requirements and distribution grid impact.

Different slow charging strategies are taken into account, to assess which parameters have the most significant grid impact, i.e., how much does fast charging impact the distribution grid compared to slow charging. Different LV distribution grid topologies are taken into account, to assess whether the conclusions are widely applicable.

Chapter 8 summarizes the general conclusions of this dissertation. Future work on the topic of PEV charging infrastructure is outlined.

1.4 Contributions

The main contributions of this dissertation are:

- An improved PEV load modeling (Chapter 3), by taking into account mobility behavior, fleet composition, battery capacity, standardized charging power rating, and charging opportunities.
- The identification of the need for local PEV charging strategies, to mitigate the residential LV (<500 households) and MV (<5000 households) grid impact (Chapter 4). These strategies are required to manage local clusters of PEVs, that will occur prior to a widespread penetration of PEVs, and therefore, prior to the presence of widespread coordinated PEV charging strategies.
- An improved residential distribution grid scenario modelling: real (sub-) urban distribution grid topologies, measured (Chapter 5) or realistically modeled (Chapter 6 and 7) household load profile, and real PV power generation profiles.
- The use of an unbalanced load flow methodology, to improve the grid impact assessment of the single-phase grid connection of the LV loads and generation. The methodology allows to assess the different types of three-phase grid topologies that occur, by making use of Carson's equation (to include the neutral conductor impedance) and Kron's reduction (to reduce the impedance matrix to 3x3) [25]. The load flow methodology can easily be expanded to split-phase grid topologies, as commonly used in North-America and Japan.
- The design and assessment of local charging strategies (which are implemented within each PEV separately), both for active (Chapter 6) and reactive power (Chapter 7), that can be implemented in currently available PEVs. Therefore, these strategies are to be considered to mitigate the distribution grid impact of PEV clusters that are expected to occur in the near-term future.
- The combined modeling of slow and fast charging behavior, as they complement each other (Chapter 7), resulting in a more accurate assessment of the fast charging requirements.

2. Plug-in electric vehicle charging

The general aspects of PEVs and PEV charging are explained briefly in this chapter. A classification of EV types is given (Section 2.1), followed by a brief overview of PEV batteries (Section 2.2), and the charging infrastructure and its related standards (Section 2.3). The distribution grid aspects related to PEV charging are discussed (Section 2.4), followed by the conclusions (Section 2.5).

2.1 Electric vehicle types

All electric vehicle (EV) types make use of electric propulsion to some extent. They recover kinetic energy during braking, by using the electric motor as a generator, which further increases their energy efficiency. There are large differences between the different EV types in their usage of electric propulsion. Battery electric vehicles (BEVs) fully rely on electric propulsion (Section 2.1.1), whereas (plug-in) hybrid electric vehicles ((P)HEVs) combine this with an ICE (Section 2.1.2). BEVs and PHEVs are both PEV types, as their propulsion batteries can be charged via the electric grid.

2.1.1 Battery electric vehicles

The propulsion energy for BEVs is fully supplied by the on-board batteries that are charged via the electric power system and via regenerative braking (Figure 2.1). The electric motor is connected to the wheels via a transmission that typically has one fixed gear ratio, as the electric motor has a wide torque range. However, it is possible that future BEVs will have multi-speed transmissions, in order to further increase the operating range.

All current commercially available BEVs and (P)HEVs make use of AC electric motors, and different types are being used by different BEV manufacturers (e.g., permanent magnet synchronous motors [26], induction motors [27], and synchronous motors with external excitation [28]). As a result, a DC to AC conversion is needed to feed these AC motors with energy supplied by a battery. Typically, both a DC/DC convertor and a DC/AC convertor are used. Hereby, the DC input voltage for the DC/AC convertor can be kept constant when the DC output voltage of the battery drops when its state of charge (SOC) decreases.

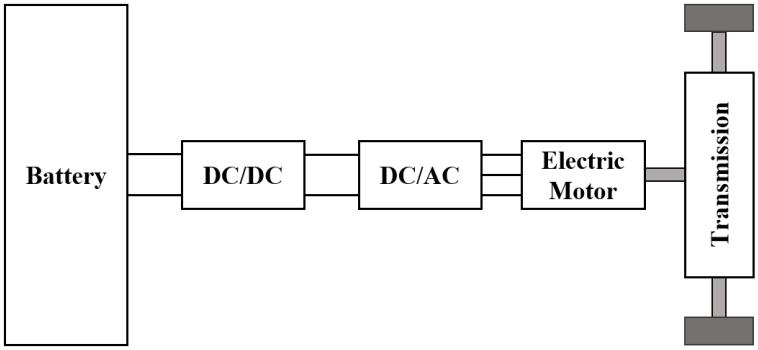

Figure 2.1: BEV powertrain topology.

2.1.2 (Plug-in) hybrid electric vehicles

(P)HEVs occur in many topologies, which differ in the way how the energy supplied by the ICE and the electric motor are combined. There are HEVs with and without the option to be grid-connected for recharging the battery. The former can recharge their battery through regenerative braking, and through the ICE. In this way, braking power is recovered and the ICE can operate in a more efficient working point. PHEVs further improve energy efficiency by recharging the battery through the electric power system instead of through the ICE. Typically, PHEVs have a larger battery capacity compared to HEVs, so that more pure electric driving occurs [29]-[30].

2.1.2.1 Series hybrid

In the series hybrid topology, the (P)HEV is exclusively propelled by the electric motor (Figure 2.2). Therefore, the series hybrid topology shows a lot of similarities with the BEV topology. The required electric energy is delivered by the battery, by the ICE, or a combination of both. The ICE is connected to an electric generator, to convert mechanical into electrical power. The addition of both power sources happens electrically in the series hybrid topology. The power rating of the battery pack determines to which extent the vehicle can drive purely on battery power [31].

As there is no mechanical connection between the ICE and the wheels, there is no need for a multi-gear transmission for the ICE. This allows the drivetrain designer to size the ICE for steady-state power requirements, as the power peaks can be supplied by the battery, if properly sized [32]. Therefore, there are less stringent performance requirements for the ICE, which allows to optimize its thermodynamic cycle and operation strategy for improved energetic efficiency.

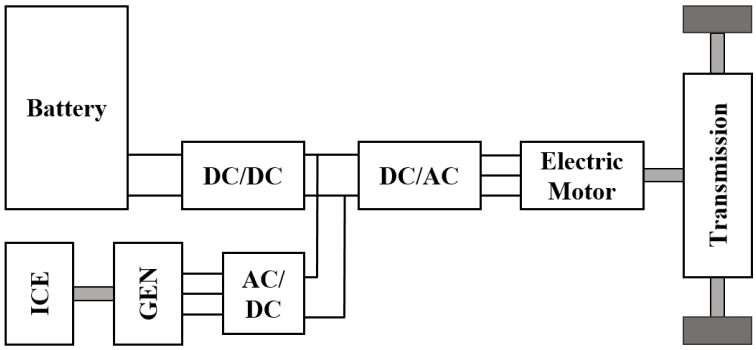

Figure 2.2: Series hybrid powertrain topology.

2.1.2.2 Parallel hybrid

In the parallel hybrid topology, the addition of the ICE and electric motor torques is performed mechanically (Figure 2.3). Both the ICE and the electric motor are mechanically connected to the wheels via a transmission, but implementations differ. Typically, the electric motor also makes use of the multi-gear transmission of the ICE [33]. Therefore, the parallel hybrid shows lots of similarities to conventional ICE vehicles, and the electric motor is typically built into the transmission, thereby making the powertrain similar to a conventional one.

Similar to the series hybrid topology, the power rating of the battery and electric motor determines to determine to which extent the vehicle can drive purely on battery power. Typically, both power sources are required to deliver the peak power [33]. However, peak power is only required for a fraction of the driving conditions, and there are many situations where the driving power requirements are relatively limited. Therefore, even with a limited power rating for the battery and the electric motor, a large fraction of the driven distances can be covered with electric power.

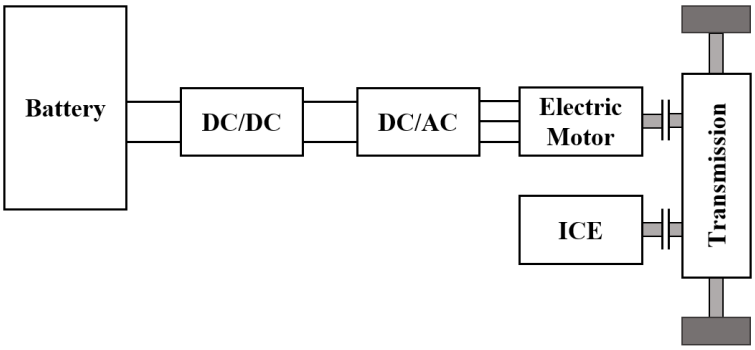

Figure 2.3: Parallel hybrid powertrain topology.

An alternative parallel hybrid system combines the electric and ICE power through the two different axes (Figure 2.4) [34]. In this way, the ICE is connected to the wheels in an identical manner as in a conventional vehicle, there is no influence of the electric propulsion on the ICE powertrain. Therefore, this system is well suited for vehicles that are offered with both (plug-in) hybrid and conventional powertrains. The electric motor is typically connected with a single-speed transmission to its axis. An additional advantage of this system is the possibility to provide an energy-efficient four-wheel drive powertrain, which is very popular in colder climates.

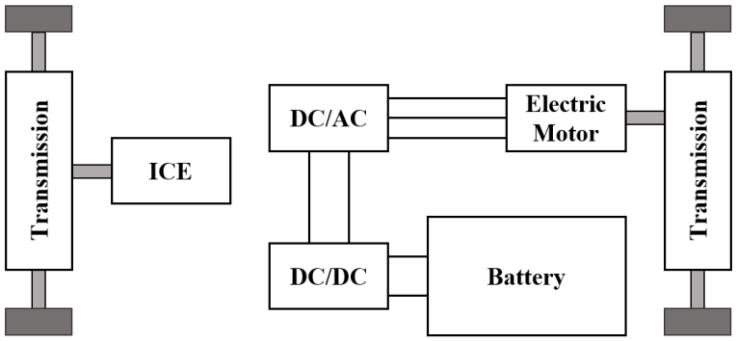

Figure 2.4: four-wheel drive parallel powertrain topology.

2.1.2.3 Combined series-parallel hybrid

Besides the pure series and parallel topologies, there are combined topologies (Figure 2.5). One of the best known examples is the Toyota Prius [30], which actually blends both modes continuously by means of a power-split device. At lower speed, most of

the ICE power flows via the series hybrid path to the wheels, while at higher speeds, the majority of the ICE power flows through the parallel hybrid path. Other topologies switch between both series and parallel hybrid modes, typically operating as a series hybrid at low speeds and as a parallel hybrid at high speeds, to maximize overall energy efficiency.

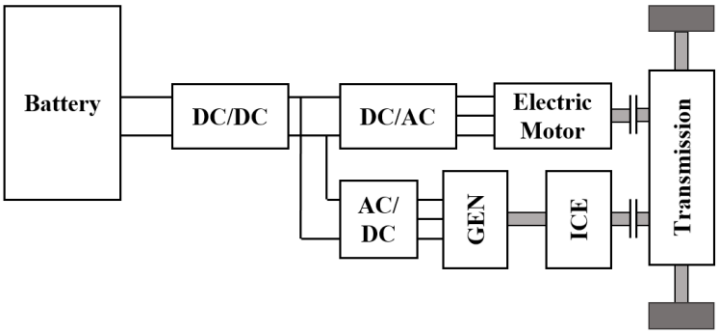

Figure 2.5: Combined series-parallel hybrid power train topology.

For example, the Mitsubishi Outlander PHEV works as a front-wheel driven series hybrid at low speeds, but provides a single-speed direct connection between the ICE and the front wheels at high speeds [31]. In this way, the conversion losses at higher speeds are eliminated. Furthermore, there is another electric motor connected to the rear axle [31], to provide four-wheel drive. This example shows that many topologies are being used and combined, and there is no clear convergence at this moment.

2.2 Plug-in electric vehicle batteries

All modern PEVs make use of lithium-ion (Li-ion) battery cells for the propulsion battery pack. Nevertheless, PEVs still have a 12 V battery to supply the auxiliaries, which is also required to start the vehicle. This battery is charged by the propulsion battery pack via a DC/DC converter, when the vehicle is engaged or when the vehicle is charging. As a consequence, it is still not possible to start the vehicle if the 12 V battery is fully discharged.

Li-ion refers to a group of battery cell chemistries in which lithium ions flow from the negative electrode to the positive electrode through the electrolyte and separator during discharging, and in the reverse direction during charging [35]. Different cathode and anode materials are being used, which determine the properties of the battery cells (Figure 2.6). The anode is typically carbon, with the exception of LTO

batteries ($Li_4Ti_5O_{12}$). They are used in some electric buses that are used for public transport [36], because they are well suited for fast-charging, and in that application a low energy density is less of an issue.

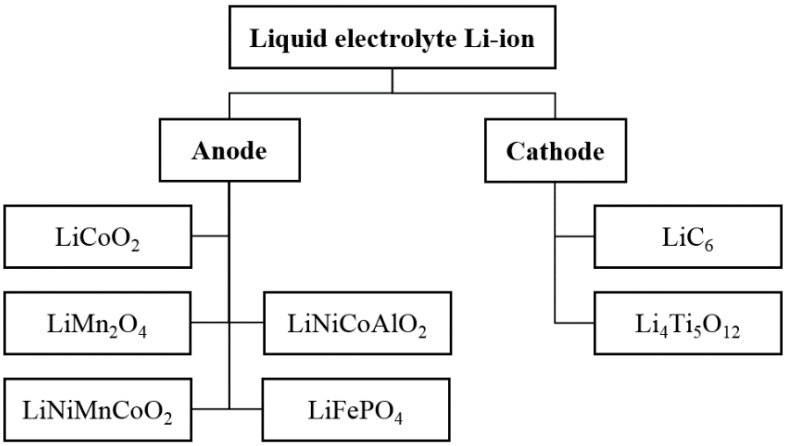

Figure 2.6: Frequently used cathode and anode materials for PEV Li-ion batteries.

2.2.1 Cell types

In the past, LCO-anode batteries ($LiCoO_2$) were used [37], which is the same cell type as used in consumer electronics. These cells have a high specific energy density, but a low specific power and a limited life span, which makes them less suited for PEVs. Therefore, different anode materials have been developed, of which four are typically applied nowadays in PEVs. These can be used for single-material anodes, or in a mix to combine the advantages of the different materials.

The LMO battery ($LiMn_2O_4$) was developed as an improvement compared to the LCO battery. The lower internal resistance supports a higher power density and fast-charge capability [26], but the trade-off is a reduced lower energy density compared to LCO batteries. A newer chemistry is used in the NMC battery ($LiNiMnCoO_2$), which tries to combine the good properties of LCO and LMO [32], while lowering the raw material cost due to the lower amount of cobalt compared to LCO. LMO and NMC are currently the typical anode materials for mass-production PEVs.

NCA batteries ($LiNiCoAlO_2$) are used in applications where the combination of high specific power and energy is very important, such as high-performance BEVs [27] and PHEVs [29]. The trade-off is a higher cost and more attention is needed to

guarantee safe operation, through a more sophisticated battery management system and thermal management. On the other side of the spectrum, LFP batteries ($LiFePO_4$) are characterized by their very low internal resistance, thermal stability, robustness, high current rating and long cycle life. The trade-off is the lower energy density, below that of LMO batteries. This makes them also more suitable for fleet vehicles that can make frequently use of fast charging [38].

2.2.2 Battery pack

Multiple battery cells are connected, in series and in parallel, to obtain a usable voltage and current rating on a pack-level. Typical rated voltages for BEV are between 350 V and 400 V [26]-[27], while for PHEVs the voltages range between 200 V and 400 V, depending on the battery capacity [29], [39]. Because each battery pack consist out of multiple battery cells that are not identical, a battery management system (BMS) is essential. The BMS is needed to keep each cell within its safety margins, determined by the temperature, current, and voltage envelopes [40].

Furthermore, the SOC of the cells might deviate considerably after multiple (dis)charging cycles, because they are not identical. Then, if one of the cells within a series connection reaches the lower SOC limit, while the others do not, the entire series connection cannot discharge anymore. As a result, the usable capacity of the battery pack is reduced when the cells are not balanced. Therefore, the BMS also provides balancing between the cells, so that the SOC of all cells stays approximately the same. Several balancing algorithms are used (e.g., voltage-based, final voltage-based, and SOC history-based), of which the vast majority performs balancing only during the charging process [40].

Discharging common lithium batteries to an extreme low SOC limits the power output, and such a high depth of discharge (DOD) may also impact the battery lifetime [41]. Some manufacturers allow a relatively high DOD, e.g., the 2012 Renault Fluence ZE uses 22 of the 25.87 kWh rated capacity [42], resulting in a DOD of 85 %. Other manufacturers are more conservative, e.g., the 2012 Chevrolet Volt uses 10.8 of the 16.5 kWh [39], keeping the SOC between 19.5 and 85 %. The upper SOC is limited, as this increases the battery lifetime as well [41]. Some manufacturers, such as Nissan and Tesla, make the upper SOC charging limit adaptable for the PEV user, to maximize the driving range when required, while increasing the battery lifetime when the maximal driving range is not needed [26]-[27].

Typically, the constant current constant voltage charging profile (CCCV) is typically used for charging Li-ion cells (Figure 2.7). Sometimes, this charging profile is implemented in a discretized manner, with a multistage constant current phase, during

which the charging current is reduced in a set of discrete steps, as the battery cell is approaching full charge (Figure 2.8).

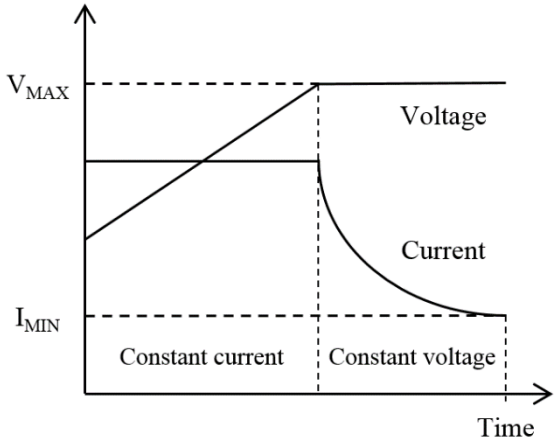

Figure 2.7: Constant current constant voltage charging profile for a single battery cell.

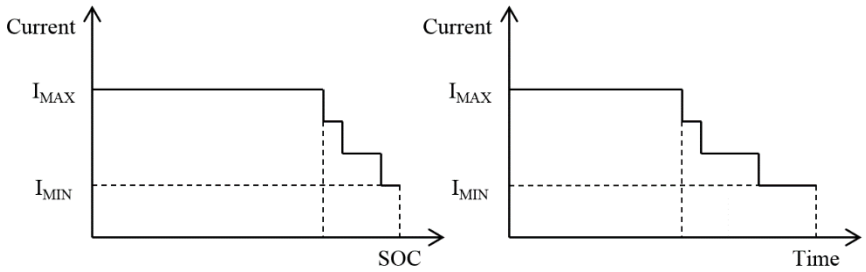

Figure 2.8: Illustration of a multilevel constant current charging profile for a battery pack.

Depending on the balancing algorithm, the aggregated charging profile of the battery pack might differ significantly for the charging profile of an individual battery cell. Three different PEV charging profiles where measured on currently available PEVs (Figure 2.9) [43]. Charging profile A looks very similar to the CCCV charging profile of an individual cell, which indicates that the balancing occurs in a continuous manner during (a part of) the charging process [40]. Charging profiles B and C look substantially different from charging profile A, as the charger works in a discontinuous manner during the constant voltage phase, to perform balancing during the off-time intervals [40].

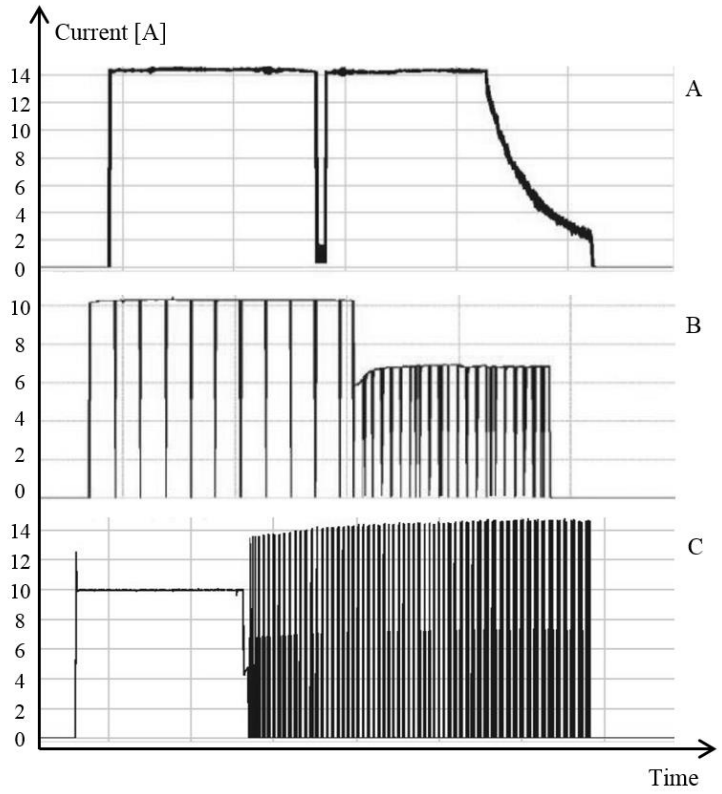

Figure 2.9: Charging current measurements for 3 commercially available PEV models [43].

2.2.3 Battery charger

For all types of PEVs, the battery pack is charged from the electricity grid. The battery charger performs several functions during the charging process. First, there is the AC/DC convertor, which rectifies the AC current that is drawn from the grid. Second, the DC/DC converter connects the DC bus to the battery pack that has a voltage that depends on the SOC and the charging current. The AC grid current must be drawn with a low distortion to keep the power quality impact within the regulatory bounds, and the power factor must be high enough to efficiently make use of the available utility power [44]. There are multiple standards that limit the allowable harmonic current injections into the grid [45]-[47], to which PEV chargers are designed to comply with, just like other power-electronic grid interfaces [44].

The most common topology for on-board battery chargers is the (interleaved) boost rectifier combined with a unidirectional DC/DC convertor (Figure 2.10). A diode bridge rectifies the AC input voltage to DC, and the DC current amplitude can be controlled through the switching behavior of the boost section. By controlling the rectified DC current to be in phase with the amplitude of the AC grid voltage, a unity power factor current is drawn from the grid. Interleaving is typically used for power ratings above 1 kW, to reduce the charging current ripple and the component size. However, as the power rating increases, the diode bridge losses significantly degrade the efficiency [48].

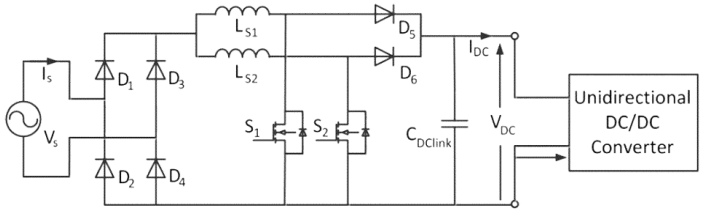

Figure 2.10: Interleaved boost rectifier topology [44].

A single-/three-phase full-bridge active rectifier is commonly used for higher power ratings and/or efficiency (Figure 2.11). The forced modulation allows to introduce a certain phase angle between the charging current and the grid voltage, thereby being able to provide reactive power grid support. Because the active full-bridge rectifier can also create a 180-degree current phase angle, it allows for bidirectional power flows, if the charger is equipped with a bidirectional DC/DC convertor [49]. Some PEVs use a full-bridge active rectifier in their on-board charger that allows to charge through both single-phase and three-phase grid connections [27].

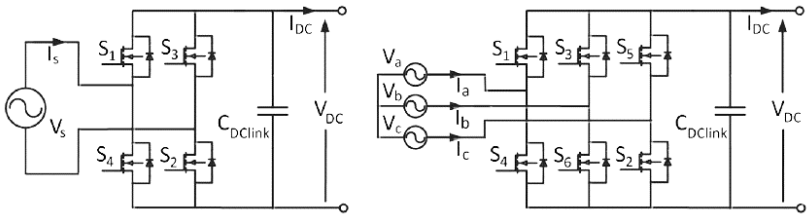

Figure 2.11: Single-phase (left) and three-phase (right) full-bridge active rectifier topology [44].

2.3 Charging infrastructure

Generally, the off board charging infrastructure is named electric vehicle supply equipment (EVSE). The PEV is connected to the EVSE via a cable, which has a connector on the PEV side and a plug on the EVSE side (Figure 2.12). The PEV battery charger rectifies the AC electricity and controls the resulting DC charging current that flows to the battery.

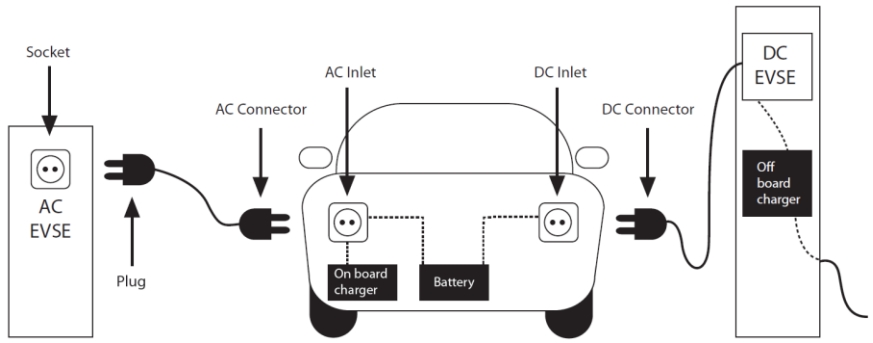

Figure 2.12: Charging infrastructure for PEV charging [35].

AC charging occurs if the battery charger is located inside the PEV, which is supplied with AC grid power from the EVSE. For DC charging, the charger is located inside the EVSE and the PEV is supplied with DC power (Figure 2.12). For inductive charging, the charger is split between the vehicle and the EVSE, and the power transfer is realized via inductive power transfer. Inductive charging will not be further discussed, as it is not fully standardized yet. The International Electrotechnical Commission (IEC) created the standard IEC 61851-1 for conductive charging [50].

2.3.1 Charging cases

According to IEC 61851-1, there are three charging cable configuration cases:

- Case A: the charging cable is attached to the PEV. The cable plug must be compatible to the EVSE socket.
- Case B: a loose cable is used, with a connector at the PEV side and a plug at the EVSE side.
- Case C: the cable is attached to the EVSE. The cable connector must be compatible with the PEV inlet.

Case A is rarely used, as there is no flexibility in EVSE sockets to connect with. Only for PEVs with a limited energy demand, such as electric bicycles and the Renault Twizy [51], Case A is implemented, thereby equipped with a standard domestic plug at the cable end.

Most PEVs are Case B and C compatible, whether being BEVs (e.g., Nissan Leaf [26], Kia Soul EV [52], and VW e-Golf [53]) or PHEVs (e.g., Chevrolet Volt [39], Mitsubishi Outlander PHEV [31], and VW Golf GTE [33]). These PEVs all have a dedicated PEV inlet, and the charging mode will depend on the EVSE to which they are connected. Case B allows to create a high degree of compatibility between different vehicle inlets and EVSE sockets. This is relevant for areas where multiple PEV inlet types and EVSE socket types occur, such as Europe.

2.3.2 Charging modes

The IEC 61851-1 standard also defines four different charging modes:

- Mode 1: single- and three-phase AC charging currents up to 16 A (3.3/9.9 kW for 230/400 V), for which the grid connection occurs through a standard domestic socket.
- Mode 2: single- and three-phase AC charging currents up to 32 A (6.6/19.8 kW for 230/400 V), for which the grid connection occurs through a standard socket and cable that is equipped with an in-cable protection device.
- Mode 3: hard-wired AC charging infrastructure for currents up to 32 A (6.6/19.8 kW for 230/400 V) for Case B, and up to 63 A (13.2/39.6 kW) for Case C.
- Mode 4: DC charging up to 400 A, making use of an off-board charger.

Mode 1/2 charging are carried out from a common single- or three-phase household socket. For Mode 1, the maximum continuous current is set through resistive coding between the in-cable power indicator and the ground [54]. Mode 2 is equipped with an In-Cable Control and Protection Device (IC-CPD) integrated into the charging cable. The IC-CPD incorporates a residual current device (RCD), protective earth (PE) monitoring and a pilot control (communication) function [54].

A charging current rating of 10 A is typically used for Mode 2 chargers in Europe, as the 16 A maximum rating of most sockets can cause overload in the household wiring [55]. For Mode 3, the RCD, PE, and control pilot function are located in the off-board charging infrastructure [54]. Common current ratings for Mode 3 charging are 16 A and 32 A, which can be supplied by LV power circuits with a 20 A and 40 A miniature circuit breaker rating (MCB), respectively.

Most PEVs are Case B/C compatible and they are typically delivered with a Mode 1/2 adapter cable that has an inlet-compatible connector on the one side, and a domestic socket on the other side. This allows the use of standard domestic sockets, albeit at a low power rating, resulting in long charging times. The in-cable resistive coding for Mode 1, and the pulse width modulation (PWM) control pilot signal for Mode 2/3 put a limit on the PEV charging current [54]. The effective instantaneous current the PEVs draw is controlled by the on-board charger and cannot exceed its current rating. Furthermore, the charging power is reduced when the battery reaches its maximum SOC [56].

Mode 3/4 charging make more effective use of the available power supply, because the EVSE has a dedicated power circuit to which it is connected. This results in a shorter charging time compared to Mode 2, as typically a current rating above 10 A is available. Mode 3 charging offers the possibility to continuously adapt the charging current limit of each PEV through variations in the control pilot signal, to which the chargers have to respond within 5 s. This provides a higher degree of flexibility for controlled charging strategies compared to on-off switching. For instance, the allowable charging current could be adapted to anticipate on fluctuating local photovoltaic power generation. For power ratings exceeding the on-board charger rating, Mode 4 charging is used, as there are less stringent space and weight limitations for an off-board charger.

However, Mode 3/4 charging also has disadvantages. A dedicated infrastructure is required, which results in fewer charging opportunities compared to Mode 1/2. Therefore, it must be considered whether the advantages of Mode 3/4 charging infrastructure outweigh the disadvantages. For instance, the investments in Mode 3 charging infrastructure at home, which allows to charge at 16 A/3.3 kW, might be unnecessary if the vehicle is parked at home for a sufficiently long time. Furthermore, resistive charging losses and battery aging are lower with lower charging currents [57]. From this point of view, it is better to charge at a lower current for a longer amount of time.

The charging power rating should be matched to the standstill time at the charging location. At home and at the workplace, Mode 2 or low-power Mode 3 (up to 10 kW) charging infrastructure is sufficient to recharge the battery within the typical standstill time span. At locations where a short standstill time is crucial, e.g., at public or highway recharging stops, high-power Mode 3/4 charging infrastructure is more suited. These will be used for the occasional trips that exceed the electric driving range. Therefore, they are only needed for a minority of the charging actions, but are crucial for BEVs to become a valid alternative for conventional vehicles.

2.3.3 Connection types

Different types of plugs/sockets and inlet/connector types are used for the connection between the PEV and the AC EVSE (Table 2.1):

- Domestic type plug/socket: usable for Case A/B and Mode 1/2, so the vehicle can charge at a standard domestic socket.
- IEC 62196-2 Type 1: this inlet/connector is also known as SAE J1772, and is usable for Case B/C and Mode 1/2/3. It is the standard inlet/connector for Japanese and American PEVs, also for the ones being sold in Europe.
- IEC 62196-2 Type 2: this is both inlet/connector and plug/socket, for Case B/C and Case A/B, respectively, for Mode 1/2/3 charging. It is the standard inlet/connector for European PEVs, and the standard Mode 3 EVSE socket in most European countries.
- IEC 62196-2 Type 3: this plug/socket type is usable for Case A/B, for Mode/3 charging. This plug/socket type is used in some European countries, but will be phased out in favor of Type 2.

In the USA and Japan, PEVs are always equipped with Type 1 inlets, which allows all PEVs to perform Mode 1/2 charging with a charging cable that has a Type 1 connector. Only Case C occurs for Mode 3 charging infrastructure in the USA, eliminating the need to carry along a Mode 3 charging cable. PEV users only need to carry a cable for Mode 1/2 charging in the USA.

Table 2.1: Overview of the AC plug/socket and inlet/connector types.

IEC 62196-2	**Type 1**	**Type 2**	**Type 3**
	Maximum current [A]		
Mode 2	32	32	/
Mode 3	80	63	32
Vehicle inlet/ connector	Yes	Yes	No
Plug/socket	No	Yes	Yes
	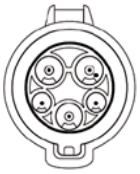		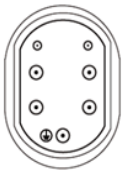

In Europe, both Type 1 and Type 2 PEV inlets occur. Therefore, two types of Mode 1/2 charging cables exist. For Mode 3 charging, both Case B and Case C occur. The advantage of Case B is that all different combinations of EVSE sockets and vehicle inlets are compatible, by making use of the appropriate charging cable. Therefore, Case B is typically used for public charging infrastructure with currents up to the allowable limit of 32 A. However, a specific vehicle only needs one Mode 3 charging cable, as there is a preferred socket type in most geographic areas [58].

In January 2013, the European Commission has announced the use of the Type 2 plug/socket as the common standard for public charging infrastructure, thereby phasing out the Type 3 plug/socket over time. A common configuration for public AC charging infrastructure in Europe is supplied with both a standard domestic socket and Type 1 or Type 2 socket. This guarantees that all PEVs can be charged due to the presence of the domestic socket, and that Mode 3 charging is possible with the appropriate charging cable. At home, Case C charging infrastructure can be used to increase the user comfort, as the PEV inlet type is known.

For DC charging, two systems are found in Europe and will likely remain in use (Figure 2.13). European and North-American PEV manufacturers use the Combined Charging System (CCS), with the appropriate AC inlet/connector type for the region where it is deployed, while the Japanese manufacturers use the CHAdeMO system. Tesla motors has its own dedicated fast-charging infrastructure, which currently cannot be used by vehicles from other manufacturers, but it is backwards compatible with the CHAdeMO system, when using the appropriate adapter [59]. Furthermore, Tesla has released a series of patents, including those concerning fast charging. Therefore, it might be possible that this charging infrastructure might be shared with others in the future.

Figure 2.13: European Combined Charging System (left) and CHAdeMO (right).

The different fast-charging systems are not compatible, but fast charger manufacturers already offer multi-standard chargers. Only the vehicle interface is different, while the power electronic topology is identical for each standard. Therefore, it is easier to implement fast charging stations than conventional fuel stations, as they have to provide different fuels to be compatible with different ICE-vehicle types. Furthermore, the grid connection guaranties a supply of electricity, opposed to a comprehensive logistic system for supplying fuels to conventional fuel stations. Therefore, it requires substantially less effort to operate a fast charging station compared to a conventional fuel station.

2.3.4 Grid connection

All types of EVSE require a LV grid connection, which can be single-phase (230 V in Europe) or three-phase (400 V line-to-line in Europe). The typical current ratings for electric installations, and the resulting apparent power ratings are summarized in Table 2.2, as well as the effective charging current. The charging current is a function of the grid voltage, which can deviate up to 10 % during normal operation (Section 2.4.3).

Table 2.2: Current ratings, corresponding single- and three-phase power ratings, and the effective charging current as a function of the grid voltage, for European LV grids.

Current rating [A]	**Power rating [kVA]**		**Charging current [A]**		
			Grid voltage [pu]		
	Single-phase	**Three-phase**	**0.9**	**1.0**	**1.1**
6	1.2	3.7	6	5.4	4.9
10	2.1	6.2	10	9.0	8.2
16	3.3	9.9	16	14.4	13.1
32	6.6	19.9	32	28.8	26.2
63	13.0	39.1	63	56.7	51.5
80	16.6	49.7	80	72.0	65.5
100	20.7	62.1	100	90.0	81.8
250	51.8	155.3	250	225.0	204.5

Many mode 2 charging cables foresee an option to reduce the charging current to a value as low as 6 A [60], the lowest current rating that can be communicated through the control pilot signal for Mode 2/3 [54]. This reduced charging current rating can be

applied to avoid overloading, when the EVSE is connected to a power circuit that not allows to supply higher currents continuously. As a result, even though the power rating is significantly reduced, the PEV can still be charged. As a result, each properly functioning domestic socket can be considered as a grid connection for PEV charging.

For Mode 3 charging, typically single-phase or three-phase current ratings of 16 A or 32 A are used, depending on the topology and current rating of the PEV charger and the EVSE. For example, a typically occurring single-phase current rating for a residential grid connection is 40 A [61]. Because this grid connection supplies all the domestic loads, the EVSE current rating is typically limited to 16 A, also if the PEV charger itself has a higher current rating (typically 32 A for recent BEVs [26], [52]). The power circuit for a 16 A load can be protected with a 20 A circuit breaker, which is commonly used in residential electric installations.

Alternatively, Mode 3 charging infrastructure could provide a variable control pilot signal. This allows to make more effective use of the available grid connection, while still not exceeding its current rating. For example, for a typical single-phase residential grid connection with a 40 A current rating and a PEV with a single-phase 32 A on-board charger, this allows to charge the PEV at currents up to its rating, as long as the non-PEV residential loads draw less than 8 A of current. Otherwise the charging current will be reduced to keep the total current below 40 A [62].

For high-power AC charging and high-power DC charging, power ratings of more than 40 kW are used. In Europe, such power ratings always require a three-phase grid connection, resulting in current ratings of more than 63 A [62]. When more than one fast charger needs to be grid connected at one spot, a separate LV feeder is often required to supply such high current ratings. For fast charging stations with more than four chargers [63], [59], the apparent power rating amounts to more than 160 kVA, which is in the order of magnitude of a typical European residential LV grid. Therefore, such fast charging stations are connected to the MV grid via their own MV/LV transformer.

2.4 Distribution grid

2.4.1 LV grid layout

Because low-power PEV charging infrastructure will be grid-connected within the existing LV grid, its layout is discussed here. Two main types of LV grid topologies can be distinguished: the European and the North-American system. The former is discussed here, as the focus in this dissertation is on Europe. The North-American LV system is discussed in Appendix A.

In Europe, relatively large MV/LV transformers serve a relatively large amount of customers, typically more than 100 households per transformer [64]-[65]. The LV feeders are typically three-phase feeders that can exceed 1 km in length in low-populated areas, to which single- and three-phase customers can be connected. Single- or two-phase grids may occur in very sparsely populated areas [65]-[66].

Three typical LV distribution grid topologies are illustrated in Figure 2.14. Each topology has a TT-grounding arrangement, i.e., with an independent grounding connection at each house, and a separate one at the transformer. In Flanders, as well as in most European (sub-) urban areas, the majority of the LV grids have a 3×400 V + N topology with a TT grounding arrangement, and a grounded-wye secondary transformer connection [61]. Single-phase customers have a 230 V line-to-neutral grid connection, and three-phase customers have a 4-wire grid connection that offers 230 V line-to-neutral and 400 V line-to-line.

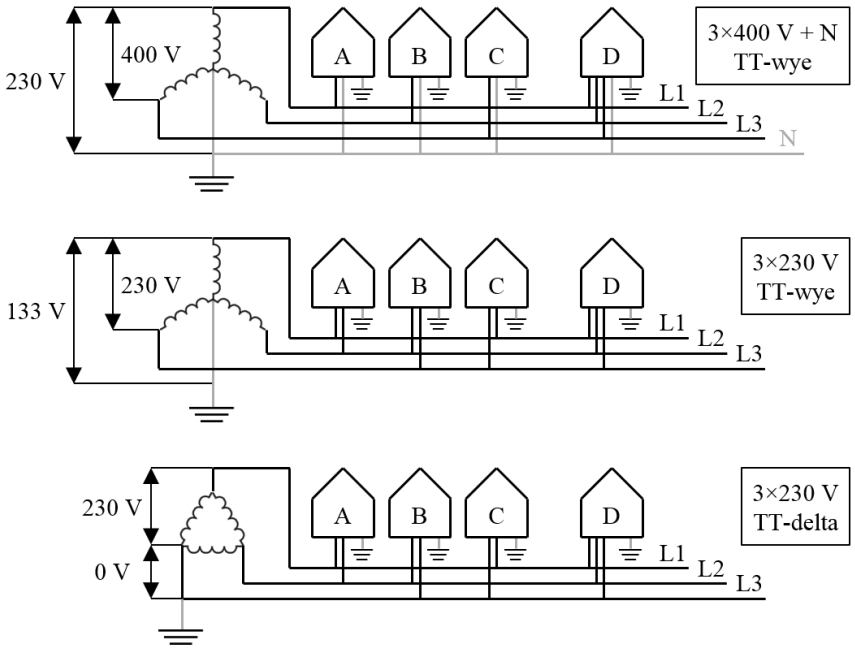

Figure 2.14: Typical Flemish distribution network topologies, with single-phase (house A, B, and C) and three-phase (house D) grid connections.

About 23 % of the Flemish residential customers have a three-phase grid connection to a 3×400 V + N grid topology, typically with a 25 A current rating [67]. About 43 % of the Flemish households have a single-phase grid connection to this grid topology, typically with a 40 A current rating [67]. The remaining 34 % of Flemish households are connected to a 3×230 V topology with a TT grounding arrangement, without a dedicated neutral conductor [67]. Grounded-wye and grounded-delta secondary transformer connections both occur in Flanders. Single-phase customers are connected line-to-line in these grids. For three-phase loads that require 400 V line-to-line, a three-phase delta-wye isolation transformer is installed.

It has been observed that the absence of a dedicated neutral conductor causes single-phase charging problems for some PEVs [67]. It is assumed that these PEVs measure the electric potential difference between the perceived neutral line and the grounding, as a safety precaution. Within the 3x230 V grid topologies, this potential difference amounts to 133 V, and the PEV assumes that there is a safety risk. These charging issues can be solved by installing a single-phase isolation transformer to create a dedicated neutral conductor.

Fast charging infrastructure needs a 3×400 V + N grid connection [68], which can be delivered through an existing MV/LV transformer, if there is sufficient capacity available. Typically, the fast charger will be connected to the MV/LV transformer through a dedicated feeder. If the available grid has a 3×230 V topology, a three-phase delta-grounded wye isolation transformer is installed to create the require voltage level. If there is insufficient capacity available, a transformer upgrade is needed. Alternatively, a dedicated MV/LV transformer can be used to feed the fast charging infrastructure, which is typically done when multiple fast chargers (≥ 4) are installed [59], [63].

2.4.2 MV grid layout

PEV charging infrastructure is connected to the MV grid, either via an existing LV grid (Section 2.4.1), or via a dedicated MV/LV transformer when the charging load is substantial, such as for fast charging stations with multiple chargers. European MV grids have a three-phase topology without a neutral conductor, to which the three-phase MV/LV transformers are connected through a delta-configuration at the primary side [65]. North-American MV grids are three-phase with a multigrounded neutral conductor, to which the single-phase MV/LV transformers are connected line-to-neutral. The three-phase MV/LV transformers are typically connected through a grounded-wye or delta connection at the primary side [65].

Both for European and North-American MV grids, there are two typical MV grid topologies. There are purely radial MV grids that can have many laterals, which can only be fed through one point. Radial grids typically occur in areas with a low load density [69]. For areas with a high load density, the open ring topology is typically used, i.e., a feeder without laterals that can be fed through either end, in order to increase reliability. During operation, the open ring topology grid is only fed through one side, thereby performing as a radial topology [69].

The voltage classes are similar in European and North-American MV grids: 5, 15, 25, and 35 kV are the typical occurring voltage classes [65]. These classes refer to a set of voltage levels that are approximately the same. For example, the operational voltage levels of 12.47 kV, 13.2 kV, and 13.8 kV are all within the 15 kV class [65]. Furthermore, both European and North-American MV grids are typically connected to the HV grid via a HV/MV transformer with at delta-grounded wye configuration [65].

2.4.3 Distribution grid constraints

Distribution grids have to operate within certain envelopes, which can be related to service standards or to grid component constraints, to assure that the customers' needs are met in a safe and satisfactory manner [70]. Voltage and quality standards are typical examples of distribution grid service standards. These standards result in operational envelopes, within which the distribution grid has to be operated. On the other hand, there are grid components constraints, such as feeder current ratings and transformer apparent power ratings. These component constraints should not be exceeded, in order not to damage the grid components. The grid operators are responsible for keeping the system parameters within their margins, and the manufacturers of electric appliances are responsible for making their products work appropriately and safely within these margins.

Current harmonics are not further discussed here, because there are standards to which PEV chargers have to comply in terms of the harmonic contamination in the currents they draw. If these standards would be insufficient, they need to become stricter. This kind of analysis is out of scope here, as this is related to the design and control aspects of power electronic interfaces in general, not specifically to PEV chargers [71]. The same counts for voltage flicker, which is typically related to the startup and shutdown of large loads with high inrush currents, such as large electric motors. For power electronic interfaces, this can be mitigated through the control of the startup and shutdown process [71].

2.4.3.1 Voltage magnitude constraints

The voltage magnitude should stay within a specified range around the rated value, to ensure that electric appliances can be operated in a safe and satisfactory manner [70], [72]. The supply voltage characteristics in Europe are standardized as described in the EN50160 standard [73]. The standard specifies that the 10 min mean rms voltage magnitude deviation at each phase ph of each grid connection node i should not exceed ±10 %, measured on a weekly base [73]. For undervoltage, a wider range is allowed in the measurement procedure: -15 % to -10 % for 5 % of time:

$$0.9 \cdot U^{\text{rat}} \leq \left|U_{ph,i}\right| \leq 1.1 \cdot U^{\text{rat}};$$
$$\text{for} > 95\ \%\ \text{of all 10 min intervals of any week;} \tag{2.1}$$

$$0.85 \cdot U^{\text{rat}} \leq \left|U_{ph,i}\right| \leq 1.1 \cdot U^{\text{rat}}. \tag{2.2}$$

U^{rat} and $\left|U_{ph,i}\right|$ are the rated voltage magnitude and the voltage rms magnitude at phase ph and grid connection node i, respectively. Thus, in the planning and design phase, the goal is to keep the grid voltage magnitude deviations within the 10 % range.

Because voltage variations occur throughout the entire supply system, a fraction of the 20 % voltage deviation range (+10 %/-10 %) is assigned to each of the voltage levels, which is illustrated in Figure 2.15 for Flanders. The distribution of the voltage deviation margins is as follows in Flanders: 4 % for HV (+2 %/-2 %), 6.5 % for MV (+1.5 %/-5 %), 7.5 % for LV (+1.5 %/-6 %), and 2 % for voltage unbalances (+1 %/-1 %) [74]. The asymmetric assignment of the voltage deviations (+6 %/-14 % in total) is corrected through the off-line transformer tap settings.

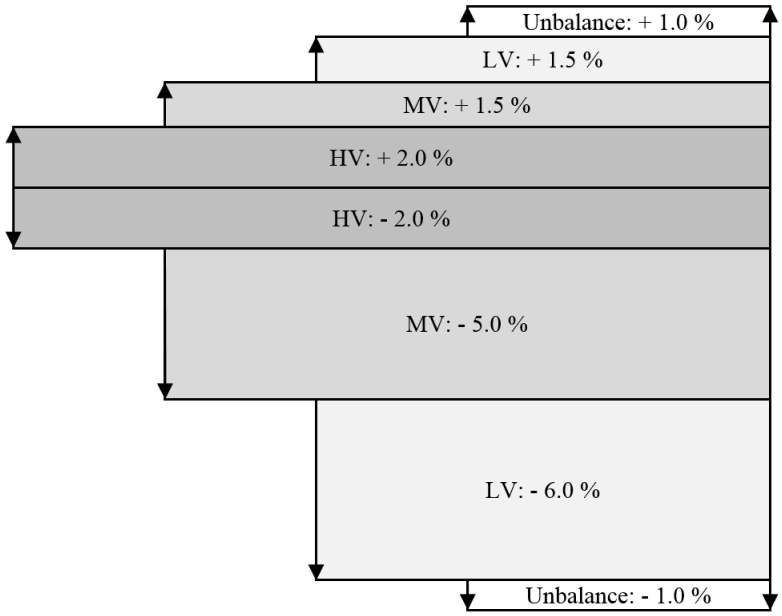

Figure 2.15: Distribution of the voltage deviation margins across the different levels of the power system, for Flanders.

2.4.3.2 Voltage unbalance constraints

The uneven distribution of single-phase loads [75] and asymmetric conductor configurations [70] lead to unequal voltage drops in the different phases of the distribution grid. In European standards, the voltage unbalance factor F_i^{VU}, for grid connection node i, is defined as follows:

$$F_i^{\mathrm{VU}} = |U_i^N / U_i^P|. \tag{2.3}$$

U_i^P and U_i^N are the positive and negative sequence voltages at grid connection node i, respectively. Due to the presence of many varying single-phase loads, a certain degree of voltage unbalance is unavoidable in residential distribution grids. However, an excessively high F_i^{VU} value negatively impacts the power system, as well as three-phase electric and electronic end-user appliances [70]. Therefore, the EN50160 standard specifies that the 10 min mean rms value of F_i^{VU} should be below 2 % for 95 % of time, measured on a weekly base [73]:

$$F_i^{\mathrm{VU}} \leq 2\ \%; \quad \text{for} > 95\ \%\ \text{of all 10 min intervals of any week.} \tag{2.4}$$

The transmission system operator (TSO) is responsible to keep the HV voltage level within the limits, and the DSO is responsible for the MV/LV voltage constraints. If the voltage magnitude or unbalance constraints are exceeded, the TSO or DSO will have to find solutions to reduce the voltage deviations. For instance, feeders will (partially) be upgraded to a larger cross section. Voltage constraints are hard real-time constraints, as they have to be met at all times, to guarantee a safe and satisfactory operation of the electrical equipment that is grid-connected.

2.4.3.3 Load ratings and grid losses

Grid components, such as feeders and transformers, have a load rating that is typically defined as an apparent power rating or current rating. If the load rating of these components is exceeded, accelerated ageing occurs, which reduces their technical lifetime [76]-[77]. This might increase the exploitation costs of the distribution system, when the technical lifetime of the system assets is reduced below the economic and strategic lifetime [76], because the grid components have to be replaced earlier than initially planned. Therefore, to a certain extent, such ratings are not hard real-time constraints, but represent an additional cost, because the component has to be replaced sooner than initially planned. This cost should be taken into account, but does not require immediate action if the accelerated ageing remains limited.

Grid losses also represent a cost to the power system, and this cost is typically recovered through the grid fees. This may create the need for grid infrastructure upgrades if this cost becomes excessively high. However, no immediate action is required when grid losses increase, as this does not directly influence the quality of service. Therefore, to some extent, load ratings and grid losses can both be considered as cost-increasing parameters, of which the cost has to be compared to the cost of a grid infrastructure upgrade, and to the increased grid operator revenues due to an increased amount of energy being delivered to end users.

For example, the increased grid load due to PEV charging could increase grid losses and cause a periodical overloading of the MV/LV transformers [22]. As long as the increase in costs can be recovered through the increased amount of grid operator revenues, it might not be necessary to invest in grid infrastructure upgrades. A slight periodical overloading of certain grid components might be compensated for by a significant increase of the amount of delivered energy, thereby increasing the profitability of the infrastructure [78].

2.5 Conclusions on PEV charging

The distribution grid operation envelopes are taken into account by DSOs in their asset planning. Load flow analyses are conducted, with a significant margin to take into account the future load increases [70]. The assumptions and predictions of the local loads are often based on historical data. In this sense, distribution system planning is a feed-forward strategy without feedback on the operational level. It is important to emphasize that the grid constraints must be met, not exceeded [70], as this will only increase the cost of the power system due to increased infrastructure investments.

As long as the grid operates within its constraints, the distribution system is operating in its normal state [79]. At normal operating state, the energy delivery should not be interrupted for grid supporting purposes, as this only leads to a decrease in the end-user comfort. However, once the system state changes from normal to disturbed, actions must take place to avoid that the grid state goes from disturbed to critical, which could result in an interruption of power delivery [79]. This is considered as being very undesirable, because this interferes with the end-user power consumption. If these interruptions occur more often than is considered reasonable, extra grid investments are required [80].

There is an increasing interest in using the flexibility of residential loads, triggered by the introduction of electronic control in household devices, such as white goods [81], and new residential loads with a significant flexibility potential, such as PEVs and residential heat pumps [82]. By using the flexibility of these devices when the grid is in the disturbed state, stabilizing actions can be performed, without affecting the end-user comfort [83]. For example, residential PEV charging may be shifted away from the evening demand peak to the valley at night. Alternatively, instead of merely shifting the charging process in time, the charging power rating may be altered. For example, the PEV charging power rating could be reduced when undervoltage is encountered, as a way to reduce the voltage drop.

The degree of charging flexibility depends on several parameters: mobility behavior, vehicle power consumption, charging locations, charging power rating, and PEV battery capacity. The assessment of the PEV charging flexibility is discussed in Chapter 3, followed by an overview of coordination strategies for PEV charging in Chapter 4. Both the active and reactive power flows can be altered during PEV charging, as a way to mitigate the grid impact. Active and reactive power control are discussed in Chapter 5 and 6, respectively.

3. Vehicle and fleet modeling

In order to have an accurate assessment for the impact of PEVs in Flanders, data of the Flemish fleet have been used to model a representative Flemish vehicle fleet. Different vehicle categories have been taken into account, according to their distribution in Flanders, because this has a significant impact on the required energy and potential charging flexibility.

The mobility behavior of a Flemish fleet is modeled in Section 3.1. The fleet segmentation is discussed in Section 3.2. The energy efficiency of the vehicles is modeled in Section 3.3. The resulting fleet power consumption, for different scenarios, is discussed in Section 3.4. The conclusions are summarized in Section 3.5.

3.1 Mobility behavior

The mobility behavior of a fleet of vehicles is modeled by the availability model, which is explained in detail in Appendix A. This model is mainly based upon the 3rd Flemish Mobility Study [84]. For each vehicle, it is known when it is driving, standing still, and also where it is standing still: at home, at the workplace, or at another location. The model can be run for any number of vehicles and days, on a one-minute time resolution. The contents of this section and Appendix B are discussed in detail in the Ph.D. dissertation:

- J. Van Roy, "Electric vehicle charging integration in buildings," Ph.D. dissertation, ESAT, KU Leuven, Leuven, Belgium, 2015.

3.1.1 Mobility modeling

The mobility model takes into account the difference between week and weekend days: 3.6 versus 2.85 trips per vehicle per day [84]-[85]. Furthermore, the difference in trip durations of each motive is taken into account, as some motifs have longer/shorter trip distances than the average trip. For instance, shopping trips are on average shorter than other trips. Seasonal variations are not taken into account, because for Flanders, no useful data is available on such variations. Intraweek variations, except for the difference between week days and weekend days, are not taken into account, as the differences are only small.

Commute trips are treated separately from other trips, since the priority of the former is assumed to be the highest. The distribution of the fraction of people as a function of the distance to the workplace is taken into account. The distance to work is fixed

vehicle-by-vehicle. Similar to the distance to work and the work shift, the departure and return hour are fixed. This is an acceptable assumption, since about 82 % of the population has fixed working hours [84]. However, to introduce some variation between the different days, a uniform probability distribution function is used to determine the exact minute of departure and return within the one-hour period for each day.

The commute trips are scheduled first, after which the characteristics of the other trips are defined. Only business trips may overlap with commute trips and the presence at work. The other trips are divided in two categories, one with a variable activity duration (business, education, and recreational trips) and one with a fixed activity duration (visits, shopping, and other trips). For the variable activity duration motifs, a distribution function for the departure and return times is used [84]. For the fixed duration motifs, only the distribution function for the departure times is used.

3.1.2 Fleet mobility behavior

To illustrate the resulting mobility behavior, Figure 3.1 shows the fraction of vehicles on the road for commute trips and other trips, for (a) weekdays, and (b) weekend days. Two fleets of 100 vehicles for a one-year period are shown: one where no vehicles are used for work (w^0), and one where all vehicles are used for work (w^{100}). They are shown separately, as both fleets have a significantly different mobility behavior. A fleet of 100 vehicles was created, because a sufficient level of aggregation is already obtained, while the computational efforts remain limited. As explained in Appendix A, 36 - 47 % of the Flemish vehicle fleet is used for work. Therefore, the mobility behavior model will create a fleet with the appropriate fraction of these two groups of vehicles.

Figure 3.1 illustrates that on average more vehicles are on the road during the week compared to the weekend since there are on average more trips per day during the week. However, on average less than 10 % of the fleet is on the road simultaneously, which is in line with the results in [86]. There is a clear morning and evening peak during the week, due to commuting, since most of the people work in normal day shifts and part-time shifts.

Figure 3.2 shows how many vehicles are at home, at work and at other locations, during (a) weekdays, and (b) weekend days. The other locations include the presence at another activity, and driving to the activity or to work and back. On average, a minimum of 15 % of the fleet is at home during a weekday and about 35 % in the weekend. The amount of vehicles at home is at its maximum during the night, with

more than 95 % parked at home. During the evening and night, only a few vehicles are parked at work.

For these two groups, the average daily driven distance is 32.2 km (w^0) and 39.0 km (w^{100}), respectively. The cumulative distribution of the daily driven distances for the two groups of vehicles is illustrated in Figure 3.3. This shows that for both groups:

- > 90 % of the daily driven distances is below 80 km;
- > 95 % of the daily driven distances is below 110 km;
- > 99 % of the daily driven distances is below 175 km.

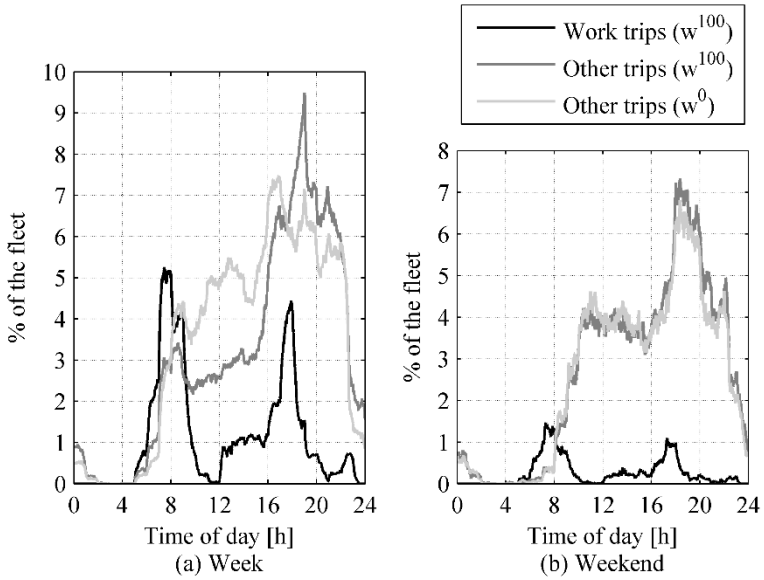

Figure 3.1: The average number of vehicles (as % of the fleet) on the road for work and other trips is higher during week days (a) than during weekend days (b).

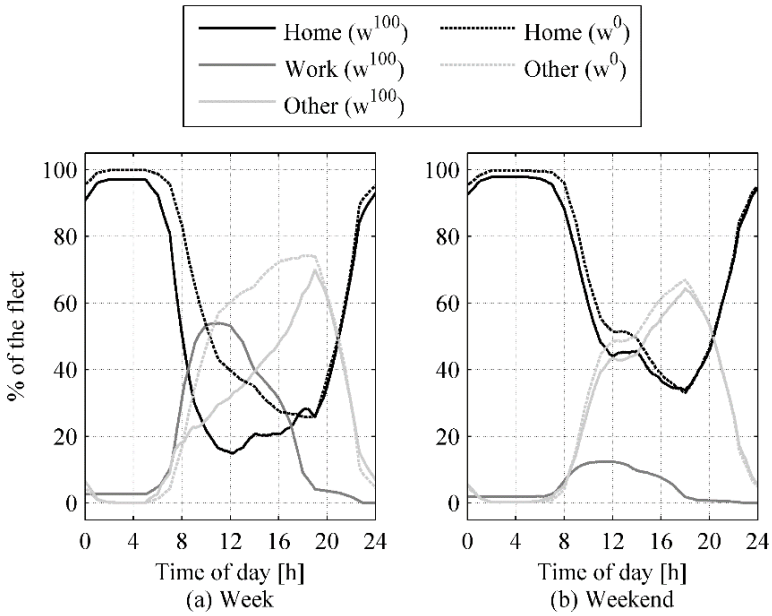

Figure 3.2: Average fraction of the fleet at home, at work, or at another location during week days (a), and weekend days (b).

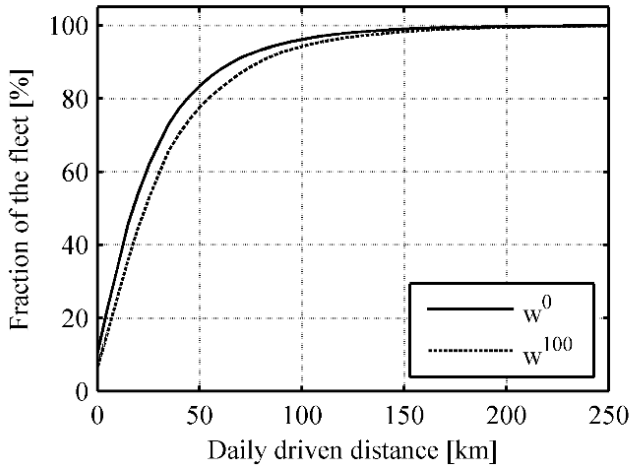

Figure 3.3: Cumulative distribution of the daily driven distances.

For the majority of the daily mobility requirements, the electric driving range of the currently available PEVs is sufficient [84], even if there is only an opportunity to charge overnight at home. In order to cover all mobility requirements, a substantially larger driving range would be needed, which would only be rarely utilized. However, there are other possibilities to fulfill the mobility requirements during the occasional days with a higher driven distance:

- using an on-board range extender if the vehicle is equipped with it;
- using low to medium power charging infrastructure (≤ 20 kW) at other locations where the vehicle is standing still for a sufficiently long time;
- using fast charging infrastructure (> 20 kW) for the occasional long distance trips that exceed the vehicle range.

The resulting impact of the mobility behavior on the electricity system is determined by the energy efficiency and the composition of the vehicle fleet, which will be discussed in the following sections.

3.2 Fleet segmentation

On average, the annual vehicle kilometers traveled are about 15,000 km in Belgium, which has been stable for the last decade, as illustrated in Figure 3.4 [87]. However, there is a large difference in the annual driven distances between the vehicle segments in the current vehicle fleet. For instance in 2010, gasoline cars drive on average 8,545 km per year, versus 19,340 km for diesel cars [85], [87]. In Belgium, the share of diesel vehicles is relatively high (60 %). The small fraction of liquefied petroleum gas (LPG, less than 1%) is neglected [85], [87]-[88].

To take into account the heterogeneity of mobility behavior, the modeled fleet is divided into segments, based upon the present vehicle characteristics. This does not necessarily mean that a future fleet will use the same fuels, but it is assumed that mobility behavior will remain the same. This assumption has been made here, because the scope of the proposed control mechanisms for PEV charging is the near-term future (less than 10 years), and it is assumed that mobility behavior will not change drastically in this time frame.

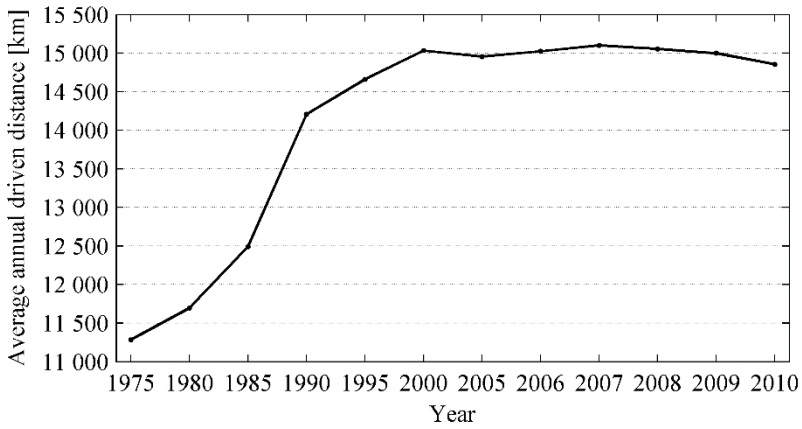

Figure 3.4: Annual vehicle kilometers traveled in Belgium by Belgian vehicles.

Table 3.1 gives the distribution of the vehicles according to the fuel type and engine displacement [88]. Small engine displacements are typically found in gasoline cars. Table 3.1 also shows the average yearly distance traveled by each vehicle, based upon the following data:

- the average number of kilometers driven as a function of the vehicle age and fuel, for each year in the period 2002–2009 [87];
- the age of the vehicles in the fleet and the number of vehicles [87].

This results in a yearly average of about 15,000 km per vehicle in the fleet, which is consistent with [84], where a sample of 8,800 people resulted in an average 15,900 km per year, and [88], where 15,000 km per year was estimated.

Table 3.1: Segmentation of the vehicles according to the engine displacement.

Engine displacement	**Fleet distribution [%]**		**Average annual driven distance [km]**	
	Gasoline	**Diesel**	**Gasoline**	**Diesel**
<1.4 l	22.64	4.86	7,960	18,045
1.4-2.0 l	14.36	44.40	9,095	19,565
>2.0 l	3.00	10.74	10,335	18,955
Total	40.00	60.00	8,545	19,340

Three vehicle categories are used to differentiate between compact, midsize and large vehicles. It is assumed that the three vehicle types coincide with the engine displacement categories, facilitating the link between the availability and efficiency model. For each vehicle category, two representative vehicles are taken, as illustrated in Figure 3.5:

- subcompact: 1) Mitsubishi i-MiEV [89], and 2) Smart ED [90];
- midsize: 3) Nissan Leaf [26], and 4) Chevrolet Volt [39];
- large: 5) Toyota RAV4 EV [91], and 6) eRuf Cayenne [92].

Figure 3.5: The six modeled PEVs.

The vehicle-specific characteristics (mass m, frontal surface S, and drag coefficient C_x) of these vehicles are listed in Table 3.2, which are available from the manufacturer's specification sheets. The other parameters, which are assumed equal for all vehicles, as will be discussed in Section 0.

Table 3.2: Characteristics of the six modeled PEVs.

Vehicle model		Mass [kg]	Frontal surface [m^2]	C_x [-]
Subcompact	Mitsubishi i-MiEV	1,100	2.37	0.33
	Smart ED	975	2.40	0.35
Midsize	Nissan Leaf	1,521	2.70	0.28
	Chevrolet Volt	1,800	2.55	0.28
Large	Toyota RAV4 EV	2,000	3.10	0.33
	eRUF Cayenne	2,670	3.30	0.36

3.3 Energy efficiency modeling

The specific power consumption (kWh/km) of PEVs is an important parameter to calculate the evolution of the SOC of the PEV batteries. Here, this parameter is calculated for the three vehicle categories, for different driving cycles. The calculations are based on the battery model discussed in [93].

3.3.1 Calculations

The power consumption is calculated with physical parameters of the vehicles as discussed in Section 3.2, and depends on the drive cycle (urban, rural, highway, or mixed). Because these parameters have a significant impact on the power consumption, they are to be defined accurately. The propulsion power P_k^p $[W]$ at each time step k (one second) is calculated from the resulting forces on the vehicle: the air resistance F_k^a, rolling resistance F_k^r, inertia F_k^i, and slope resistance F_k^s $[N]$:

$$F_k^a = (S \cdot C_x \cdot \rho \cdot {v_k}^2)/2 \; ; \tag{3.1}$$

$$F_k^r = \; m.g.f_r.\cos(\alpha) \; ; \tag{3.2}$$

$$F_k^i = m.a_k \; ; \tag{3.3}$$

$$F_k^s = m.g.\sin(\alpha) \; ; \tag{3.4}$$

$$P_k^p = \left(F_k^a + F_k^r + F_k^i + F_k^s\right).v_k \; ; \tag{3.5}$$

with:

- S the frontale surface of the vehicle $[m^2]$;
- C_x the coefficient of drag [-];
- ρ the volumetric density of the air $[kg/m^3]$;
- v_k the vehicle speed at time step k $[m/s]$;
- m the vehicle mass $[kg]$;
- g the gravity constant $[9.81 \; m/s^2]$;
- f_r the rolling resistance coefficient [-];
- α the slope of the road $[rad]$;
- a_k the acceleration of the vehicle at time step k $[m/s^2]$.

A positive value for P_k^p means that power is consumed to propel the vehicle ($P_{\text{out},k}^{\text{bat}} > 0$). For negative values, the battery will be recharged $\left(P_{\text{in},k}^{\text{bat}} > 0\right)$. A battery has a maximum charging rate $\left(P_{ch,\max}^{\text{bat}}\right)$ and the fraction of recuperation of braking energy (e^{rec}) is limited, since a part of the braking occurs mechanically (see Section 0). The following efficiencies (see Section 0) are taken into account: charging (η^{in}) and discharging (η^{out}) efficiencies of the power electronics, the battery charging $\left(\eta_{ch}^{\text{bat}}\right)$ and discharging$\left(\eta_{d}^{\text{bat}}\right)$ efficiencies and the efficiency of the electric motor in motor (η^m) and generator mode (η^g). Using these parameters, the power flow from/to the battery can be calculated as follows:

$$P_{\text{out},k}^{\text{bat}} = P_k^p / \eta^m \; ; \tag{3.6}$$

$$P_{\text{in},k}^{\text{bat}} = min\left(\left(e^{\text{rec}}.\left|P_k^p\right|.\eta^g\right), P_{ch,\max}^{\text{bat}}\right). \tag{3.7}$$

In the next step, the energy flows during the time interval ΔT are calculated: the charging energy $\left(E_{ch,k}^{\text{bat}}\right)$, the discharging energy $\left(E_{d,k}^{\text{bat}}\right)$, and the net energy flow from/to the battery $\left(\Delta E_k^{\text{bat}}\right)$. The auxiliary power consumption (P^{aux}) is also taken into account:

$$E_{d,k}^{bat} = \Delta T.\left(P_{\text{out},k}^{\text{bat}} + P^{\text{aux}}\right)/\eta^{\text{out}} \; ; \tag{3.8}$$

$$E_{ch,k}^{\text{bat}} = \Delta T.P_{\text{in},k}^{\text{bat}}.\eta^{\text{in}} \; ; \tag{3.9}$$

$$\Delta E_k^{\text{bat}} = \left(E_{ch,k}^{\text{bat}}.\eta_{ch}^{\text{bat}}\right) - \left(E_{d,k}^{\text{bat}}/\eta_{d}^{\text{bat}}\right). \tag{3.10}$$

The state of charge (SOC_k) of the battery can be updated with ΔE_k^{bat}, including the battery self-discharge losses (δ^{sd}). Each vehicle has a certain rated battery capacity ($E_{\text{rat}}^{\text{bat}}$):

$$SOC_k = SOC_{k-1} - \delta^{\text{sd}} + \left(\Delta E_k^{\text{bat}}/E_{\text{rat}}^{\text{bat}}\right); \tag{3.11}$$

$$\Delta E_{\text{cycle}}^{\text{bat}} = E_{\text{end}}^{\text{bat}} - E_{\text{start}}^{\text{bat}}. \tag{3.12}$$

The power consumption of the total driving cycle, as will be discussed in Section 3.3.3, is denoted as $\Delta E_{\text{cycle}}^{\text{bat}}$, which is the difference between the battery energy content at the beginning $\left(E_{\text{start}}^{\text{bat}}\right)$ and the end $\left(E_{\text{end}}^{\text{bat}}\right)$ of the driving cycle. By dividing this power consumption by the cycle distance (d^{cycle}) and taking into account the charging efficiency, the specific power consumption (E^{spec}) is calculated. Also, the

electric range (d^{range}) of the vehicle can be calculated. This range depends on the energy efficiency of the vehicle and the effectively usable battery capacity $\left(E_{\text{eff}}^{\text{bat}}\right)$:

$$E^{\text{spec}} = \Delta E_{\text{cycle}}^{\text{bat}} / \left(d^{\text{cycle}} \cdot \eta^{\text{in}} \cdot \eta_{ch}^{\text{bat}}\right); \tag{3.13}$$

$$d^{\text{range}} = d^{\text{cycle}} \cdot \left(E_{\text{eff}}^{\text{bat}} / \Delta E_{\text{cycle}}^{\text{bat}}\right). \tag{3.14}$$

A schematic overview of the power flows from and to the PEV battery is illustrated in Figure 3.6.

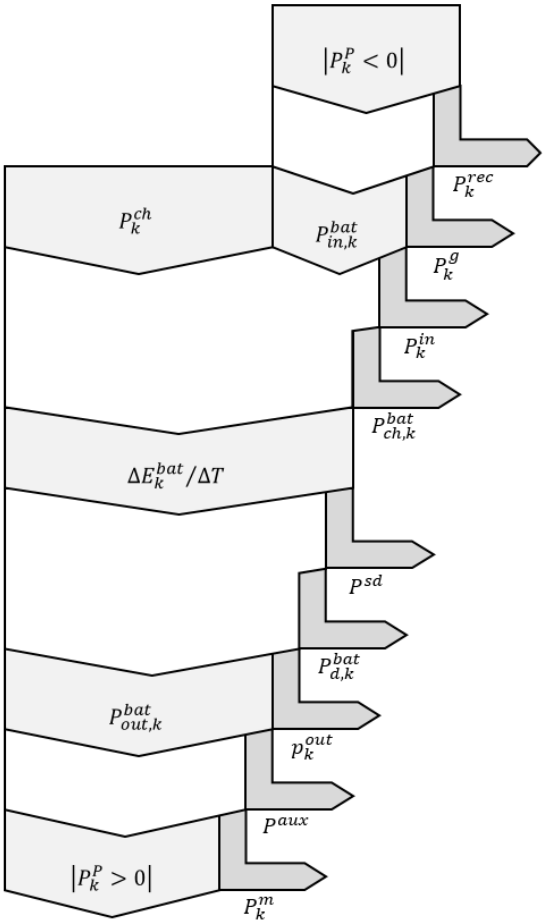

Figure 3.6: Schematic overview of the power flow from and to the PEV battery.

The battery can be charged through the grid $\left(P_k^{ch}\right)$, or through regenerative braking when the PEV is decelerating $\left(P_k^p < 0\right)$. Not all power will flow into the battery, as losses occur due to e^{rec} $\left(P_k^{rec}\right)$, η^g $\left(P_k^g\right)$, η^{in} $\left(P_k^{in}\right)$, and η_{ch}^{bat} $\left(P_{ch,k}^{bat}\right)$. Besides the propulsion power $\left(P_k^p > 0\right)$, the battery also has to supply P^{aux}. Furthermore, there are losses induced by η^m $\left(P_k^m\right)$, η^{out} $\left(P_k^{out}\right)$, η_d^{bat} $\left(P_{d,k}^{bat}\right)$, and δ^{sd} $\left(P_k^{sd}\right)$.

3.3.2 General parameters

As discussed in Section 3.2, three vehicle types are used to differentiate between subcompact, midsize, and large vehicles. The fixed parameters (Table 3.3) are discussed here.

Table 3.3: General parameters for efficiency calculation.

f_r	e^{rec}	η^{in}	η^{out}	η_{ch}^{bat}	η_d^{bat}	η^m	η^g	P^{aux}	α
0.01	90 %	95 %	95 %	95 %	95 %	90 %	90 %	500 W	0 rad

The rolling resistance of a vehicle depends on the rolling resistance coefficient factor f_r. This coefficient is not readily available in vehicle specification sheets, since it depends on the type of tire. In [94], measurement results on the rolling resistance coefficient (RRC) are presented and illustrated in Figure 3.7. Here, value of 0.01 is used for f_r, which is a typical value for modern tires with low rolling resistance.

The kinetic energy recuperation factor e^{rec} defines the amount of kinetic energy that can be recuperated during regenerative braking. This factor includes the fraction of mechanical braking, friction in bearings, etc. Efficiencies of the electric elements are not included, as they are treated separately. As no specific data on e^{rec} is available, a value of 90 % is chosen. According to [95], the overall recovery rate is in the range of 50 - 60 %. With a value of 90 % for e^{rec}, an average overall recovery rate is found in this range, due to the other losses as summarized in Table 3.3.

The efficiencies of the power electronics (η^{in} and η^{out}) and the batteries (η_{ch}^{bat} and η_d^{bat}) are based upon [93] and listed in Table 3.3. The efficiency of the electric motor is set to 90 % in both motor and generator mode ($\eta^m$and η^g). Besides the propulsion power requirements, different auxiliary loads require electrical power (P^{aux}), which have a significant impact on the specific power consumption. These loads include lights, entertainment and navigation systems, air conditioning, etc. According to [96], P^{aux} amounts to 500 W for HEVs, which is also used here for PEVs.

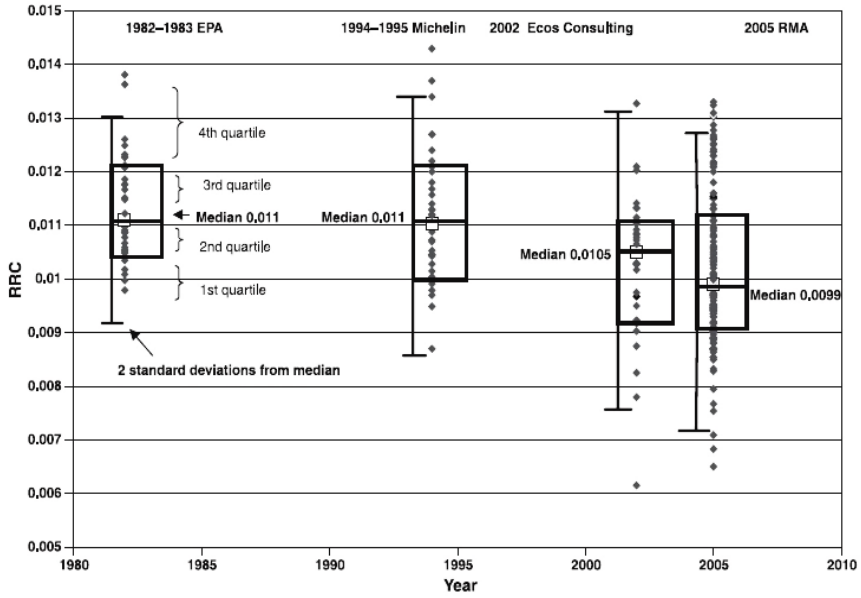

Figure 3.7: Rolling resistance coefficient (RRC) for passenger vehicle tires [94].

3.3.3 Driving cycle

A representative driving cycle is composed using the following American test cycles (Figure 3.8). These cycles are preferred instead of the artificial European cycles for emission testing, since they are based on real traffic behavior [97]:

- the New York City Cycle (NYCC) represents traffic in a dense **urban** area with low average speed (11.42 km/h) and lots of stop and-go traffic;
- the Federal Test Procedure (FTP) represents **rural** traffic with a significant share of high-speed driving (average speed of 34.11 km/h);
- the Highway Fuel Economy Driving Schedule (HWFET) represents **highway** driving with no stops (average speed of 104.94 km/h).

In the European Transient Cycle (ETC) , a weighted sum of the three drive cycles made in which the three cycles occupy the same amount of time (Figure 3.9) [98]. However, real measurements from Flanders can be used for more realistic Flemish driving behavior, where a lower fraction of highway driving occurs. The distribution of driven distances for each cycle type is as follows: 23.7 %, 39.8 %, and 36.5 %, for urban, rural, and highway traffic, respectively [99].

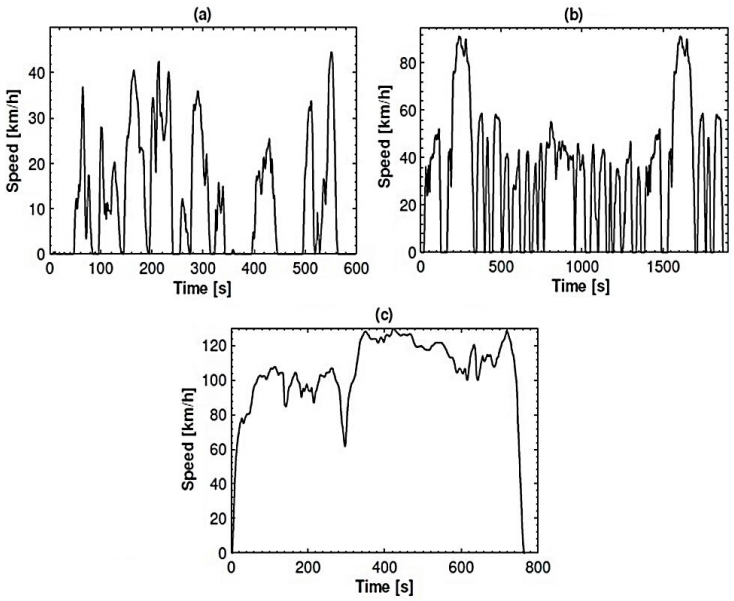

Figure 3.8: Urban (a), rural (b) and highway (c) driving cycle [97].

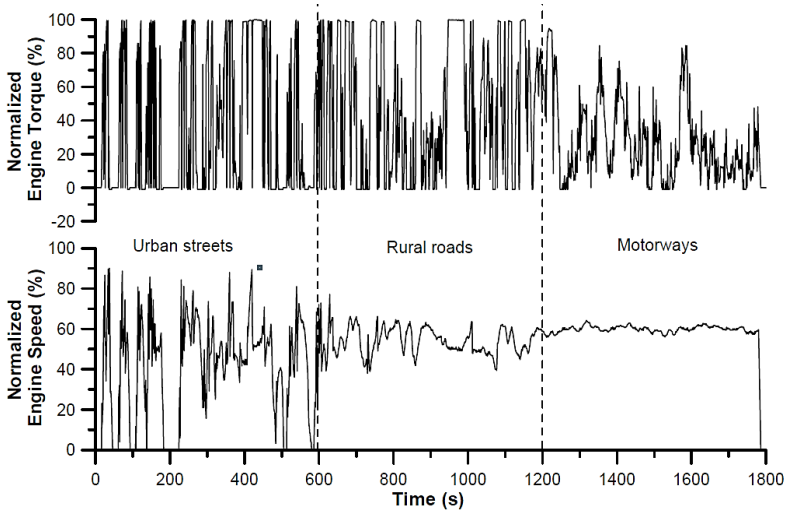

Figure 3.9: Setup of the European Transient Cycle [98].

3.3.4 Results

The power consumption of different vehicles and vehicle categories while driving is discussed in this section, using the general parameters (Table 3.3). Table 3.4 summarizes the base results for the specific power consumption. The consumption for all vehicles, and the average for each of the three vehicle categories is given. The results are shown for each separate driving cycle and the weighted combination of these cycles (Section 3.3.3).

Table 3.4: Specific power consumption for the six modeled PEVs.

	Drive cycle	NYCC	FTP	HWFET	ETC	Flanders	
Vehicle model	Mitsubishi i-MiEV	0.145	0.131	0.233	0.203	0.171	$\left[\frac{\mathbf{kWh}}{\mathbf{km}}\right]$
	Smart ED	0.136	0.126	0.240	0.206	0.170	
	Subcompact avg.	**0.141**	**0.128**	**0.236**	**0.204**	**0.171**	
	Nissan Leaf	0.179	0.152	0.230	0.208	0.187	
	Chevrolet Volt	0.203	0.173	0.252	0.230	0.209	
	Midsize avg.	**0.191**	**0.162**	**0.241**	**0.219**	**0.198**	
	Toyota RAV4 EV	0.222	0.203	0.330	0.293	0.254	
	eRUF Cayenne	0.280	0.256	0.400	0.358	0.314	
	Large avg.	**0.251**	**0.229**	**0.365**	**0.326**	**0.284**	

The results of the Flemish cycle composition is used in further simulations, since they are based on realistic behavior in Flanders. They result in 15 % less power consumption compared with the ETC-based composition. This is due to the lower amount of highway driving in the Flemish composition, which has a significantly higher specific power consumption for PEVs compared to the urban and rural drive cycles. Conversely, the lower share of highway driving would lead to a higher fuel consumption for conventional vehicles, as an ICE is the least efficient in low-speed stop-and-go traffic. The efficiencies for charging the battery are included in the results, to obtain the so-called AC power consumption.

Significant differences can be observed between the different vehicle categories. Larger vehicles, with a higher mass and larger frontal surface, consume considerably more energy: the least efficient vehicle uses approximately 75 % more energy, when driving according to the Flemish behavior, compared to the most efficient one.

3.3.5 Sensitivity analysis

The power consumption of PEVs is determined by different parameters (Section 3.3.1). A sensitivity analysis is performed for the general parameters for which an assumption has been made (Table 3.2). In the following subsections, the sensitivity of the specific power consumption to the mass m of the vehicle, the auxiliary load P^{aux}, the slope of the road α, the rolling resistance coefficient f_r and the amount of kinetic energy recuperation e^{rec}, respectively, is discussed.

3.3.5.1 Mass of the vehicle

The impact of the total vehicle mass m, including the load, on the specific power consumption is quasi linear and the relative impact is less for heavier vehicles (Table 3.5). Without taking the losses (η^m, η^g, η_{ch}^{bat}, η_d^{bat}, η^{in}, η^{out}) into account, this impact is sub-linear, because the air resistance is not mass dependent.

Table 3.5: Increase in specific power consumption for a change in vehicle mass.

Mass increase [kg]		**-200**	**-100**	**+100**	**+200**	
Vehicle category	**Subcompact**	-8.2	-4.1	+4.2	+8.5	**[%]**
	Midsize	-7.2	-3.6	+3.7	+7.4	
	Large	-5.0	-2.5	+2.5	+5.1	

3.3.5.2 Auxiliary load

The auxiliary loads P^{aux} are responsible for an increase in electric power consumption, depending on the drive cycle. The impact of the auxiliary loads are more significant for drive cycles with a lower average speed, since more energy is consumed for a given distance. The specific increase in power consumption is given in Table 3.6 for the different drive cycles. The values are given as an extra consumption per kilometer [kWh/km] for each kW of auxiliary loads.

There is a linear increase with the amount of installed auxiliary loads. The increase of the power consumption for the NYCC (urban cycle) is considerably larger. Neglecting this consumption would thus lead to an unrealistically low total power consumption. As a result, the incorporation of the auxiliary loads reduces the differences in power consumption between the drive cycles. The increase is equal for each of the three vehicle categories, as there is no influence of the vehicle parameters on the resulting power consumption due to the auxiliary loads.

Table 3.6: Increase in specific power consumption per unit of auxiliary load.

NYCC	FTP	HWFET	ETC	Flanders	
0.105	0.035	0.011	0.024	0.043	**[kWh/km] per [kW]**

3.3.5.3 Slope of the road

Realistic driving results in an average slope α of 0°. The slope of the road is an important parameter, because the required power depends on the increase and decrease of gravitational potential energy. The impact on the power consumption is investigated by applying a fixed slope on a drive cycle, for both positive and negative values and averaging the two result. The results for different road slopes are given in Table 3.7.

Table 3.7: Increase in specific power consumption for different road slopes.

Road slope [°]		**±1**	**±2**	**±3**	**±4**	**±5**	
Vehicle category	**Subcompact**	0.8	3.7	8.9	17.4	30.1	
	Midsize	1.5	6.9	17.8	33.8	54.0	**[%]**
	Large	1.4	6.2	15.0	28.5	47.2	

The results indicate a significant impact, which cannot be neglected when evaluating the power consumption. Because the extra power requirement for a slope is proportional to vehicle mass, the impact increases for heavier vehicles. However, the relative increase in power consumption is lower for large vehicles compared to midsize vehicles, as the heavier vehicles may have an advantage on the downhill sections.

3.3.5.4 Rolling resistance

The sensitivity on the power consumption is assessed for 50 % and 200 % of the reference value of the rolling resistance f_r. The resulting impact, as summarized in Table 3.8, is higher for heavier vehicles, because of the linear relationship between the vehicle mass and the required power to overcome friction. The results show the impact of the effective rolling resistance, which depends on the tire conditions (tire pressure, tire wear, etc.), on the power consumption.

Table 3.8: Impact of the rolling resistance coefficient on the specific power consumption.

f_r compared to	the reference value [%]	50	200	
Vehicle category	**Subcompact**	-10.8	+20.4	
	Midsize	-13.6	+27.5	**[%]**
	Large	-14.9	+29.7	

3.3.5.5 Kinetic energy recuperation

In the base case, there is 90 % kinetic energy recuperation e^{rec} during braking. In Table 3.9, the sensitivity of the specific power consumption is summarized for $e^{rec} = 0, 50, 100$ %. The results indicate a higher sensitivity for heavier vehicles, because more kinetic energy is lost. The increase in power consumption between 0 and 100 % recovery rate varies between 15 and 22 % for the different segments.

Table 3.9: Impact of the kinetic energy recuperation on the specific power consumption, compared to the 90 % value in the reference scenario.

e^{rec} [%]		0	50	100	
Vehicle category	**Subcompact**	+13.4	+3.8	-1.3	
	Midsize	+17.6	+5.3	-1.1	**[%]**
	Large	+23.3	+8.4	-1.8	

3.3.5.6 Conclusions on the sensitivity analysis

The sensitivity analysis shows that there are many parameters that significantly influence the specific power consumption of the vehicles. However, these parameters also influence the power consumption of conventional vehicles. To include the influence of road grade, road surface (which influences the effective rolling resistance), etc., The United States Environmental Protection Agency (EPA) includes an increase of 15 % compared to the test results [100]. Therefore, the specific power consumption results of the base case of [101] are increased with 15 %, resulting in the following values:

- 201 Wh/km for subcompact vehicles;
- 233 Wh/km for midsize vehicles;
- 334 Wh/km for large vehicles.

As mentioned before, these values are so-called net AC values, which include the losses to recharge the PEV batteries again to their initial SOC. Therefore, when assessing the evolution of the SOC of the PEVs during driving, these numbers are corrected to 181, 210, and 301 Wh/km, respectively. The charging energy losses are taken into account during the recharging process.

3.4 Fleet power consumption

The mobility behavior and specific power consumption determine the power consumption behavior of the PEVs. The results of this section are based on the book chapter:

- N. Leemput, J. Van Roy, F. Geth, J. Driesen, and S. De Breucker, *Data Science and Simulation in Transportation Research*, Hershey, PA: IGI Global, 2014, *ch. 17: Grid and fleet impact mapping of EV charge opportunities*, pp. 364-390.

3.4.1 Daily power consumption

The cumulative daily power consumption is illustrated in Figure 3.10, for two fleets of 100 PEVs (Section 3.1.2): one in which all vehicles are used for work trips (w^{100}), and one in which no vehicles are used for work trips (w^{0}). For the two groups, the average daily power consumption is 9.3 kWh and 7.4 kWh, respectively. The cumulative distribution in Figure 3.10 shows that, for both fleets:

- > 90 % of the daily fleet power consumption is below 18 kWh;
- > 95 % of the daily fleet power consumption is below 24 kWh;
- > 99 % of the daily fleet power consumption is below 40 kWh.

These results show that on average and for a majority of the days, the electric driving range of currently available PEVs is sufficient to cover the mobility needs. For the occasional days with a high power consumption, there are other possibilities (Section 3.1.2): using a range extender, making use of other charging opportunities besides at home, making use of fast charging infrastructure, or temporarily switch to another vehicle.

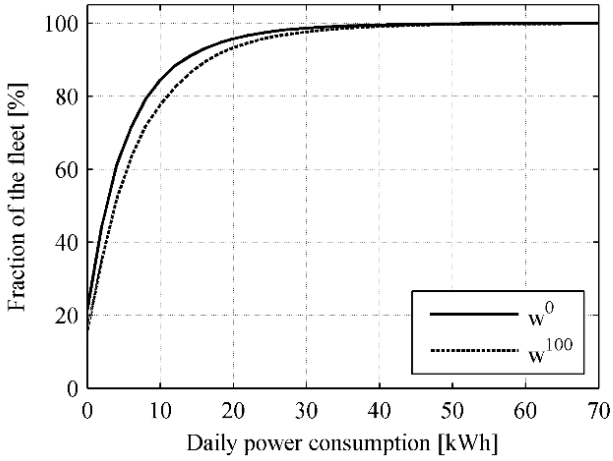

Figure 3.10: Cumulative distribution of the daily power consumption.

3.4.2 Grid impact parameters

The impact of the PEV power consumption on the electricity system is influenced by several factors. First, there is the battery capacity of the PEVs, as this determines which fraction of the driven distances can be covered on electric energy, given that there are no constraints on charging. These charging constraints are due to the charging power rating, and the charging opportunities. Therefore, these three parameters are used to construct different scenarios, to assess their on the behavior of the vehicle fleet.

3.4.2.1 Battery capacity scenarios

The PEVs are modeled as PHEVs here, to guarantee that all mobility requirements are met, even when the battery is depleted. They are assumed to be extended range EVs (EREVs), driving on battery power until depleted. Therefore, the combustion engine only runs when the battery is depleted. Three battery capacity scenarios are investigated, in which a rated battery capacity is assigned to each vehicle category:

- Battery scenario 1 (b^1) represents PEVs with a small battery capacity: 5, 7.5, and 10 kWh for subcompact, midsize, and large vehicles, respectively. Current PEVs which suit this battery scenario are the Toyota Prius PHV (4.4 kWh) [29] and the Ford C-Max Energi (7.6 kWh) [102].

- Battery scenario 2 (b^2) represents PEVs with a medium battery capacity: 10, 15, and 20 kWh. Current PEVs which suit this battery scenario are the 2014 Chevrolet Volt (16.5 kWh) [39] and the 2014 Cadillac ELR [103].
- Battery scenario 3 (b^3) is based on PEVs with a large battery capacity: 20, 30 and 40 kWh. Such values can be found in BEVs such as the Kia Soul EV (27 kWh) [52] and the Toyota RAV4 EV (42 kWh) [91].

The specific power consumption of the different segments remains as established in the efficiency model. This implies that the impact of the battery weight on the power consumption is not taken into account. The calculations in Section 3.3 make use of parameters for vehicles with relatively large battery capacities. Therefore, a rather conservative approach is used here, as the weight reduction for smaller battery capacities is not assessed. Here, it is assumed that only 80 % of the rated battery capacity is used, resulting in a DOD of 80 %, to preserve the battery lifetime [41].

3.4.2.2 Charging cases

Four different charging cases are evaluated in this chapter, with an increasing charging opportunity in each subsequent case c:

- only charging at home (c^1);
- charging at home and at the workplace (c^2);
- charging at home, at work and at 25 % of the other locations (c^3);
- charging at home, at work and at 50 % of the other locations (c^4).

For each of the four charge cases, charging is considered to occur without coordination. Thus, vehicles charge when they are grid connected, until the battery is completely recharged or until the next trip occurs. For standstill times shorter than 15´, it is assumed charging does not take place, because it is considered that PEV users won't do the effort to plug in the PEV for such a short time span.

The driving pattern for 100 PEVs is simulated with the discussed availability and efficiency model, for the duration of one year on a one-minute resolution. Furthermore, their energy requirements are calculated, based upon the efficiency model and the distribution of the vehicle segments in the Flemish fleet.

3.4.2.3 Charging power rating

Three charging power ratings are taken into consideration. First, Mode 2 charging with the typical European power rating of 2.1 kW is used (p^1). This corresponds to a single phase current rating of 10 A, which can safely be drawn from a power circuit with a 16 A circuit breaker rating (Section 2.3.4).

Second, Mode 3 charging with a power rating of 3.3 kW is used (p^2), as this is a typical power rating for single-phase PEV charging infrastructure. A single-phase charging power rating of 3.3 kW results in a current rating of 16 A which can easily be integrated within a single-phase household electric installation of 40 A, which is a typical rating in Flanders.

Third, Mode 3 charging with a power rating of 6.6 kW is used (p^3), which is the charging power rating of the on-board charger of several PEVs on the market, e.g., Nissan Leaf [26], Chevrolet Volt [39], and Kia Soul EV [52]. The medium power charging at 6.6 kW can either be realized with a single-current rating of 32 A, or a three-phase current rating of 11 A.

3.4.3 Results

3.4.3.1 Power consumption and utility factor

For the two fleets of vehicles, the average annual power consumption is 2,708 kWh/vehicle (w^0) and 3,380 kWh/vehicle (w^{100}), respectively. This power consumption is insensitive to the scenario, as the mobility behavior remains the same. This energy can be delivered through the PEV battery, or through the on-board range extender. The fraction of this energy being delivered by the PEV battery is defined as the utility function F^{U}. As a consequence, F^{U} also equals the ratio of the electrically driven distances to the total driven distances [7]. F^{U} gives an indication to which extent the mobility requirements can be covered on electric power. The results for the different scenarios are summarized in Table 3.10. For c^2 and w^0, no results are given, as this scenario is identical as for c^1 and w^0.

F^{U} depends strongly on the amount of charging opportunities. For b^1, F^{U} increases from 65 to 82 % for p^1, when the amount of charging opportunities increases. For c^4, the impact of increasing the charging power and the battery capacity on F^{U} is limited, as the high amount of charging opportunities already allows to fulfill a high fraction of the mobility requirements, even with small batteries and low charging power ratings. For b^2, F^{U} ranges between 84 and 94 % for c^1, which is up to 20 percentage points higher compared to b^1. The differences decrease significantly for the higher amount of charging opportunities, as the battery capacity remains the limiting factor. For b^3, the F^{U} is already 96 % for c^1, and therefore, the impact of the increase in charging power and charging opportunities on F^{U} remains low.

Table 3.10: Utility factor F^{U}.

Scenario		w^0			w^{100}			
		b^1	b^2	b^3	b^1	b^2	b^3	
c^1	p^1	67	87	97	64	84	96	[%]
	p^2	68	87	97	65	85	96	
	p^3	69	87	97	66	86	97	
c^2	p^1	/	/	/	70	87	97	
	p^2	/	/	/	71	88	97	
	p^3	/	/	/	71	88	97	
c^3	p^1	74	90	98	75	90	97	
	p^2	75	90	98	76	90	98	
	p^3	76	91	98	77	91	98	
c^4	p^1	80	92	98	79	92	98	
	p^2	81	93	98	80	92	98	
	p^3	82	94	99	82	93	98	

For $c^{\{1,2\}}$, the sensitivity of F^{U} to the charging power rating is insignificant, due to the relatively long standstill times of the vehicles at home and at work. For a low charging power rating, the charging is more spread out in time when the vehicle is standing still at these locations. Thus, the PEV user can decide whether or not the benefits (lower charging times) of charging infrastructure with a higher power rating outweigh the costs. A standard domestic socket is suited for p^1, whereas a dedicated power circuit is required for $p^{\{2,3\}}$. Furthermore, the household grid connection (typically 40 A single-phase) might need to be upgraded for p^3, due to the high current rating required for supplying 6.6 kW (32 A).

The share of charging at each location type is summarized in Table 3.11, and the average annual power consumption per vehicle at each location type is summarized in Table 3.12. The share of charging at home, and the resulting residential power consumption, reduces with an increasing amount of charging opportunities. Therefore, the residential grid impact will also be reduced when the amount of charging opportunities increases.

Table 3.11: Share of the charging energy.

Fleet	w^0		w^{100}			
Location	**Home**	**Other**	**Home**	**Work**	**Other**	
c^1	100	/	100	/	/	**[%]**
c^2	/	/	82-85	15-18	/	
c^3	72-81	19-28	64-71	14-17	13-20	
c^4	54-65	35-46	50-60	14-15	25-35	

Table 3.12: Average annual power consumption per vehicle.

Fleet	w^0		w^{100}			
Location	**Home**	**Other**	**Home**	**Work**	**Other**	
c^1	1 706-2 632	/	1 943-3 212	/	/	**[kWh]**
c^2	/	/	1 778-2 774	399-536	/	
c^3	1 410-2 139	467-648	1 554-2 316	392-512	398-573	
c^4	1 115-1 734	865-1 144	1 315-1 975	385-491	761-1 054	

The share of charging at the workplace, and the resulting amount of charging energy, remains limited to below 20 %. It is only limitedly influenced by the battery size, charging power rating, and the presence of charging opportunities at other places than home ($c^{\{3,4\}}$). Therefore, low-power charging infrastructure (Mode 2 at 2.1 kW) might be sufficient to fulfill the workplace charging requirements. This is due to the limited distance between home and the workplace, and the long standstill times there.

Charging at locations other than home and the workplace ($c^{\{3,4\}}$) accounts for a significant share of the charging energy, also for larger battery capacities (b^3), which already have a high F^{U} without these charging opportunities. Then, there is a substitution of charging at home to charging at these locations, thereby reducing the residential grid impact of PEV charging.

As an indication on the utilization of the battery capacity in the fleet, the yearly electric power consumption of the fleet is divided by the effective battery capacity of the entire fleet, and by the number of days in a year. A battery utilization factor F^B of 100 % would mean that the effective battery capacity of the fleet is being used 365 times during the year (on average once a day). A higher F^B is beneficial for the user as this corresponds to a higher return on investment on the battery. The F^B values are summarized in Table 3.13.

Table 3.13: Battery utilization factor F^B for the different scenarios.

Scenario		w^0			w^{100}			
		b^1	b^2	b^3	b^1	b^2	b^3	
c^1	p^1	87	58	34	99	68	40	[%]
	p^2	88	58	34	100	69	40	
	p^3	89	59	34	103	70	41	
c^2	p^1	/	/	/	111	72	41	
	p^2	/	/	/	112	73	41	
	p^3	/	/	/	114	73	41	
c^3	p^1	97	61	34	119	74	41	
	p^2	99	61	34	122	75	41	
	p^3	100	62	34	124	76	42	
c^4	p^1	105	63	34	127	76	42	
	p^2	108	63	34	130	77	42	
	p^3	109	64	34	133	78	42	

Significant differences are visible for the different battery scenarios. The highest F^B occurs for b^1, and increases with an increasing amount of charging opportunities, exceeding 100 % in many of the scenarios. For b^1, the average effective battery capacity is lower than the average daily power consumption, therefore it limits F^U. Thus, when there are sufficient charging opportunities, the battery capacity is intensively being used. For b^1, the charging power rating has a limited impact on F^B, as the limited battery capacity results in a low charging time, even at a low power rating.

For $b^{\{2,3\}}$, the battery capacity is significantly exceeds the average daily power consumption. Because F^U is already high for c^1, an increase in charging opportunities has no significant impact. Consequently, F^B does not increase significantly with an increasing amount of charging opportunities, it just reduces the share of residential charging energy as it increases the share of charging energy at the other locations.

3.4.3.2 PEV charging power profile

The charging behavior for fleet w^{100} is illustrated in Figure 3.11, for battery scenario b^2, for $c^{\{2,4\}}$. The yearly average charging profile is shown for one weekday. For c^2, the residential charging power profile is much more impacted by the charging power

rating than for c^4. This is due to the mobility behavior, as most trips to locations other than the workplace mostly occur after work, before going home. On the other hand, there are almost no trips to other locations before going to work, for the vehicles that effectively are used for work trips on that day. Therefore, the workplace charging profile is almost identical for both charging cases, as most vehicle drive straight to work in the morning.

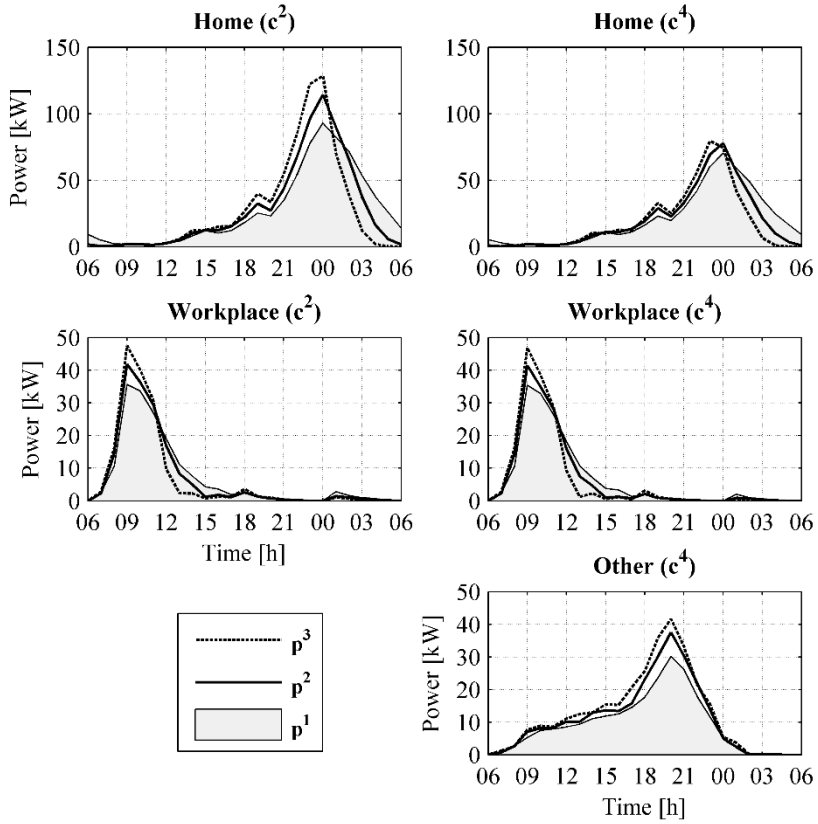

Figure 3.11: Charging power profiles for $c^{\{2,4\}}$, for battery capacity scenario b^2.

The workplace charging profile shows a steep increase in the morning, with a peak around 09:00 and a fast decrease. This is due to the average limited distance from home to work, resulting in a relatively short charging time. The charging profile for the other locations shows a peak in the evening, prior to the residential charging peak,

when the vehicles visit other locations after work, before going home. During the course of the day, there is a gradual increase in the charging power at the other locations. This is due to vehicles that are not used for work trips on the specific day, so these vehicles can visit the other locations during the day, when the others are at the workplace.

The charging power peak at the different charging locations is summarized in Table 3.14, for all scenarios. These results confirm that the opportunity to charge at other locations than at home and at the workplace significantly reduces the residential charging power peak at home, for all scenarios, while it has no significant influence on the charging profile at the workplace. The impact of residential PEV charging on the residential power profile of 100 households is illustrated in Figure 3.12, for fleet w^{100} and for b^2. The yearly average charging profile is shown for one weekday, as in Figure 3.11.

Table 3.14: Charging power peak at the different charging locations.

Scenario		w^0 Peak at home/other [kW]			w^{100} Peak at home/work/other [kW]		
		b^1	b^2	b^3	b^1	b^2	b^3
c^1	p^1	125/-	132/-	132/-	124/-/-	137/-/-	137/-/-
	p^2	178/-	188/-	188/-	145/-/-	187/-/-	191/-/-
	p^3	211/-	304/-	310/-	191/-/-	238/-/-	257/-/-
c^2	p^1	/	/	/	120/60/-	130/60/-	130/60/-
	p^2	/	/	/	139/76/-	162/76/-	165/76/-
	p^3	/	/	/	191/112/-	224/112/-	238/112/-
c^3	p^1	110/33	118/33	119/33	109/60/44	122/60/44	122/60/44
	p^2	158/46	172/46	162/46	129/73/53	146/76/50	145/76/49
	p^3	172/66	211/73	211/73	178/112/73	191/112/92	205/112/92
c^4	p^1	108/46	114/50	114/50	93/60/60	99/60/62	101/60/62
	p^2	129/63	139/66	132/69	115/76/79	129/76/79	131/76/79
	p^3	165/85	211/92	211/92	149/112/99	172/112/106	185/112/106

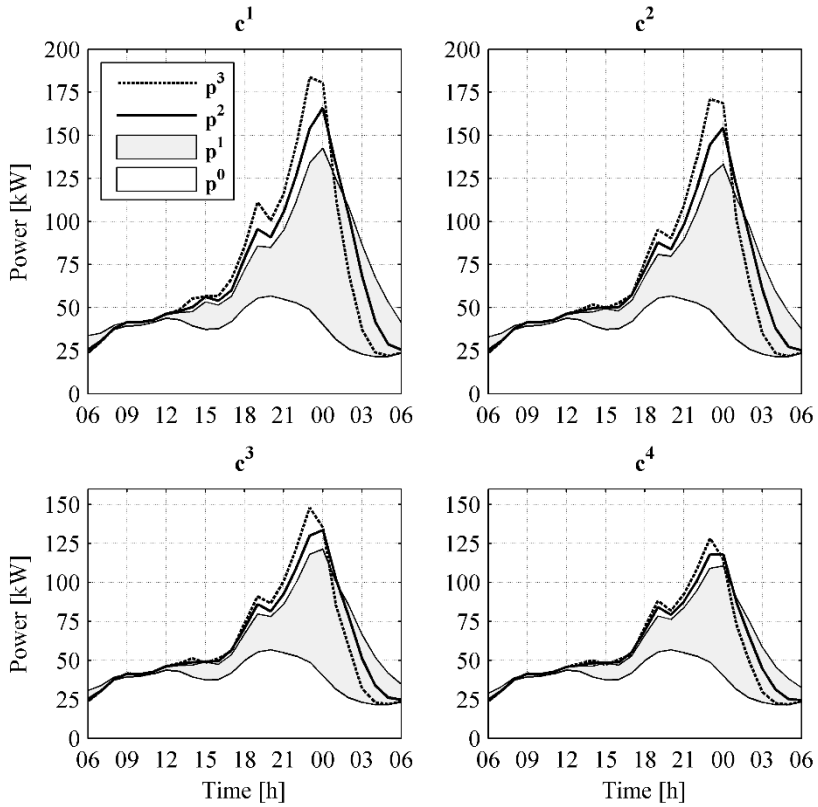

Figure 3.12: Power profile for 100 households and 1 PEV per household, for a vehicle fleet that is used for work trips (100 %) and for the medium battery capacity scenario.

For all scenarios, the residential power peak is summarized in Table 3.15. The residential charging profile without vehicles (p^0) is the sum of 100 synthetic household load profiles that are representative for the Flemish region, which has a peak value of 849 W per household in 2012 [105]. The results show how the residential charging profile is heavily impacted by residential PEV charging, and the magnitude depends significantly on the charging case and the charging power rating. The presence of more charging opportunities reduces the impact on the residential power profile, and it reduces the impact of a higher charging power rating. Thus, the residential grid impact of an increasing amount of PEVs can be mitigated by increasing the amount of charging opportunities, and by incentivizing users to charge at a lower charging power rating.

Table 3.15: Residential power peak for the different scenarios.

Scenario		w^0			w^{100}			
		b^1	b^2	b^3	b^1	b^2	b^3	
c^1	p^1	179	184	184	179	192	192	[kW]
	p^2	234	244	244	197	242	247	
	p^3	287	361	368	247	293	313	
c^2	p^1	/	/	/	175	186	186	
	p^2	/	/	/	193	217	220	
	p^3	/	/	/	247	280	293	
c^3	p^1	166	174	175	166	177	177	
	p^2	216	227	219	179	202	200	
	p^3	224	269	269	233	247	260	
c^4	p^1	164	170	170	146	155	155	
	p^2	186	196	189	170	184	178	
	p^3	222	269	269	194	212	225	

3.4.3.3 Grid services

The PEV fleet is investigated and expressed in terms of the grid connection availability, the energy stored in the PEV batteries, and the energy required to fully charge the PEV batteries. These parameters provide information to assess the interaction with the power system, in terms of energy requirements and charging flexibility. This indicates the potential for a fleet of PEVs to deliver ancillary services to the power system, such as peak power delivery, load shifting, or even spinning reserves [14]. Ancillary services will gain importance in the envisioned future power system, which contains a significant amount of intermittent renewable energy sources [106].

The grid connection availability a^{gc}, as summarized in Table 3.16, is defined as the fraction of the fleet that is grid connected for all but 1 hour of the year (99.99 % of time). Vehicles are grid connected when they are standing still at a location with a charging opportunity for more than 15´. These results show how a^{gc} increases significantly for an increasing amount of charging opportunities. This is due to the fact that vehicles are standing still for the majority of the day, and even during rush hour there is still a large fraction of vehicles standing still.

Table 3.16: Grid connection availability a^{gc} for 99.99 % of time.

Scenario	c^1	c^2	c^3	c^4	
w^0	13	13	29	47	**[%]**
w^{100}	6	18	32	49	

The lowest value of a^{gc} occurs for c^1, and it is lower for w^{100} than for w^0, as the latter fleet is more of its time standing still at home. However for c^2, a^{gc} is higher for w^{100} than for w^0, as the latter fleet is standing still at the workplace for a lot of time. For more charging opportunities, a^{gc} increases further, because of the high standstill time of vehicles in general.

The minimum amount of discharging energy per vehicle that is available for 99.99 % of time (a^{dc}) is summarized in Table 3.17, for both fleets. This parameter indicates how much energy could be discharged to the grid by the vehicles, for all but 1 hour of the year, if the vehicles would be equipped with a bidirectional charger. No change in the mobility behavior compared to conventional vehicles is assumed here, as it is unclear to which extent the mobility behavior will change.

Table 3.17: Discharging energy availability a^{dc}.

Scenario		w^0			w^{100}			
		b^1	b^2	b^3	b^1	b^2	b^3	
c^1	p^1	60	121	260	30	60	120	**[kWh]**
	p^2	63	125	263	30	60	120	
	p^3	66	131	271	31	61	123	
c^2	p^1	/	/	/	76	168	352	
	p^2	/	/	/	82	175	359	
	p^3	/	/	/	90	182	370	
c^3	p^1	123	242	559	132	250	609	
	p^2	135	273	564	152	283	689	
	p^3	144	285	580	166	290	708	
c^4	p^1	207	423	877	202	383	911	
	p^2	222	432	910	210	457	976	
	p^3	232	448	924	225	481	996	

Logically, higher battery capacities significantly increase a^{dc}, as the average SOC of the batteries increases. An increasing charging power ratings only increases a^{dc} to a limited extent, as the average charging time is already relatively limited for low power ratings. The increase in charging opportunities also significantly increases a^{dc}, because it increases the average SOC, as well as it increases the time being grid-connected. For w^{100}, the presence of workplace charging (c^2) increases e^{gc} with more than 150 %, compared to c^1. This increase is higher than what can be achieved by doubling the battery capacity for c^1 and w^{100}, as can be seen by comparing a^{dc} for b^1, b^2, and b^3. This illustrates the importance of workplace charging infrastructure for vehicle to grid (V2G) services.

The amount of available discharging energy in fully charged vehicles for 99.99 % of time $a_{\mathrm{fc}}^{\mathrm{dc}}$ is summarized in Table 3.18. These results give an indication on the amount of fully charged vehicles being grid connected at each moment, except for one hour per year. This fraction of the fleet is unable to participate in down-regulation, i.e. these vehicles can't charge any further to consume excess energy available in the grid. Obviously, these values are lower than the ones in Table 3.17. The major difference with a^{dc} is the more significant influence of the charging power rating, as an increased power rating reduces the time to fully recharge the batteries, which decreases the number of vehicles being available for down-regulation.

The charging energy availability of the fleet for 99.99 % of time a^{ch} turns out to be near zero for all cases. This is caused by the long duration of the grid connection availability when almost all vehicles are charging at home, and some at work, at the end of the night and all batteries are simultaneously fully charged. As all batteries are fully charged, the fleet is unable to accept any additional charge energy for up-regulation. Table 3.19 and gives the minimum available charge energy which is present for 75 % a_{75}^{ch} of time. The results are only shown for p^1, as a_{75}^{ch} is practically zero for higher charging power ratings.

The results show that the available charging energy is negligible in comparison with the available discharging energy. This implies that, for the uncoordinated charging strategy being used here, a fleet of PEVs with bidirectional chargers can be relied upon to provide up-regulation by injecting the energy stored in the onboard batteries, but not to provide down-regulation by charging the batteries, as the probability that the fleet is already fully charged is high.

Table 3.18: Discharging energy availability of fully charged vehicles $a_{\mathrm{fc}}^{\mathrm{dc}}$.

Scenario		w^0			w^{100}			
		b^1	b^2	b^3	b^1	b^2	b^3	
c^1	p^1	36	68	136	20	40	64	[kWh]
	p^2	48	88	176	22	44	88	
	p^3	58	112	224	26	52	104	
c^2	p^1	/	/	/	46	84	168	
	p^2	/	/	/	60	120	240	
	p^3	/	/	/	74	148	288	
c^3	p^1	78	132	296	84	152	304	
	p^2	96	192	408	102	196	432	
	p^3	124	232	488	136	240	552	
c^4	p^1	142	276	512	118	212	440	
	p^2	176	316	664	156	300	608	
	p^3	206	380	784	190	392	778	

Table 3.19: Charging energy availability for 75 % of time a_{75}^{ch}.

Scenario		w^0			w^{100}			
		b^1	b^2	b^3	b^1	b^2	b^3	
p^1	c^1	1	6	18	2	9	26	[kWh]
	c^2	/	/	/	6	17	35	
	c^3	3	9	23	8	20	41	
	c^4	4	11	25	9	22	42	

3.5 Conclusions

In order to implement PEV charging infrastructure in an efficient manner, the requirements of the PEV fleet need to be assessed. Therefore, the modeling of representative Flemish mobility behavior is discussed in this chapter. Furthermore, the specific power consumption of a representative Flemish vehicle fleet has been modeled, to calculate the power consumption requirements that result from the mobility behavior and the fleet composition. The effective grid impact depends on several impact parameters (battery capacity, charging power, and charging opportunities), which are explored through several scenarios. The resulting grid impact and the potential opportunities for grid supporting services have been assessed, for maximum comfort charging (no coordination).

The results indicate that Mode 2 charging, with a power rating as low as 2.1 kW, is able to supply energy to meet a significant amount of the mobility requirements. More than two thirds of the distances can be driven electrically when Mode 2 charging is possible at home and at the workplace, even if the PEVs are equipped with a relatively small battery capacity. This fraction increases to more than 85 % for larger battery capacities. An increase in charging opportunities at other locations, other than at home and at the workplace, will further increase this fraction. For home and workplace charging, low power charging infrastructure appears to provide sufficient energy to fulfill typical mobility requirements. Furthermore, as the initial rollout of PEVs will rely on uncoordinated charging, the grid impact of charging at 2.1 kW on the residential grid is much smaller, compared to higher power ratings.

Charging infrastructure that is capable of providing a variable power rating might be a solution to combine the advantages of both low power ratings (low grid impact), and high power ratings (short charging duration), by selecting the lowest power rating required to still get the PEV fully charged for the next trip. Such charging infrastructure is already commercially available [60], but an effective incentive is needed for users to use a charging power rating that is lower than the highest it can deliver.

The results support the increasingly popular assumption that a carefully chosen set of small battery capacities already allow to obtain a high F^U, thereby already using battery energy for more than half of the driven distances, instead of using the combustion engine. With battery capacities ranging between 5 and 10 kWh, F^U values between 64 % and 82 % can be achieved. A decisive factor in obtaining those high F^U values is the availability of charge opportunities. Charging at home and at work will result in F^U up to 70 %, but to obtain an extra 10 pp in F^U, charging opportunities at other locations are required.

With larger battery capacities, F^U values are high even when charging occurs only at home and at the workplace. More charging opportunities do increase F^U values, but they mainly shift a part of the charging process away from home and the workplace to these other locations. An increase in the charging power rating has only a small impact, as the higher battery capacity provides a larger buffer for situations where the charging time is too short to fully recharge the battery for the next trip. Thus, conversely to common wisdom, larger battery capacities tend to decrease the need for high power charging infrastructure. The above mentioned conclusions also hold when the charging is modeled with a higher resolution and when PEVs would also charge during standstill times shorter than 15 min, as this results in an increased amount of charging opportunities.

The available energy for up-regulation for the modeled fleet strongly depends on the battery capacity and the amount of grid-connection opportunities. An increasing amount of charging opportunities is beneficial for the grid as both the grid-supporting potential increases, and the residential grid impact decreases. Unfortunately, the minimum grid to vehicle (G2V) services of the fleet for down-regulation can be almost non-existent as the batteries are fully charged near the end of the night, when uncoordinated charging is applied. This prevents the vehicles from storing any excess energy available in the grid. Therefore, in order to provide grid supporting services with PEVs in an effective manner, some form of controlled or coordinated charging needs to be implemented.

4. Coordinated charging

A structured literature overview of coordinated charging strategies for PEVs is discussed in this chapter. The coordination objective, scale and method of each coordination strategy are the three degrees of freedom used to characterize and compare different approaches. The correlation between the three parameters and the research category are investigated, resulting in a correlation mapping of the different approaches. The contents of this section are based upon the conference paper:

- N. Leemput, J. Van Roy, F. Geth, P. Tant, B. Claessens, and J. Driesen, "Comparative analysis of coordination strategies for electric vehicles," in *IEEE PES ISGT Europe*, 2011, pp. 1-8.

More recent literature has been added to the literature study in the conference paper. The chapter is structured as follows. The background and history of coordinated charging is discussed in Section 4.1. The relevant layers of control for coordination are defined in Section 4.2. The coordination objectives are discussed in Section 4.3, followed by the coordination methods in Section 4.4, and the scale of coordination in Section 4.5. The correlation mapping is summarized in Section 4.6. The conclusions are discussed in Section 4.7.

4.1 Background

As the number of PEVs grows, they are likely to have an increasing impact on the electricity system. A lot of research has already been done on this topic, which can be categorized according to the research focus.

Research on PEV charging was pioneered with impact and scenario analysis studies [7]-[8], [12], [107]-[108]. Impact analysis studies investigate the impact of PEVs, taking into account all stakeholders and evaluating the impact on welfare [109]-[110]. Parameters such as air quality, public health, external costs etc. are taken into account. Scenario analysis studies focus on the impact of the PEVs on the electricity system, based on the charging behavior, e.g., charging locations, charging timing, and charging power rating. The results of these studies indicate the possible power and energy demand related to PEV charging (Section 4.1.1). Although research on these topics already exists for several decades, it is still an active field of research, taking into account new developments and knowledge on PEVs and power systems [111]-[136].

As there is a certain flexibility for PEV charging, due to their long vehicle standstill time and the relatively low distances driven, an additional objective besides mobility can be included in the PEV charging process. In benchmarking studies (Section 4.1.2), the potential of coordinated charging to obtain these objectives, is calculated [24], [130]-[132], [137]-[155]. Grid planning studies use these results to estimate the expected electrical load of PEVs (Section 4.1.2), which can be taken into account when considering investments in grid infrastructure [133]-[175].

The next step is the practical implementation of coordination systems [57], [24]-[23], [154]-[155], [175]-[220]. They can be assessed in their effectivity, i.e., to which extent they can achieve the results of the benchmarking studies. Practical considerations of the implementation are taken into account here: required components, robustness, execution time, etc. (Section 4.1.3).

4.1.1 Impact and scenario analysis

Most impact analysis studies conclude that there is an opportunity for PEVs to reduce CO_2-emissions and to improve air quality due to a reduction of transport-related emissions [1]. Because emissions are shifted from the tailpipe to the power plants, the amount of reduction is strongly dependent on the composition of plants for electric power generation (gas, coal, nuclear, solar, wind, etc.) [7], [107].

A common finding of the scenario analysis studies is the rise in household peak power demand when no charging coordination is applied. This increase can be understood through the correlation of the arrival time of vehicles at home in the evening with the evening peak of the residential power consumption. Even though the energy demand has a relatively limited impact at the scale of the entire electric energy system, the local impact at the distribution and low-voltage level can be significant [116]. For instance for Belgium, a PEV having an efficiency of 200 Wh/km and an annually driven distance of 15 000 km (Section 3.2), the annual electricity consumption (3,000 kWh) is of the same magnitude as the average annual residential electricity consumption per household (3,500 kWh) [105].

4.1.2 Grid planning and benchmarking

Benchmarking studies gives an indication of the maximum potential of coordinated charging, the optimal solution, assuming perfect knowledge of vehicle behavior when solving for the optimization objective [137]-[149].

Different objectives are investigated: minimizing power losses, voltage deviations, unbalance, charging cost, etc. These studies typically do not propose practical coordination systems, but rather calculate what would be optimal solution. The

opportunities for bidirectional energy flows between the PEV and the grid, known as Vehicle-to-Grid (V2G), are also being investigated in literature [221]-[228].

The combination of the results from the scenario analysis, which give a worst-case scenario, and the optimal solution from benchmarking, gives an indication of the expected power and energy demand of PEVs. Grid operators can use this information to evaluate and plan future investments [150]-[168].

4.1.3 Coordination systems

Combining the results of the discussed categories, allows for designing practical coordinated PEV charging systems [176]-[189]. A coordination system is assumed to be effective if it approaches the benchmark linked to the coordination objective. The translation into an online algorithm has to take into account behavior of the individual vehicles and their mobility needs, instead of considering a group of vehicles at an aggregated level.

In the following sections, three parameters for coordinated charging are discussed: the objective, method and scale of the coordination strategy. The correlation between these parameters is investigated. The layers of control will be discussed in Section 4.2. The correlation between the three parameters and the research categories will be discussed in Section 4.6.

4.2 Layers

Extensive experience was attained in operating the electricity system in a stable and robust manner, because the system must remain intact and it must be able to withstand a variety of disturbances. Therefore, it is designed and operated so that the more probable contingencies can be sustained with no overall loss of load, and so that the most adverse possible contingencies do not result in uncontrolled, widespread and cascading power interruptions [79]. The philosophy that has evolved to cope with the diverse requirements of system control comprises a hierarchical structure [79].

As PEV charging interacts with the electricity system, the control mechanisms should be compatible with each other. Therefore, the hierarchical structure with different control layers also applies to PEV charging. Three principles govern the control system as a whole:

- higher levels operate on longer time scales;
- the levels interact with each other;
- lower layer control actions have priority to higher layer control actions.

Seven control layers are identified here for PEV charging, as illustrated in Figure 4.1. Control action examples at each of these layer are summarized in Table 4.1, for both conventional power system actions and for PEV charging actions. There are three control layers on the planning level (Section 4.2.1), which is linked to the operational level that contains three control layers (Section 4.2.3), through the implementation layer (Section 4.2.2).

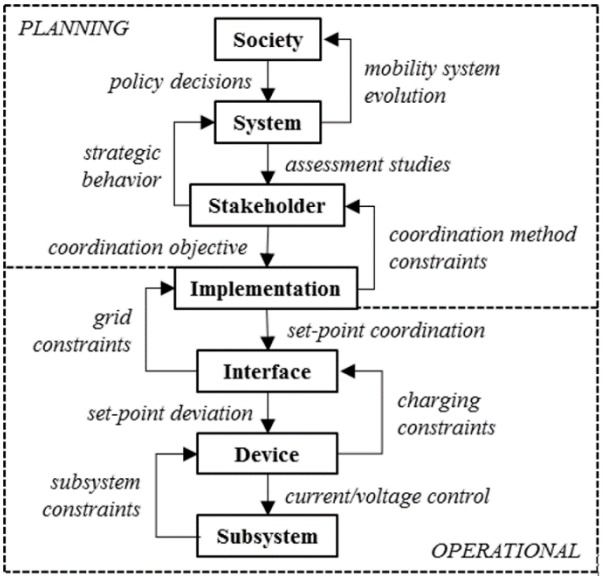

Figure 4.1: Control layers for PEV charging.

Table 4.1: Control layer examples for the power system and for PEV charging.

Layer	Time scale	Example of control action	
		Power system	**PEV charging**
Society	Decades	Climate agreements	
System	Years	EU energy policy	EU transport policy
Stakeholder	Minutes-years	TSO/DSO grid planning	PEV grid impact assessment
Implementation	Seconds-hours	Secondary frequency control	Charging coordination method
Interface	Milliseconds-seconds	Primary frequency control	PEV voltage droop control
Device	Milliseconds-seconds	Power plant ramp rate	Battery pack constraints
Subsystem	Milliseconds-seconds	Turbine thermal limitations	Battery cell constraints

4.2.1 Planning layers

4.2.1.1 Society

The society layer is the highest and most abstract one, as it considers objectives for the entire society. This layer obviously contains exactly the same elements for PEV charging as for the rest of the power system, as this layer is about the entire society. The maximization of general welfare can be considered as the final target for each new technology, combination of new technologies, application, etc. Decisions at society layer will serve as boundary conditions for each of the systems within society, including the power system. As a result, this control layer will influence the evolution of society's systems. Control actions in this layer are taken on a time scale of years/decades.

However, it is impossible to unambiguously define or measure total welfare. Therefore, different methods are used as an attempt to define welfare. Examples of such approaches are found in economic analysis theory (e.g., total welfare definition) [229] and the Human Development Index [230]. Policy making and governance are situated at this control layer, where choices are made that have an impact on the society. Examples of such policy decisions are the European Union climate and energy pack [231] and the Kyoto protocol [232].

4.2.1.2 System

The system layer includes all stakeholders involved in the PEV system. The targets that are set at the society layer, are translated into boundary conditions for this system. These boundary conditions are used to perform cost-benefit analyses and impact assessment studies, to evaluate the most efficient way to obtain society's targets through the PEV system.

Because the PEV charging infrastructure is a part of the power system, some of the stakeholders are mutual. Power system models such as PRIMES [233] and MARKAL [234] are used on the system layer, they can make predictions on the evolution of the energy system (supply, demand, emissions, etc.), given a certain energy policy. Institutions such as the International Energy Agency [235] and the Electric Power and Research Institute Energy Technology Assessment Center [236] operate on this layer. They conduct research and provide advice and support on energy policy.

The power system-related models and institutions will need to incorporate the power system impact of PEV charging infrastructure. Furthermore, mobility-related stakeholders are also at this level for the PEV system, because of the mobility objective function of a PEV. This mix of power system-related and transportation-related stakeholders is one of the major differences between the power system and the PEV charging system. A significant amount of research is carried out on the potential benefits of electric vehicle PEV grid integration and supporting policies [11], [86]. Furthermore, research from the mobility point of view that takes into account multiple stakeholders is also situated at this layer [237].

4.2.1.3 Stakeholder

On this layer, each of the PEV stakeholders defines is own objective. For PEV users and fleet operators, this will typically be an economical objective, i.e., to charge the vehicle in the most cost effective way [6]. Grid operators are technically oriented in their objectives, as they are responsible to keep their grids operational at an acceptable cost to society [142]. Producers and suppliers, being private companies in an unbundled electricity system, typically have the objective to maximize their profit or market share.

Based on their own objective, each stakeholder determines its strategic behavior. As a consequence, a change in energy or transportation policy can change the behavior or adapt the objectives of the PEV stakeholders. This layer has a time scale of years down to a quarter of an hour (the typical time constant in short-term energy markets). Grid planning (DSO and TSO), power plant investment planning (producers), load

forecasting (suppliers), etc., are examples of decisions and activities on this layer [19], [86].

Even though the objectives are clearly different for each stakeholder, they all have an indirect economic consequence. For example, reducing grid losses through coordinated PEV charging will reduce the running costs of the electricity system, which are typically financed through the grid tariffs [238]. More general, delivering grid supporting services with PEVs can be considered as a technical service with an economic value [146]. Through the economic values, the trade-off between different sorts of coordination objectives can be made.

4.2.2 Implementation layer

At this layer, the stakeholder's objectives are translated into operational practice. This layer can be considered as the interface between the planning and the operational layers. The dispatching of power plants within a producer's portfolio and the power output set-point coordination of the power plants through automatic generation control (AGC) are examples of power system actions at this layer [239]. The effectiveness of the methods used for set-point coordination can be evaluated by comparing the obtained results with benchmark values. The benchmark defines the optimal solution, if perfect knowledge would be available [236].

The implementation layer contains the methods for the set point coordination of PEV charging. Depending on the fleet size, the time resolution of coordination actions, etc., one can choose a suitable method. Centralized, hierarchical and distributed methods are being proposed in the literature [240]. The method will determine the required amount of communication, the time resolution of coordination actions, etc. [241]-[243]. This layer has a time scale of a quarter of an hour down to seconds (time constant for secondary frequency and voltage control).

The method for coordinated charging is dependent on the circumstances: a fleet of vehicles at a centralized charging location (e.g., vehicles at an office parking lot) is suited to use a centralized coordination method. For a large distributed fleet (e.g., vehicles located in residential areas), a distributed algorithm seems more suited. For some objectives, such as frequency support, a cascade of control methods is used. Because frequency is a highly variable grid parameter, a distributed method is required (primary frequency support) in addition to other methods (secondary and tertiary control). The distributed mechanism can be continuously active, or only once the frequency deviation is exceeds a predefined dead band [14], [228].

4.2.3 Operational layers

4.2.3.1 Interface

This layer is related to the physical grid constraints and grid regulation. Primary frequency regulation and voltage droop regulation through active and reactive power, respectively, are examples of actions on this control layer at the transmission system [73], [244]. This layer creates deviations from the set-point that is created by the mechanism on the implementation layer, if needed. This layer has a time scale of seconds down to 20 milliseconds (time constant of grid frequency variations).

Control mechanisms on this layer typically require no communication, as they are embedded in the device and are activated through locally measured parameters (e.g., frequency and voltage). Therefore, this control layer provides a stabilizing mechanism in case of absent or malicious communication on the implementation layer. The implementation of control mechanisms on the interface layer typically occur through grid compliance codes for grid-connected devices.

Because PEVs are charged through the low-voltage grid, the distribution grid constraints have a significant influence e.g., feeder current ratings, transformer power rating, and grid voltage deviations [73], [185]. For example, in case of an under voltage or an under frequency event, PEV charging may be altered or interrupted. It should be stressed that the actions only occur once a constraint is exceeded, as these actions interfere with the coordination mechanisms at the implementation layer.

4.2.3.2 Device

The device layer takes into account the physical constraints of the grid-connected device, e.g., ramp rates of thermal and nuclear power plants [246], and variable output of wind power generation [247]. Limitations and constraints on this layer are dependent on the type of device. No matter what higher control layers decide, the physics of the device cannot be overruled. This layer has a time scale down to milliseconds.

In case of PEVs, this layer contains control mechanisms such as the Battery Management System (BMS). This system monitors the battery pack parameters (e.g., cell unbalances, temperature, and voltage) and will actively modify the power flow if one of the battery constraints becomes active (e.g., thermal constraints, end-of-charge behavior) [248].

This layer can reduce/curtail the output of the device due to device-specific reasons, thereby overruling control actions of the higher control layers. One can already (partially) take into account some of the known limitations in the implementation layer

(e.g., end-of-charge behavior), to reduce the impact of this layer during normal operation.

4.2.3.3 Subsystem

This layer is below the device layer: it includes physical phenomena that occur within subsystems of the device, e.g., limitations on turbine blades in thermal power plants [249], and switching frequency limitations for power electronic interfaces [250]. The effects of subsystems of the device are all represented in an aggregated way in the device physics layer. This layer has a time scale going down to sub-millisecond level.

Research on this layer will is performed by the component manufacturers (e.g., semiconductor manufacturers), which has no direct relation with the electricity system. One could define several subsystems eventually, going down to the molecular level. Because this is out of scope, these layers are not further discussed.

4.3 Objectives

Different (technical, economic and combined) objectives can be taken into consideration when defining a PEV charging strategy. They are linked to different stakeholders, and each of them wants to minimize its own cost through objective-focused decision making.

4.3.1 Technical objectives

Technical objectives are linked to the physical assets and constraints of the energy system. These objectives include the minimization of energy losses, minimal voltage deviations, reducing peak power demand, balancing power supply and demand, supporting higher penetration of renewable energy, increased robustness, etc. [114]-[121]. They have often been discussed from the point of view of electrical energy storage [224]-[226], considering V2G functionality.

Technical objectives are related to electricity system stakeholders such as Transmission (TSO) and Distribution System Operators (DSO), electricity producers, retailers and consumers. The technical constraints are to be taken into account as boundary conditions.

4.3.2 Economic objectives

Economic objectives are linked to the energy market-related stakeholders (consumers, producers, and retailers). Electrical energy is traded on markets in which the prices may vary as a function of time. When anticipating on these price fluctuations, by

shifting the charging process in time to minimize the cost of charging, one can achieve financial benefits compared to uncoordinated charging [141]-[143], [189]-[252]. Dual-tariff schemes, real-time pricing, etc. are examples of time-of-use (TOU) pricing schemes.

The optimization for economic objectives takes place on the level of electricity markets where the energy is purchased, grid constraints are not taken into account.

For instance the Virtual Power Plant concept applied on electric vehicles (EV-VPP) focuses on an economic optimization of a large fleet of electric vehicles [145], [253]. The energy demand of a large group of PEVs is aggregated to conform to market entry requirements. By anticipating on the energy markets, charging costs can be minimized. The available capacity of the vehicle batteries could be a competitive alternative for certain high-value energy markets which include capacity payments (e.g. spinning reserves) [224]-[228].

4.3.3 Coupled techno-economic objectives

Both technical and economic aspects are part of the total energy price to be paid by the consumer. The commercial part is set by the electricity trading markets, by balancing demand and supply of electrical energy on these markets. The technical part is determined by the assets of the energy systems and are dependent on the location [79], [163]. E.g. a low-voltage congestion has a great influence on the local grid condition, but has no influence on the wholesale market price.

Although commercial operation based on an open market model serves as a base model for European electricity supply, one cannot disregard the technical constraints due to the grid [254]. At TSO-level, the technical constraints are already taken into account. In most European countries a power exchange market is used to establish a market price for the next day [255]. This commercial allocation is followed by a technical approval in case of network limitations in order to ensure security of supply [256].

Nodal pricing is another example that combines technical constraints and economic objectives. Both are reflected in the price at each node [257]-[261]. The technical aspects are translated into a cost function, which is the weighting factor in the optimization. Another possibility is to perform a multi-objective analysis, whereby the trade-off between the different objectives is determined [168], [238].

4.4 Methods

Objectives are translated into coordination systems by using a certain method. The methods found in literature are categorized into three types: centralized, distributed and hierarchical.

4.4.1 Centralized methods

With a centralized method, a central scheduler optimizes the charging strategy for each vehicle simultaneously. Each vehicle has to follow the schedule set by the scheduler. A centralized method requires communication between each vehicle and the central optimizer. When the size of the system increases, the amount of data will grow significantly. This will require a large infrastructure to handle all data, and typically has a high complexity [79], [182]-[183], [229]-[252].

On the other hand, centrally organized coordination can obtain a highly optimal strategy, since the optimization takes into account all relevant information of the control area. For this reason, benchmarking studies typically use a centralized optimization method (Section 4.6.4) [137]-[140].

4.4.2 Distributed methods

When using distributed methods, the decisions are not made centrally, the intelligence is distributed throughout the system [184], [262]. The electric network is a distributed system with millions of consumers and multiple producers on different grid levels. With a distributed method, the structure of the coordination system may be matched to the grid structure. The communication overhead is limited compared to a centralized approach. Distributed (network) algorithms provide the scalability needed to control the large number of components in a smart grid [79], [263].

A possible distributed method is a distributed multi-agent system (MAS). A MAS consists of several autonomous entities (agents) which operate in an environment where they can cooperate to achieve a certain common goal [149]. Other distributed methods proposed in literature are based upon heuristics, game-theory or Particle Swarm Optimization [147]-[148], [179], [184], [264]. These methods run a local optimization (differentiating them from completely distributed multi-agent methods). Some of these local optimization strategies even obtain the global optimum, e.g. when using game-theoretic power consumption scheduling [184].

For some stability-related time-critical control mechanisms, only distributed control can be used because the time lag due to communication, needed for a centralized method, is too long [79], [176]-[180], [185]-[228].

4.4.3 Hierarchical methods

In hierarchical methods, the decisions are being made following a hierarchical structure. Each hierarchical level only communicates with the adjacent levels. Higher levels receive aggregated information from the lower level. The higher level in the hierarchy will optimize the aggregated energy flows. The lower levels receive a charging profile for their aggregated energy flow, which they dispatch to the level below them [177], [184]-[187].

Hierarchical methods are well-suited to match the multi-agent character of the energy system, with a combination of market and grid-oriented stakeholders at different levels. Grid-related agents can influence or adapt the market-oriented transactions to take into account grid constraints (e.g. capacity limitations). An example of a hierarchical methodology is a hierarchical multi-agent methodology [79], [183], [262]-[266].

4.5 Scale of coordination

The scale of the coordination strategy defines the number of PEVs being coordinated: one vehicle, those located at one feeder at low-voltage level, those within one distribution-voltage area or within an entire TSO area.

- *Vehicle Scale:* This is the smallest possible scale of coordination in which the coordination strategy only takes into account the information being available at that location and the optimization is focused on the individual benefits: charging at minimal cost, reduction of peak-power demand, etc. [120], [188], [267]-[268]. Coordination at this scale typically takes into account the power demand of the building [189].
- *Low-Voltage Scale:* This is the residential low-voltage level, with vehicles connected to one low-voltage feeder [115], [19], [137], [139]. Low-voltage micro grids are also considered at this scale [161], [177]. Local constraints are the ampacity of the feeder and the maximal allowed voltage deviation, taking into account the relatively high R/X-ratio of low-voltage feeders. The resistive behavior, compared to the inductively behaving transmission level, requires adapted control strategies for frequency and voltage control [79], [185]-[228].
- *Distribution-Voltage Scale:* At this level, the distribution grid and medium-voltage micro-grids are situated [114], [118]-[20], [21], [140], [146], [149], [160], [162], [178], [180], [263], [257]-[259], [264]. This level is being characterized by the expansive medium-voltage grid, which links the high-voltage transmission and low-voltage distribution level. Due to the

historical growth of these grids, standardization is limited. Coordination strategies at this scale should take into account the variety in grid topologies.

- *Transmission-Voltage Scale:* At this level (high-voltage), the TSO and energy trading markets operate. This level is also the level at which energy-policy is formulated [12], [116], [15], [121], [123]-[138], [141]-[145], [176], [179]-[183], [9]-[228], [253], [269]-[270]. Because of the aggregation of a high amount of PEVs, quite accurate predictions can be made considering the stochastic parameters of the fleet. Therefore, coordination systems at this level can approach the benchmarks fairly well.

4.6 Correlation mapping

4.6.1 Research category vs. coordination objective

The correlation between the research category and the coordination objective gives an indication where the interest of research lies (Figure 4.2). Most of the literature focuses on the technical objectives, followed by coupled techno-economic objectives. Most literature is about scenario analysis, followed by benchmarking.

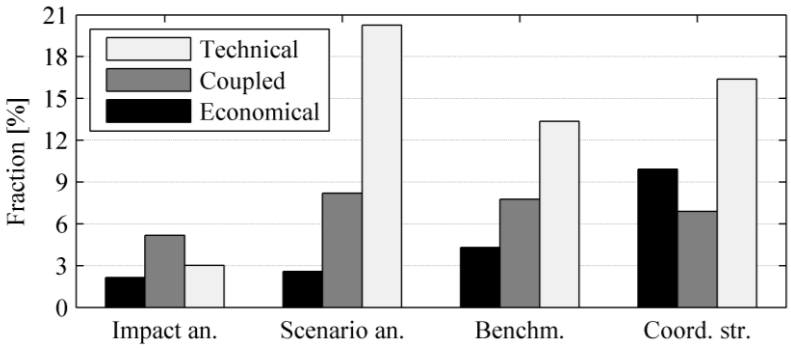

Figure 4.2: Research category vs. coordination objective.

In the category of impact analysis literature, coupled objectives are the most present, as impact analysis studies typically have an integrated high-level approach in which different stakeholders are taken into account (Section 4.1.1). These studies look further than only the technical or economic aspect separately. When an entire area, with all stakeholders, is taken into account, it is called an economic impact analysis.

The scenario analysis studies on the other hand have a strong focus on technical and techno-economic objectives. These studies typically investigate the impact on the electric energy system, in terms of peak-power demand, load profile, etc. The same is observed for benchmarking studies, which is obvious because of the strong ties between scenario analysis and benchmarking.

For practical coordination systems, the economic objectives become more important. This can be understood due to the possibility to anticipate on a variable electricity price. These economic strategies focus on minimization of the cost for PEV charging on an individual base. If the electricity price incorporates technical constraints, one can achieve a coupled techno-economic charging strategy which anticipates on the economic focus of the consumer.

4.6.2 Research category vs. scale of coordination

This correlation indicates at which level of the energy system the different categories are investigated (Figure 4.3). Most research on coordinated PEV charging has been done at TSO-scale, for each category of research besides coordination strategies. As mentioned before, the integrated approach in impact analysis studies and the focus on the electric energy system in both scenario analysis and benchmarking studies, are implicitly more oriented at large scale.

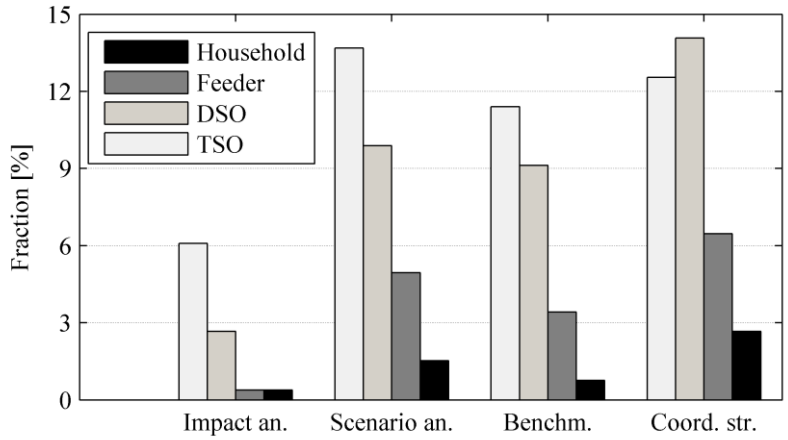

Figure 4.3: Research category vs. scale of coordination.

The share of the smaller scale strategies increases when going from theoretical to practical research on coordination systems. It is more realistic to start with smaller-scale coordination systems, which can be implemented more easily, than to immediately set up an expansive large-scale coordination strategy. Especially at the DSO-level, practical coordination strategies are investigated, as the distribution grids will be significantly impacted due to PEV charging.

4.6.3 Scale of coordination vs. coordination objective

This correlation indicates which coordination objective is being tackled at the different scales (Figure 4.4). At feeder and DSO-scale, the focus lies on technical objectives, due to the importance of technical constraints. More diversification is encountered at the TSO-level, due to the presence of the electricity markets and centralized power generation at this level. Large amounts of distributed generation, grouped in VPPs, can also participate at that level when their energy is traded on these markets. At household level, both technical and economic objectives are being investigated, while coupled objectives seem to be less present. Therefore, the household level is more present for practical coordination systems, typically focusing on one single objective.

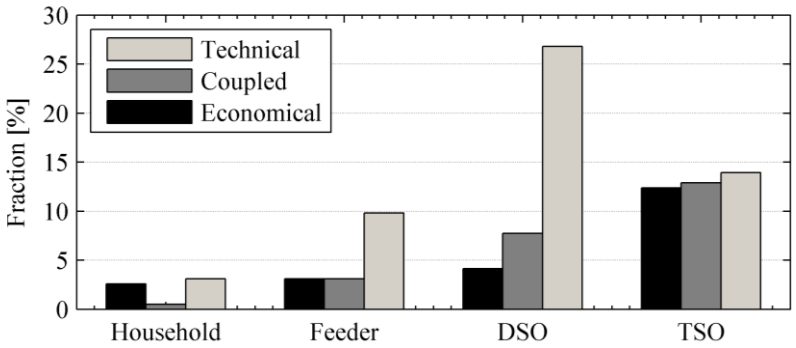

Figure 4.4: Scale of coordination vs. coordination objective.

4.6.4 Research category vs. coordination method

This correlation shows a high presence of a centralized methodology at all categories, except for the practical coordination systems (Figure 4.5). The other categories are making abstraction of practical considerations and focus on the optimally achievable result, being obtained through centralized optimization. For practical coordination

systems, distributed and hierarchical methods are more present than centralized methods. This can be understood due to the larger share of small-scale strategies in practical coordination systems, which are more distributed levels.

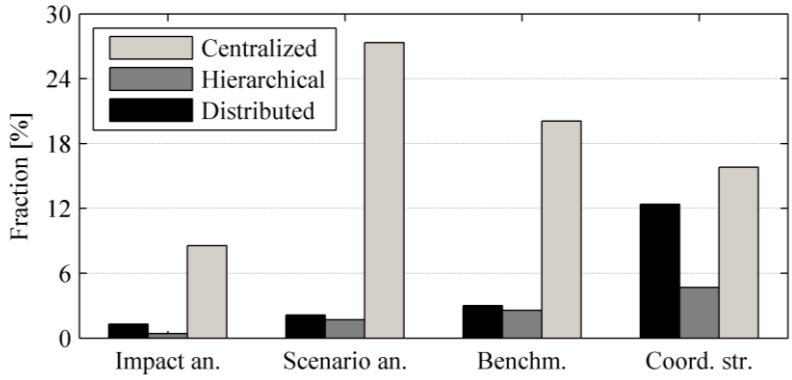

Figure 4.5: Research category vs. coordination method.

4.6.5 Scale of coordination vs. coordination method

The correlation shows that most literature focuses on centralized methods, followed by distributed methods (Figure 4.6). As seen earlier, most literature is on scenario analysis and benchmarking, in which a central optimization is being used. The hierarchical methods are the least present in current literature.

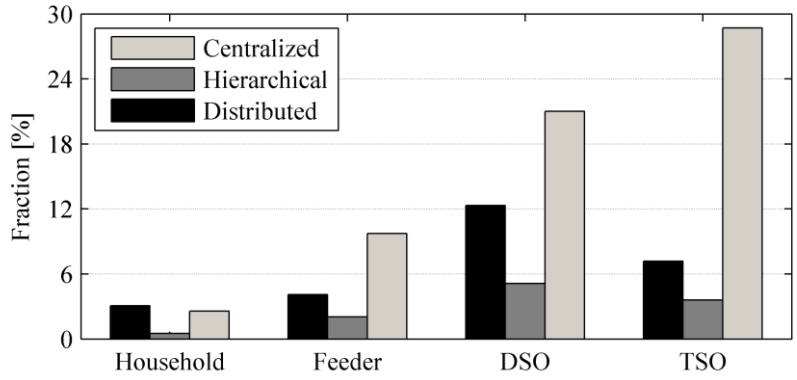

Figure 4.6: Scale of coordination vs. coordination method.

The larger share of the distributed method on DSO-level can be understood due to the distributed nature of this level, combined with the relatively large size of it. At feeder level, the amount of vehicles to be coordinated is smaller, limiting the overhead for centralized coordination systems.

4.6.6 Coordination method vs. coordination objective

This correlation shows that the hierarchical methods are primarily focused on technical objectives (Figure 4.7). This is related to the hierarchical structure in the grid, for which technical constraints are relevant. The large amount of literature on centralized methods is related to the large amount of scenario analysis and benchmarking studies, as explained earlier. Distributed methods are more related to practical coordination systems (Figure 4.5).

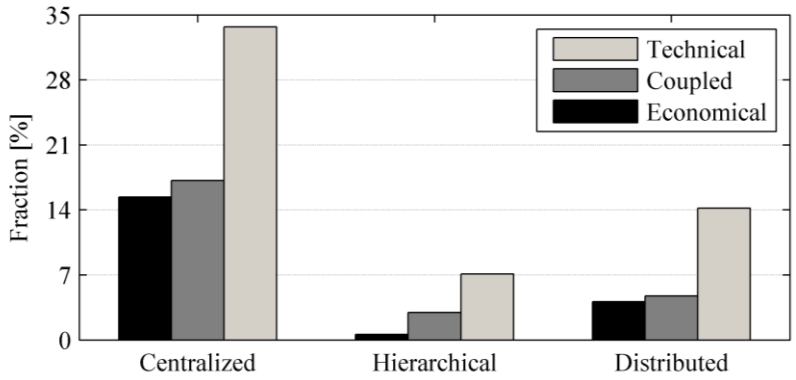

Figure 4.7: Coordination method vs. coordination objective.

4.7 Conclusion

The opportunities of coordinated PEV charging for the society and its stakeholders are well investigated in the literature. PEV charging can be coordinated to maximize different objectives, where each stakeholder has its own objectives. For example, PEV owners want to charge at the lowest cost, while grid operators want to minimize infrastructure upgrades. Most of the proposed coordination systems only consider set-point coordination for one or more coordination objectives, of which some seem to be in conflict with each other, because only direct costs and benefits are considered.

A multi-objective trade-off should be performed at the society and system layer, to create policy decisions and incentives which maximize the overall benefit for all stakeholders. In this way, the coordination objective at the stakeholder layer and the effective set-point coordination at the implementation layer are influenced to create a charging behavior that is more beneficial for the entire society. The benefits for the society will only occur in the long term, because a high number of PEVs on the national scale is required to have sufficient impact on the larger scale.

Control actions at the device and subsystem layer are already implemented in PEVs, as they are required for a correct execution of the charging process. At the interface level, grid-stabilizing control actions are not yet taken into account for PEV charging. However, such mechanisms have already been investigated for distributed energy resources, for which they are already part of grid compliance codes in some countries. Control mechanisms for PEV charging at the interface layer should be considered, as local clusters of PEVs may significantly impact the distribution grid. Control actions at the interface layer create deviations from the coordination set-point once grid constraints are exceeded.

Control actions at the interface layers thus provide a robust mechanism for the initial rollout of PEVs in the near term future, prior to the implementation of large-scale coordinated charging mechanisms. Furthermore, these set-point deviating control actions will remain relevant afterwards, to provide a robust fallback mechanism in case of absent or malicious coordination. In this way, control actions at the interface layer act as a primary control mechanism, e.g., primary frequency and voltage regulation.

Grid-supporting control actions should become part of the grid compliance requirements for PEV chargers in the near-term future, to ensure that all new PEVs have the desired grid-supporting behavior. Therefore, it needs to be assessed which control actions provide the desired grid-supportive behavior. In the following two chapters, active and reactive charging power control strategies, respectively, are assessed and discussed.

5. Active power control

The residential distribution grid impact of active power control strategies for PEV charging are investigated in this chapter. Uncontrolled and on-board controlled charging mechanisms are compared to each other, both with and without voltage droop-corrected charging behavior. This behavior is complementary with coordination, but can also be implemented without, it merely creates power set point deviations as a function of the grid voltage. Voltage droop charging behavior is implemented on the on-board charger, and it does not need communication between the PEV and the distribution grid. On-board controlled charging only needs one user input (the next departure time), as the other information (required recharging energy) is already available within the PEV.

The content of this chapter has been based on the peer-reviewed paper:

- N. Leemput, F. Geth, J. Van Roy, A. Delnooz, J. Büscher, and J. Driesen, "Impact of electric vehicle on-board single-phase charging strategies on a Flemish residential grid," *IEEE Trans. Smart Grid*, vol. 5, no. 4, pp. 1815-1822, Jul. 2014.

The chapter is structured as follows. The background on active power control for PEV charging is summarized in Section 5.1. The materials used and methods applied are explained in Section 5.2. The results are discussed in Section 5.3, followed by the conclusions in Section 5.4.

5.1 Background

As discussed in Chapter 4, there is a need for local control strategies for PEV charging, as local clusters with a high PEV penetration rate might occur in the near-term future, while the average penetration rate remains low. Therefore, no widespread coordination mechanism for PEV charging will be implemented in the near-term future. Therefore, local control mechanisms are needed, which have the objective to keep the distribution grid within operational constraints. These mechanisms will remain present in the long-term future, as a robust fallback mechanism, in case of absent or malicious coordination. These control mechanisms can be considered as the equivalent of primary voltage/frequency control mechanisms, as implemented on large generating units. The primary mechanisms avoid the system to go from a disturbed state to a critical state, and the secondary/tertiary mechanisms are activated to bring the system back from the disturbed state to the normal state.

Local off-line control mechanisms can make use of locally available grid and user information. The battery charger always measures the voltage waveform, as this information is needed to create a grid-compliant charging current, as discussed in Section 2.2.3. The voltage magnitude and frequency can be derived from this waveform, so this information could be used to alter the charging behavior. Such local control mechanisms are already required for photovoltaic (PV) installations in Germany, as part of their grid compliance requirements. PV installations have to reduce their active power output with a gradient of 40 % per Hertz from 50.2 Hz through 51.5 Hz, and disconnect from the grid above 51.5 Hz [271]. Furthermore, PV installations must adapt their reactive power behavior as a function of the grid voltage, (Chapter 6).

Opposed to PV installations, active power control of PEV charging does not lead to a loss in user functionality, as long as the PEV is sufficiently charged by the next departure time. This is not the case for PV installations, as a deviation from the maximal power point leads to a decrease in energy yield. As active power control is already implemented for PV installations, where it has an inherent cost, it should definitely be investigated for PEV charging as well. PEV battery chargers always have the functionality to adapt the active charging power, as this is required anyway for the end of charge behavior, as discussed in Section 2.2.2. Therefore, no hardware adaptations are required to implement active power control for PEV charging.

When a PEV charger draws a purely active current I_d, i.e., unity power factor (PF), the voltage magnitude impact can be calculated as follows:

$$|U_2| = \sqrt{|U_1|^2 - |I_d X|^2} - (I_d R). \tag{5.1}$$

U_1 represents a voltage source, e.g., the voltage magnitude at the interface between the distribution and the transmission grid, and U_2 is the resulting voltage at the point where the active current offtake I_d takes place. I_d influences the resulting voltage magnitude $|U_2|$, due the impedance $(R + jX)$ between U_1 and U_2, as illustrated in Figure 5.1. Thus, by altering the charging current, voltage magnitude can be altered to reduce the induced distribution grid voltage drop. Reactive currents also influence the grid voltages, but it requires a full-bridge active rectifier to control reactive currents, which not all PEVs are equipped with (Chapter 6) [44]. Voltage droop charging (Section 5.2.4) will be assessed in this chapter as an active power control strategy for PEV charging.

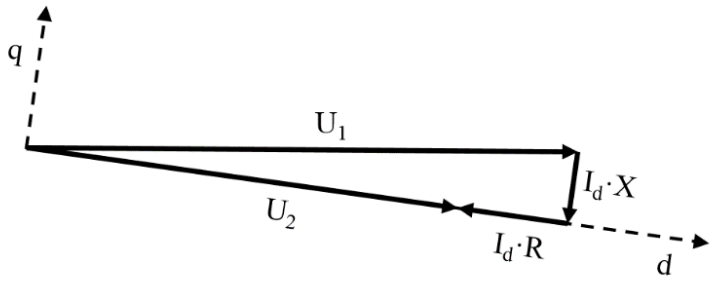

Figure 5.1: Voltage magnitude impact of active power consumption.

Beside the active PEV charging power control for grid purposes (Chapter 4), local coordination mechanisms can be considered to further reduce local grid impacts. The difference between the control and the coordination mechanisms is when they are activated. Control actions only occur when the grid is in the disturbed state, not in the normal state, as the grid constraints only need to be met, not exceeded [70]. Coordination mechanisms on the other hand are continuously active, also when the grid is in the normal state, in order to avoid the disturbed state as well. Because a local coordination mechanism will also be active when the distribution grid is within the normal state, the charging process is more influenced than when only control actions occur. Therefore, incentives might be required to participate in such local coordination mechanisms, similar as for other demand response mechanisms [272]-[273].

PEV charging can be controlled locally to smoothen the power profile of the distribution system [19], e.g., distribution grid peak shaving as explicit objective [114], [146], [169], or as a constraint in cost-minimizing coordination strategies [170]-[171]. Distribution grid peak shaving can be chosen as an optimization objective, to mitigate local load peaks in the distribution grid. This reduces the simultaneity of household and PEV power demand, which positively impacts voltage deviations [169] and grid losses [146]. Voltage deviation reduction can also be considered as a coordination objective during times of excessive deviations [19]. A wide range of programming techniques are used to implement these coordination strategies, e.g., linear programming [171]-[172], sequential quadratic programming [19], [274], dynamic programming [19], [228], convex quadratic programming [146], and heuristic programming [10], [111]. The choice of the programming technique is a trade-off between optimality, completeness, accuracy, complexity, robustness, and execution time.

Alternatively, local parameters can be used for a rule-based coordination strategy of the PEV charging process, opposed to the abovementioned optimization strategies. These rule-based coordination strategies do not require communication between the PEVs, and they do not require predictive knowledge. Furthermore, as there is no optimization to be conducted, there is no calculation time which needs to be taken into account, and the execution time of the rule-based coordination strategy is independent of the amount of participating PEVs. For example, the PEV charging power rating can be reduced based on the required charging energy, which can be calculated by the PEV itself based on the time until the next departure, which can be delivered as an input by the PEV user. This coordination strategy is hereafter referred to as PEV-based peak shaving (Section 5.2.4).

5.2 Materials and methods

5.2.1 Distribution grid data

A real urban feeder topology is used here (Figure 5.2 and Table 5.1), provided within the EIT-KIC InnoEnergy EVCity project [275]. The 39 residential loads h are grid connected through 29 nodes i. The distance between these nodes and the transformer varies between 310 and 550 m. All households have a single-phase grid connection between one of the three phases ($ph \in \{a, b, c\}$) and the common neutral conductor n; the rated neutral-to-phase voltage U^{nom} is 230 V. Cable parameters are taken from the standard NBN C33-322 [276]. Cable type EIAJB 1 kV 3×70 + 1×50 mm^2 is used for the main feeder. Cable type EXVB 1 kV 4×16 mm^2 is used to connect the household supply terminals with the main feeder, except at node 28, where cable type EXVB 1 kV 4×35 mm^2 is used, because of the high load that is connected there. These cables are between 5.3 and 14.8 m in length.

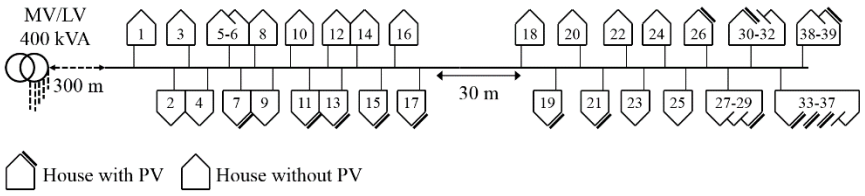

Figure 5.2: Schematic overview of the residential low voltage feeder topology, with 29 connection nodes i serving 39 households h.

Table 5.1: LV grid parameters.

		Primary	Secondary
Cable type		Cu-3×70 + 1×50 mm^2	Cu-4x16 mm^2
I^{max} **[A]**		245	120
Z^{cable} **[Ω/km]**		0.268 + 0.085i	1.15 + 0.083i
Parallel feeders	**# parallel feeders**	5	
	Length [m]	300	
# loads/feeder		39 (29 nodes)	
Total # household loads		234	
S^{tr} **[kVA]**		400	
Z^{tr} **[Ω]**		0.007 + 0.029i	

The feeder is connected to a MV/LV transformer with a power rating $S^{tr} = 400$ kVA. The transformer impedance is derived from [277]. Because multiple LV feeders are connected to the transformer, five simplified feeders with a length of 300 m are added. An aggregated unbalanced load, with an equivalent number of households as for the detailed feeder, is added to each parallel feeder. As a result, the transformer capacity equals 1.7 kVA per household, a realistic value for urban LV distribution grids.

5.2.2 Residential load and generation

A stochastically representative set H_o of 39 real single-phase household electric power consumption profiles h was sampled in 2008 [278], with a 15 min time resolution. The profiles are self-identified in the survey as within an urban environment. Only active power consumption was measured, and therefore reactive power consumption is neglected in the simulations. The households are alternatingly connected to the three phases $ph \in \{a, b, c\}$.

On the main feeder, 14 houses are assigned a photovoltaic (PV) installation (Figure 5.2). The PV power generation profiles for these installations are based upon measurements at an installation of the KU Leuven, with a 15 min resolution. The PV power profile is scaled to match the annual power generation to the annual household power consumption at the selected locations. The single-phase regulatory inverter power rating limit of 5 kVA is taken into account [279], and a unity PF of 1 is assumed for the PV power generation [280].

5.2.3 PEV charging load

A representative set $\mathcal{E}_o$ of charging profiles e, with a 1 min time resolution ΔT, is generated. The fleet modeling (Chapter 3) is used to create a representative fleet of PEVs. Each household $h \in H_o$ is assigned a PEV $e \in \mathcal{E}_o$. The rated battery capacities are 10, 15, and 20 kWh for subcompact, midsize, and large vehicles, respectively. The usable battery capacity is limited to 80 % of the rated capacity, to extend the battery life [41].

The PEVs are modeled as Extended Range Electric Vehicles (EREVs), using battery power as long as the battery is not depleted. Consequently, the combustion engine only runs when the battery is depleted. Therefore, all mobility requirements are met, even if the battery is depleted.

The PEVs are grid-connected at home and at the workplace, whenever they are standing still at these locations for more than 15′. Mode 3 charging infrastructure is assumed [104], with the commonly occurring power rating of 3.3 kW, which results in a current rating of 16 A at 90 % of U^{nom} in continental Europe. A PF of 1 is assumed for slow charging, as the default PF for PEV chargers is well above 0.99 [127].

5.2.4 Charging cases

Four different PEV charging cases c are investigated (Table 5.2), and compared to the case without PEVs (c^0).

Table 5.2: Summary of the charging cases.

Case c	Description
0	No PEVs
1a	Uncoordinated charging
1b	Uncoordinated charging with voltage droop
2a	PEV-based peak shaving
2b	PEV-based peak shaving with voltage droop

5.2.4.1 Uncoordinated charging

Uncoordinated charging is represented by c^1. The PEVs start charging immediately when they are grid connected, until fully charged or until leaving for the next trip.

Thus, the battery is recharged as soon as possible. The flexibility of PEV charging is completely dedicated to increase the comfort of the PEV user.

For c^{1a}, during each time step k, the charging power P_k^{1a} equal to the rated power $P_{\text{rat}}^{ch} = 3.3$ kW:

$$P_k^{1a} = P_{\text{rat}}^{ch}. \tag{5.2}$$

For c^{1b}, voltage droop charging is used [281]. The charging power P_k^{1b} depends on the voltage magnitude $|U_{ph,i,k}|$ at the phase ph and connection node i where the PEV is grid connected, during the time step k:

$$P_k^{1b} = 3.3 \text{ kW} \cdot f(|U_{ph,i,k}|). \tag{5.3}$$

The function $f(|U_{ph,i,k}|)$ linearly decreases from 1 to 0 at voltage magnitudes between 0.90 and 0.85 pu (Figure 5.3), which will increase the charging time when the voltage magnitude is below 0.9 pu. The range 0.85-0.90 pu is chosen, as this coincides with the voltage magnitude threshold values of the EN50160 grid compliance code (Section 2.4.3). As a result, the charging is only altered if the voltage magnitude goes outside the normal operating range, and charging is completely stopped when the voltage goes to the critical range.

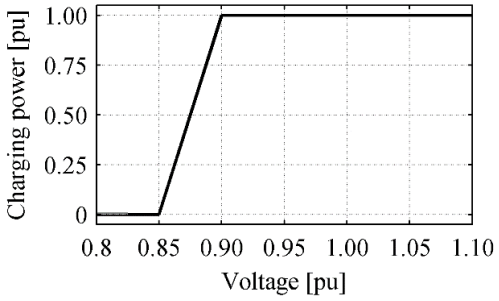

Figure 5.3: Piece-wise linear voltage droop charging behavior.

A grid voltage measurement is already present in PEV chargers, because the charging current waveform needs to be controlled to be grid compliant. PEV chargers can adapt their charging power within a wide range, which is required to stay below the maximal charging current that is allowed by the Mode 2 or Mode 3 charging infrastructure. Therefore, voltage droop charging behavior can be implemented in current PEV chargers, by adapting their control scheme.

5.2.4.2 PEV-based peak shaving

For c^2, the charging power set point $P_k^{2,\text{set}}$ is equal to the minimal power that is needed to get the PEV battery fully charged during the standstill time span until the next trip ΔT_k^{dep}. Therefore, $P_k^{2,\text{set}}$ depends on ΔT_k^{dep}, the SOC at the considered time step SOC_k, and E^{nom}. To avoid a too low efficiency at partial load [48], the charging power set point lower limit is 25 % of 3.3 kW (825 W):

$$P_{k,\text{avg}}^{2,\text{set}} = (1 - SOC_k).\, E_{\text{nom}}^{\text{bat}} / \Delta T_{\text{dep}}; \tag{5.4}$$

$$P_k^{2,\text{set}} = \begin{cases} 825\ \text{W} & P_{k,\text{avg}}^{2,\text{set}} \leq 825\ \text{W} \\ P_{k,\text{avg}}^{2,\text{set}} & 825\ \text{W} < P_{k,\text{avg}}^{2,\text{set}} < 3.3\ \text{kW}. \\ P_{\text{rat}}^{ch} & P_{k,\text{avg}}^{2,\text{set}} \geq P_{\text{rat}}^{ch} \end{cases} \tag{5.5}$$

Thus, if a PEV is standing still for 10 h until the next departure and 10 kWh is needed to recharge the battery, $P_k^{2,set}$ will be 1 kW.

For c^{2a}, the battery charger has a constant power behavior:

$$P_k^{2a} = P_k^{2,\text{set}}. \tag{5.6}$$

For c^{2b}, a voltage droop charging behavior is implemented, as illustrated Figure 5.3. The droop behavior limits the maximal power the charger can draw, dependent on $f(|U_{ph,i,k}|)$:

$$P_{k,\text{max}}^{2b} = P_{\text{rat}}^{ch} \cdot f(|U_{ph,i,k}|); \tag{5.7}$$

$$P_k^{2b} = \begin{cases} P_k^{2,\text{set}}, & P_k^{2,\text{set}} < P_{k,\text{max}}^{2b} \\ P_{k,\text{max}}^{2b}, & P_k^{2,\text{set}} \geq P_{k,\text{max}}^{2b} \end{cases}. \tag{5.8}$$

For example, if the voltage magnitude is 0.875 pu, the maximal charging power is limited to 1.65 kW, i.e. 50 % of 3.3 kW. If the charging strategy already limits the charging power to 1 kW, the charging process will not be influenced. If the voltage droop influences the charging process, the charging power will be adapted in the following time step to get the PEV fully charged by the next departure, given the charging power rating of 3.3 kW.

5.2.5 Simulation approach

The simulations are conducted for 25 randomly selected weeks out of a one-year scenario, resulting in a number of time steps n_t = 252,000, i.e., $k \in \{1, 2, \dots, n_t\}$. This same selection is used for each case, to make a correct assessment. For each 1 min time step ΔT, the evolution of SOC_k for each PEV is calculated. The resulting residential PEV charging profiles are added to the residential load and generation profile at the respective grid nodes. The residential load profiles are constant for their 15 min period. The workplace charging profiles are not added, as it is assumed that there are no workplace charging locations in this residential grid.

A three-phase unbalanced load flow analysis is implemented in MATLAB. Unbalanced loads are taken into account, as well as the resulting zero-point shifting due currents running through the common neutral conductor. The backward-forward sweep technique is used, because of the radial layout of the grid [282]. The problem is converged when the worst time step voltage error ε^V is below 0.1 V. A supplementary convergence criterion is used for the PEV loads: the worst time step power error ε^P is below 33 W, which is 1 % of the charging power rating.

All loads are modeled with unity power factor for all cases. The loads are modeled as constant power loads for $c^{\{0,1a,2a\}}$. For $c^{\{1b,2b\}}$, the voltage dependent PEV charging behavior is implemented within the backward-forward sweep, while the other loads are modeled as constant power loads.

5.3 Results and discussion

The simulation results are discussed in this section. The impact of the charging strategies on the charging behavior is summarized in Section 5.3.1. The voltage droop charging behavior is discussed in detail in Section 5.3.2. The impact on the power profile, voltage magnitude, and voltage unbalance are discussed in Section 5.3.3, 5.3.4, and 5.3.5, respectively.

5.3.1 Charging behavior

The PEV charging simultaneity is defined as the number of PEVs that are charging simultaneously at the feeder (Table 5.3), on which each of the 39 households has a PEV. For all cases, the maximal charging simultaneity is below 30 PEVs, and even below 20 PEVs for $c^{\{2a,2b\}}$. During more than 50 % of time, at least 3 PEVs are charging for $c^{\{1a,1b\}}$, and 9 PEVs for $c^{\{2a,2b\}}$. The higher simultaneity for $c^{\{2a,2b\}}$ is due to the spreading of the charging process over the full standstill time at home.

Table 5.3: PEV charging simultaneity.

# PEVs charging simultaneously	Fraction of the total time [%]		
	c^{1a}	c^{1b}	$c^{\{2a,2b\}}$
> 0	85.4	85.5	99.8
> 5	27.0	27.4	74.5
> 10	9.3	9.8	46.4
> 15	1.3	1.5	31.8
> 20	0.0	0.0	17.5
> 25	0.0	0.0	4.1

The impact of the different charging cases on the PEV charging time differs significantly (Table 5.4). The charging time increase for c^{1b} vs. c^{1a} is less than 5 % for all vehicles in the fleet. The charging time for c^{2a} and c^{2b} are identical and substantially longer than for $c^{\{1a,1b\}}$, since both fully make use of the standstill time at home.

Table 5.4: PEV charging time.

Distribution within the PEV fleet	Fraction of total time [%]		
	c^{1a}	c^{1b}	$c^{\{2a,2b\}}$
Minimum	3.8	3.9	13.9
Mean	10.4	10.5	30.1
Maximum	16.2	16.3	43.2

The cumulative charging time increase, for each charge event per PEV, remains below 7.2, 16.2, 30.8, and 72.8 % for 85, 90, 95, and 100 % of all charging actions, respectively (Figure 5.4). This illustrates the significant impact of voltage droop behavior on the charge duration at some moments, but a limited impact most of the times.

The minimum, mean and maximum value for the utility function F^{U} in the fleet are 57.4, 70.8, and 85.5 %, respectively. F^{U} remains identical in all cases for each PEV in the fleet. This indicates that there is sufficient charging flexibility to implement voltage dependent charging behavior, even in this constrained grid situation.

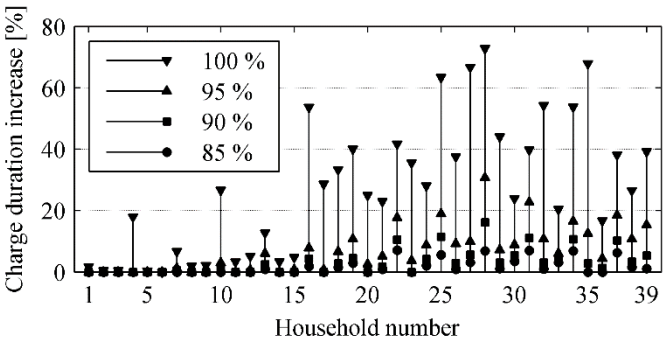

Figure 5.4: Duration increase per PEV of cumulative charge events for c^{1b} vs. c^{1a}.

5.3.2 Voltage droop charging behavior

To illustrate the voltage droop charging behavior in detail, a four-hour period between 22.30 and 02.30 on one specific day is visualized for c^{1a} and c^{1b}. The charging simultaneity for c^{1a} (black curve) and c^{1b} (grey area) are illustrated in Figure 5.5. The simultaneity varies between 6 and 18 PEVs for both cases. The charge simultaneity is slightly higher for c^{1b} than in c^{1a}, due to the charge duration increase that occurs if the droop behavior is active, which compensates for the charging power reduction.

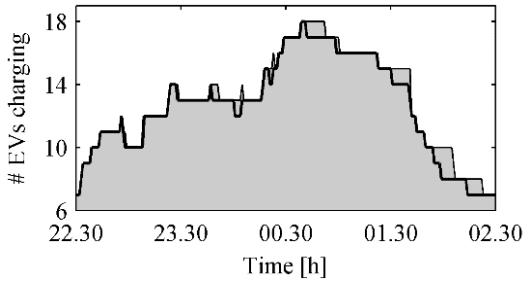

Figure 5.5: Charging simultaneity for c^{1a} (black curve) and c^{1b} (grey area).

For three households $h \epsilon \{23, 31, 39\}$, each on a different phase, the voltage magnitude and PEV charging profile are illustrated in Figure 5.6 for c^{1a} (black curve) and c^{1b} (grey area). The PEVs at $h = 31$ and $h = 39$ reduce their charging power for c^{1b}, because the voltage magnitude goes below 0.9 pu. The resulting charging time increase and the substantial impact on the voltage magnitude can be observed.

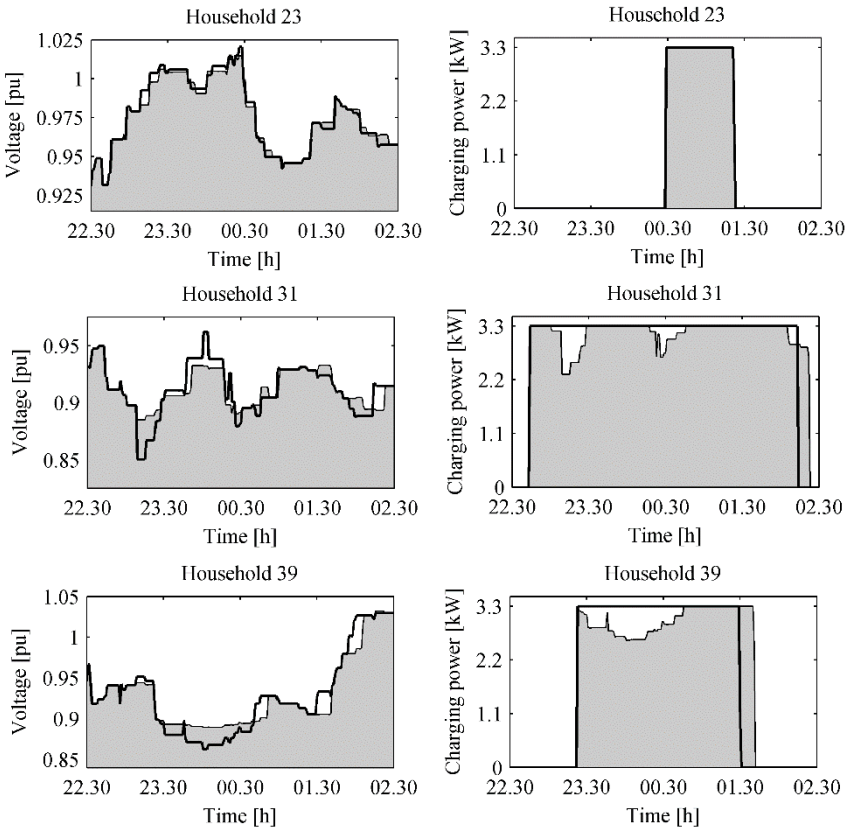

Figure 5.6: Nodal voltage profiles and charging power profiles for c^{1a} (black curve) and c^{1b} (grey area).

The voltage droop behavior of all PEVs that face voltage magnitudes below 0.9 pu during charging influences all nodal voltages on the feeder. This can be seen at $h = 23$, where the voltage profile changes, while the charging profile of the PEVs is identical. Also, there are changes in the voltage profile when the PEV is not charging, due to the voltage droop behavior of other PEVs that are charging at that time.

5.3.3 Power profile

The maximum transformer load $S_{\max}^{\mathrm{tr}}$, delivered energy E^{del}, and grid losses E^{grid} are summarized in Table 5.5, for both positive (pos) and negative (neg) values. The negative power values occurs at times when instantaneous PV power generation

exceeds power consumption in the LV grid. This is due to the difference in timing of PV power generation and household power consumption.

The load $S_{ph,k}^{\text{tot}}$ on each phase ph is defined as follows:

$$S_{ph,k}^{\text{tot}} = P_{ph,k}^{\text{grid}} + jQ_{ph,k}^{\text{grid}} + \sum_{h\epsilon H_0} P_{ph,h,k}^{\text{load}} + \sum_{e\in\mathcal{E}_o} P_{ph,e,k}^{\text{ch}}; \quad (5.9)$$

where $P_{ph,k}^{\text{grid}}$ and $Q_{ph,k}^{\text{grid}}$ are the active and reactive grid power losses for each phase on each time step. $P_{ph,h,k}^{load}$ is the residential load, including PV power generation, $P_{ph,e,k}^{\text{ch}}$ is the active power consumption of a PEV during charging.

Table 5.5: Impact of the charging strategy on the power profile.

Case	$S_{\max}^{tr}$ [kVA]		E^{del} [MWh]		E^{grid} [MWh]
	pos	neg	pos	neg	
c^0	264.2	271.5	324.2	43.8	6.0
c^{1a}	588.3	234.1	647.1	31.1	24.1
c^{1b}	572.2	234.1	647.2	31.1	23.6
c^{2a}	375.3	222.0	641.3	25.6	17.9
c^{2b}	364.1	222.0	641.3	25.6	17.9

$S_{\max}^{tr}$ is the maximum of the sum of the load on each phase:

$$S_{\max}^{tr} = \max_k\left[\sum_{ph\epsilon\{a,b,c\}} |S_{ph,k}^{\text{tot}}|\right]. \quad (5.10)$$

E^{del} and E^{grid} are defined as follows:

$$E^{\text{del}} = T_s \sum_{k=1}^{n_t} \sum_{ph\epsilon\{a,b,c\}} \left(\sum_{h\epsilon H_p} P_{ph,h,k}^{\text{load}} + \sum_{e\in\mathcal{E}_o} P_{ph,e,k}^{\text{ch}}\right); \quad (5.11)$$

$$E^{\text{grid}} = T_s \sum_{k=1}^{n_t} \sum_{ph\epsilon\{a,b,c\}} P_{ph,k}^{\text{grid}}; \quad (5.12)$$

where E^{del} only contains the energy the households effectively consume (pos) and produce (neg), as the grid losses are not of interest for the residential end user.

Compared to c^0, $S_{\max}^{tr}$ is more than doubled for $c^{\{1a,1b\}}$. As a result, the transformer is loaded above its rating for $c^{\{1a,1b\}}$. The increase is significantly less for $c^{\{2a,2b\}}$. Because $S_{\max}^{tr}$ is at 93.8 and 91.0 % of the transformer rating for c^{2a} and c^{2b}, respectively, a transformer upgrade is not required. When comparing c^{1a} and c^{1b}, it

can be concluded that the presence of voltage droop behavior only has a limited impact on the peak power.

E^{del} approximately doubles due to PEV charging. The difference in power generation and consumption between $c^{\{1a,1b\}}$ and $c^{\{2a,2b\}}$ is due to a higher self-consumption for $c^{\{2a,2b\}}$, because the simultaneity between PEV charging and PV power generation increases. However, the limited difference indicates that the simultaneity remains low.

E^{grid} for $c^{\{1a,1b\}}$ is approximately the fourfold compared to c^0, due to the increase in peak power and power consumption. E^{grid} for $c^{\{2a,2b\}}$ is approximately 25 % lower than for $c^{\{1a,1b\}}$, due to the lower peak power values.

5.3.4 Voltage magnitude profile

The impact of PEV charging on the voltage magnitude is summarized in Table 5.6. The voltage magnitude stays below 1.1 pu for all cases, so only the minimum voltage U_{min} is discussed. For c^0 the voltage magnitudes are compliant with EN50160 (Eq. 2.1 and 2.2), U_{min} is just below 0.9 pu, for only 0.2 % of time in one week at one location.

Table 5.6: Impact of the charging cases on the voltage magnitudes.

Case	U^{min} [pu]	Max weekly duration [%]	
		$U_{ph,i,k}$ < 0.85 pu	$U_{ph,i,k}$ < 0.9 pu
c^0	0.90	0.0	0.2
c^{1a}	0.75	2.1	8.5
c^{1b}	0.86	0.0	10.4
c^{2a}	0.85	0.0	1.4
c^{2b}	0.87	0.0	1.4

For c^{1a}, the grid is not compliant with the EN50160 standard. U^{min} is 0.75 pu and the voltage magnitude goes below 0.85 pu in each of the 25 weeks of the simulation, affecting 37 households.

For c^{1b}, U^{min} is above 0.85 pu. However, the grid is still not compliant with EN50160. The voltage magnitude is below 0.9 pu in 8 weeks of the simulation for up to 10.4 % of time per week, affecting 13 households.

For $c^{\{2a,2b\}}$, the voltage magnitude is compliant with EN50160. $U^{\min}$ is above 0.85 pu and the voltage magnitude is between 0.9 and 0.85 pu for a maximum of 1.4 % of time per week.

5.3.5 Voltage unbalance factor

The impact of PEV charging on the voltage unbalance factor F^{VU} is summarized in Table 5.7. For c^0 the voltage unbalances are compliant with EN50160 (Eq. 2.3 and 2.4), as the maximum voltage unbalance factor $F^{VU}_{\max}$ remains below 2 %.

Table 5.7: Impact of the charging cases on F^{VU}.

Case	$F^{VU}_{\max}$ [%]	Max weekly duration $VUF > 2$ % [%]
c^0	1.9	0.0
c^{1a}	5.0	7.7
c^{1b}	3.4	4.5
c^{2a}	2.6	0.3
c^{2b}	2.5	0.3

For c^{1a}, F^{VU} is above 2 % for up to 7.7 % of time per week, in 7 of the 25 weeks. This affects 24 of the 39 households, in up to 7 weeks for individual households. For c^{1b}, F^{VU} values are compliant with the standard. F^{VU} only exceeds 2 % for a maximum of 4.5 % of time per week. Thus, voltage droop behavior substantially reduces F^{VU}.

For $c^{\{2a,2b\}}$, F^{VU} exceeds 2 % for a maximum of 0.3 % of time per week, which is compliant with EN50160. This is significantly lower than for $c^{\{1a,1b\}}$, due to the increased charging simultaneity and lower peak power values.

5.4 Conclusions

The residential grid impact of PEV charging can be substantially reduced with on-board strategies that do not require communication between the PEVs and the DSO or PEV aggregator. Voltage droop charging and on-board peak shaving both can be implemented within the PEVs.

Voltage droop charging eliminates PEV-induced voltage magnitudes below 0.85 pu. F^{VU} values higher than 2 % occur for less than 5 % of time per week. However,

because the voltage magnitude is below 0.9 pu for more than 5 % of time per week, the grid is not compliant with the EN50160 standard. On-board peak shaving makes the grid fully compliant with EN50160, and the peak power remains below the transformer rating. As a result, there is no need for grid infrastructure reinforcements.

For all cases, the voltage droop behavior reduces PEV-induced voltage deviations and voltage unbalance. The combination of both strategies enables the integration of PEVs prior to the widespread availability of coordination. Once available, PEV-based peak shaving can be bypassed, while the voltage droop enabled charger provides an effective fallback mechanism in case of erroneous coordination.

The electrically driven fraction remains identical to uncontrolled charging for both strategies. However, the impact on the charging time is different. For voltage droop charging, there is a significant impact at some moments, but a limited impact at most of the time. Therefore, the total charging time is only impacted marginally. For PEV-based peak shaving, the charging time increases significantly because the full standstill time at home and at the workplace is used. Therefore, incentives will be required to convince PEV users to participate.

Another way of mitigating the grid impact of PEV charging is to make use of reactive power, instead of active power. The advantage of this approach is that it does not influence the charging process, given that the PEV chargers is appropriately sized. Therefore, reactive power control during PEV charging is investigated in the following chapter.

6. Reactive power control

The residential distribution grid impact of reactive power support of single-phase electric vehicle chargers is investigated in this chapter. Reactive power support is investigated for three different electric vehicle charging strategies: uncoordinated charging, residential off-peak charging, and PEV-based peak shaving. For an increasing amount of reactive power support, the grid impact is compared in terms of LV voltage deviations, MV/LV transformer peak load, and distribution grid losses.

The results are used to assess which level of reactive power support allows for the highest PEV hosting capacity, before grid infrastructure investments are required, taking into account different active power charging strategies. The level of reactive power injection can be implemented by including the resulting capacitive PF in the grid compliance code for PEV chargers.

The content of this chapter has been based on the peer-reviewed paper:

- N. Leemput, F. Geth, J. Van Roy, J. Büscher, and J. Driesen, "Reactive power support in residential LV distribution grids through electric vehicle charging," *Sust. Energy, Grids and Networks*, vol. 3, pp. 24-35, Sept. 2015.

The chapter is structured as follows. Background information on reactive power in distribution grids is briefly discussed in Section 6.1. In Section 6.2, the materials used and methods applied are explained. The results are discussed in Section 6.3, followed by a grid topology sensitivity analysis in Section 6.4. The conclusions are summarized in Section 6.5.

6.1 Background

The active power charging strategies discussed in Chapter 5 increase the charging time, compared to uncontrolled charging, as the average active power rating is reduced. As a result, the user comfort is impacted to some extent [150], which implies that incentives are needed to convince him to participate. PEVs are grid connected via a power electronic interface, allowing for the implementation of more advanced charging strategies. Reactive power support could be implemented, if the on-board charger is suitably designed and sized.

With a typical average R/X ratio between 0.5 and 5 for LV distribution grids [283], the contribution of reactive power to grid voltage variations may be substantial. The reactive power behavior for different PEV types is investigated in [127]. All of the investigated PEVs have a power factor (PF) that is well above 0.99, but their reactive

power contributions vary significantly. As for a PF of 0.99, the reactive power injection or consumption already amounts to up to 14.25 % of the active power consumption, which may already have a noticeable influence on the LV grid.

For residential photovoltaic (PV) installations, grid-supporting reactive power behavior has already been investigated. The use of an inductive PF between 0.95 and 1 is an effective manner to mitigate the grid impact of residential PV installations [284]. Reactive power support of (large) PV installations is already part of the grid code in some countries. For example in Germany, LV grid-connected PV installations rated above 3.68 kVA have to follow a specified PF droop curve as a function of their instantaneous power output [271].

A similar approach can be used for PEV charging, by injecting reactive power during PEV charging, i.e., capacitive behavior. The voltage magnitude impact of reactive current offtake I_q (i.e., reactive power injection) during active current offtake I_d (i.e., active power offtake) is illustrated with a simple example (Figure 6.1). U_1 represents a voltage source, and U_2 is the resulting voltage at the point where the current offtake $I_d + jI_q$ takes place. Both I_d and I_q influence the resulting voltage magnitude $|U_2|$, due to the series impedance $(R + jX)$ between U_1 and U_2:

$$|U_2| = \sqrt{|U_1|^2 - \left|\left(I_q R\right) + \left(I_d X\right)\right|^2} - \left(I_d R\right) + \left(I_q X\right). \tag{6.1}$$

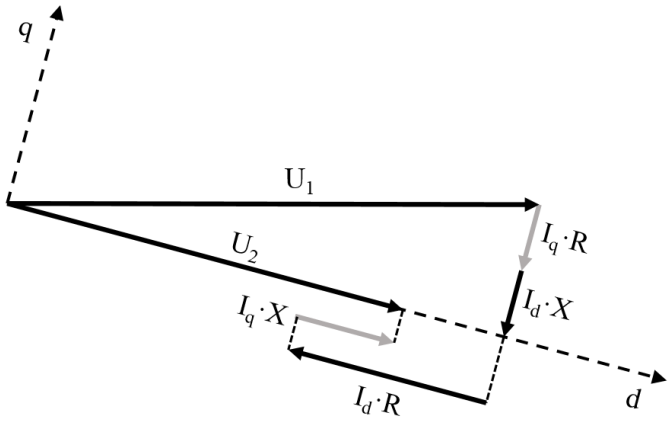

Figure 6.1: Voltage magnitude impact of active and reactive power.

The voltage drop due to active current $-(I_d R)$ is partially compensated for by a voltage rise due to reactive current $+(I_q X)$. Instead of adapting the active charging power profile, and thereby impacting the user comfort, reactive power can be used to support the grid during PEV charging. However, the apparent power rating of the PEV charger is not to be exceeded. For example, in order to obtain a 0.95 PF value, the apparent power rating of the PEV charger should be 105.3 % of the active power rating. Thus, for a typical PEV charger active power rating of 3.3 or 6.6 kW, an apparent power rating of 3.5 or 7.0 kVA, respectively, is enough to provide a 0.95 capacitive PF. The reactive power injection for this 5.3 % oversizing already amounts to up to 32.9 % of the active power consumption.

To the best of the authors' knowledge, the LV grid impact assessment of reactive power support for PEV chargers is not investigated in the literature, neither for uncoordinated charging, nor in conjunction with a control strategy for PEV charging. The objective is to assess which capacitive PF could be used for all suitable PEV chargers to provide a beneficial overall result. This approach is similar to the above-mentioned research conducted on grid-supporting reactive power support of PV installations, for which an inductive PF is implemented [284]. The grid impact of reactive power injection could be further optimized by differentiating the PF between the PEV chargers, but this is not the objective here, as this would require knowledge on the specific location of each vehicle, and also communication between the PEVs.

6.2 Materials and methods.

6.2.1 Distribution grid data

A real urban feeder topology is used to model a residential LV grid (Figure 6.2 and Table 6.1), the grid modeling is explained in detail in Section 5.2.1. Also for this grid, S^{tr}=400 kVA, and five simplified parallel feeders are added [283]. The resulting R/X value for the aggregated series impedance (MV/LV transformer, primary feeder, and secondary feeder) ranges from 1.3 to 2.9, when moving from the household the closest to the transformer $(h = 1)$ to the one the furthest away from it $(h = 42)$.

The LV voltage deviations at each node should remain within 7.5 % of U^{rat} (Section 2.4.3.1). The voltage magnitude and unbalance constraints, together with the feeder current constraints, determine how much PEV charging load the distribution grid can accept, additional to the residential load and the PV power generation. As opposed to the current and voltage constraints, the transformer power rating is not a hard real-time constraint (Section 2.4.3.3).

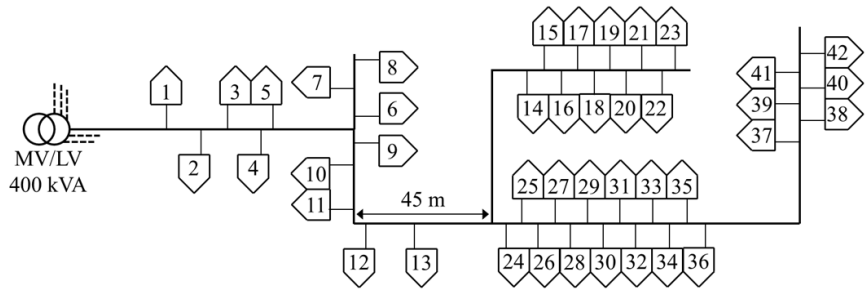

Figure 6.2: Urban LV feeder topology, with lengths drawn to scale.

Table 6.1: LV grid parameters.

	Primary	**Secondary**
Cable type	Al-4x95 mm^2	Cu-4x16 mm^2
$I^{\max}$ **[A]**	245	120
Z^{cable} **[Ω/km]**	0.320 + 0.078i	1.15 + 0.083i
Parallel feeders	**# parallel feeders**	5
	Length [m]	250
# loads/feeder	42	
Total # household loads	252	
S^{tr} **[kVA]**	400	
Z^{tr} **[Ω]**	0.005 + 0.015i	
R/X	1.3 – 2.9	

6.2.2 Residential load and generation

A residential electric load profile generator is used to create a statistically representative set H^o of single-phase household electric power consumption profiles h, with a 15 min time resolution [285]. Variations between week and weekend days, as well as seasonal variations, are included. The reactive power consumption of household loads highly depends on the type of appliance that is active. In general, the PF increases with increasing active power consumption. However, a fixed inductive PF is typically used in grid impact assessment studies, underestimating reactive power consumption at low, and overestimating at high load.

As a detailed analysis of the reactive power consumption of household loads is out of scope, the reactive power behavior is based upon a 48 h duration measurement with a 6 s time resolution. Using the Curve Fitting Toolbox of MATLAB, a two-term power series is fitted on the measured data:

$$PF_{h,k}^{\text{load}} = 0.9928 - 0.003705 \cdot \left(\left(P_{h,k}^{\text{load}}/8\right) + 0.005\right)^{-0.923}. \quad (6.2)$$

$PF_{h,k}^{\text{load}}$ and $P_{h,k}^{\text{load}}$ are the inductive PF and the power consumption, respectively, of household load profile h at time step k (Figure 6.3). With this model, the PF increases from 0.50 to 0.99 inductive when the load increases from 0 to 8 kW, the range in which the single-phase household power profiles vary.

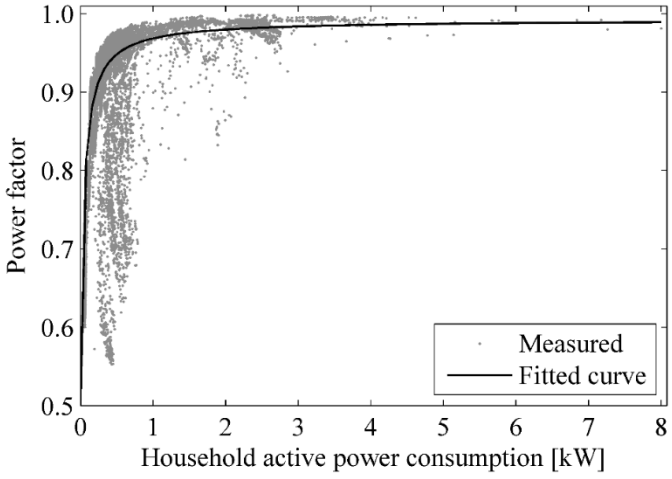

Figure 6.3: Measurements and fitted curve of the household load reactive power behavior.

In Flanders, residential grid-connected PV power generation amounts to approximately 10 % of the residential power consumption [286]. Therefore, a random selection of 10 % of the houses is assigned a PV installation. The PV power profiles are based upon full-year measurements on an installation at the KU Leuven, with a 1 min time resolution. Therefore, seasonal variations in PV power generation are included. The profiles are scaled to match the annual generation volume to the annual consumption at the selected household. The single-phase regulatory inverter power rating limit of 5 kVA is taken into account [279], and a unity PF of 1 is assumed for the PV power generation [280].

6.2.3 PEV charging behavior

The fleet modeling (Chapter 3) is used to create a representative set of PEVs, as explained in detail in Section 5.2.3. The same battery capacities (10, 15, and 20 kWh) are used here, as well as the same single-phase Mode 3 charger power rating $P_{\text{rat}}^{ch} = 3.3$ kW. The charging process is modeled in more detail here, by taking into account the end-of-charge power limit $P^{\text{EOC}}(SOC_k)$ (Figure 6.4), which is based upon measurements performed on real vehicles [43]. When the SOC exceeds 92 %, $P^{\text{EOC}}(SOC_k)$ limits the effective charging to below P^{ch}.

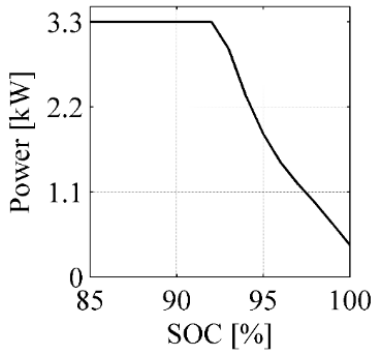

Figure 6.4: End-of-charge power limitation.

Three residential charging cases c are investigated (Table 6.2) and compared to the case without PEVs (c^0). The three rule-based charging strategies represent three typical charging targets: high comfort, low charging cost, and low grid impact through active power management. More advanced charging strategies could be considered, but is out of scope here.

Table 6.2: Summary of the charging cases.

Case c	**Description**
0	No PEVs
1	Uncoordinated charging
2	Off-peak charging
3	PEV-based peak shaving

For c^1, the target is to maximize the user's comfort. Each PEV immediately starts charging when it is grid-connected. This case represents the situation without any form of controlled charging. For c^1; during each time step k, the charging power $P_k^{1,set}$ equal to the rated power $P_{\text{rat}}^{ch} = 3.3$ kW:

$$P_k^{1,\text{set}} = P_{\text{rat}}^{ch} \tag{6.3}$$

For c^2, the target is to decrease the residential charging cost. Therefore, the PEVs are only charged at home during the off-peak tariff period, when the tariff is about 30 % lower [287]. In many areas, this tariff occurs when the time T_k is between 10 pm and 7 am:

$$P_k^{2,\text{set}} = \begin{cases} P_{\text{rat}}^{ch}, & 10\text{ pm} \le T_k \le 7\text{ am} \\ 0, & 7\text{ am} < T_k < 10\text{ pm} \end{cases}. \tag{6.4}$$

At the workplace, the PEVs are still able to charge between 7 am and 10 pm, because the charging cost at the workplace might be significantly different from the one at home. This rule-based strategy only uses the time of day (T_k), known by the onboard computer.

For c^3, the target is to reduce the local grid impact by adapting the active charging power, with a strategy that can be implemented without interaction between the end-user and the grid. PEV-based peak shaving is used (Section 5.2.4.2), adapted here to take into account the end-of-charge behavior. The set point $P_k^{\text{set},3}$ is the minimum power rating required to get the battery charged in the timespan until the next departure ΔT^{dep}, taking into account the upper limit of P_{rat}^{ch} and the end-of-charge power limitation $P^{\text{EOC}}(SOC_k)$:

$$P_k^{3,\text{set}} = f\left(E_{\text{rat}}^{\text{bat}}, E_k^{\text{bat}}, \Delta T^{\text{dep}}, P_{\text{rat}}^{ch}, P^{\text{EOC}}(SOC_k)\right). \tag{6.5}$$

As a result, the battery is charged to the same level at the departure time as for c^1. This charging strategy uses one driver input: the next departure time. The other parameters are already available in the onboard computer.

For all cases, the end-of-charge power profile $P^{\text{EOC}}(SOC_k)$ limits the effective charging power $P_k^{\text{ch},c}$ at SOC values above 92 %:

$$P_k^{c,\text{ch}} = \begin{cases} P_k^{c,\text{set}}, & SOC_k \le 92\ \% \\ P^{\text{EOC}}(SOC_k), & SOC_k > 92\ \% \end{cases}. \tag{6.6}$$

For the three cases, different capacitive PF values are implemented in the simulations, to assess the grid impact of reactive power support during charging.

6.2.4 Simulation approach

The simulations are conducted for a one-week scenario, resulting in a number of time steps n_t = 10 080, i.e., $k \in \{1, 2, \ldots, n_t\}$. For each 1 min time step ΔT, the evolution of SoC_k for each PEV is calculated (Eq. 3.11). The resulting residential PEV charging profiles are added to the residential load and generation profile at the respective grid nodes. The residential load profiles are constant during the 15′ period. The workplace charging profiles are not added, as there are no workplace charging locations in the residential grid. The simulations are conducted for a PEV penetration that increases in steps of 10 % until 100 %, or until the load flow offers no feasible solution (no load flow convergence or exceeding the feeder current constraints).

For the three cases, this assessment is performed with an increasing ratio r^{ch} of reactive power injection Q_k^c to active power consumption P_k^c ($Q_k^c = r^{\mathrm{ch}} \cdot P_k^c$), in steps of 10 % until 50 % $\left(r^{\mathrm{ch}} = 0, 10, \ldots, 50\ \%\right)$. The resulting PF, apparent power rating S^{ch}, and charging current rating I^{ch} for the PEV chargers are summarized in Table 6.3. The increase in power and current requirements stays below 12 %. For Mode 3 charging infrastructure with an active power rating of 3.3 kW, a 20 A fuse must be used anyway, which remains sufficient for all the r^{ch} values being investigated here.

Table 6.3: Power factor, power rating, and current rating for different levels of reactive power injection.

r^{ch} [%]	0	10	20	30	40	50
PF [-]	1.000	0.995	0.981	0.958	0.929	0.894
S^{ch} **[kW]**	3.30	3.32	3.37	3.45	3.55	3.70
I^{ch} **[A]**	16.0	16.1	16.3	16.7	17.2	17.9

Seasonal and intraweek residential load variations, seasonal PV power generation variations, and intraweek PEV load variations are taken into account by conducting the simulation for a representative one-week scenario for each season. Furthermore, the sensitivity of the results to the nodal location of the residential loads is taken into account by performing the simulations for ten different permutations of the load locations.

For each permutation, a new random selection of 10 % of the households is chosen to be equipped with a PV installation, to take into account the sensitivity of the results to their location. Obviously, the yearly energy generation is matched to the household load it is assigned to (Section 2.2). Finally, for each permutation, the random selection

of the locations for the sequence of the increasing PEV penetration rate is changed, to take into account the sensitivity of the results to the specific location of the PEV loads.

To obtain grid impact results (Section 3.3-3.5), a three-phase unbalanced load flow algorithm is implemented in MATLAB. Unbalanced loads are taken into account, as well as the resulting LV neutral conductor voltage drop. The backward-forward sweep technique is used, because of the radial layout of the grid [282]. The problem is converged when the worst time step voltage error ε^V is below 0.1 V. The resulting impact of the reactive power injection is compared in terms of LV voltage deviations, MV/LV transformer peak load, and grid losses.

6.3 Results and discussion

6.3.1 User impact

The charging metrics (F^{U}, PEV charging energy, and share of charging energy per location) are summarized in Table 6.4 for the simulated fleet of 252 PEVs.

Table 6.4: Charging metrics for the fleet of 252 PEVs.

Charging case c		{1, 3}	2
F^{U} [%]	Min	56.3	52.0
	Mean	87.4	85.3
	Max	100.0	100.0
PEV charging energy [kWh]		50 674	48 930
Share of charging energy [%]	Home	93.5	92.8
	Workplace	6.5	7.2

The values for $c^{\{1,3\}}$ are identical, as they provide the same SOC by the next departure from a charging location. The F^{U} values are lower for c^2, but the differences are small, because the required charging time at home is sometimes shorter than the off-peak time span. Therefore, for most of the time, the PEV batteries can be fully recharged during off-peak during standstill at home. The minimal value of F^{U} is above 50 % for each case: each of the PEVs covers more than half of its driven distances purely electrically. The maximum value of F^{U} is 100 % for each case: at least one PEV always drives purely electrically. F^{U} values are relatively high, even though the battery capacities are relatively limited.

Larger battery capacities result in even higher values for F^{U}, as more distance can be covered purely electrically between charging locations. For example, for a doubling of the battery capacities (20, 30, and 40 kWh for the three vehicle categories, respectively), the minimal and mean F^{U} values are 77.6 % and 97.3 % for $c^{\{1,3\}}$, and 76.0 % and 97.0 % for c^{2}, respectively. This significant increase in battery capacity firmly influences the minimum F^{U} values, but has a more limited impact on the mean F^{U} values, as for most PEVs, this extra battery capacity only has an impact for a limited amount of long distance trips. Therefore, it might be more advisable to only provide a higher battery capacity to PEVs that are more frequently used for long distance trips.

The PEV fleet charging energy is 50.7 MWh for $c^{\{1,3\}}$, and 48.9 MWh for $c = 2$, for the fleet of 252 PEVs during the 4 week simulation. 114 of the 252 PEVs are used at least once for work trips. This fraction, i.e., about 45 % of the fleet, is a realistic number for a vehicle fleet (Section 3.1). For the three cases, the vast majority of this charging energy (>90 %) is provided through residential charging. The share of workplace charging is slightly higher for c^{2}, but the total amount of charging energy is lower. As a result, the increase in workplace charging energy is only 225 kWh, as the reduction in residential charging energy for c^{2} is mainly compensated for by the range extender, which translates into the lower F^{U} values for c^{2}.

6.3.2 Charging behavior

As an example, the impact of the three charging cases on a single PEV is illustrated for a 72 h timespan in Figure 6.5. For each case, the charging power at home, at work, and the evolution of the SOC are shown. The residential charging power profile is similar in shape for c^{1} and c^{2}, but the latter is shifted in time, as the PEV arrives at home before the start of the off-peak tariff period. For both c^{1} and c^{2} the PEV is recharged during standstill at home, therefore, the SOC is identical when the PEV leaves for the next trip. As a result, the workplace charging power profile is identical for both cases, for the 72 h time span (Figure 6.5).

For c^{3}, the residential charging power profile significantly differs, as the charging process is spread out over the standstill time at home. As a result, the charging power magnitude is much lower for c^{3} than for $c^{\{1,2\}}$. This results in a slower increase in SOC during the charging process and might be considered as a reduction in user comfort, as the PEV is only fully charged by the planned departure time. However, at the time of leaving a charging location, the SOC is identical as for c^{1} (Figure 6.5).

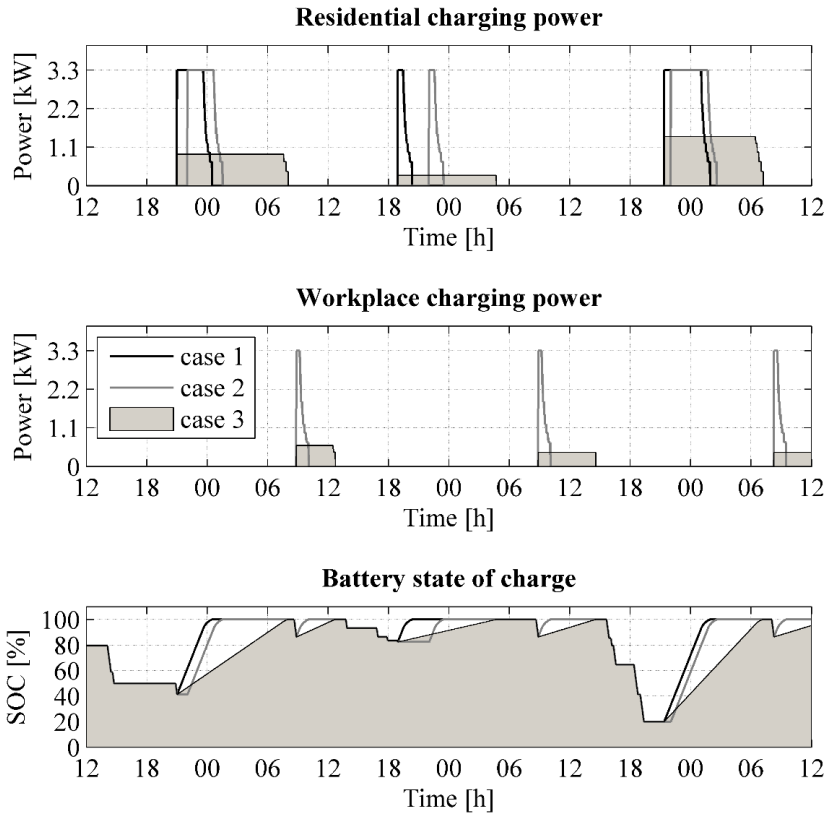

Figure 6.5: Charging behavior of a single PEV for the three cases, during a 72 h timespan.

To illustrate the aggregated effect of the charging cases, the charging behavior of the total PEV fleet is displayed in Figure 6.6 for the same 72 h time span. The aggregated residential charging profile for c^2 differs significantly from the profile for c^1. For the latter, the PEVs that arrive at home before 10 pm would immediately start charging. However, for c^2, these PEVs all start at exactly 10 pm. The synchronization of residential charging actions results in an increased charging power peak. Each PEV will reduce its charging power as much as possible for c^3, which results in a significantly decreased aggregated charging power peak.

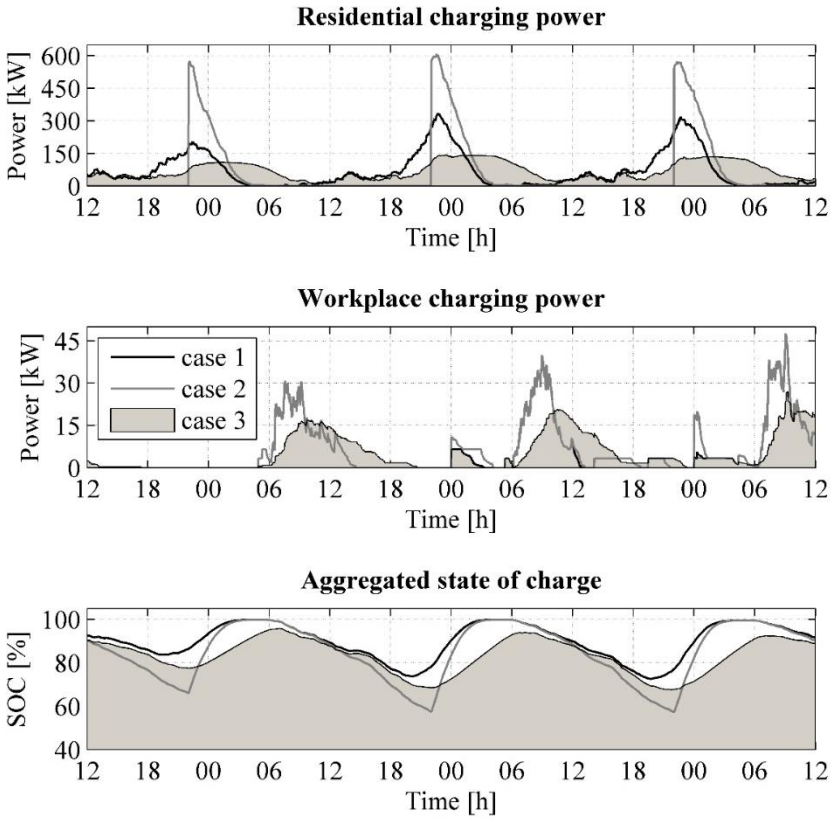

Figure 6.6: Charging behavior of the entire PEV fleet during a 72 h time span.

The highest mean SOC occurs for c^1 (Figure 6.6), because each PEV is charged as soon as possible. For c^2, there are larger variations in the aggregated SOC, because the PEVs can only start charging at home after 10 pm. The minimum of the aggregated SOC is at 10 pm, when it is lower than for both other cases. Starting from 10 pm, the mean SOC increases at a much faster rate than for the other charging cases, due to the high amount of PEVs that are charging synchronously at that moment. Finally, between 3 and 6 am, the mean SOC is approximately the same as for c^1, because the majority of PEVs have sufficient time to fully recharge their battery. For c^3, the aggregated SOC always stays below the profile for c^1, as the SOC during standstill of each PEV is lower than or equal to the value for c^1.

6.3.3 Grid voltages

The per-phase instantaneous grid loads differs significantly, due to the single-phase grid connection of the houses. Therefore, most residential PV installations and the residential PEV charging infrastructure are single-phase as well. These single-phase connections induce unbalanced grid loading, resulting in noticeable differences in nodal phase voltages. The added value of performing an unbalanced load flow is not to underestimate phase voltage deviations. The impact of reactive power injection of PEV charging (c^1) on the voltage profile is illustrated in Figure 6.7 for an 8 h period, for three different houses and for a 50 % PEV penetration.

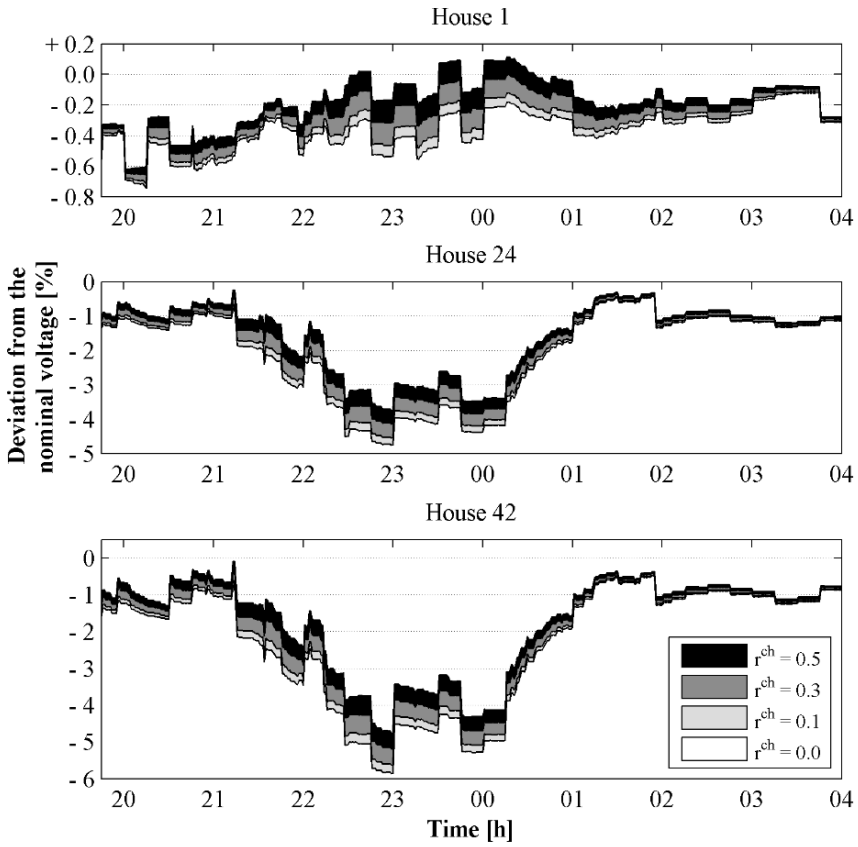

Figure 6.7: Deviation from the rated voltage, for a 50 % PEV penetration.

The impact of reactive power injection on the lower voltages is clearly visible, as these low voltages are induced by the simultaneous charging of multiple PEVs. The profile for house 1 has the lowest voltage deviations, as it is closest to the transformer, house 24 is somewhere halfway, and house 42 is the one the furthest away, resulting in significant voltage deviations. House 1 is connected to a different phase than house 24 and 42, both connected to the same phase. Therefore, the voltage profile for house 1 has a different shape. The results in Figure 6.7 illustrate how the impact of reactive power injection on the voltage magnitude is quasi-linear at a given moment, due to the factor $+(I_q \cdot X)$. For instance, for house 42 at 22.50, the increase of the voltage due to reactive power injection is 0.24 % for $r^{\text{ch}} = 0.1$, 0.71 % for $r^{\text{ch}} = 0.3$, and 1.17 % for $r^{\text{ch}} = 0.5$.

As the F^{VU} values stay below 2 % for more than 95 % of time, for each of the cases and each value of r^{ch}, only the results for the voltage deviations are shown. The highest LV voltage deviations out of the ten conducted permutations are illustrated in Figure 6.8, for an increasing r^{ch}, for a penetration up to 90 %, 50 %, and 100 %, for $c^{\{1,2,3\}}$, respectively. For higher penetration rates, the feeder current limits are exceeded. Also, for c^2 and a PEV penetration of 50 %, r^{ch} is limited to 0.4, as for higher values the feeder current limits are exceeded.

For c^1 and $r^{\text{ch}} = 0$, the LV voltage deviations exceed 7.5 % for a PEV penetration above 70 %. A residential LV distribution grid sized according to the current criteria can already accept a high PEV penetration for uncoordinated charging. For $r^{\text{ch}} \geq 0.3$ (PF ≤ 0.958), the PEV penetration can be further increased up to 90 % without exceeding the LV voltage deviation limit of 7.5 %. A higher PEV penetration is not possible for c^1, because the feeder current limits are exceeded. Thus, by reducing the PF with less than 5 %, the PEV penetration rate for uncoordinated can be increased by more than 28 %.

For c^2 and $r^{\text{ch}} = 0$, only 20 % PEV penetration can be accepted, otherwise the LV voltage deviations exceed 7.5 %, which is due to the PEV charging synchronization at the start of the off-peak tariff period. For $r^{\text{ch}} \geq 0.3$, PEV penetration can be increased up to 40 % while staying below the LV voltage deviation limit. Thus, by reducing the PF with less than 5 %, PEV penetration can be doubled. For $r^{\text{ch}} = 0.4$ (PF = 0.929), the PEV penetration rate can even be increased up to 50 %. However, this implies that a PF of less than 0.95 would be applied, while this is a typical regulatory limit for loads and generation in LV grids. Higher PEV penetration cannot be obtained, because the feeder current limits would be exceeded anyway.

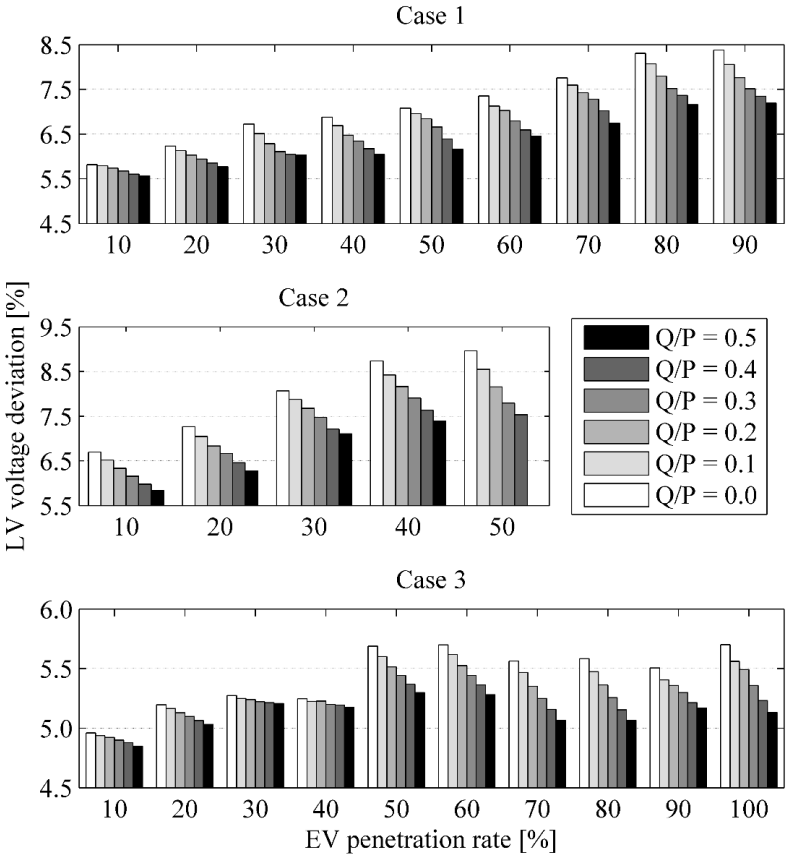

Figure 6.8: Highest occurring LV voltage deviations.

For c^3, a PEV penetration of 100 % can be accepted, regardless of the value of r^{ch}, because the PEV active power peak is significantly lower than for the other two cases (Figure 6.8). Nevertheless, reactive power support also results in significant reductions in the LV voltage deviations, especially for high PEV penetration.

The results indicate a positive impact of reactive power support during PEV charging on LV voltage deviations, for each of the three cases. This impact becomes more significant for an increasing PEV penetration rate, as reactive power injection increases too. Furthermore, the beneficial impact of reactive power support increases as the grid impact of the charging case increases. Therefore, the implementation of a capacitive PF in PEV chargers is very effective in mitigating the grid impact of PEV charging.

6.3.4 Transformer peak load

The highest occurring transformer peak load out of the ten permutations, for each charging case and PEV penetration that does not violate the feeder current limits, is illustrated in Figure 6.9 for increasing r^{ch}. For c^1, the transformer rating (400 kVA) is exceeded for a 80 % PEV penetration rate. The value of r^{ch} only has a marginal impact. For PEV penetration up to 50 %, the peak load slightly decreases when r^{ch} increases. For higher penetration rates, there is an initial decrease in peak load, followed by an increase for higher values of r^{ch}.

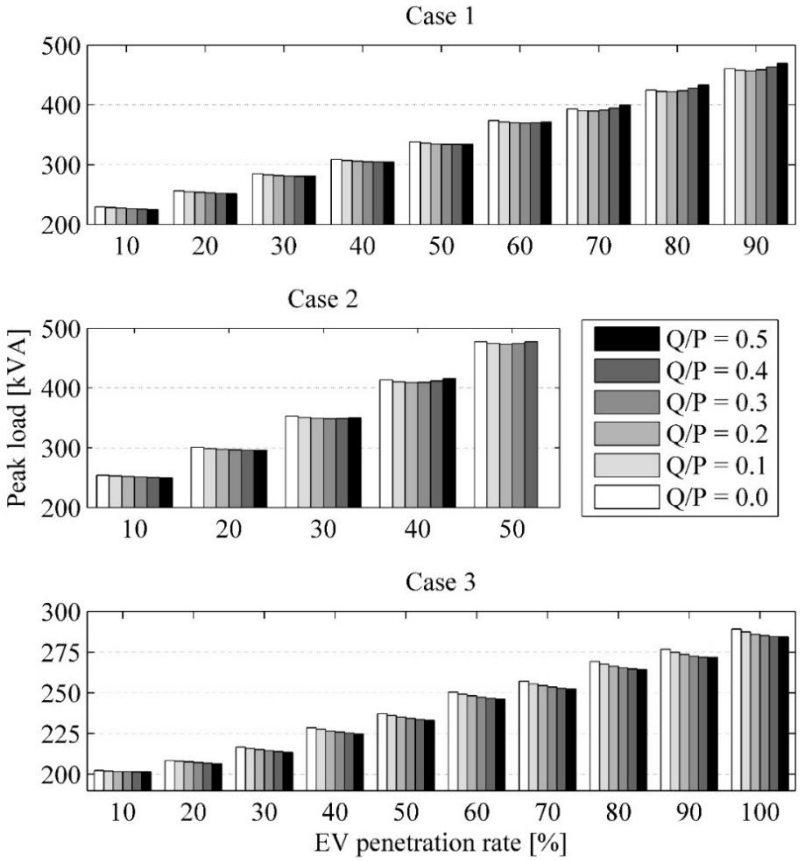

Figure 6.9: Highest occurring LV peak load.

Low amounts of reactive power injection ($r^{\text{ch}} \leq 0.3$) have a beneficial effect, as they supply the required reactive power to offset the reactive power consumption of the LV grid itself, as well as the reactive power consumption of household loads at that moment. Higher amounts of reactive power injection ($r^{\text{ch}} \geq 0.4$) supply more reactive power than required, and the surplus flows to the MV grid, thereby increasing the transformer peak load.

For c^2, the transformer peak load is significantly higher than for c^1, given equal PEV penetration. The transformer rating is exceeded for a 40 % PEV penetration, compared to 80 % for c^1, due to the PEV peak load at the start of the off-peak tariff period. However, the impact of the reactive power on the transformer peak power is similar. For an increasing value of r^{ch}, there is an initial small decrease in peak load followed by a small increase. The lowest peak load occurs for c^3, as it allows for a 100 % PEV penetration while staying below the transformer rating. An increasing value of r^{ch} results in an increasing reduction of the peak load. Similar as for $c^{\{1,2\}}$, the impact of the reactive power injection on the peak load remains relatively small.

The LV transformer peak load is an important metric for the DSO, because of accelerated transformer ageing. For $r^{\text{ch}} \leq 0.3$, there is a beneficial impact on the LV peak load for each charging case and for each PEV penetration. Therefore, no additional transformer ageing is caused by the implementation of reactive power injection in PEV chargers with $r^{\text{ch}} \leq 0.3$.

6.3.5 Grid losses

The power consumption of the LV distribution grid itself is an operational cost for the DSO, which most of the time is recovered through grid tariffs. The ratio of the LV grid power consumption to the energy exchange between the households and the LV grid is illustrated in Figure 6.10.

The trends are similar to these for the LV peak load. The highest and lowest losses occur for $c^2$and c^3, respectively. Furthermore, an increasing r^{ch} leads to an initial small reduction of the grid losses, followed by an increase for $c^{\{1,2\}}$ at higher PEV penetration. As a result, for $r^{\text{ch}} \leq 0.3$, there is no increase in grid losses, and therefore, no additional operational costs for the DSO caused by the implementation of reactive power injection in PEV chargers.

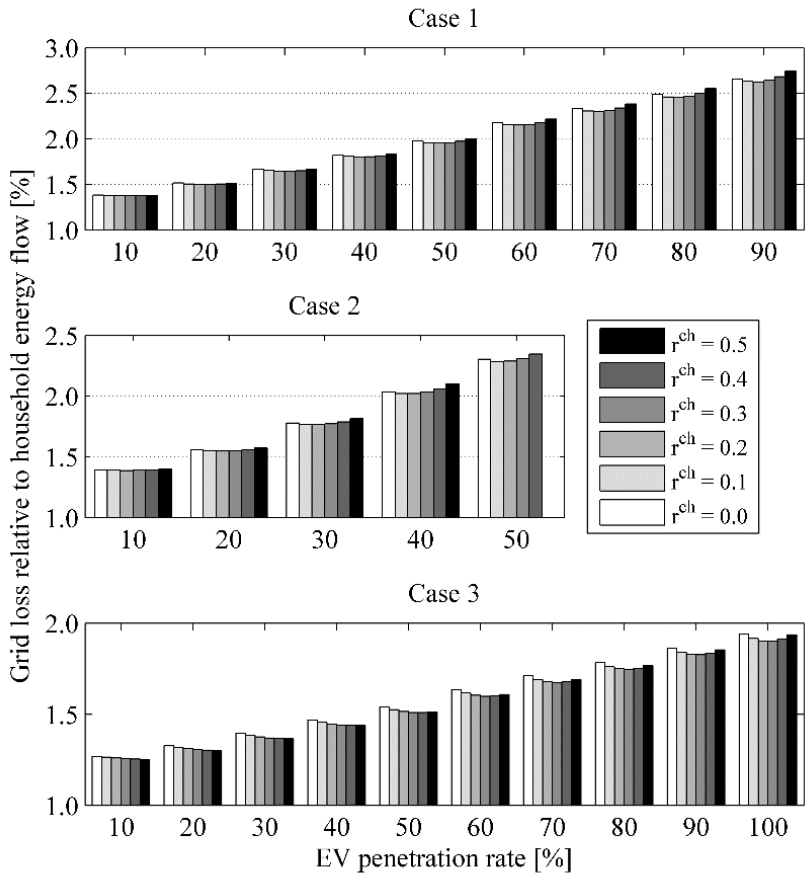

Figure 6.10: Grid losses relative to the household energy flow.

6.4 Grid topology sensitivity

The results from the previous sections are for one specific urban grid, whereas many LV grid layouts occur. Three other real feeder topologies are illustrated in Figure 6.11, representing rural, city, and semi-urban grid topologies, respectively. The main characteristics are summarized in Table 6.5.

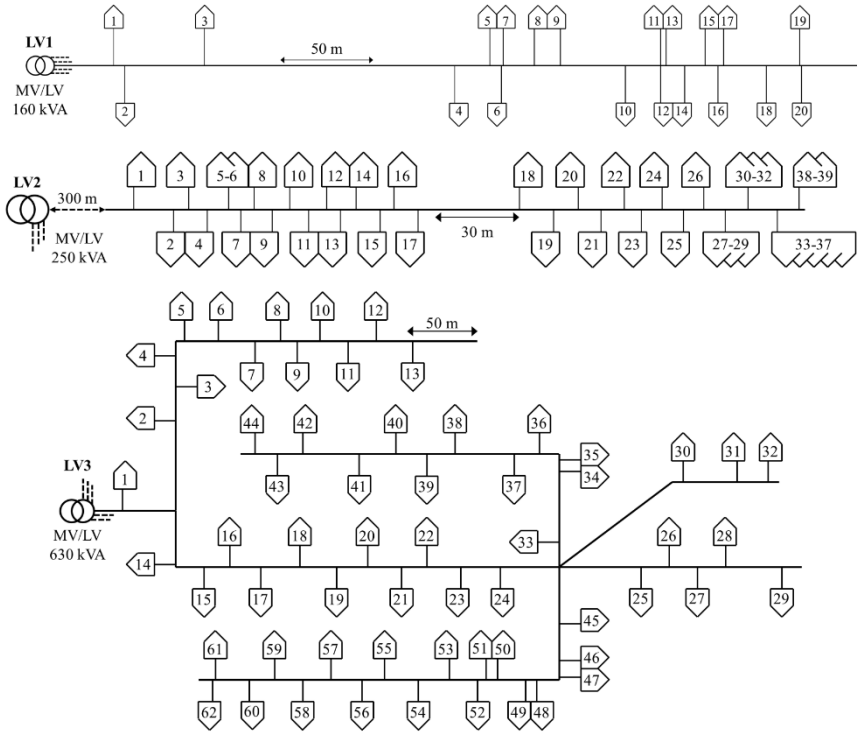

Figure 6.11: Other representative residential LV grid topologies.

Even though the three grids are significantly different, the R/X ratio between the house connection point and the MV grid is within the same range for each of them (1.0 < R/X <3.5), due to the interaction between the impedances of the feeders (primary and secondary) and the distribution transformer. In densely populated areas, cables with a relatively large cross section (R/X < 5) are used, in order not to exceed the current and voltage constraints, which are connected to relatively large distribution transformers. For rural areas, cables with a smaller cross section (5< R/X < 10) are connected to smaller transformers.

The lower R/X ratio for larger cable cross sections is mainly due to the lower specific R value, as the specific X value barely changes for increasing cable cross-sections. As a result, the voltage rise due to reactive power injection $+(I_q X)$ is approximately the same for different cross sections, for a given feeder length. The transformer impedance is mainly inductive and relatively high, characterized by their relative short-circuit voltage u^{sc}.

Table 6.5: LV grid parameters.

Grid		**LV1**	**LV2**	**LV3**
Type		**Rural**	**City**	**Semi-urban**
Cable type	**Primary**	BuAl-4 × 70 mm^2 (areal bundled cable)	Al-4 × 150 mm^2 (underground cable)	
	Secondary	Cu-4 × 16 mm^2 (35 mm^2 at 2th last node LV2)		
I^{max} **[A]**	**Primary**	245	315	
	Secondary	120 (175)		
Z^{cable} **[Ω/km]**	**Primary**	0.551 + 0.088i	0.206 + 0.078i	
	Secondary	1.15 + 0.083i (0.524 + 0.081i)		
# loads/feeder		20	39	62
Parallel feeders	**# Added feeders**	4	3	5
	Length [m]	250	250	300
Total # LV loads		100	156	372
S^{tr} **[kVA]**		160	250	630
Z^{tr} **[Ω]**		0.012 + 0.038i	0.008 + 0.024i	0.003 + 0.010i
R/X		1.24 – 3.04	1.64 - 1.92	1.38 – 2.41

Typically for distribution transformers ($S^{tr} < 630$ kVA), $u^{sc} = 4$ - 6 %. For the MV/LV transformers discussed here, $u^{sc} = 4$ %, in order not to overestimate the grid supportive impact of the reactive power control strategy. The city grid topology is also used in Chapter 5, the urban, city, and semi-urban grid topologies in Chapter 7. However, in those chapters, $u^{sc} = 6$ %, as a conservative approach for the amount of distribution grid resistance, in order not to underestimate the voltage impact of PEV charging.

For a given u^{sc}, smaller transformers have a higher reactance than larger ones ($X^{tr} \sim 1/S^{tr}$), as the fault current limit for the former is smaller than for the latter. Therefore, rural grids have a higher resistance (due to the smaller cable cross-sections), and a higher reactance (due to the higher transformer reactance), compared to urban grids. The resulting voltage drop due to active power offtake $-(I_d R)$ is larger for rural grids, but the voltage rise due to reactive power injection $+(I_q X)$ is also higher, compared to urban grids. Therefore, the total R/X values are in the same order of magnitude.

The results for LV1 are illustrated in Figure 6.12 for c^1, the grid with the highest R/X ratios. The simulation approach and assumptions are identical as in Section 6.2. The voltage deviation constraints are exceeded for a PEV penetration above 20 %, as the grid is already operating close to its limits without PEVs. The feeder current constraints would be exceeded too for a PEV penetration above 20 %. Therefore, a grid infrastructure upgrade is required for PEV penetration rates above 20 %. However, even though the primary feeder has an R/X ratio of 6.26, the impact of reactive power support is still significant, due to the high reactance of the distribution transformer, and the reactance of the feeders. This shows that reactive power injection (PF > 0.95) during PEV charging is an effective measure.

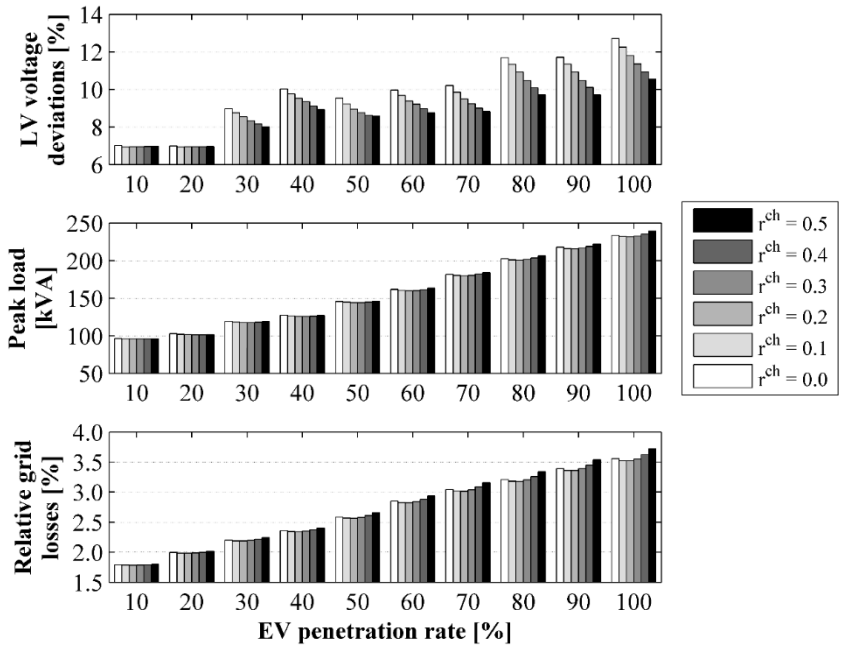

Figure 6.12: Impact of PEVs on LV1.

6.5 Conclusions

The implementation of a capacitive PF for PEV charging provides several benefits for the distribution grid. The voltage deviations in LV grids reduce for an increasing amount of reactive power injection, resulting in an increased PEV hosting capacity for uncoordinated charging and for off-peak residential charging. As a result, LV feeder upgrading investments are deferred. For PEV-based peak shaving, the LV grid can already host 1 PEV for each household (i.e., a 100 % PEV penetration rate) for a unity PF, but there are still significant LV voltage deviation reductions due to the reactive power injection of PEV chargers.

The provision of PEV chargers with a capacitive $PF \geq 0.95$ barely influences the MV/LV transformer peak load, compared to unity PF. Therefore, it does not induce any increased transformer aging, for any of the charging strategies investigated here. The implementation of a capacitive $PF \geq 0.95$ in PEV chargers does not advance transformer upgrade investments, but it also does not postpone them. To obtain the latter, a peak shaving charging strategy is required, for instance PEV-based peak shaving. For a capacitive $PF \geq 0.95$, the grid losses are not higher compared to a unity PF, for each of the charging strategies. Reactive power injection of PEV chargers does not increase the operational costs for the DSO. Similar as for the MV/LV transformer peak load, a peak shaving strategy is required to reduce grid losses.

From the DSO point of view, a capacitive $PF \geq 0.95$ for PEV chargers is beneficial, as it allows deferring infrastructure investments in residential LV distribution grids. Even though the active power control strategies have a vastly more significant grid impact than reactive power injection, its impact is beneficial for the three active power control strategies discussed. Moreover, the beneficial grid impact of reactive power injection increases for an increasing PEV penetration and for active power control strategies that lead to high peak loads. Thus, when the grid impact of PEV charging is high, the beneficial impact of a capacitive PF is high as well, thereby making it an effective means for grid impact mitigation of PEV charging.

From the PEV user point of view, a capacitive PF has no impact on the charging behavior, opposed to the active power control strategies, if the PEV chargers are adequately sized for the higher required apparent power requirement. For a capacitive $PF \geq 0.95$, the required PEV charger apparent power rating needs to be increased by less than 5.5 %. This limited increase in power and current requirements does not require an upgrade of the charging infrastructure, as it falls well within the safety margins of the infrastructure sizing. Otherwise, for an equal apparent power, the charging time would only increase by less than 5 %, which only has a limited marginally impact on the user comfort.

Given the considerable benefits, it should be considered to include capacitive power behavior in the grid compliance requirements for PEV chargers. The efficacy of voltage support through reactive power injection is strongly dependent on the R/X ratio, as a high ratio results in a low efficacy and vice versa (Eq. 6.1 and Figure 6.1). Even though the R/X ratio for feeders with different cross section can significantly differ, the total R/X ratio between the grid connection and the MV grid is similar for the different grid topologies, as the MV/LV transformer impedance is not negligible. It is up to the stakeholders to determine which is the most suitable PF to include in the grid compliance requirements, as a lower PF leads to decreased voltage deviations, but trade-offs include increased PEV charger power ratings, increased grid losses, and increased LV peak loads, for PF < 0.95.

7. Fast charging

The combined LV and MV residential grid impact is investigated for slow and fast PEV charging, for an increasing local penetration and for different residential slow charging strategies. A realistic case study is used, for which three residential slow charging strategies are modeled: uncoordinated charging, residential off-peak charging, and PEV-based peak shaving. For each slow charging strategy, the PEV hosting capacity is determined, with and without the possibility of fast charging, while keeping the grid within its operating limits.

The content of this chapter has been based on the peer-reviewed paper:

- N. Leemput, F. Geth, J. Van Roy, P. Olivella-Rosell, J. Driesen, and A. Sumper, "MV and LV residential grid impact of combined slow and fast charging of electric vehicles," *Energies (Special Section on "Electrical Power and Energy Systems for Transportation Applications")*, vol. 8, no. 3, pp. 1815-1822, March 2015.

The chapter is structured as follows. The background on fast charging infrastructure for PEVs is discussed in Section 7.1. The used materials and methods are explained in Section 7.2. The results are discussed in Section 7.3, followed by the conclusions in Section 7.4.

7.1 Background

7.1.1 Complementarity of slow and fast charging

Due to the typically long standstill times at home and at the workplace [128], and the low average daily driven distances [288], a low charging power at these locations is sufficient to fulfill the majority of the mobility needs, thereby keeping the charging infrastructure investments low. Typically, Mode 2 or Mode 3 charging, as defined in the IEC 61851-1 standard [104] and discussed in Section 2.3, are used to charge PEVs at their standstill locations. The standstill times at charging locations exceed the required charging time for the vast majority of the mobility requirements, as discussed in Section 3.4. As a result, the majority of mobility requirements can be met with low power charging infrastructure.

For occasional long-distance trips, fast charging is a necessary addition to slow charging, to allow for long-distance electric driving. The implementation of fast charging networks that cover large contiguous regions make BEVs a viable alternative

for conventional vehicles [59], [63]. The power rating for fast chargers vary from 50 kW [63] up to 120 kW [59], which allows to recharge PEVs within an acceptable time span, typically within half an hour. Multistandard fast chargers provide compatibility with the different types of fast charging standards used nowadays [63].

For fast charging, two typical infrastructure configurations are used. The first one is a network of single- or dual-outlet fast chargers that allow to reach the next fast charger. This is a configuration for the initial rollout of fast charging infrastructure [289]. The fast chargers are connected to the local LV grid, and therefore, the grid impact will strongly depend on the local situation, e.g., being connected to the distribution transformer through a separate or an existing feeder.

In the second configuration, fast charging stations with multiple fast chargers (≥ 4) are located next to the busy traffic arteries. These stations resemble conventional highway refueling stations in their setup, and are typically commercially operated [63], or they are dedicated to one specific brand [59]. Because the total power rating of such stations is in the order of magnitude of a typical European residential LV grid (≥ 200 kVA), they are connected to the medium voltage (MV) grid through a dedicated transformer.

7.1.2 Research on fast charging infrastructure

Several aspects of fast charging are investigated in the literature: economic, infrastructure usage optimization, MV grid impact, and power electronic converter design. An economic analysis on fast charging infrastructure is performed for Germany [290] and China [291]. For both countries, it is concluded that fast charging infrastructure is hardly profitable with the present energy pricing and battery costs, and a high PEV penetration is required for a profitable exploitation [290]. Both [290] and [291] do not use a time-based fast charging scenario in their modeling, as this is not the scope of an economic analysis.

Traffic modeling is used to determine the fast charging demand in space and time in [292]. The optimization of PEV charging scheduling for highway fast chargers is discussed in [293] and [294]. The time-based occupation of the fast charging stations, and the variation of the PEV battery state of charge at the start of the highway trip are based on a mathematical distribution, not on mobility behavior or slow charging behavior.

The MV grid impact of fast charging stations is discussed in [295]-[297]. A static worst-case load scenario is modeled in [295], assuming all fast chargers are used simultaneously at their rated power. Time-based vehicle arrival pattern of conventional refueling stations are used in [296], and time-based road occupation

profiles are used in [297], to model the demand for fast charging. No slow charging behavior is taken into account, and in [296] and [297] it is assumed that the PEVs continuously draw the rated fast charging power. Voltage unbalance, due to single-phase loads connected to the MV grid, besides the three-phase fast charging infrastructure, is not taken into account.

The electric and power electronic design of fast chargers is discussed in [298] and [299]. As these components need to be sized for the peak load, a worst-case scenario for the fast charging demand is used. The design of a fast charging station with local energy storage and local photovoltaic power generation is discussed in [300]. The fast charging demand is based upon mobility behavior and takes into account residential slow charging. The load flow is not assessed, because the scope is on sizing the fast charging station and the power flow between its components.

7.1.3 Scope

To the best of the authors' knowledge, neither the combination of slow nor fast charging, nor the combined MV and LV grid impact assessment are investigated in the literature. Both slow and fast charging behavior are modeled here, because they interact, thereby influencing the MV and LV grid impact, as both network levels influence each other. A realistic distribution grid topology and scenario are used here: realistic single-phase household load profiles and measured photovoltaic (PV) power generation profiles. The PEV charging behavior is based upon Flemish mobility behavior and passenger vehicle fleet composition.

Three residential slow charging strategies are compared in terms of their PEV hosting capacity, with and without the presence of fast charging. Fast charging is modeled to supplement slow charging at home and the workplace, when the battery capacity is insufficient to fulfill the mobility requirements otherwise. The fast charging infrastructure is assumed to consist of charging stations with multiple fast chargers, sized to fulfill the fast charging demands in the area it covers. The fast charging stations are connected to the MV grid through a dedicated transformer.

7.2 Materials and methods

7.2.1 Distribution grid data

Three (semi-) urban feeder topologies are used to model three residential LV grids (Figure 7.1 and Table 7.1). The grid modeling is explained in detail in Section 5.2.1. These three feeders, which are also used in Chapter 6 (Section 6.4), are connected to

three different MV/LV transformers with three common power ratings: 250, 400, and 630 kVA. Also for these grids, simplified parallel feeders are added [283] (Table 7.1).

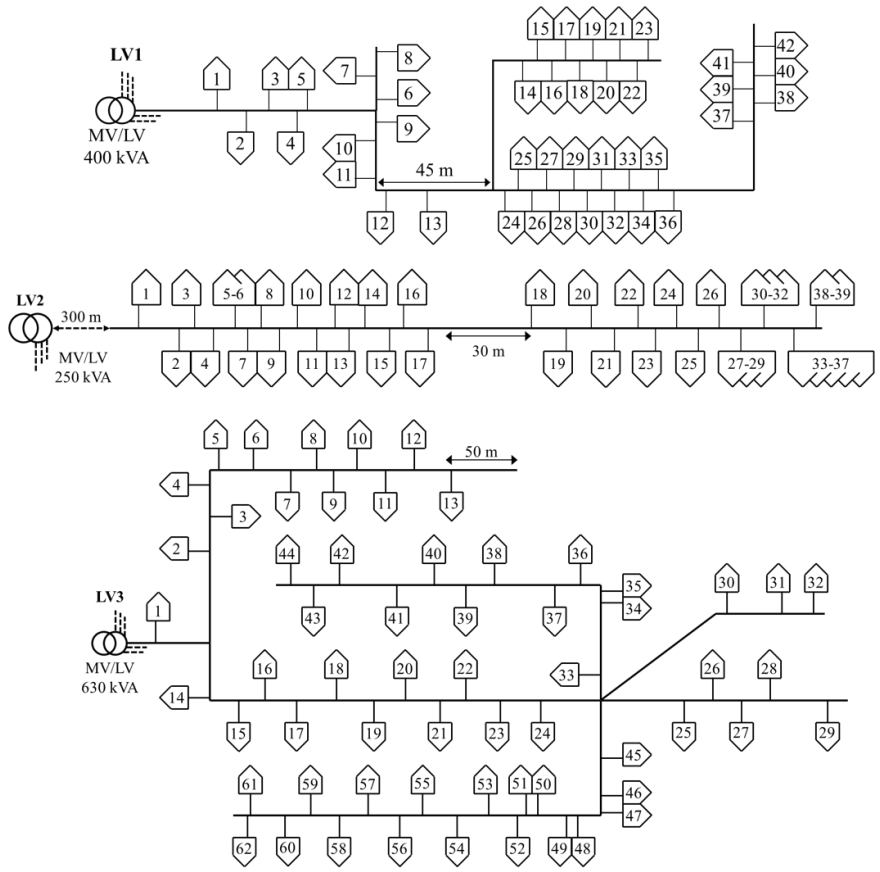

Figure 7.1. LV grid topologies.

The transformer taps are set at 1 pu. A higher tap could be selected to increase the lowest occurring voltages, which would reduce the impact of PEV charging on voltage deviations. However, this would also increase the highest occurring voltages, as no on-load tap changers are used at MV/LV transformers. This can cause overvoltages at moments of high residential PV generation [301]. Therefore, the taps are chosen at 1 pu here, to provide a realistic scenario for a residential distribution grid with PV power generation. Different tap settings would obviously influence the results, but qualitatively the comparative analysis remains the same.

Table 7.1: LV grid parameters.

Grid		LV1	LV2	LV3
Cable type	**Primary**	Al-4x95 mm^2	Al-4x150 mm^2	
	Secondary	Cu-4x16 mm^2 (35 mm^2 at 2th last node LV2)		
I^{max} **[A]**	**Primary**	245	315	
	Secondary	120 (175)		
Z^{cable} **[Ω/km]**	**Primary**	0.320+0.078i	0.206+0.078i	
	Secondary	1.15+0.083i (0.524+0.081i)		
# nodes/feeder		42	29	62
# loads/feeder		42	39	62
Parallel feeders	**# Added feeders**	5	3	5
	Length [m]	250	250	300
Total # LV loads		252	156	372
Z^{tr} **[Ω]**		0.008+0.029i	0.013+0.045i	0.004+0.020i

The three LV grids are each used three times, together with the fast charging station (FCS), to connect to a MV feeder with 9 nodes (Figure 7.2). As a result, a total of 2340 household loads are connected to the MV feeder. The rated MV line-to-line voltage is 11 kV, and the distance between each node is 600 m. This is a realistic urban MV feeder topology [66], where MV grids are operated in an open-ring topology with few or absent laterals [302]. The MV cable is a three-core armored aluminum conductor, i.e., Al 11 kV-3x95 mm^2, with an impedance of 0.411+0.105i Ω/km, and a current rating of 200 A [303].

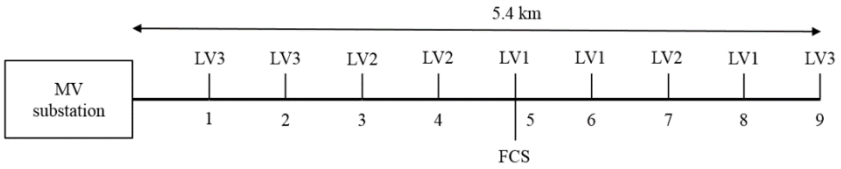

Figure 7.2: MV grid topology to which the LV grids and the fast charge station (FCS) are connected.

The end-user distribution grid voltages should stay within the operation limits of the EN50160 standard [73], as discussed in Section 2.4.3 for the voltage magnitude and voltage unbalance, respectively. In the planning and design phase, the goal is to keep the grid voltage magnitude deviations within the 10 % range (Eq. 2.1). During measurements in the field, a 15 % deviation for under voltage is allowed for 5 % of time on a weekly base (Eq. 2.2). Thus, for the simulation-based grid impact assessment that is conducted here, the limits of Eq. 2.1 are applicable. If the voltage deviations exceed the grid constraints, the DSO will have to invest in grid reinforcements. For instance, the LV feeder will (partially) be upgraded to a larger cross section.

The voltage magnitude and unbalance constraints, together with the feeder current constraints, determine how much PEV charging load the distribution grid can accept, additional to the residential load and the PV power generation. As a result, these constraints determine the PEV hosting capacity. The transformer power rating is not a hard real-time constraint (Section 2.4.3). Therefore, the impact of both slow and fast PEV charging are discussed in Section 7.3.5.

7.2.2 Residential load and generation

A residential electric load profile generator is used to create a statistically representative set H_o of single-phase Flemish household electric power consumption profiles h, with a 15 min time resolution, as discussed in detail in Section 6.2.2. Here, a unity PF is assumed for the household loads, because reactive power is not includes in the profile generator, and the impact of reactive power behavior is discussed in detail in Chapter 6.

Similar to Chapter 6, a PV installation is randomly assigned to 10 % of the houses. The random assignment of the PV installation locations on the detailed feeders, is done to take into account the locational sensitivity of their grid impact. In Appendix C, the specific location are summarized (Table C.1). Also here, the profiles are based upon full-year measurements, and they are scaled to match the annual generation volume to the annual consumption at the selected household. The single-phase regulatory inverter power rating limit of 5 kVA is taken into account [279], and a unity PF of 1 is assumed for the PV power generation [280].

7.2.3 PEV charging behavior

The fleet modeling (Chapter 3) is used to create a representative set of PEVs, as explained in detail in Section 5.2.3. For slow charging, the same single-phase Mode 3 charger power rating $P_{\text{rat}}^{ch} = 3.3$ kW is used as in Chapter 5 and 6, and the same end-

of-charge power limit $P^{\mathrm{EOC}}(SOC_k)$ as in Chapter 6 (Figure 7.3). The three slow charging cases c (Table 7.2) are compared to the case without PEVs (c^0). These strategies are explained in detail in Section 6.2.3, and represent three typical charging objectives: high comfort (uncoordinated charging), low charging cost (off-peak charging), and low grid impact (PEV-based peak shaving). Each slow charging case is simulated (a) without and (b) with fast charging. The PEVs are modeled as EREVs for the cases without fast charging (as in Chapter 5 and 6), while they are modeled as BEVs for the cases with fast charging. The battery capacities are doubled in this chapter (20, 30, and 40 kWh), to provide a realistic scenario for the fast charging requirements of BEVs.

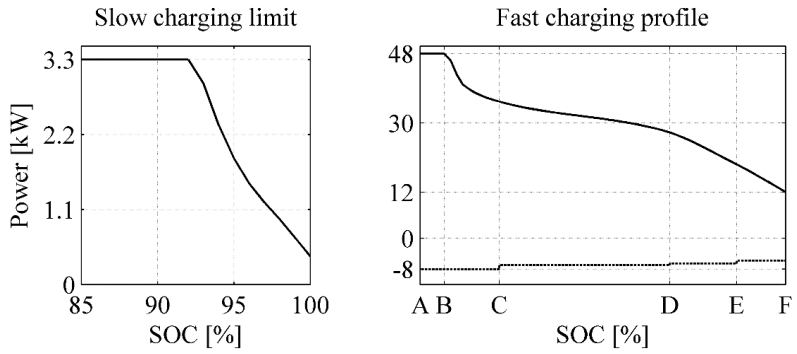

Figure 7.3: Charging power limit for slow charging (left), and for active (solid line) and reactive (dashed line) power profile for fast charging (right).

Table 7.2: Summary of the slow charging cases.

Case c	**Description**
0	No PEVs
1a	Uncoordinated charging without fast charging
1b	Uncoordinated charging with fast charging
2a	Off-peak charging without fast charging
2b	Off-peak charging with fast charging
3a	PEV-based peak shaving without fast charging
3b	PEV-based peak shaving with fast charging

The fast charging demand is modeled as discussed in [300]. The PEVs interrupt their trip if the SOC goes below the threshold value $SOC(th)$, chosen uniformly between 20 and 30 % for each trip: $SOC(th)\ \epsilon\ \{20\ \%\ ...\ 30\ \%\}$, to take into account that a PEV is not exactly located at a fast charging station when the SOC reaches the 20 % limit. When fast charging occurs, it is assumed that the battery will be fast charged up to 80 % SOC. The fast charging power profile $P^{\mathrm{FC}}(SOC_k)$, as illustrated in Figure 7.3, is based upon real measurements [43]. Point A and point F coincide with $SOC(th)$ and point 80 %, respectively. As a result, depending on $SOC(th)$, points B to E occur at a different SOC values (Table 7.3).

Table 7.3: Calculation of the SOC values for the fast charging profile.

Point	SOC **value**
A	$SOC(th)$
B	$SOC(th) + \big((SOC(F) - SOC(th)) \cdot (1/15)\big)$
C	$SOC(th) + \big((SOC(F) - SOC(th)) \cdot (1/5)\big)$
D	$SOC(th) + \big((SOC(F) - SOC(th)) \cdot (2/3)\big)$
E	$SOC(th) + \big((SOC(F) - SOC(th)) \cdot (5/6)\big)$
F	80 %

Reactive power injection Q^{FC} of fast chargers into the grid is included in the simulations [43]. The reactive power injection decreases in 4 discrete steps, as a function of the active fast charging power that is drawn. This capacitive behavior is implemented in the fast charger by the manufacturer, as a way to reduce the voltage drop induced by the fast charger.

7.2.4 Simulation approach

The simulations are conducted for a one-week scenario, resulting in a number of time steps n_t = 10 080, i.e., $k\ \epsilon\ \{1, 2, \dots, n_t\}$. The scenario is conducted for a week representative for the first quarter of the year, because this is the period of the year when high grid loads occur in Northwestern Europe. Therefore, the grid constraints are exceeded the soonest when additional load, due to PEV charging, is added. The simulations are conducted for a PEV penetration increasing in steps of 10 % up to 100 %, or until the load flow offers no feasible solution. In Appendix C, the LV feeder locations of the PEVs added for each step are summarized (Table C.2). The locations are diversified, to take into account the locational sensitivity of the results.

For each 1′ time step ΔT, the evolution of SOC_k for each PEV is calculated (Eq. 3.11). The resulting residential PEV charging profile is added to the residential load and generation profile at the respective LV grid nodes. The residential load and generation profiles are kept constant for 15′. The aggregated fast charging load is added to the 5th node on the MV grid through a separate MV/LV transformer (Figure 7.2). No workplace charging locations are assumed in this residential grid.

To obtain grid impact results, a three-phase unbalanced load flow algorithm is implemented in MATLAB. Unbalanced loads are taken into account, as well as the resulting LV neutral conductor voltage drop. The backward-forward sweep technique is used, because of the radial layout of the grid [282]. The problem is converged when the worst time step voltage error eV is below 0.1 V. All loads are modeled as constant power loads with unity power factor, except for the fast chargers, injecting a reactive power $Q^{\mathrm{FC}}(SOC_k)$ during fast charging (Figure 7.3).

For each charging case, the PEV hosting capacity is calculated, which is the highest PEV penetration rate that can be achieved without exceeding the feeder current constraints and the grid voltage constraints.

7.3 Results and discussion

7.3.1 User impact

To assess the dependency of the PEVs on their range extender for the cases without fast charging, the utility function F^{U} is used [7]. Obviously, F^{U} is 100 % for each PEV when fast charging is possible, given that the fast charging stations have a sufficient geographical distribution. For all cases without fast charging, the maximum F^{U} is 100 %, i.e., there is at least one vehicle in the fleet of 2,340 PEVs that will drive purely electrically during the simulated week. For $c^{\{1\mathrm{a},\,3\mathrm{a}\}}$, the minimal and mean F^{U} are 84.2 % and 96.7 %, respectively. The values are identical for both cases, because they provide the same SOC by the next departure time. For $c^{2\mathrm{a}}$, it has a marginally lower minimal and mean F^{U} (82.6 % and 96.2 %). The difference compared to $c^{\{1\mathrm{a},\,3\mathrm{a}\}}$ is very small, because the charging time is usually well below the standstill time within the off-peak time span.

The total required electric driving energy for the PEVs is 171 MWh, for the fleet of 2340 PEVs during the one-week simulation period. This accounts for the energy being delivered to the PEV batteries, by slow and fast charging for the b-cases, and by slow charging and the range extender for the a-cases. The share of charging energy at the different locations is summarized in Table 7.4. The majority of PEV charging occurs

at home, while workplace charging only accounts for 5.6 % to 6.7 % of the charging energy, due to the low average distance between home and the workplace. For c^2, the slightly higher share in workplace charging energy is due to the limitation of the charging time at home. Therefore, sometimes the PEV is not fully charged when leaving home to go to work. As a result, more charging energy is delivered at the workplace.

Table 7.4: Share of charging energy for the different locations.

Case *c*	**1/3a**	**1/3b**	**2a**	**2b**	
Home (slow)	94.0	83.3	93.3	81.1	
Work (slow)	6.0	5.6	6.7	6.0	**[%]**
Fast	/	11.1	/	12.9	

Fast charging delivers 11.1 % up to 12.9 % of the charging energy, depending on the slow charging case. The presence of fast charging mainly reduces the share of residential charging energy, as can be seen when comparing the shares of charging energy at home of the a-cases with the b-cases. The share of fast charging energy strongly depends on the assumptions being made.

In theory, fast charging could be used to charge the batteries exactly up to the SOC required to reach the next charging destination, instead of charging up to 80 % by default. Also, if the fast charging infrastructure would be perfectly spread out, each PEV would reach a fast charge station when their battery SOC reaches the 20 % threshold value. Under these theoretical assumptions, the share of fast charging energy would equal the share of energy being delivered by the range extenders for the cases without fast charging, i.e., 3.3 % for $c^{\{1b,\,3b\}}$, and 3.8 % for c^{2b}. Furthermore, larger battery capacities will also decrease the need for fast charging. For example, a doubling of the battery capacities decreases the share of fast charging energy to 2.3 % for $c^{\{1b,\,3b\}}$, and 3.2 % for c^{2b}.

7.3.2 Charging behavior

As a detailed illustration of the differences in charging behavior, the charging profile for a single PEV is shown in Figure 7.4 for a 17 h timespan, for $c^{\{1b,\,2b,\,3b\}}$. Also, the evolution of the SOC is shown. The fast charging profiles are identical for the three cases, while the residential charging profiles are different. The latter is similar in shape for c^{1b} and c^{2b}, but shifted in time. For c^{1b}, the charging process at home starts

immediately when the PEV arrives there (around 21:15), while for c^{2b}, it starts at 22:00, when the off-peak tariff period starts. For c^{3b}, the charging also starts immediately when arriving at home, but with charging power significantly reduced, because in this example, there is a long standstill time at home before the next departure (> 15 h). As a result, the SOC rises more slowly for c^{3b} than for $c^{\{1b,\,2b\}}$. This clearly illustrates how the slow charging profiles are significantly affected by the applied charging strategy.

The aggregated grid impact of the PEV charging behavior is illustrated for a 40 % PEV penetration (936 PEVs), for a 12 h timespan (Figure 7.5). The highest residential charging peak occurs for c^{2b}, which results in the highest MV feeder load, due to the synchronization effect that occurs at the start of the off-peak tariff period, which does not occur for c^{1b}, because the distribution of the arrival at home of PEVs. The lowest peak power occurs for c^{3b}, resulting in the lowest MV feeder load, due to the combination of the spread on the PEV arrival times at home, the SOC when arriving at home, and the time until the next departure. Therefore, there is a spread on the charging time and charging power, significantly reducing the peak load (Figure 7.5).

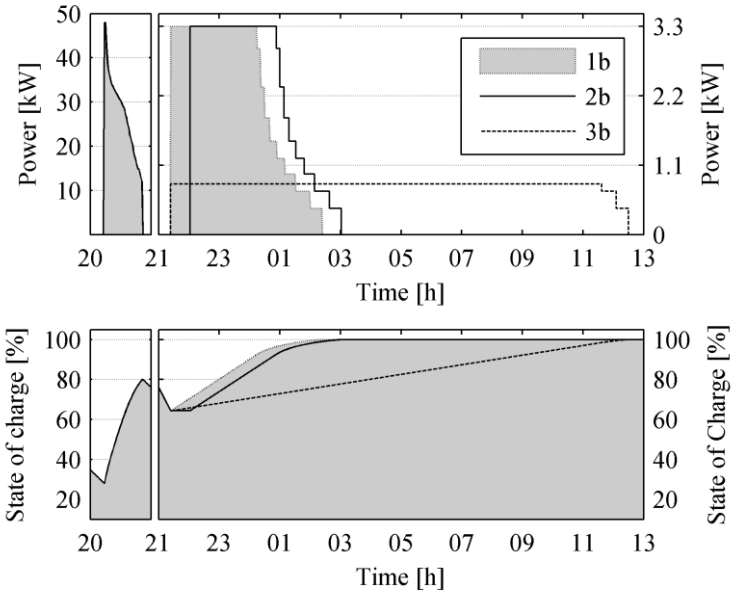

Figure 7.4: Fast (left) and slow (right) charging profiles (top), and the evolution of the state of charge (bottom).

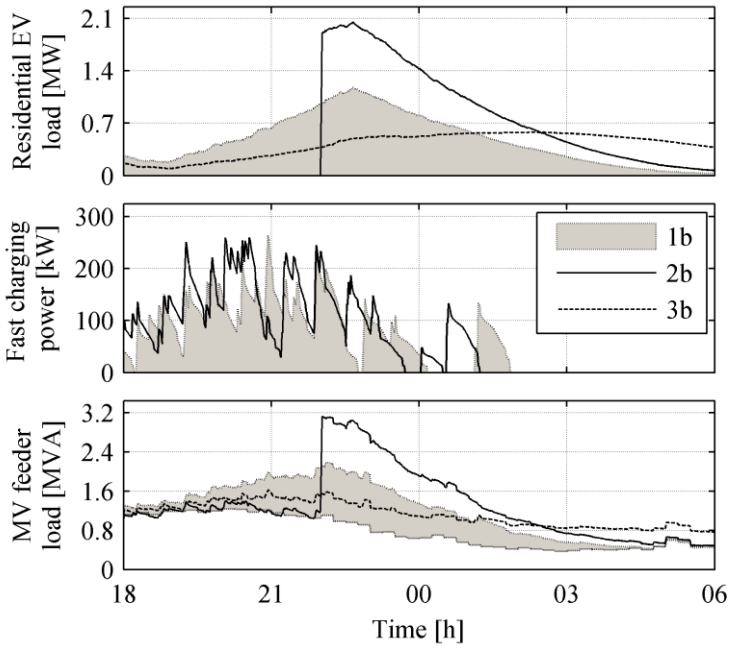

Figure 7.5: Load impact for a 40 % PEV penetration rate. The white surface in the bottom figure represents the non-PEV residential load.

The fast charging profiles are identical for c^{1b} and c^{3b}, as the SOC for both cases is identical at the time of departure. As a consequence, the SOC profiles are identical during driving, so there is an identical need for fast charging for both cases. The fast charging profile is different for c^{2b}, but it has similar peak values, as the need for fast charging is only slightly higher (Table 7.4).

The fast charge peak load is significantly lower than the residential slow charging peak, as it only accounts for a small share of the charging actions. Therefore, the grid impact of the slow charging strategy is more significant than the presence of fast charging. The aggregated fast charging infrastructure occupation and the resulting power consumption peaks during the evening traffic peak [300], but in contrast to conventional petrol station occupation, there is no peak during the morning traffic peak, as the PEVs charged at home overnight.

7.3.3 PEV hosting capacity

The impact of the PEV load on the grid per-phase nodal voltages is illustrated in detail, for a one-hour time period between 19 h and 20 h, for c^{1b}, with a 40 % PEV penetration (Figure 7.6). The per-phase MV feeder load and the resulting per-phase voltages at the 9th node of the MV feeder are shown. The per-phase LV grid load at the 9th MV node are illustrated, as well as the nodal voltages at the LV node the farthest away from the MV/LV transformer (node 62 of feeder topology LV3) that is connected to the 9th MV node.

The fast chargers each have a three-phase grid connection, therefore they act as a balanced grid load. The unbalanced residential loads and PV power generation result in noticeable differences in the nodal phase voltages. The difference in the per-phase voltage magnitudes exceeds 0.01 pu at the 9th node of the MV feeder, and they exceed 0.05 pu at the 62th node of the LV feeder. This illustrates the added value of performing an unbalanced load flow (as will be discussed below), otherwise the voltage deviations are underestimated when assuming a balanced situation at the MV/LV interface. As a result, the PEV hosting capacity would be overestimated.

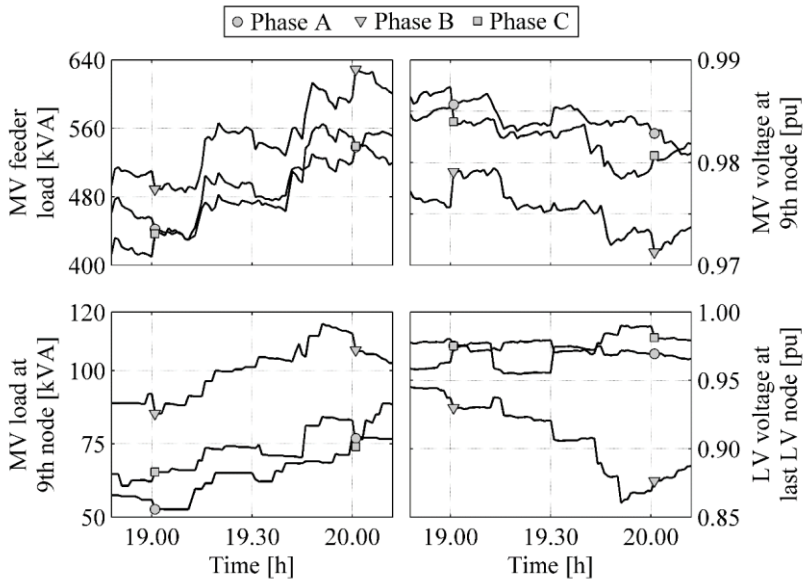

Figure 7.6: Per-phase load profiles (left) and voltage magnitudes (right), at the last MV node (top) and the last LV node (bottom), for c^{1b} with a 40 % PEV penetration.

For each charging case c, the PEV hosting capacity is calculated as the maximum PEV penetration rate $R_{\mathrm{MAX}}^{\mathrm{PEV}}$ that can be accepted, while not exceeding the grid voltage and feeder current constraints. The resulting PEV hosting capacity for the charging cases are summarized in Table 7.5. For each case considered, the voltage magnitude constraints (Eq. 2.1) are the most stringent. The cases without fast charging result in an equal or higher $R_{\mathrm{MAX}}^{\mathrm{PEV}}$ than ones with fast charging. However, the differences are limited to only 10 percentage points, which is equal to only 1 step of increase in the PEV penetration rate. This is due to the limited share of fast charging in the charging behavior of the PEVs, while residential charging accounts for the vast majority of charging actions.

Table 7.5: PEV hosting capacity [%].

Case c	1a	1b	2a	2b	3a	3b
$\boldsymbol{R_{\mathrm{MAX}}^{\mathrm{PEV}}}$	80	70	50	40	100	100

$R_{\mathrm{MAX}}^{\mathrm{PEV}}$ is more influenced by slow charging than whether or not fast charging occurs, as differences up to 60 percentage points occur. These results show that the additional grid impact due to the presence of fast charging can easily be compensated for by the implementation of a more grid-friendly residential charging strategy. For instance, by incentivizing PEV users to start charging immediately when arriving at home $\left(c^{\{1\mathrm{a},\,1\mathrm{b}\}}\right)$ instead of waiting until the off-peak tariff period starts $\left(c^{\{2\mathrm{a},\,2\mathrm{b}\}}\right)$, a significantly higher $R_{\mathrm{MAX}}^{\mathrm{PEV}}$, even if fast charging is possible. This is due to the synchronization effect of PEV charging at the start of the off-peak tariff period for $c^{\{2\mathrm{a},\,2\mathrm{b}\}}$, creating a peak in the power demand.

This off-peak PEV charging synchronization creates a voltage drop that negates the beneficial effect of shifting the charging load away from the time of the residential peak demand. An even higher $R_{\mathrm{MAX}}^{\mathrm{PEV}}$ is possible when PEV-based peak shaving is applied $\left(c^{\{3\mathrm{a},\,3\mathrm{b}\}}\right)$, as it allows for a 100 % PEV penetration rate for the scenario discussed here, whether or not fast charging occurs. Therefore, when the local PEV penetration rate increases to significant levels, the PEV users should be incentivized to charge in a more grid-friendly manner, as this can allow for a substantially higher PEV hosting capacity with the same grid infrastructure.

7.3.4 Fast charging requirements

The fast charging power peak and the one percent peak (OPP) value are illustrated in Figure 7.7 for PEV penetration rates up to $R_{\mathrm{MAX}}^{\mathrm{PEV}}$. The OPP is the value above which only 1 % of the values are situated. For $c^{1\mathrm{b}}$ and $c^{3\mathrm{b}}$, the values are identical for fast charging, but the values for penetration rates above 70 % are only applicable for $c^{3\mathrm{b}}$, as this is the $R_{\mathrm{MAX}}^{\mathrm{PEV}}$ for $c^{1\mathrm{b}}$. For $c^{2\mathrm{b}}$, the values only marginally differ from those of the other two cases, as the fast charging requirements are very similar.

The OPP for fast charging power is significantly smaller than the peak value, as the maximal fast charging power is only drawn for a short period and quickly declines as the SOC increases (Figure 7.3). Therefore, the MV/LV transformer that connects the fast charging station to the MV grid, might be sized for a power rating smaller than the expected peak value, as this value only occurs for a very short time.

As 19 fast chargers are needed to cover the peak occupation, but 16 fast chargers are sufficient for the OPP, it might be more efficient to allow for a limited waiting time during peak situations, to avoid investing in additional chargers. Furthermore, this would lower the grid impact of the fast charging infrastructure. These results are in line with [300], where the number of fast chargers is reduced by 40 %, resulting in waiting times below 10′ for 99.7 % of time.

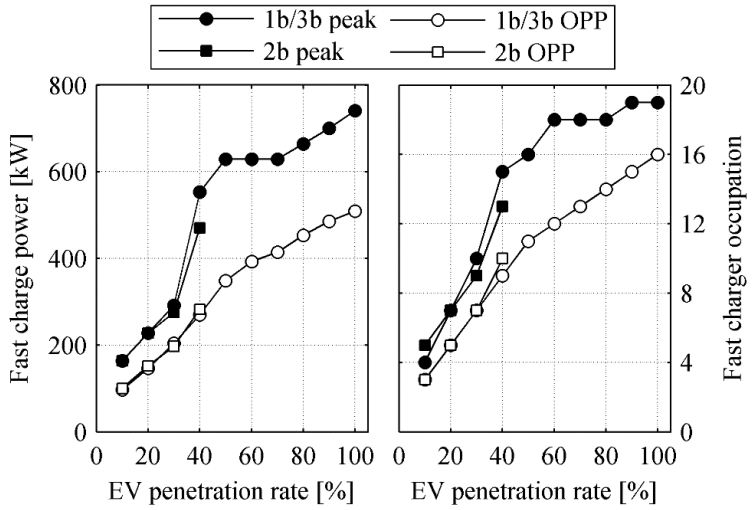

Figure 7.7: Peak values and one percent peak (OPP) for the fast charging load (left), and fast charger occupation (right).

For an increasing PEV penetration (from 10 % to 100 % for $c = 3b$), the ratio of fast chargers to PEVs lowers significantly: from 3 % to 0.9 % for the peak value, and from 1.7 % to 0.7 % for the OPP. This means that there is a need for one fast charger for each 111-142 PEVs, when there are sufficient PEVs on the roads This number can be compared to the ratio of fuel stations per car in Europe, which varies from 1/1500 (Luxembourg) to 1/3500 (Germany) stations per vehicle [304]. Thus, for a fast charging infrastructure with the same spatial spreading as the current fueling infrastructure and a 100 % PEV penetration rate , the fast charging infrastructure would consist of stations with on average 11-25 fast chargers to cover the OPP, or with on average 14-32 fast chargers to cover the peak value.

An increase in PEV battery capacity would decrease the ratio of fast chargers to PEVs significantly, because the share of fast charging increases significantly when the PEV battery increases (Section 3.1). For the cases discussed here, a doubling of the PEV battery capacities would reduce the peak value and the OPP value for the ratio to 0.4 % and 0.3 %, for a 100 % PEV penetration. The resulting fast charging infrastructure would consist of stations with on average 5-11 fast chargers to cover the OPP, or on average 6-14 fast chargers to cover the peak value. These results show that the fast charging infrastructure needs to be extensive, even though it only account for a minority of the charging actions, as fast charging fuels a vehicle more slowly than a fuel pump.

7.3.5 Peak load

The MV distribution feeder peak load, and the highest MV/LV residential grid transformer load are shown in Figure 7.8. The presence of fast charging reduces the LV residential peak load, but only slightly, as the presence of fast charging only accounts for a limited amount of the charging energy. Fast charging increases the peak load on the MV feeder. These opposing trends show how the presence of fast charging substitutes a fraction of the home charging actions. However, the difference in grid impact between the three slow charging cases is substantially larger than the difference between the situation with or without fast charging. Therefore, the increased grid impact of fast charging can be mitigated in an effective manner by implementing a grid-friendly slow charging strategy.

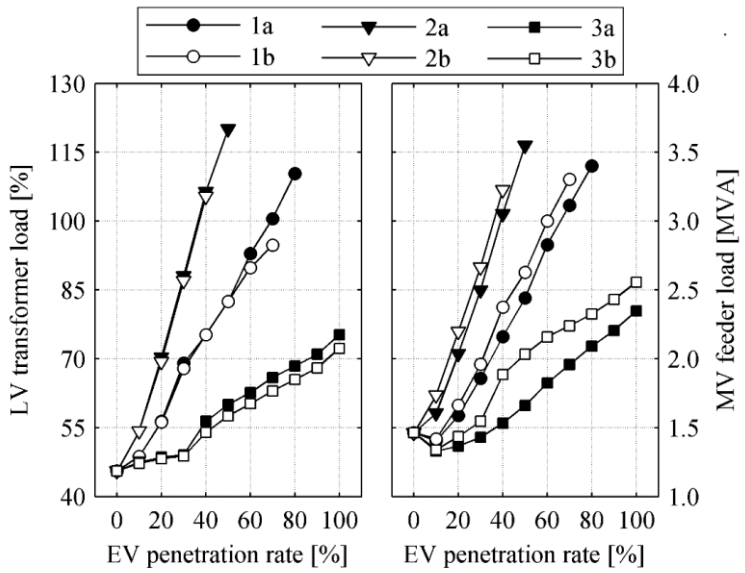

Figure 7.8: Highest MV/LV transformer peak load (left) and MV feeder peak load (right).

For $c^{\{1a,\,1b\}}$ and $c^{\{2a,\,2b\}}$, the LV residential peak loads are approximately the double at $R_{\mathrm{MAX}}^{\mathrm{PEV}}$, compared to the case without PEVs. The peak load is above 100 % for c^{1a} and $c^{\{2a,\,2b\}}$ at higher PEV penetration: at least one of the 9 residential grid MV/LV transformers is loaded above its rated power. It must be assessed whether the increase in transformer ageing is acceptable, or a transformer upgrade is required. For $c^{\{3a,\,3b\}}$, the peak load increases to a smaller degree, as the PEVs on average charge at a significantly lower effective power rating. As a result, the transformer peak load stays well below the rated power for $c^{\{3a,\,3b\}}$. The initial drop in the MV feeder load is due to an initial reduction in load unbalance, as the low amount of PEV charging load reduces the load unbalance on the grid.

7.4 Conclusions

The distribution grid impact of PEV charging is found to be far more sensitive to the applied residential slow charging strategy, than to fast charging. For a given residential slow charging strategy, the presence of fast charging decreases the PEV hosting capacity with 10 percentage points or less. A more grid-friendly residential slow charging strategy increases the PEV hosting capacity much more than fast charging decreases it, as charging at home accounts for the vast majority of PEV

charging. Fast charging only accounts for a low share of the PEV charging energy, which even decreases further if PEV battery capacities increase. As a result, fast charging stations have a limited impact on the medium voltage level, because the load increase is limited, compared to the load caused by residential slow charging. However, despite the limited share in the charging energy, fast charging infrastructure is indispensable to allow the vehicle fleet to drive close to purely electric.

The choice of the slow charging strategy at home strongly influences the PEV hosting capacity, which varies from 40 % up to 100 %. The highest hosting capacity occurs when PEV-based peak shaving is implemented, both with and without fast charging, as for most of the time the effective charging power is significantly below the rated power. Therefore, PEV-based peak shaving significantly reduces the distribution grid impact, compared to both other strategies. The lowest PEV hosting capacity occurs for off-peak residential charging, due to the synchronization of the charging actions, creating a peak that is higher than for the other cases. Therefore, distribution grid operators should consider adapting the peak/off-peak tariff scheme for households with a PEV, when a significant local PEV penetration occurs. By incentivizing more grid-friendly PEV charging strategies, a higher PEV penetration can be accepted.

Fast charging stations fundamentally differ from refueling stations for conventional vehicles. The latter are responsible for *all* of the refueling needs, while the former only supply a fraction of the charging needs (less than 13 % for the scenarios in this chapter). However, because the charging actions take much more time than for conventional refueling, the infrastructure is still substantial.

8. Summary, conclusions, and future work

8.1 Summary & conclusions

This dissertation handles the distribution grid impact of PEV charging infrastructure. Local control strategies for impact mitigation are proposed and assessed. Even though a vast amount of research has already been conducted on PEV charging and its coordination, the impact mitigation of local clusters of PEVs was not treated critically, while this is also required to allow for a widespread rollout of PEVs.

The general aspects of PEVs and PEV charging are discussed in Chapter 2, in order to frame the PEV charging process within the distribution grid context. This overview shows that there is already an advanced level of standardization for the functional objective of the charging aspect. For AC charging, the charging process is standardized and different systems are interoperable by means of the appropriate adapters. For DC fast charging, multistandard chargers are becoming increasingly common, similar to multifuel pumps in conventional fossil fuel stations. However, on the grid interface level, standardization is insufficient. The reactive power behavior, the voltage dependency, and the power profile during the charging process, substantially vary for currently available PEVs. These aspects are not part of the grid compliance requirements of PEV chargers.

The mobility behavior and the power consumption of the vehicles needs to be accurately modeled, in order to obtain the resulting energy requirements and charging opportunities. The modeling of the charging requirements is discussed in Chapter 3, for a representative vehicle fleet. The results show that for the vast majority of mobility requirements, the battery capacity of currently available BEVs is sufficient, from a technical perspective. The typically long standstill times allow to recharge the PEV batteries with a low power rating, if there are sufficient charging opportunities at such standstill locations. There is little need for high power ratings or high battery capacities, for the vast majority of mobility needs. Furthermore, with an increasing amount of moments the vehicles are grid-connected, the charging flexibility and the potential to deliver grid services increases.

The charging flexibility can be used to coordinate the charging process (Chapter 4). A systematic overview of coordinated PEV charging is conducted. The coordination objective, scale, and method of each strategy are the three parameters used to characterize and compare different approaches. The correlation between the three

parameters and the research category are investigated, resulting in a correlation mapping of the different approaches. Most coordination systems being proposed only consider set-point coordination for one or more coordination objectives. Grid-stabilizing control at the grid interface typically is not taken into account for PEV charging, but has already been investigated for distributed energy resources. A control mechanism at this level is to be considered, because of the potentially large impact of PEV charging on the electricity system. It implies a deviation from the coordination set-point once grid constraints are active. As a consequence, the set-point coordination can take place without risking grid incidents and failures due to grid constraints.

In Chapter 5, the impact of single-phase on-board active power PEV charging strategies on unbalanced three-phase low voltage residential grids are discussed. In the considered case, voltage droop charging behavior eliminates critical voltages below 0.85 pu and excessive voltage unbalances, with only a limited impact on the charge duration. Peak shaving at vehicle level makes the grid fully compliant with the EN50160 standard, and avoids the need for an infrastructure upgrade. The results show that local grid constraints and critical conditions can be mitigated in an effective manner with local active power strategies. As a result, grid infrastructure investments are deferred when using these on-board charging strategies.

Chapter 6 discusses the distribution grid impact of reactive power support of single-phase PEV charging. For a representative case study, reactive power support is investigated for three different electric vehicle charging strategies: uncoordinated charging, residential off-peak tariff charging, and PEV-based peak shaving. The impact on the residential voltage deviations, peak load, and grid losses is calculated. The results of the case study show that the implementation of a capacitive load behavior in electric vehicle chargers has a beneficial impact on voltage deviations. Furthermore, for a capacitive power factor of 0.95 or higher, there is no disadvantage with respect to the residential peak load and the residential grid losses. However, the cost related to the increased apparent power rating of the vehicle chargers, required to supply the reactive power, should be assessed compared to the mentioned advantages. If the benefits outweigh the costs, reactive power support could be considered in the grid compliance requirements of electric vehicle chargers, as it allows deferring distribution grid infrastructure investments.

Chapter 7 investigates the combined LV and MV residential grid impact for slow and fast PEV charging. A realistic case study for an urban distribution grid is used, for which three residential slow charging strategies are modeled, as in Chapter 6: uncoordinated, residential off-peak, and PEV-based peak shaving. For each slow charging strategy, the PEV hosting capacity is determined, with and without fast

charging. The results show that the distribution grid impact is much less sensitive to the presence of fast charging compared to the slow charging strategy. PEV-based peak shaving results in the lowest grid impact, allowing for the highest PEV hosting capacity. Residential off-peak charging has the highest grid impact, due the load synchronization effect, resulting in the lowest PEV hosting capacity. Therefore, the PEV users should be incentivized to charge their PEVs in a more grid-friendly manner when the local PEV penetration becomes significant.

Voltage-dependent charging behavior can be implemented on all types of onboard PEV chargers used. Therefore, a prescribed voltage-dependent behavior could be made part of the grid compliance requirements for PEV chargers. Reactive power injection can be implemented on PEV chargers using a full-bridge active rectifier topology. For such chargers, a prescribed non-unity capacitive power factor could be made part of the grid compliance requirements, similar to the grid compliance requirements for photovoltaic installations, which have to adapt their active and reactive power as a function of the grid frequency and voltage, respectively.

Even though fast charging only supplies a minor fraction of the required energy, becoming even lower with increasing battery capacities, it is necessary to allow for a full electrification of passenger vehicles. Therefore, given the limited medium-voltage grid impact of fast charging infrastructure for the currently available battery capacities, the relative grid impact of fast charging infrastructure will remain limited. However, due to the fact that fast charging still takes longer than refueling a conventional vehicle, the required amount of fast chargers is substantial.

8.2 Future work

The different grid load types, i.e., household power consumption, PEV charging, and PV power generation, are modeled independently. For PV power generation, this is a correct assessment, as it is determined by the solar irradiation. However, for the household power consumption and the PEV charging, there is a correlation between the presence of the PEV at home and the activities taking place. By modeling the household power consumption and the vehicle mobility together, this correlation could be taken into account. In this way, the potential for coordination on a building level, can be fully assessed.

Houses with a three-phase grid connection still have a non-negligible fraction of single-phase electric loads (e.g., dishwasher, washer, and dryer). Therefore, the grid load of such a house is not balanced, and this may be taken into account in the household load model for three-phase connected residential consumers. If this unbalance is ignored, their grid impact is significantly underestimated.

The vehicle and fleet modeling (Chapter 3) distinguishes week and weekend days, but not seasonal variations or exceptional days, such as holidays. For a full quantitative assessment of the grid and user comfort impact, the mobility requirements during exceptional days should be modeled, for which the input data need to be collected.

The voltage droop PEV charging behavior (Chapter 5) makes full use of the voltage magnitude constraints as defined in the EN50160 standard. However, different voltage droop settings should be compared to assess which one provides the best trade-off between grid support and user comfort.

As each grid node has a different voltage magnitude, there is an inherent damping present in the voltage droop control mechanism, because the PEV chargers are operating on a different point. Furthermore, due to filtering of the grid measurements, and due to the time constant of the control loops of in the charger, additional damping is introduced. However, when considering to make voltage droop charging behavior part of the grid compliance requirements of PEV chargers, the dynamic requirements should also be taken into account.

For the reactive power behavior (Chapter 6), different settings should be compared, as the active and reactive power behavior for PV installations as a function of the grid frequency and voltage, respectively. For PV installations, the active power output and the inductive PF are at most reduced to 0.48 pu and 0.9, respectively [271].

For fast charging, it is assumed that each PEV will fast charge up to the upper limit, regardless of the remaining range to the next standstill location. In reality, PEV drivers might charge to a SOC sufficient to reach the next standstill location that offers a charging opportunity. Therefore, for PEVs with a charging opportunity at home, the share of fast charging in the charging energy delivery is lower. As a consequence, the relative grid impact of fast charging compared to slow charging is lower, and the required amount of fast chargers too. For PEVs without a charging opportunity at home (no private parking), the fast charging requirements might be substantially different, depending the available charging opportunities.

The active and reactive power control mechanisms affect the charging behavior and the resulting distribution grid impact. Therefore, it also impacts the behavior of large-scale coordination mechanisms, as the aggregated charging behavior deviates from its set point. For example, voltage droop charging reduces the PEV charging power, when the voltage deviations exceed their bounds. Therefore, more PEVs have to be activated, to compensate for the set point deviation. The extent of this set point deviation should be assessed, by taking into account the typical grid topologies present within the investigated region investigated.

Besides the voltage-dependent charging behavior discussed here, which provides local grid support, frequency-dependent charging behavior could be implemented to provide primary frequency support. Once there is a substantial amount of PEVs, the impact of this behavior will become relevant. Furthermore, the voltage-dependent charging behavior could be expanded from unidirectional to bidirectional energy flows, i.e., vehicle-to-grid (V2G), if the PEV charger offers bidirectional functionality. In this way, PEVs could actively provide voltage support, by discharging the PEV battery when the grid voltage magnitude is low. Frequency-dependent charging behavior could also be made bidirectional, if the charger offers bidirectional functionality.

Appendix A North-American grid layout

Three typical North-American LV distribution grid topologies are illustrated in Figure A.1. Residential grids typically have a 120/240 V split-phase topology, so that two single-phase voltage levels are available. The 120 V level is used for low-power appliances such as lighting and electronic devices. Mode 2 charging cables that are compatible with the 120 V level typically have a 1.3-1.7 kW current rating [305]. The 240 V level is used for the high-power appliances such as electric cookers and air conditioning. Mode 2 and Mode 3 charging infrastructure that are compatible with the 240 V level typically have current ratings up to 6.9 and 17.3 kW, respectively [305].

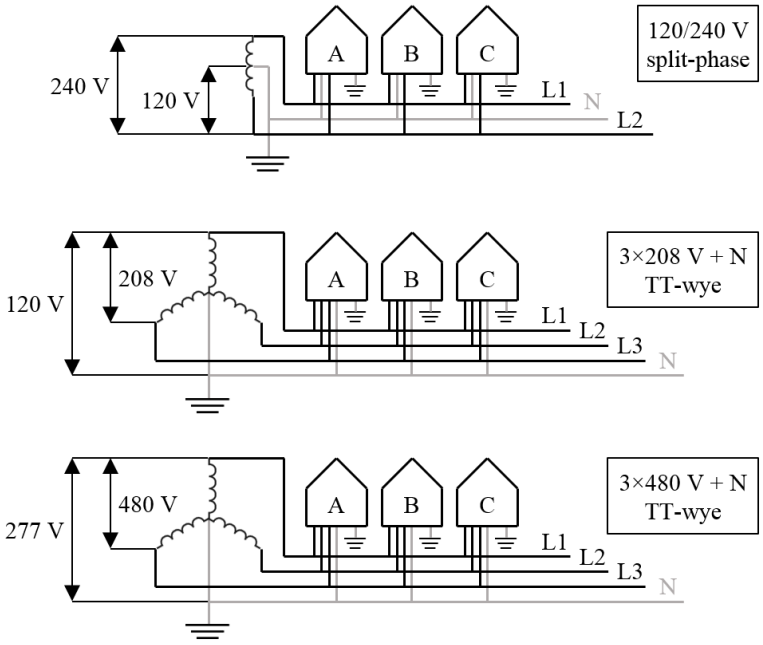

Figure A.1: Typical North-American distribution network topologies, for single-phase (120/240 V split-phase), and three-phase (120/208 V and 277/480 V) grid connections.

If three-phase power is required, a 3×208 V + N topology is typically used for residential and small-scale commercial buildings. The customers can use 120 V line-to-neutral for low power appliances, and 208 V line-to-line for three-phase appliances. Single-phase high-power appliances can use the 208 V line-to-line voltage, as most of them are designed to be compatible with both 208 V and 240 V, including PEV charging infrastructure [305]. For large-scale commercial and industrial customers, and for fast charging infrastructure [68], a 3×480 V + N grid topology is typically used.

Appendix B Availability analysis

An availability analysis model is developed to determine the driving behavior for each vehicle in the fleet. This model is created by Juan Van Roy, and the content of this appendix is based upon his PhD dissertation [306]. From this analysis, it is known when each vehicle is driving, when it is at home, at work or another activity.

B.1 Flemish travel behavior data

The third Flemish Mobility Study (OVG3) has been conducted between September 2007 and 2008 among 8,800 people (≥ 6 years old) [84]. This research is commissioned by the Flemish government. The people surveyed, were asked to keep track of all their trips (all transport means):

- number of trips per day;
- distance;
- duration;
- motive;
- departure and return times;
- etc.

In this context, only the vehicle trips are considered. A distinction is made between week and weekend days, since the travel behavior is different. The other data are taken from *Febiac* [87], the Belgian *Algemene Directie Statistiek en Economische Informatie* [85], the *FOD Mobiliteit en Vervoer [99]*, and the *Vlaamse Milieumaatschappij* [88].

On August 1, 2014, the Belgian vehicle fleet consisted of 5 555 499 vehicles [88]. Table B.1 shows the number of cars per household [84]. More than half of the households has only 1 vehicle. The average number of vehicles per household is about 1.1. Therefore, only one vehicle per household is assumed here. However, for all trips, the average occupancy of a vehicle is 1.86 persons, while for commute trips this is only 1.20 persons.

Table B.1: Number of cars per household.

Number of cars	fraction of households [%]
0	18.21
1	53.65
2	24.75
≥3	3.39

B.1.1 Duration of the vehicle trip

A trip is defined as the trip from home to the activity and back home, since about 73.4 % of the trips are limited to one activity and going back home [84]. However, it is possible to start another trip while being at another activity.

There are commute and non-commute trips. For the OVG-survey, people had to keep track of the motif of each trip. Here, the categorization of the non-commute trips are limited to the following motifs:

- Business trips;
- Visits;
- Shopping;
- Education;
- Recreation;
- Other trips (e.g. doctor visit, picking up someone,).

On average there are 3.14 trips per day per person by all transport means, of which about 65 by car (as driver and/or passenger). Other important transport means are by foot (13.4 %) and by bike (14.2 %). About 75 % of all vehicle trips are less than 15 km. For most distances, between 50 to 60 % of all trips is by car. Going on foot and by bike also has a high share for short distances, for which their share increases to about 20 % for each. For distances less than 1 km, travelling by foot has the highest share. For high distances, it is clear that moving by train becomes more and more important. Still, moving by car is very popular for very short trips. The share of travelling by foot or bike is higher for lower distances and travelling times.

Considering the total travelled kilometers, vehicles take about 71 % of the average daily travelled kilometers. About 34 % of this distance is for commute trips. Of these 3.14 trips, 1.47 trips are as a driver of a vehicle. Considering an average of 2.3 inhabitants [85] and assuming one vehicle per household in Flanders, this results in

3.39 trips per day per vehicle. During the weekend there are less trips, as can be seen in Table B.2.

Table B.2: Number of trips per day per vehicle.

Average week	Weekday	Weekend day
3.39	3.60	2.85

B.1.2 Duration of the vehicle trip

OVG provides data for the duration (indirectly this means the distance) of an average vehicle trip [84]. Figure B.1 shows the distribution of the average number of trips of a certain duration. The surface below the graph is equal to the average number of trips per day per vehicle (3.39 trips per vehicle per day). This graph represents the average trip, thus it has to be adapted for:

- The difference between week and weekend days: 3.60 versus 2.85 trips per vehicle per day.
- The difference in trip durations of each motif: some motifs have longer/shorter trip distances. For instance, shopping trips are on average shorter than work or business trips. Table B.3 shows the scale factors, as the result of the average driven distance for each motive with respect to the average driven distance for all trips.

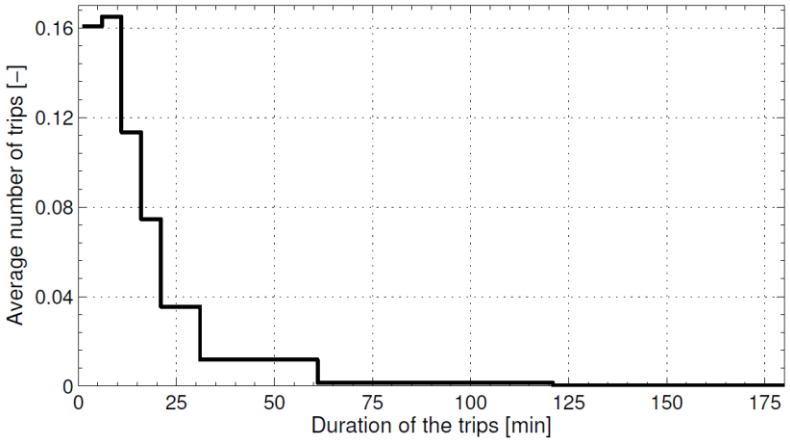

Figure B.1: Distribution of average number of trips as a function of the duration of a trip.

Table B.3: Scale factors for the distance of the different motives.

Motive	Scale factor
Work	1.37
Business	1.92
Visits	0.99
Shopping	0.51
Education	1.13
Recreation	1.00
Others	0.76

B.2 Commute trips

The most important subdivision are the commute versus the non-commute trips, since the priority of the former is the highest. No other trips but business trips may overlap during the trip to work and the presence at work. Therefore, commute trips will be treated separately, as they are very predictable and can be scheduled well in advance. It is also important to simulate them, because they form a great part in the absence of vehicles. Furthermore, it is possible in the future that vehicles can be charged at work.

The mean average distance to work in Flanders is 18.82 km (the mean average time needed to get to work from home is 25.8 minutes). 82 % of the people live less than 30 km from their work (Table B.4). Only at the coast there are some areas with an average work distance of more than 30 km.

The distance of the commute trips is defined using Figure B.1 and fixed for a vehicle during the year. This figure is normalized, since it is assumed that a vehicle is only used for a maximum of one commute trip a day. Table B.5 shows the probability for a working trip for working people during week and weekend days [84].

Table B.4: Number of working people in function of distance to work.

Distance to work [km]	Fraction of working people [%]	Fraction of people who go to work with a vehicle [%]
0 – 1	6.58	2.59
1.1 – 2.5	6.77	4.36
2.6 – 5	14.73	12.75
5.1 – 7.5	8.69	8.70
7.6 – 10	9.75	10.87
10.1 – 15	13.45	16.43
15.1 – 20	9.60	12.01
20.1 – 30	12.59	14.32
30.1 – 50	10.18	11.41
≥ 50	7.66	6.55

Table B.5: Probability for a work trip [%].

Weekday	Weekend day
65.81%	13.01%

In 2010, about 67.1 % of all working people traveled to work by car [99]. According to [85], about:

- 54 % of the Flemish population (≥ 18 years old) were active on the labor market.
- 69.9 % of the Flemish population (18–64 years old) were active on the labor market.

This results in 36.2 % to 46.9 % of all vehicles being used for commuting, with the assumption that there is only one vehicle per household. The actual number is expected to be closer to 46.9 %. Generally, the average number of vehicles in households with working people (higher net income) is higher than one [84]. However, this is not included, as there is no data available to model this. A fixed work shift is assigned to each vehicle. The probability a certain shift is attributed to a vehicle is given in Table B.6 [307]. Depending on the work shift, the departure and return hour are defined according to the distribution functions given in Figure B.2 [307].

Table B.6: Probability for a shift for a work trip.

Shift	Probability
Day	73.3%
Evening	3.7%
Morning	3.7%
Part-time	12.5%
Night	6.8%

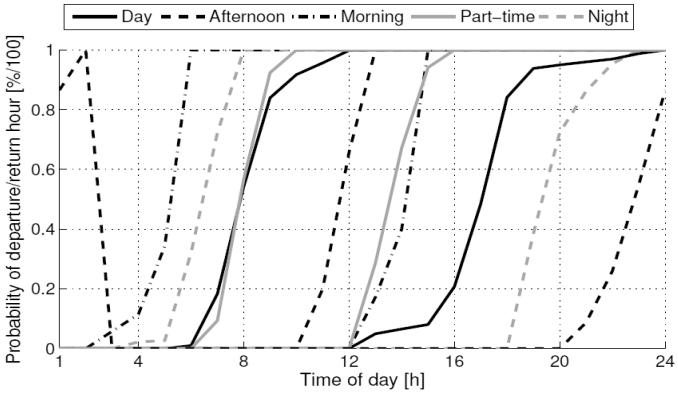

Figure B.2: Cumulative probability density function for the departure and return hours for work shifts.

Similar to the distance and the shift, the departure and return hour (on hourly basis) are fixed for each vehicle. This is an acceptable approximation, since about 82 % of the population have fixed working hours [84]. To introduce some variation, the exact moment of departure and return (on minute basis) is variable. A uniform probability distribution function is used to determine the exact minute of departure and return. It is assumed that the return trip is within 24 h.

B.3 Other trips

Different motifs are available for non-commute trips, with each their probability of occurrence (Table B.7). For the weekend, it is supposed that Saturday and Sunday are identical, as is done for weekdays. For each motive, OVG provides a distribution function for the departure and return times.

Table B.7: Probability for non-commute trips.

Motive	Weekday	Weekend day
Business	8.54%	2.07%
Visits	12.50%	19.38%
Shopping	23.82%	28.45%
Education	10.52%	0.82%
Recreation	23.56%	32.42%
Others	21.06%	16.86%

However, the distribution function for the return times is not given as a function of the departure times, nor a distribution of the total activity duration (including the trip duration) is available. This could result in less reliable results (e.g. picking up someone takes a whole day, even if the distance is limited). Therefore, the data from OVG is adapted. The following assumptions have been made:

- **Variable activity duration**: Probability distribution functions for both the departure and return hours are used. It is assumed that education trips end the same day. Motifs: Business, education, and recreation.
- **Fixed activity duration**: The total duration of the activity (trip and presence at the activity) is fixed. The probability distributions for the departure hour are used. Motifs: Visits, shopping, and others.

Table B.8: Fixed activity duration.

Motif	Duration [min]
Visits	180
Shopping	120
Others	60

The cumulative probability functions are shown in Figure B.3, for (a) week days and (b) weekend days, respectively. For the motifs with a fixed activity duration, only the distribution function for the departure hour is shown. The first graph of each motif represents the departure trip; the second represents the return trip. Business and recreation trips may end during the first hours of the next day.

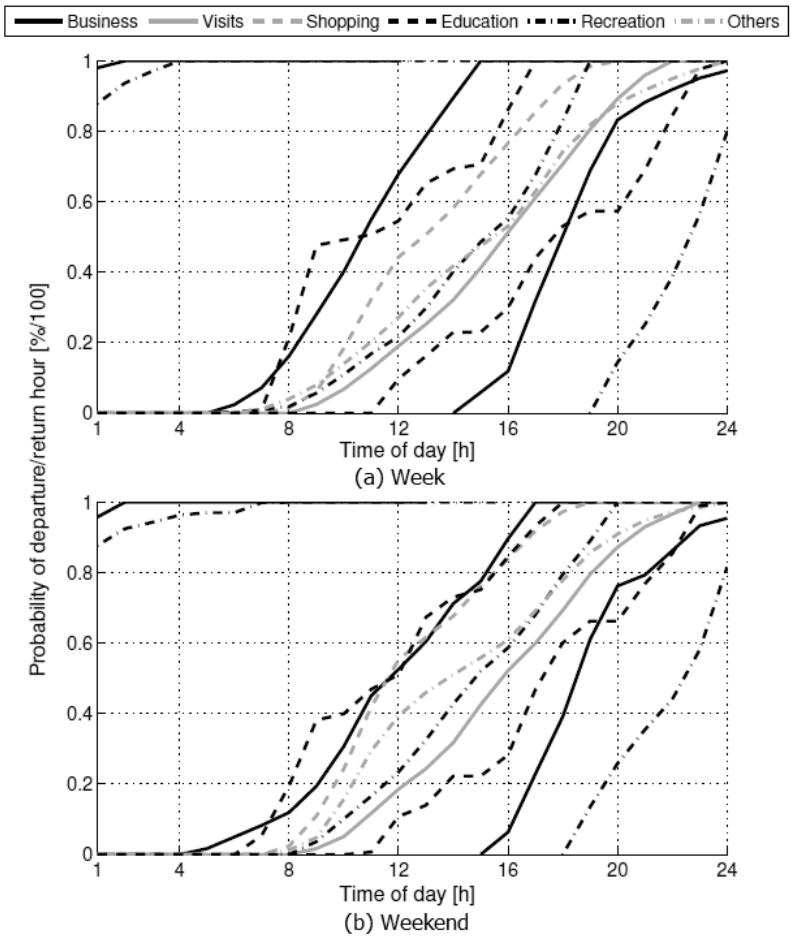

Figure B.3: Cumulative probability density function for the departure and return hour for other motifs during week days (a), and weekend days (b).

The duration of the trip is defined with Figure B.1 and the scale factors in Table B.3. For the days where a vehicle has a work trip, Figure B.1 has to be scaled in such a way that the average number of trips of that day is not higher than given in Table B.1. As mentioned earlier, the commute trips are scheduled first. Afterwards, the characteristics of the other trips (number of trips, distance, and departure and return time) are defined. A distinction is made between business trips and other motifs regarding the scheduling of the trips in time:

- **Business trips** may overlap with commute trips. They can also take place on days without a commute trip. Furthermore, it is not only possible to start a business trip at work, but also on the way to or from work.
- **Other trips** have more constraints. There is no overlap between these trips, trips to work and the time at work. These trips will be placed before or after work. It is also important to take into account any commute trip during the next day.

Since commute trips are scheduled first, it is important to check if a trip can be scheduled before leaving for work when a departure hour is found before work. If not, the trip will be done after work. These non-commute trips are allowed to overlap with each other, e.g., shopping after a visit.

Appendix C Fast charging scenario

Table C.1: LV feeder locations of the randomly assigned PV installations.

MV node	Houses with a PV installation
1	1, 17, 21, 24, 42, 46, 50
2	6, 15, 20, 27, 43, 57, 58
3	10, 16, 17, 23
4	10, 17, 20, 25
5	1, 6, 17, 21, 37
6	3, 26, 28, 30, 42
7	9, 21, 25, 31
8	2, 8, 22, 27, 33
9	6, 7, 18, 23, 37, 49, 58

Table C.2: Location (house number) of the PEVs on the LV feeders.

PEV group	MV grid node								
	1	**2**	**3**	**4**	**5**	**6**	**7**	**8**	**9**
10 %	4-7-13-16-27-37-54	10-17-31-33-44-58-60	4-25-27-37	4-7-8-30	10,11-13-24-50	6-11-14-28-38	22-25-28-38	2-11-18-33	3-6-8-10-20-22-23-
20 %	10-15-41-44-46-57	14-32-41-43-46-53	3-7-14-22	6-17-18-35	8-25-27-42	1-3-19-30	7-17-34-37	5-13-19-42	7-27-32-40-52-55-
30 %	6-11-12-34-35-51	16-24-27-35-45-49	16-19-33-39	3-5-28-38	12-15-38-39	7-12-32-33	1-14-30-32	24-26-30-32	17-33-41-43-46-62
40 %	18-21-30-40-43-61	13-37-42-51-56-62	2-11-21-23	15-20-25-29	4-6-7-41	5-8-9-39	6-13-19-29	7-20-36-40	21-24-43-49-53-60
50 %	20-36-39-52-53-56	3-8-28-34-52-55	1-15-17-31	1-13-19-32	9-16-18-34	2-16-18-29	3-8-21-26	15-35-39-41	2-9-14-26-37-56
60 %	2-19-23-24-33-38-60	5-9-20-26-29-50-61	10-24-28-35	21-27-31-33	14-22-30-33-37	10-15-23-27-41	24-27-31-39	4-8-9-25-29	13-18-35-47-48-54-61
70 %	3-8-17-28-42-48	18-21-36-38-47-59	9-26-29-34	11-14-16-26	2-19-24-35	20-21-35-40	2-12-16-33	3-17-23-38	11-15-34-42-57-59
80 %	5-14-22-25-47-55	2-6-7-12-48-57	8-24-28-37	2-10-36-39	3-28-31-32	4-22-26-36	5-18-20-35	6-10-27-34	4-12-16-29-45-58
90 %	1-31-32-45-50-59	1-4-19-22-23-25	5-6-12-20	12-22-24-37	1-16-21-29	13-25-37-42	4-11-23-36	12-16-28-37	1-19-25-28-36-39
100 %	9-26-29-49-58-62	11-15-30-39-40-54	13-18-30	9-23-26	5-20-26-36	17-24-31-34	9-10-15	1-21-22-31	5-30-31-38-50-51

Bibliography

[1] L. Fulton *et al.*, *Transport, energy and CO_2*, Paris, France: IEA Publications, 2009.

[2] OECD, *The cost of air pollution - Health impacts of road transport*, Paris, France: OECD Publishing, 2014.

[3] WHO Regional Office for Europe and OECD, *Economic cost of the health impact of air pollution in Europe - Clean air, health and wealth*, Copenhagen: WHO Regional Office for Europe, 2015.

[4] L. Fulton *et al*, *Technology roadmap - Electric and plug-in hybrid electric vehicles*, Paris, France: IEA Publications, 2011.

[5] European Commission, *A sustainable future for transport - towards an integrated, technology-lead and user-friendly system*, Luxembourg City, Luxembourg: Publications Office of the European Union, 2009.

[6] F.C. Boureima, J. Matheys, V. Wynen, N. Sergeant, J. Van Mierlo, and M. Messagie, "Comparative LCA of electric, hybrid, LPG and gasoline family cars in a Belgian context"**,** in *EVS-24.*, 2009, pp. 1-8.

[7] M. Duvall *et al.*, "Environmental assessment of plug-in hybrid electric vehicles, volume 1: nationwide greenhouse gas emissions", EPRI, Palo Alto, CA, U.S.A., Rep. 1015325, Jul. 2007.

[8] M. Duvall *et al.*, "Environmental assessment of plug-in hybrid electric vehicles, volume 2: United States air quality analysis based on AEO-2006 assumptions for 2030," EPRI, Palo Alto, CA, Rep. 1015326, Jul. 2007.

[9] W. Kempton and J. Tomic, "Vehicle-to-grid power fundamentals: calculating capacity and net revenue", *Elsevier J. Power Sources*, vol. 144, no. 1, pp. 268-249, Jun. 2005.

[10] A.Y. Saber and G.K. Venayagamoorthy, "Plug-in vehicles and renewable energy sources for cost and emission reductions,", *IEEE Trans. Ind. Electron.*, vol. 58, no. 4, pp. 1229-1238, Apr. 2011.

[11] W. Kempton and J. Tomic, "Vehicle-to-grid power implementation: from stabilizing the grid to supporting large-scale renewable energy," *Elsevier Journal of Power Sources*, vol. 144, no. 1, pp. 280-297, Jun. 2005.

[12] J.T. Salihi, "Energy requirements for electric cars and their impact on electric power generation and distribution systems," *IEEE Trans. Ind. Appl.*, vol. 9, no. 5, pp. 516-532, Sept. 1973.

[13] S.G. Wirasingha, N. Schofield, and A. Emadi, "Plug-in hybrid electric vehicle developments in the US: trends, barriers, and economic feasibility," in *IEEE VPPC*, 2008, pp. 1-8.

[14] J.A.P. Lopes, F.J. Soares, and P.M.R. Almeida, "Integration of electric vehicles in the electric power system," *Proc. IEEE*, vol. 99, no. 1, pp. 168-183, Jan. 2011.

[15] C. Camus, C.M. Silva, T.L. Farias, and J. Esteves, "Impact of plug-in hybrid electric vehicles in the Portuguese electric utility system," in *Int. Conf. Energy Elect. Drives*, 2009, pp. 258-290.

[16] H.U. Gerbracht, D. Most, and W. Fichtner, “Impacts of plug-in electric vehicles on Germany's power plant portfolio: a model based approach,” in *7th Int. Conf. Eur. Energy Market*, 2010, pp. 1-7.

[17] “More than 400,000 electric cars on the road worldwide,” Zentrum für Sonnenergie- und Wasserstoff-Forschung Baden-Württemberg, 2014. [Online]. Available: http://www.zsw-bw.de/uploads/media/pr04-2014-ZSW-Electromobilityworldwide.pdf.

[18] S. Rahman and G.B. Shrestha, “An investigation into the impact of electric vehicle load on the electric utility distribution system,” *IEEE Trans. Power Del.,* vol. 8, no. 2, pp. 591-597, Apr. 1993.

[19] K. Clement-Nyns, E. Haesen, J. Driesen, “The impact of charging plug-in hybrid electric vehicles on a residential distribution grid,” *IEEE Trans. Power Syst.*, vol. 25, no. 1, pp. 371-380, Feb. 2010.

[20] L. Pieltain-Fernandez, T. Gomez-San Roman, R. Cossent, C. Mateo-Domingo, and P. Frias, “Assessment of the impact of plug-in electric vehicles on distribution networks,” *IEEE Trans. Power Syst.*, vol. 26, no. 1, pp. 206-213, Feb. 2011.

[21] A. Karnama and V. Knazkins, “Scenario-based investigation of the effects of plug-in hybrid electric vehicles (PHEVs) in 11 kV substations in Stockholm,” in *Int. Conf. Eur. Energy Market*, 2010, pp. 1-6.

[22] Q. Gong, S. Midlam-Mohler, V. Marano, and G. Rizzoni, “Study of PEV charging on residential distribution transformer life,” *IEEE Trans. Smart Grid*, vol. 3, no. 1, pp. 404-412, March 2012.

[23] A.D. Hilshey, P.D.H. Hines, P. Rezaei, and J.R. Dowds, “Estimating the impact of electric vehicle smart charging on distribution transformer aging,” *IEEE Trans. Smart Grid,* vol. 4, no. 2, pp. 905-913, Jun. 2013.

[24] E. Veldman and R.A. Verzijlbergh, “Distribution grid impacts of smart electric vehicle charging from different perspectives,” *IEEE Trans. Smart Grid,* vol. 6, no. 1, pp. 333-342, Jan. 2015.

[25] W.H. Kersting and W.H. Phillips, “Distribution feeder line models,” *IEEE Trans. Ind. Appl.*, vol. 31, no. 4, pp. 715-720, Aug. 1995.

[26] “2015 Nissan Leaf,” Nissan USA, 2015. [Online]. Available: http://www.nissanusa.com/electric-cars/leaf/

[27] “Tesla Model S,” Tesla Motors, 2015. [Online]. Available: http://www.teslamotors.com/models

[28] “Renault Zoe,” Renault België, 2015. [Online]. Available: http://www.renault.be/nl/gamma-renault/elektrische-wagens/zoe/zoe/

[29] “2015 Toyota Prius Plug-in Hybrid,” Toyota Motor Sales U.S.A, 2015. [Online]. Available: http://www.toyota.com/prius-plug-in-hybrid/

[30] “2015 Toyota Prius,” Toyota Motor Sales U.S.A, 2015. [Online]. Available: http://www.toyota.com/prius/

[31] “Mitsubishi Outlander PHEV,” Beherman Motors, 2015. [Online]. Available: http://www.mitsubishi-motors.be/nl-be/models/outlander-phev

[32] “BMW i3 Model Overview,” BMW North America, 2015. [Online]. Available: http://www.bmwusa.com/bmw/bmwi/i3

[33] “Golf GTE,” Volkswagen UK, 2015. [Online]. Available: http://www.volkswagen.co.uk/new/golf-gte-vii/home

[34] "Volvo V60 Twin Engine," Volvo Car Corporation, 2015. [Online]. Available: http://www.volvocars.com/nl/modellen/model/v60/twin-engine

[35] "Electric Vehicles," KU Leuven Energy Institute, 2014. [Online]. Available: https://set.kuleuven.be/ei/images/ei-factsheet7-eng-web.pdf

[36] "Proterra," Proterra, 2015. [Online]. Available: http://www.proterra.com/

[37] "Roadster Features and Specifications," Tesla Motors, 2015. [Online]. Available: http://my.teslamotors.com/roadster/specs

[38] "e6," BYD Global, 2015. [Online]. Available: http://www.bydeurope.com/vehicles/e6/

[39] "2011 Chevrolet Volt Specifications," General Motors, 2011. [Online]. Available: http://media.gm.com/media/us/en/chevrolet/vehicles/volt/2011.tab1.html

[40] D. Andrea, *Battery management systems for large lithium-ion battery packs*, Norwood, MA, U.S.A.: Artech House, 2010.

[41] J. Dogger, B. Roossien, and F. Nieuwenhout, "Characterization of Li-ion batteries for intelligent management of distributed grid-connected storage," *IEEE Trans. Energy Convers.*, vol. 26, no. 1, pp. 256–263, Mar. 2011.

[42] "Technische eigenschappen van Renault Fluence Z.E.," Renault België, 2011. [Online]. Available: http://www.media-renault.eu/fluence-ze/files/108_nl_tech.pdf

[43] H. Seljeseth, H. Taxt, and T. Solvang, "Measurements of network impact from electric vehicles during slow and fast charging", in *CIRED*, 2013, pp. 1-4.

[44] M. Yilmaz and P.T. Krein, "Review of battery charger topologies, charging power levels, and infrastructure for plug-in electric and hybrid vehicles," *IEEE Trans. Power Electron.*, vol. 28, no. 5, pp. 2151-2169, May 2013.

[45] *IEEE Standard for Interconnecting Distributed Resources with Electric Power Systems*, IEEE Standard 1547, 2003.

[46] *Power Quality Requirements for Plug-in Vehicle Chargers—Part 1: Requirements*, SAE International Standard J2894, 2011.

[47] *Electromagnetic Compatibility (EMC)—Part 3: Limits - Section 2: Limits for Harmonic Current Emissions*, IEC Standard 1000-3-2, 1995.

[48] F. Musavi, M. Edington, W. Eberle, W.G. Dunford, "Evaluation and efficiency comparison of front end AC-DC plug-in hybrid charger topologies," *IEEE Trans. Smart Grid*, vol. 3, no. 1, pp. 413-421, March 2012.

[49] K. Stengert, "On-board 22 kW fast charger "NLG6"," in *EVS-27*, 2013, pp. 1-11.

[50] P. Van Den Bossche, "The electric vehicle: raising the standards," Ph.D. dissertation, ETEC, VUB, Brussels, Belgium, 2003.

[51] "Renault Twizy," Renault België, 2015. [Online]. Available: http://www.renault.be/nl/gamma-renault/elektrische-wagens/twizy/twizy/

[52] "The new Kia Soul EV," Kia Motors Europe, 2015. [Online]. Available: http://www.kia.com/eu/future/soul_ev/

[53] "2015 VW e-Golf," Volkswagen of America, 2015. [Online]. Available: https://www.vw.com/models/e-golf/

[54] A. Mathoy, "Definition and implementation of a global EV charging infrastructure," Brusa Elektronik, 2008. [Online]. Available: http://www.park-charge.ch/documents/EV-infrastructure%20project.pdf

[55] C. Ricaud and P. Vollet, “Connection system on the recharging spot: a key element for electric vehicles,” Schneider Electric, 2010. [Online]. Available: http://www2.schneider-electric.com/documents/support/white-papers/connection-system-recharging-spot.pdf

[56] I. Buchmann, “Types of Lithium-ion Batteries,” Cadex Electronics Inc., 2015. [Online]. Available: http://batteryuniversity.com/learn/article/types_of_lithium_ion

[57] B. Lunz, Z. Yan, J.B. Gerschler, and D.U. Saurer, “Influence of plug-in hybrid electric vehicle charging strategies on charging and battery degradation costs,” *Elsevier Energy Policy*, vol. 46, pp. 511-519, Jul. 2012.

[58] “Facilitating e-mobility: EURELECTRIC views on charging infrastructure,” EURELECTRIC, 2012. [Online]. Available: http://www.eurelectric.org/media/27060/0322_facilitating_emobility_eurelectric_views_-_final-2012-030-0291-01-e.pdf

[59] “Supercharger,” Tesla Motors, 2015. [Online]. Available: http://www.teslamotors.com/supercharger

[60] “Brochure Charging Solutions,” Ratio Electric B.V., 2015. [Online]. Available: http://www.ratio.nl/files/Brochure%20Charging%20Solutions.pdf

[61] “Van productie tot stopcontact,” Eandis, 2013. [Online]. Available: http://www.eandis.be/sites/eandis/files/documents/9010059_van_productie_tot_stopcontact.pdf

[62] “Aangesloten op de toekomst - Laadstations voor E-Mobility,” Hager, 2015. [Online]. Available: http://www.hager.nl/nieuws-acties/nieuwe-producten/energiedistributie/laadstation-witty/82191.htm

[63] “Fastned – Home,” Fastned, 2015. [Online]. Available: http://fastned.nl

[64] H.L. Willis, “Service Layout and Planning,” in *Power Distribution Planning Reference Book*, New York, New York, U.S.A.: Marcel Dekker, 1997, ch. 13, sec. 3, pp. 539-545.

[65] T.A. Short, “Fundamentals of Distribution Systems,” in *Electric Power Distribution Handbook*, Boca Raton, Florida, U.S.A.: CRC Press, 2004, ch. 1, pp. 1-31.

[66] M. Lehtonen *et al.*, “Fault management in electrical distribution systems,” in *CIRED*, 1999, pp. 1-4.

[67] B. Rotthier, T. Van Maerhem, P. Blockx, P. Van den Bossche, and J. Cappelle, “Home charging of electric vehicles in Belgium,” in *EVS-27*, 2013, pp. 1-6.

[68] “Global product offering,”ABB, 2015. [Online]. Available: http://new.abb.com/ev-charging/full-global-portfolio

[69] H.L. Willis, “Distribution Feeder Layout,” in *Power Distribution Planning Reference Book*, New York, New York, U.S.A.: Marcel Dekker, 1997, ch. 8, pp. 285-340.

[70] H.L. Willis, “Planning Criteria,” in *Power Distribution Planning Reference Book*, New York, New York, U.S.A.: Marcel Dekker, 1997, ch. 4, pp. 129-153.

[71] A. Cziker, Z. Hanzelka, and I. Wasiak, “Power Quality Phenomena and Indicators,” in *Electrical Energy Efficiency*, Hoboken, New Yersey, U.S.A.: John Wiley & Sons, 2012, ch. 5, pp. 125-163.

[72] H. Seljeseth, T. Rump, and K. Haugen, “Overvoltage immunity of electrical appliances - Laboratory test results from 60 appliances,” in *CIRED* ,2011, pp. 1–4.

[73] *Voltage Characteristics of Electricity Supplied by Public Electricity Networks*, CENELEC Standard EN 50160, 2010.

[74] F. Hindryckx, “Spanningskwaliteit - Automatisering cabine,” Eandis, 2013, unpublished.

[75] A. von Jouanne and B. Banerjee, “Assessment of voltage unbalance,” *IEEE Trans. Power Del.*, vol. 16, no. 4, pp. 782-790, Oct 2001.

[76] A. Franzen and L. Bertling, .”State of the art - lifetime modeling and management of transformers,” KTH Electrical Engineering. Stockholm, Sweden, Rep. TRITA_EE 2007:041, 2007.

[77] C. Dang, J. L. Parpal, and J. P. Crine, “Electrical aging of extruded dielectric cables: review of existing theories and data”, *IEEE Trans. Dielectr. Electric. Insul.*, vol. 3, no. 2, pp. 237-247, Apr. 1996.

[78] H.L. Willis, “Profit-based Planning Paradigms,” in *Power Distribution Planning Reference Book*, New York, New York, U.S.A.: Marcel Dekker, 1997, ch. 18, sec. 5 pp. 789-802.

[79] P. Kundur, *Power System Stability and Control*, New York, New York, U.S.A.: McGraw-Hill, 1994.

[80] M.D. Ilic, “From hierarchical to open access electric power systems,” *Proc. IEEE*, vol. 95, no. 5, pp. 1060-1084, May 2007.

[81] F. Rahimi and A. Ipakchi, “Demand response as a market resource under the smart grid paradigm,” *IEEE Trans. Smart Grid*, vol. 1, no. 1, pp. 82-88, Jun. 2010.

[82] A. Molderink, V. Bakker, M.G.C. Bosman, J.L. Hurink, and G.J.M. Smit, “Management and control of domestic smart grid technology,” *IEEE Trans. Smart Grid*, vol. 1, no. 2, pp. 109-119, Sept. 2010.

[83] H. Saele and O.S. Grande, “Demand response from household customers: experiences from a pilot study in Norway,” *IEEE Trans. Smart Grid*, vol. 2, no. 1, pp. 102-109, March 2011.

[84] D. Janssens, E. Moons, E. Nuyts, and . Wets, “Onderzoek verplaatsingsgedrag Vlaanderen 3,” Instituut voor Mobiliteit, 2009. [Online]. Available: http://www.mobielvlaanderen.be/ovg

[85] “Statistics Belgium,” Belgian Federal Governement, 2015. [Online]. Available: http://statbel.fgov.be

[86] S. Huang, and D. Infield, “The potential of domestic electric vehicles to contribute to power system operation through vehicle to grid technology,” in *Int. Universities Power Eng. Conf.*, 2009, pp. 1-5.

[87] “FEBIAC,” FEBIAC v.z.w., 2015. [Online]. Available: http://www.febiac.be

[88] “Milieurapport Vlaanderen - Achtergronddocument 2010 - Sector Transport,” Vlaamse Milieumaatschappij, 2011. [Online]. Available: http://www.milieurapport.be/upload/main/miradata/mira-t/01_sectoren/01_06/ag_transport.pdf

[89] “Mitsubishi i-MiEV,” Beherman Motors, 2015. [Online]. Available: http://www.mitsubishi-motors.be/nl-be/models/i-miev

[90] “Smart electric drive,” Smart USA, 2015. [Online]. Available: http://www.smartusa.com/models/electric-drive/overview.aspx

[91] “Toyota Concept Vehicles: RAV4 EV,” Toyota Motor Sales USA, 2012, [Online]. Available: http://www.toyota.com/concept-vehicles/rav4ev.html

[92] “eRUF Stormster Electric Porsche Cayenne,” RUF Automobile GmbH, 2012. [Online]. Available: http://www.ruf-automobile.de/en/en-aktuelles-eruf.php

[93] F. Geth, J. Tant, D. Six, P. Tant, T. De Rybel, and J. Driesen, "Techno-economical and life expectancy modeling of battery energy storage systems," in *CIRED*, 2011, pp. 1-4.

[94] D.F. Stein *et al.*,"Tires and passenger vehicle fuel economy: informing consumers, improving performance," TRB, Washington, D.C., U.S.A., Special Rep. 286, 2006.

[95] R. Barrero, X. Tackoen, and J. Van Mierlo, "Improving energy efficiency in public transport: stationary supercapacitor based energy storage systems for a metro network," in *IEEE VPPC*, 2008, pp. 1-8.

[96] R. Farrington and J. Rugh, "Impact of vehicle air-conditioning on fuel-economy, tailpipe emissions and electric vehicle range," presented at the *Earth Technol. Forum*, Washington, D.C., U.S.A., 2000.

[97] "Tesing and measuring emissions," U.S. Environmental Protection Agency, 2014. [Online]. Available: http://www.epa.gov/nvfel/testing/

[98] E.G. Giakoumis and A.I. Alafouzos, "Study of diesel engine performance and emissions during a transient cycle applying an engine mapping-based methodology," *Elsevier Appl. Energy*, vol. 87, no. 4, pp. 1358-1365, Apr. 2010.

[99] "FOD Mobiliteit," FOD Mobiliteit en Vervoer, 2015. [Online]. Available: http://www.mobilit.fgov.be.

[100] Office of Transportation and Air Quality, "Fuel economy labeling of motor vehicles: revisions to improve calculation of fuel economy estimates," EPA, Washington, D.C., U.S.A., Rep. EPA420-R-06-017, 2006.

[101] J. Van Roy, N. Leemput, S. De Breucker, F. Geth, P. Tant, and J. Driesen: "An availability analysis and energy consumption model for a Flemish fleet of electric vehicles," presented at the *EEVC*, Brussels, Belgium, 2011.

[102] "2015 Ford C-MAX Energi," Ford Motor Company, 2015. [Online]. Available: http://www.ford.com/cars/cmax/trim/energi/

[103] "2016 ELR Coupe," General Motors, 2015. [Online]. Available: http://www.cadillac.com/coupes/elr-coupe.html

[104] *Electric vehicle conductive charging system - Part 1: General requirements*, IEC Standard 61851-1, 2010.

[105] "Verbruiksprofielen," Vreg, 2013. [Online]. Available: http://www.vreg.be/verbruiksprofielen-0

[106] C. Budischak, S. DeAnna, H. Thomson, L. Mach, D.E. Veron, and W. Kempton, "Cost-minimized combinations of wind power, solar power and electrochemical storage, powering the grid up to 99.9 % of the time," *Elsevier J. Power Sources*, vol. 225, pp. 60-74, March 2013.

[107] A. Brooks and T. Gage, "Integration of electric drive vehicles with the electric power grid: a vew value stream," presented at *EVS-18,* Berlin, Germany, 2001.

[108] M. Duvall *et al.*, "Comparing the benefits and impacts of hybrid electric vehicle options for compact sedan and sport utility vehicles", EPRI, Palo Alto, CA, U.S.A., Rep. 1006892, 2002.

[109] A. Simpson, "Cost-benefit analysis of plug-in hybrid electric vehicle technology," presented at the *EVS-22,* Yokohama, Japan, 2006.

[110] B. Sovacool and R.Hirsh, "Beyond batteries: an examination of the benefits and barriers to plug-in hybrid electric vehicles (PHEVs) and a vehicle-to-grid (V2G) transition", *Elsevier Energy Policy*, vol. 37, no. 3, pp. 1095-1103, Dec. 2008.

[111] K.P. Schneider, C.E. Gerkensmeyer, M.C.W. Kintner-Meyer, and R. Fletcher, “Impact assessment of plug-in hybrid vehicles on pacific northwest distribution systems,” in *IEEE PES General Meeting*, 2008, pp. 1–6.

[112] N. DeForest, J. Funk, A. Lorimer, B. Ur, I. Sidhu, P. Kaminsky, B. Tenderich, “Impact of Widespread Electric Vehicle Adoption on the Electrical Utility Business”, Tech. Rep., Center for Entrepreneurship & Technology (CET), University of California, Aug. 2009.

[113] A.S. Masoum, S. Deilami, P.S. Moses, and A. Abu-Siada, “Impacts of battery charging rates of plug-in electric vehicle on smart grid distribution systems,” in *IEEE PES ISGT Europe*, 2011, pp. 1-6.

[114] S. Shao, T. Zhang, M. Pipattanasomporn, and S. Rahman, “Impact of TOU rates on distribution load shapes in a smart grid with PHEV penetration,” in *IEEE PES Transmission Distribution Conf. Expo.*, 2010, pp. 1-6.

[115] A.S. Masoum, S. Dei, P. S. Moses, and A.A. Siada, “Voltage profile and THD distortion of residential network with high penetration of plug-in electrical vehicles”, in *IEEE PES ISGT Eur.*, 2010, pp.1-6.

[116] K. Clement, K. Van Reusel, J. and Driesen, “The consumption of electrical energy of plug-in hybrid electric vehicles in Belgium,” presented at the *EET-Eur. Ele-Drive Transportation Conf.*, Brussels, Belgium, 2007.

[117] K. Clement-Nyns, E. Haesen, and J. Driesen, “Stochastic analysis of the impact of plug-in hybrid electric vehicles on the distribution grid,” presented at the *CIRED*, Prague, Czech Republic, 2009.

[118] G.A. Putrus, P. Suwanapingkarl, D. Johnston, E.C. Bentley, and M. Narayana “Impact of electric vehicles on power distribution networks”, in *IEEE VPPC,* 2009, pp. 827-831.

[119] B.A. Hacker, S. Azongha, and C.S. Edrington, “PHEV impacts on microgrid systems,” in *IEEE Electr. Power & Energy Conference*, 2009, pp. 1-7.

[120] A. Bedir, B. Ozpineci, and J.E. Christian, “The impact of plug-in hybrid electric vehicle interaction with energy storage and solar panels on the grid for a zero energy house,” in *IEEE PES Transmission Distribution Conf. Expo.*, 2010, pp.1-6.

[121] K. J. Dyke, N. Schofield, and M. Barnes, “The impact of transport electrification on electrical networks,” *IEEE Trans. Ind. Electron.*, vol. 57, no. 12, pp. 3917-3926, Dec. 2010.

[122] H. Valizadeh Haghi, S.M. Hakimi, M. Aliakbar Golki, “Considering impacts of plug-in electric vehicles in planning optimal hybrid systems;” in *CIRED*, 2011, pp : 1-4.

[123] X. Zhong, A. Cruden, D. Infield, P. Holik, and S. Huang, “Assessment of vehicle to grid power as power system support,” *Universities Power Eng. Conf.*, 2009, pp. 1-5.

[124] Y. Ota *et al.*, “Effect of autonomous distributed vehicle-to-grid (V2G) on power system frequency control,” in *Int. Conf. Ind. Inform. Syst.*, 2010, pp. 481-485.

[125] S.W. Hadley, “Evaluating the impact of plug-in hybrid electric vehicles on regional electricity supplies,” *iREP Symp. Bulk Power Syst. Dynamics and Control*, 2007, pp. 1-12.

[126] S.W. Hadley and A. Tsvetkova, “Potential impacts of plug-in hybrid electric vehicles on regional power generation,” *Elsevier The Electricity J.*, vol. 22, no. 10, pp, 56-68, Dec. 2009.

[127] E. Sortomme, A.I. Negash, S.S. Venkata, and D.S. Kirschen, “Voltage dependent load models of charging electric vehicles,” in *IEEE PES General Meeting*, 2013, pp. 1-5.

[128] R. Bruninga and J.A.T. Sorensen, “Charging EVs efficiently now while waiting for the smart grid,” In *IEEE Green Technologies Conf.*, 2013; pp. 1-7.

[129] S. Shahidinejad, S. Filizadeh, and E. Bibeau, “Profile of charging load on the grid due to plug-in vehicles,” *IEEE Trans. Smart Grid*, vol. 3, no. 1, pp.135-141, March 2012.

[130] D. Wu; D.C. Aliprantis, and L. Ying, “Load scheduling and dispatch for aggregators of plug-in electric vehicles,” *IEEE Trans. Smart Grid*, vol. 3, no. 1, pp. 368-376, March 2012.

[131] C. Liu, J. Wang, A. Botterud, Y. Zhou, and A. Vyas, “Assessment of impacts of PHEV charging patterns on wind-thermal scheduling by stochastic unit commitment,” *Smart Grid, IEEE Trans. Smart Grid*, vol. 3, no. 2, pp. 675-683, Jun. 2012.

[132] R.A. Verzijlbergh, M.O.W. Grond, Z. Lukszo, J.G. Slootweg, and M.D. Ilic, “Network impacts and cost savings of controlled EV charging,” *IEEE Trans. Smart Grid*, vol. 3, no. 3, pp. 1203-1212, Sept. 2012.

[133] S.F. Abdelsamad, W.G. Morsi, and T.S. Sidhu, “Impact of wind-based distributed generation on electric energy in distribution systems embedded with electric vehicles,” *IEEE Trans. Smart Grid*, vol. 6, no. 1, pp. 79-87, Jan. 2015.

[134] M.S. ElNozahy and M.M.A. Salama, “Studying the feasibility of charging plug-in hybrid electric vehicles using photovoltaic electricity in residential distribution systems,” *Elsevier Elect. Power Syst. Res.*, vol. 110, pp. 133-143, May 2014.

[135] C. Pang, P. Dutta, and M. Kezunovic, “BEVs/PHEVs as dispersed energy storage for V2B uses in the smart grid,” *IEEE Trans. Smart Grid*, vol. 3, no. 1, pp.473-482, March 2012.

[136] G. Li and X.P. Zhang, “Modeling of plug-in hybrid electric vehicle charging demand in probabilistic power flow calculations,” *IEEE Trans. Smart Grid*, vol. 3, no. 1, pp. 492-499, March 2012.

[137] K. Clement-Nyns, E. Haesen, and J. Driesen, “Coordinated charging of multiple plug-in hybrid electric vehicles in residential distribution grids,” in *IEEE PES Power Syst. Conf. Expo.*, 2009, pp. 1-7.

[138] P. Denholm and W. Short, “An evaluation of utility system impacts and benefits of optimally dispatched plug-in hybrid electric vehicles,” NREL, Golden, CO, U.S.A., Rep. TP-620-40293, 2006.

[139] K. Mets, T. Verschueren, W. Haerick, C. Develder, and F. De Turck, “Optimizing smart energy control strategies for plug-in hybrid electric vehicle charging,” in *IEEE/IFIP Network Oper. Manage. Symp. Workshops*, 2010, pp. 293-299.

[140] S. Acha, T.C. Green, and N. Shah, “Effects of optimized plug-in hybrid vehicle charging strategies on electric distribution network losses,” in *IEEE Transmission Distribution Conf. Expo.*, 2010, pp. 1-6.

[141] S. Acha, T.C. Green, and N. Shah, “Optimal charging strategies of electric vehicles in the UK power market,” in *IEEE PES ISGT*, 2011, pp. 1-8.

[142] N. Rotering and M. Ilic, “Optimal charge control of plug-in hybrid electric vehicles in deregulated electricity markets,” *IEEE Trans. Power Syst.*, vol. 26, no. 3, pp. 1021-1029, Aug. 2011.

[143] M. Doostizadeh, M. Khanabadi, A. Esmaeilian, and M. Mohseninezhad, “Optimal energy management of a retailer with smart metering and plug-in hybrid electric vehicle,” in *10th Int. Conf. Environment Electr. Eng.*, 2011, pp. 1-5.

[144] O. Sundstrom and C. Binding, “Optimization methods to plan the charging of electric vehicle fleets,” in *Proc. Int.Conf. Control Commun. Power Eng.*, 2010, pp. 28-29.

[145] A. Brooks, E. Lu, D. Reicher, C. Spirakis, and B. Weihl, “Demand dispatch,” *IEEE Power Energy Mag.*, vol. 8, no. 3, pp.20-29, May/Jun. 2010.

[146] E. Sortomme, M.M. Hindi, S.D.J. MacPherson, and S.S. Venkata, “Coordinated charging of plug-in hybrid electric vehicles to minimize distribution system losses,” *IEEE Trans. Smart Grid*, vol. 2, no. 1, pp. 198-205, March 2011.

[147] M.D. Gallus, R. La Fauci, and G. Andersson, “Investigating PHEV wind balancing capabilities using heuristics and model predictive control,” in *IEEE PES General Meeting*, 2010, pp. 1-8.

[148] M.D. Gallus and G. Andersson, “Demand management of grid connected plug-in hybrid electric vehicles (PHEV),” in *IEEE Energy 2030 Conf.*, 2008, pp. 1-8.

[149] M. Pipattanasomporn, H. Feroze, and S. Rahman, “Multi-agent systems in a distributed smart grid: design and implementation,” in *IEEE/PES Power Syst. Conf. Expo.*, 2009, pp. 1-8.

[150] S. Shao, M. Pipattanasomporn, and S. Rahman, “Grid integration of electric vehicles and demand response with customer choice,” *IEEE Trans. Smart Grid*, vol. 3, no. 1, pp. 543-550, March 2012.

[151] S.J. Gunter, K.K. Afridi, and D.J. Perreault, “Optimal design of grid-connected PEV charging systems with integrated distributed resources,” *IEEE Trans. Smart Grid*, vol. 4, no. 2, pp. 956-967, Jun. 2013.

[152] E. Sortomme and M.A. El-Sharkawi, “Optimal scheduling of vehicle-to-grid energy and ancillary services,” *IEEE Trans. Smart Grid*, vol. 3, no. 1, pp. 351-359, March 2012.

[153] E. Sortomme and M.A. El-Sharkawi, “Optimal combined bidding of vehicle-to-grid ancillary services,” *IEEE Trans. Smart Grid*, vol. 3, no. 1, pp. 70-79, March 2012.

[154] H. Yifeng, B. Venkatesh, and G. Ling, “Optimal scheduling for charging and discharging of electric vehicles,” *IEEE Trans Smart Grid*, vol. 3, no. 3, pp.1095-1105, Sept. 2012.

[155] H. Weihao, S. Chi, C. Zhe Chen, and B. Bak-Jensen, “Optimal operation of plug-in electric vehicles in power systems with high wind power penetrations,” *IEEE Trans. Sustain. Energy*, vol. 4, no. 3, pp. 577-585, Jul. 2013.

[156] E. Haesen, “Multi-objective optimization of the integration of stochastic distributed energy resources in electricity grids,” Ph.D. dissertation, K.U.Leuven, 2009.

[157] E. Haesen, J. Driesen, and R. Belmans, “Robust planning methodology for integration of stochastic generators in distribution grids,” *IET Renewable Power Generation*, vol. 1, no. 1, pp. 25-32, Mar. 2007.

[158] P. Papadopoulos, S Skarvelis-Kazakos, I. Grau, L.M. Cipcigan, and N. Jenkins, “Predicting electric vehicle impacts on residential distribution networks with distributed generation,” in *IEEE VPPC*, 2010, pp. 1-5.

[159] S. Blumsack, C. Samaras, and P. Hines, “Long-term electric system investments to support plug-in hybrid electric vehicles,” in *IEEE PES General Meeting*, 2008, pp. 1-6.

[160] K. Qian, C. Zhou, M. Allan, and Y. Yuan, "Modeling of load demand due to EV battery charging in distribution systems," *IEEE Trans. Power Syst.*, vol. 26, no. 2, pp. 802-810, May. 2011.

[161] J.A. Peças Lopes, C.L. Moreira, and A.G. Madureira, "Defining control strategies for microgrids islanded operation," *IEEE Trans. Power Syst.*, vol. 21 no. 2, pp. 916-924, May 2006.

[162] J.A. Peças Lopes, F.J. Soares, and P.M. Rocha Almeida, "Identifying management procedures to deal with connection of electric vehicles in the grid;" in *IEEE PowerTech*, 2009; pp. 1-8.

[163] "Integral: integrated ICT-platform based distributed control in electricity grids," Energy research Centre of the Netherlands, 2011. [Online]. Available: http://www.integral-eu.com

[164] S.S. Hernandez, P.P. Galindo, and A.Q. Lopez, "EPV project: technology to integrate EV inside smart grids," in *7th Int. Conf. Eur. Energy Market*, 2010, pp. 1-6.

[165] Q. Wu, A.H. Nielsen, J. Østergaard, S.T. Cha, F. Marra, and P.B. Andersen, "Modeling of electric vehicles (EVs) for EV grid integration study," in *Eur. Conf. SmartGrids & E-Mobility*, 2010, pp. 1-8.

[166] B. Adornato, R. Patil, Z. Filipi, Z. Baraket, and T. Gordon, "Characterizing naturalistic driving patterns for plug-in hybrid electric vehicle analysis," in *IEEE VPPC*, 2009, pp. 665-660.

[167] "Bottling electricity: storage as a strategic tool for managing variability and capacity concerns in the modern grid", Electricity Advisory Committee, 2008. [Online]. Available: http://energy.gov/sites/prod/files/oeprod/DocumentsandMedia/final-energy-storage_12-16-08.pdf

[168] M. Aliakbar Golki and H. Valizadeh Haghi, "Using a multivariate DOE method for congestion study in distribution systems under impacts of plug-in electric vehicles," in *CIRED*, 2011, pp. 1-4.

[169] N. Leemput, F. Geth, B. Claessens, J. Van Roy, R. Ponnette, and J. Driesen, "A case study of coordinated electric vehicle charging for peak shaving on a low voltage grid," in *IEEE PES ISGT Eur.*, 2012, pp. 1-7.

[170] S. Vandael, B. Claessens, M. Hommelberg, T. Holvoet, and G. Deconinck, "A scalable three-step approach for demand side management of plug-in hybrid vehicles," *IEEE Trans. Smart Grid*, vol. 4, no. 2, pp. 720–728, Jun. 2013.

[171] K. De Craemer, S. Vandael, B. Claessens, and G. Deconinck, "An event-driven dual coordination mechanism for demand side management of PHEVs," *IEEE Trans. Smart Grid*, vol. 5, no. 2, pp. 751–760, March 2014.

[172] P. Richardson, D. Flynn, and A. Keane, "Local versus centralized charging strategies for electric vehicles in low voltage distribution systems," *IEEE Trans. Smart Grid*, vol. 3, no. 2, pp. 1020–1028, Jun. 2012.

[173] S. Shafiee, M. Fotuhi-Firuzabad, and M. Rastegar, "Investigating the impacts of plug-in hybrid electric vehicles on power distribution systems," *IEEE Trans. Smart Grid*, vol. 4, no. 3, pp.1351-1360, Sept. 2013.

[174] O. Sundstrom and C.Binding, "Flexible charging optimization for electric vehicles considering distribution grid constraints," *IEEE Trans Smart Grid*, vol. 3, no. 1, pp. 26-37, March 2012.

[175] N. O'Connell, Q. Wu, J. Østergaard, A.H. Nielsen, S.T. Cha, and Y.Ding, "Day-ahead tariffs for the alleviation of distribution grid congestion from electric vehicles," *Elsevier Electr. Power Syst. Research*, vol. 92, pp. 106-114, Nov. 2012.

[176] P.M. Rocha Almeida, J.A. Peças Lopes, F.J. Soares, and M.H. Vascones, "Automatic generation control operation with electric vehicles," in *iREP Symp. Bulk Power Syst. Dynamics Control,* 2010. pp. 1-7.

[177] N.J. Gil and J.A. Peças Lopes, "Hierarchical frequency control scheme for islanded multi-microgrids operation," in *IEEE Power Tech*, 2007, pp. 473-478.

[178] J.A. Peças Lopes, P.M. Rocha Almeida, and F. J. Soares, "Using vehicle-to-grid to maximize the integration of intermittent renewable energy resources in islanded electric grids," in *Int. Conf. Clean Electr. Power*, 2009, pp. 290-295.

[179] A.Y. Saber and G.K. Venayagamoorthy, "Unit commitment with vehicle-to-grid using particle swarm optimization," in *IEEE PowerTech*, 2009, pp. 1-8.

[180] W. Kempton *et al.*, "A Test of Vehicle-to-Grid (V2G) for Energy Storage and Frequency Regulation in the PJM System", University of Delaware, Pepco Holdings, PJM Interconnect, and Green Mountain College, 2008. [Online]. Available: http://www.udel.edu/V2G/resources/test-v2g-in-pjm-jan09.pdf

[181] P. Mitra and G.K. Venayagamoorthy, "Wide area control for improving stability of a power system with plug-in electric vehicles," *IET Generation, Transmission & Distribution*, vol. 4, no. 10, pp. 1151-1163, Oct. 2010.

[182] S. Vandael, N. Boucké, T. Holvoet, and G. Deconinck, "Decentralized demand side management of plug-in hybrid vehicles in a smart grid," in *Proc. 1st Int. Workshop Agent Technol. Energy Syst.*, 2010, pp. 67-74.

[183] S. Vandael, K. De Craemer, N. Boucké, T. Holvoet, and G. Deconinck, "Decentralized coordination of plug-in hybrid vehicles for imbalance reduction in a Smart Grid," in *Proc. 10th Int. Conf. on Autonomous Agents Multiagent Syst.*, 2011, pp. 803-810.

[184] A. Mohsenian-Rad, V.W.S. Wong, J. Jatskev, R. Schrober, and A. Leon-Garcia, "Autonomous demand side management based on game-theoretic energy consumption scheduling for the future smart grid," *IEEE Trans. on Smart Grid*, vol. 1, no. 3, Dec. 2010.

[185] K. De Brabandere, B. Bolsens, J. Van den Keybus, A. Woyte, J. Driesen, and R. Belmans, "A voltage and frequency droop control method for parallel inverters," *IEEE Trans. Power Electron.,* vol. 22, no. 4, pp. 1107-1115, Jul. 2007.

[186] S. De Breucker, P. Jacqmaer, K. De Brabandere, J. Driesen, and R. Belmans, "Grid power quality improvements using grid-coupled hybrid electric vehicles," in *3rd IET Int. Conf. Power Electron. Machines Drives*, 2006, pp. 505-509.

[187] M. Prodanovic , K. De Brabandere, J. Van den Keybus, T. Green, and J. Driesen, "Harmonic and reactive power compensation as ancillary services in inverter-based distributed generation," *IET Generation, Transmission & Distribution,* vol. 1, no. 3, pp. 432-438, May 2007.

[188] S. Bashash, S.J. Moura, and H.K. Fathy, "Charge trajectory optimization of plug-in hybrid electric vehicles for energy cost reduction and battery health enhancement," in *Amer. Control Conf.*, 2010, pp. 5824-5831.

[189] I. Momber *et al.*, "Plug-in electric vehicle interactions with a small office building: an economic analysis using DER-CAM," in *IEEE PES General Meeting*, 2010, pp. 1-8.

[190] B. Khorramdel, H. Khorramdel, J. Aghaei, A. Heidari, and V.G. Agelidis, “Voltage security considerations in optimal operation of BEVs/PHEVs integrated microgrids,” *IEEE Trans. Smart Grid,*, vol. 6, no. 4, pp. 1575-1587, Jul. 2015.

[191] X. Bai and W. Qiao, “Robust optimization for bidirectional dispatch coordination of large-scale V2G,” *IEEE Trans. Smart Grid*, vol. 6, no. 4, pp. 1944-1954, Jul. 2015.

[192] M. Ansari, A.T. Al-Awami, E. Sortomme, and M.A. Abidoeric, “Coordinated bidding of ancillary services for vehicle-to-grid using fuzzy optimization,” *IEEE Trans. Smart Grid*, vol. 6, no. 1, pp.261-270, Jan. 2015.

[193] W. Lee, L. Xiang, R. Schober, and V.W.S. Wong, “Electric vehicle charging stations with renewable power generators: a game theoretical analysis,” *IEEE Trans. Smart Grid*, vol. 6, no. 2, pp.608-617, March 2015.

[194] G. Wang, J. Zhao, F. Wen, Y. Xue, and G. Ledwich, “Dispatch strategy of PHEVs to mitigate selected patterns of seasonally varying outputs from renewable generation,” *IEEE Trans. Smart Grid*, vol. 6, no. 2, pp. 627-639, March 2015.

[195] Y. Mou, H. Xing, Z. Lin, and M. Fu, "Decentralized optimal demand-side management for PHEV charging in a smart grid,” *IEEE Trans. Smart Grid*, vol. 6, no. 2, pp. 726-736, March 2015.

[196] F. Baccino, S. Grillo, S. Massucco, and F. Silvestro, “A two-stage margin-based algorithm for optimal plug-in electric vehicles scheduling,” *IEEE Trans. Smart Grid*, vol. 6, no. 2, pp. 759-766, March 2015.

[197] D.T. Nguyen and L.B. Le, “Joint optimization of electric vehicle and home energy scheduling considering user comfort preference,” *IEEE Trans. Smart Grid*, vol. 5, no. 1, pp. 188-199, Jan. 2014.

[198] P. Rezaei, j. Frolik, and P.D.H. Hines, “Packetized Plug-In Electric Vehicle Charge Management,” *IEEE Trans. Smart Grid*, vol. 5, no. 2, pp. 642-650, March 2014.

[199] L. Yang, J. Zhang, and H.V. Poor, “Risk-aware day-ahead scheduling and real-time dispatch for electric vehicle charging,” *IEEE Trans. Smart Grid*, vol. 5, no. 2, pp. 693-702, March 2014.

[200] J. Hu, S. You, M. Lind, and J. Ostergaard, “Coordinated charging of electric vehicles for congestion prevention in the distribution grid,” *IEEE Trans. Smart Grid*, vol. 5, no. 2, pp. 703-711, March 2014.

[201] I. Sharma, C. Canizares, and K. Bhattacharya, “Smart charging of PEVs penetrating into residential distribution systems,” *IEEE Trans. Smart Grid*, vol. 5, no. 3, pp. 1196-1209, May 2014.

[202] W. Leterme, F. Ruelens, B. Claessens, and R. Belmans, “A flexible stochastic optimization method for wind power balancing with PHEVs,” *IEEE Trans. Smart Grid*, vol. 5, no. 3, pp. 1238-1245, May 2014.

[203] W. Qi, Z. Xu, Z.J.M. Shen, Z. Hu, and Y. Song, “Hierarchical coordinated control of plug-in electric vehicles charging in multifamily dwellings,” *IEEE Trans. Smart Grid*, vol. 5, no. 3, pp. 1465-1474, May 2014.

[204] J. Tan and L. Wang, “Integration of plug-in hybrid electric vehicles into residential distribution grid based on two-layer intelligent optimization,” *IEEE Trans. Smart Grid*, vol. 5, no. 4, pp. 1774-1784, Jul. 2014.

[205] O. Ardakanian, S. Keshav, and C. Rosenberg, “Real-time distributed control for smart electric vehicle chargers: from a static to a dynamic study,” *IEEE Trans. Smart Grid*, vol. 5, no. 5, pp. 2295-2305, Sept. 2014.

[206] S. Bahrami, M. Parniani, “Game theoretic based charging strategy for plug-in hybrid electric vehicles," *IEEE Trans. Smart Grid*, vol. 5, no. 5, pp. 2368-2375, Sept. 2014.

[207] L. Hua, J. Wang, and C.Zhou, “Adaptive electric vehicle charging coordination on distribution network,” *IEEE Trans. Smart Grid*, vol. 5, no. 6, pp. 2666-2675, Nov. 2014.

[208] W. Tang, S. Bi, and Y.J.A. Zhang, “Online coordinated charging decision algorithm for electric vehicles without future information,” *IEEE Trans.Smart Grid*, vol. 5, no. 6, pp. 2810-2824, Nov. 2014.

[209] S. Weckx, R. D'Hulst, B. Claessens, and J. Driesen, “Multiagent charging of electric vehicles respecting distribution transformer loading and voltage limits,” *IEEE Trans. Smart Grid*, vol. 5, no. 6, pp. 2857-2867, Nov. 2014.

[210] C.J. Tang and P. Ghosh, “Optimizing electric vehicle charging with energy storage in the electricity market,” *IEEE Trans. Smart Grid*, vol. 4, no. 1, pp. 311-320, March 2013.

[211] C. Goebel and D.S. Callaway, “Using ICT-controlled plug-in electric vehicles to supply grid regulation in California at different renewable integration levels,” *IEEE Trans. Smart Grid*, vol. 4, no. 2, pp. 729-740, Jun. 2013.

[212] M.E. Khodayar, L. Wu, and Z. Li, “Electric vehicle mobility in transmission-constrained hourly power generation scheduling," *IEEE Trans. Smart Grid*, vol. 4, no. 2, pp. 779-788, Jun. 2013.

[213] Y. Mu, J. Wu, J. Ekanayake, N. Jenkins, and H. Jia, “Primary frequency response from electric vehicles in the Great Britain power system,” *IEEE Trans. Smart Grid*, vol. 4, no. 2, pp. 1142-1150, Jun. 2013.

[214] B. Geng, J.K. Mills, and D. Sun, “Two-stage charging strategy for plug-in electric vehicles at the residential transformer level,” *IEEE Trans. Smart Grid*, vol. 4, no. 3, pp. 1442-1452, Sept. 2013.

[215] N. Taheri, R. Entriken, and Y. Ye, “A dynamic algorithm for facilitated charging of plug-in electric vehicles,” *IEEE Trans. Smart Grid*, vol. 4, no. 4, pp. 1772-1779, Dec. 2013.

[216] P. Papadopoulos, N. Jenkins, L.M. Cipcigan, I. Grau, and E. Zabala, “Coordination of the charging of electric vehicles using a multi-agent system,” *IEEE Trans. Smart Grid*, vol. 4, no. 4, pp. 1802-1809, Dec. 2013.

[217] R.J. Bessa, M.A. Matos, F.J. Soares, and J.A.P. Lopes, “Optimized bidding of a EV aggregation agent in the electricity market,” *IEEE Trans. Smart Grid*, vol. 3, no. 1, pp. 443-452, March 2012.

[218] S. Weckx and J. Driesen, “Load Balancing With EV Chargers and PV Inverters in Unbalanced Distribution Grids,” *IEEE Trans. Sustain. Energy*, vol. 6, no. 2, pp. 635-643, Apr. 2015.

[219] P.M. Rocha Almeida, F.J. Soares, and J.A. Peças Lopes, “Electric vehicles contribution for frequency control with inertial emulation,” *Elsevier Electr. Power Syst. Research*, vol. 127, pp. 141-150, Oct. 2015.

[220] M.A. López, S. Martín, J.A. Aguado, and S. de la Torre, “V2G strategies for congestion management in microgrids with high penetration of electric vehicles,” *Elsevier Electr. Power Syst. Research*, vol. 104, pp. 28-34, Nov. 2013.

[221] V. Brslica, “Plug-in hybrids and new energy storages,” in *IEEE VPPC*, 2009, pp. 516-523.

[222] S. Inage, "Modelling load shifting using electric vehicles in a smart grid environment," IEA, Paris, France, Working paper, 2010. [Online]. Available: https://www.iea.org/publications/freepublications/publication/load_shifting.pdf

[223] P. Lombardi, P. Vasquez, and Z.A. Styczynski, "Plug-in electric vehicles as storage devices within an autonomous power system: optimization issue," in *IEEE PowerTech*, 2009, pp. 1-7.

[224] W. Kempton, J. Tomic´, S. Letendre, A. Brooks, and T. Lipman, "Vehicle-to-grid power: battery, hybrid, and fuel cell vehicles as resources for distributed electric power in California," University of Delaware, Newark, DE, U.S.A, Rep. UCD-ITS-RR-01-03, 2001.

[225] W. Kempton and S. Letendre, "Electric Vehicles as a new power source for electric utilities," *Elsevier Science*, vol. 2, no. 3, pp. 157-175, Dec. 1996.

[226] W. Kempton and T. Kubo, "Electric-drive vehicles for peak power in Japan," *Elsevier Energy Policy*, vol. 28, pp. 9-18, Aug. 1999.

[227] H. Lund and W. Kempton, "Integration of renewable energy into the transport and electricity sectors through V2G," *Elsevier Energy Policy*, vol. 36, no. 9, pp. 3578-3587, Sept. 2008.

[228] H. Sekyung, H. Soohee, and K. Sezaki, "Development of an optimal vehicle-to-grid aggregator for frequency regulation," *IEEE Trans. Smart Grid*, vol. 1, no. 1, Jun. 2010.

[229] P.A. Samuelson, *Foundation of economic analysis*, Harvard University Press, Cambridge, MA, U.S.A., 1947.

[230] "Human Development Report 2011," United Nations Development Programme, 2012. [Online]. Available: http://hdr.undp.org/en/

[231] "The EU climate and energy package," European Commission, 2012. [Online]. Available: http://ec.europa.eu/clima/policies/package/index_en.htm

[232] "Kyoto Protocol to the United Nations Framework Convention on Climate Change," United Nations, 1998. [Online]. Available: http://unfccc.int/kyoto_protocol/items/2830.php

[233] "The PRIMES model," E3MLab, 2012. [Online]. Available: http://www.e3mlab.ntua.gr

[234] "MARKAL," IEA-ETSAP, 2012. [Online]. Available: http://www.iea-etsap.org

[235] "International Energy Agnency," IEA, 2012. [Online]. Available: http://www.iea.org

[236] "Electric Power Research Institute," EPRI, 2012. [Online]. Available: http://www.epri.com

[237] L. Chen, H. Suzuki, T. Wachi, and Y. Shimura, "Components of nodal prices for electric power systems," *IEEE Trans. Power Syst.*, vol. 17, no. 1, pp. 41-49, Feb. 2002.

[238] P. Maghouli, S.H. Hosseini, M.O. Buygi, and M. Shahidehpour, "A multi-objective framework for transmission expansion planning in deregulated environments," *IEEE Trans. Power Syst.*, vol. 24, no. 2, pp. 1051-1061, May 2009.

[239] A. Kazarlis, A.G Bakirtzis, and V. Petridis, "A genetic algorithm solution to the unit commitment problem," *IEEE Trans. Power Syst.*, vol. 11, no. 1, pp. 83-92, Feb. 1996.

[240] D.S. Callaway and I.A. Hiskens, "Achieving controllability of electric loads," *Proc. IEEE,* vol. 99, no. 1, pp. 184-199, Jan. 2011.

[241] L.R. Chang-Chien, O. Chee-Mun, and R.A. Kramer, "Field tests and refinements of an ACE model," *IEEE Trans. Power Syst.,* vol. 18, no. 2, pp. 898-903, May 2003.

[242] S.D. Helmick and R.R. Shoults, "A practical approach to an interim multi-area economic dispatch using limited computer resources," *IEEE Trans. Power App. Syst.,* vol. 104, no. 6, pp. 1400-1404, Jun. 1985.

[243] F. Daneshfar and H. Bevrani, "Load-frequency control: a GA-based multi-agent reinforcement learning," *IET Generation, Transmission & Distribution*, vol. 4, no. 1, pp. 13-26, Jan. 2010.

[244] N.R. Ullah, T. Thiringer, and D. Karlsson, "Temporary primary frequency control support by variable speed wind turbines: potential and applications," *IEEE Trans. Power Syst.,* vol. 23, no. 2, pp. 601-612, May 2008.

[245] R.C. Schaefer and K. Kim, "Excitation control of the synchronous generator," *IEEE Ind. Appl. Mag.*, vol. 7, no. 2, pp. 37-43, Mar./Apr. 2001.

[246] C. Wang and S.M. Shahidehpour, "Effects of ramp-rate limits on unit commitment and economic dispatch," *IEEE Trans. Power Syst.*, vol. 8, no. 3, pp. 1341-1350, Aug. 1993.

[247] B.C. Ummels, M. Gibescu, E. Pelgrum, W.L. Kling, and A.J. Brand, "Impacts of Wind Power on Thermal Generation Unit Commitment and Dispatch," *IEEE Trans. Energy Convers.*, vol. 22, no. 1, pp. 44-51, Mar. 2007.

[248] S. Lukic, "Charging ahead," *IEEE Ind. Electron. Mag.*, vol. 2, no. 4, pp. 22-31, Dec. 2008.

[249] L.W. Pierce, "Predicting liquid filled transformer loading capability," *IEEE Trans. Ind. Appl.*, vol. 30, no. 1, pp. 170-178, Jan. 1994.

[250] M.M. Morcos, N.G. Dillman, and C.R. Mersman, "Battery chargers for electric vehicles," *IEEE Power Eng. Rev.*, vol. 20, no. 11, pp. 8-11, Nov. 2000.

[251] M.P.F. Hommelberg, C.J. Warmer, I.G. Kamphuis, J.K. Kok, and G.J. Schaeffer, "Distributed control concepts using multi-agent technology and automatic markets: an indispensable feature of smart power grids," in *IEEE PES General Meeting*, 2007, pp. 1-7.

[252] M.P.F. Hommelberg, B.J. van der Velde, C.J. Warmer, I.G. Kamphuis, and J.K. Kok, "A novel architecture for real-time operation of multi-agent based coordination of demand and supply," in *IEEE PES General Meeting*, 2008, pp. 1-5.

[253] B. Jansen, C. Binding, O. Sundstr, and D. Gantenbein, "Architecture and communication of an electric vehicle virtual power plant," in *1st Int. Conf. Smart Grid. Commun.*, 2010, pp. 149-154.

[254] "EU's energy-related strategies," European Comission, 2011. [Online]. Available: ec.europa.eu/energy/strategies/index_en.htm

[255] "Belgian Power Exchange," Belpex, 2011. [Online]. Available: www.belpex.be

[256] Y. Hase, *Handbook of Power System Engineering*, Hoboken, NJ, U.S.A: John Wiley & Sons, 2007.

[257] R.K. Singh, N.B.D. Choudhury, and S.K. Goswami, "Effect of load models on nodal pricing and revenue evaluation of DG in distribution network," in *Annu. IEEE India Conf.*, 2008, pp. 229-233.

[258] R.K. Sing and S.K. Goswami, "Evaluation of nodal prices and revenue of distributed generation in distribution network including load model,", *IEEE Int. Conf. Ind. Inform. Syst.,* 2008, pp. 1-6.

[259] P.M. Sotkiewicz and J.M. Vignolo, “Nodal pricing for distribution networks: efficient pricing for efficiency enhancing DG,” *IEEE Trans. Power Syst.*, vol. 21, no. 2, pp. 1013-1014, May 2006.

[260] P. Van Roy, T. Van Craenenbroeck, R. Belmans, D. Van Dommelen, G. Pepermans, and S. Proost, “Comparison of transmission tariff methods in a free market for electricity”, in *Int. Conf. Electr. Power Eng.*, 1999, pp. 159.

[261] P. Wang, Y. Ding, and Y. Xiao, ”Technique to evaluate nodal reliability indices and nodal prices of restructured power systems,” *IEE Proc. Generation Transmission Distribution*, vol. 152, no. 3, pp. 390-396, May 2005.

[262] K. De Brabandere, K. Vanthournout, J. Driesen, G. Deconinck, and R. Belmans, “Control of microgrids,” in *IEEE PES General Meeting*, 2007, pp. 1-7.

[263] C.J. Warmer, M.P.F. Hommelberg, J.K. Kok, and I.G. Kamphuis, “Local DER driven grid support by coordinated operation of devices,” *IEEE PES General Meeting*, 2008, pp. 1-5.

[264] M.A.A. Pedrasa, T.D. Spooner, and I.F. MacGill, “Coordinated scheduling of residential distributed energy resources to optimize smart home energy services,” *IEEE Trans. Smart Grid*, vol. 1, no. 1, pp. 134-144, Sept. 2010.

[265] B. Roossien and P.C. van der Laag, “Universal power manager: integrating ECN’s PowerMatcher with Nedap’s Atrium,” ECN, Petten, The Netherlands, Rep. ECN-E-10-003, 2010.

[266] D.A. Cohen, “GridAgents™: intelligent agent applications for integration of distributed energy resources within distribution systems,” *IEEE PES General Meeting*, 2008, pp. 1-5.

[267] P. Jacqmaer, S. De Breucker, K. De Brabandere, J. Driesen, and R Belmans, “Plug-in HEVs using d,q current components for single-phase grid-coupling,” in *23th Int. Electr. Veh. Symp.*, 2007, pp. 1432-1442.

[268] H. Makkonen, J. Partanen, and P. Silventoinen, “Concept of battery charging and discharging in automotive applications,” in *Int. Symp. Power Electron. Electr. Drives Automation Motion*, 2010, pp. 1664-1669.

[269] N. Lu and D.J. Hammerstrom, “Design considerations for frequency responsive grid griendly^{TM} appliances,” in *IEEE PES Transmission Distribution Conf. Exhibition*, 2006, pp. 647-652.

[270] M. Bragard, N. Soltau, S. Thomas, and R.W. De Doncker, “The balance of renewable sources and user demands in grids: power electronics for modular battery energy storage systems,” *IEEE Trans. Power Electron.*, vol. 25, no. 12, pp. 3049-3056, Dec. 2010.

[271] “Technology compendium 3.4: PV grid integration,” SMA Solar Technology, 2012. [Online]. Available: http://files.sma.de/dl/10040/PV-Netzint-AEN123016w.pdf

[272] P. Bradley, M. Leach, and J. Torriti, “A review of the costs and benefits of demand response for electricity in the UK,” *Elsevier Energy Policy*, vol. 52, pp. 312-327, Jan. 2013.

[273] R. Earle, E.P. Kahn, and E. Macan, “Measuring the capacity impacts of demand desponse,” *Elsevier The Electricity Journal*, vol. 22, no. 6, pp. 47-58, Jul. 2009.

[274] A. Hajimiragha, C.A. Canizares, M.W. Fowler, and A. Elkamel, “Optimal transition to plug-in hybrid electric vehicles in Ontario, Canada, considering the electricity-grid limitations,” *IEEE Trans. Ind. Electr.*, vol. 57, no. 2, pp. 690-701, Feb. 2010.

[275] A. Delnooz, D. Six, C. Mol, and E. Gielen, "State-of-the-art in business models for charging services: the EVCITY approach," presented at the *EEVC*, Brussels, Belgium, 2012.

[276] *Kabels Voor Ondergrondse Aanleg, met Synthetische Isolatie en Versterkte Mantel (Type 1kV)*, NBN Standard C33-322, 1975.

[277] R. Belmans, G. Deconinck, and J. Driesen. "Deel IV: Transformatoren," in *Elektrische energie. Deel 1*, Leuven, Belgium: ACCO, 2010, ch. 4, sec. 2.2.3, pp. 269-270.

[278] W. Labeeuw and G. Deconinck, "Customer sampling in a smart grid pilot," in *IEEE PES General Meeting*, 2012, pp. 1–7.

[279] *Specifieke Technische Voorschriften Voor Decentrale Productie-Installaties die in Parallel Werken met het Distributienet*, Synergrid Standard C10/11 (Rev. 12), 2009.

[280] "Sunny Boy 240," SMA Solar Technology AG, 2015. [Online]. Available: http://files.sma.de/dl/18925/SB240-DEN1442web.pdf

[281] F. Geth, N. Leemput, J. Van Roy, J. Büscher, R. Ponnette, and J. Driesen, "Voltage droop charging of electric vehicles in a residential distribution feeder," in *IEEE PES. ISGT Eur.*, 2012, pp. 1–8.

[282] C. Cheng and D. Shirmohammadi, "A three-phase power flow method for real-time distribution system analysis," *IEEE Trans. Power Syst.*,vol. 10, no. 2, pp. 671–679, May. 1995.

[283] N. Leemput, F. Geth, J. Van Roy, A. Delnooz, J. Büscher, and J. Driesen, "Impact of electric vehicle on-board single-phase charging strategies on a Flemish residential grid," *IEEE Trans. Smart Grid*, vol. 5, no. 4, pp. 1815-1822, Jul. 2014.

[284] T. Vu Van *et al.*, "The Meta PV project: photovoltaics for active distribution systems," in *EU PVSEC*, 2009, pp. 4132-4135.

[285] W. Labeeuw and G. Deconinck, "Residential electrical load model based on mixture model clustering and Markov models," *IEEE Trans. Ind. Inform.*, vol. 9, no. 3, pp. 1561-1569, Aug. 2013.

[286] "De cijfers," Organisatie Duurzame Energie, 2014. [Online]. Available: http://www.ode.be/zonnestroom/de-cijfers

[287] "Onze diensten," Vlaamse regulator van de elektriciteits- en gasmarkt, 2014. [Online]. Available: http://www.vreg.be/

[288] N. Leemput, J. Van Roy, F. Geth, J. Driesen, and S. De Breucker, "Grid and fleet impact mapping of EV charge opportunities," in *Data Science and Simulation in Transportation Research*, Hershey, PA: IGI Global, 2014, ch. 17, pp. 364-390.

[289] "Electric car charging: electric vehicle charging points in Ireland," ESB ecars, 2015. [Online] Available: http://www.esb.ie/electric-cars/electric-car-charging.jsp

[290] A. Schroeder, and T. Traber, "The economics of fast charging infrastructure for electric vehicles," *Elsevier Energy Policy*, vol. 43, pp. 136-144, Apr. 2012.

[291] Z. Li and M. Ouyang,"The pricing of charging for electric vehicles in China-Dilemma and solution," *Elsevier Energy*, vol. 36, pp. 5765-5778, Sept. 2011.

[292] S. Bae and A. Kwasinski, "Spatial and temporal model of electric vehicle charging demand," *IEEE Trans. Smart Grid*, vol. 3, no. 1, pp. 394-403, Mar. 2012.

[293] S.N. Yang, W.S. Cheng, Y.C. Hsu, C.H. Gan, and Y.B. Lin, "Charge scheduling of electric vehicles in highways," *Math. Comput. Modeling*, vol. 57, no. 11-12, pp. 2873-2882, Jun. 2013.

[294] C. Coninckx, R. Claes, S. Vandael, N. Leemput, T. Holvoet, and G. Deconinck, "Anticipatory coordination of electric vehicle allocation to fast charging infrastructure," in *Advances in Practical Applications of Heterogeneous Multi-Agent Systems - The PAAMS Collection*, Cham, Switzerland: Springer International Publishing AG, 2014, pp 74-85.

[295] M. Etezadi-Amoli, K. Choma, and J. Stefani, "Rapid-charge electric-vehicle stations," *IEEE Trans. Power Delivery*, vol. 25, no. 3, pp. 1883-1887, Jul. 2010.

[296] K. Yunus, H. Zelaya-De La Parra, and M. Reza, "Distribution grid impact of plug-in electric vehicles charging at fast charging stations using stochastic charging model," in *Proc. Eur. Conf. Power Electron. Appl.*, 2011, pp. 1937-1947.

[297] G. Mauri and A. Valsecchi, "Fast charging stations for electric vehicle: the impact on the mv distribution grids of the Milan metropolitan area," in *IEEE Int. Energy Conf. Exhibition*, 2012, pp. 1055-1059.

[298] A. Arancibia and K. Strunz, "Modeling of an electric vehicle charging station for fast DC charging" in *IEEE IEVC*, 2012, pp. 1-6.

[299] D. Aggeler, F. Canales, H. Zelaya-De La Parra, A. Coccia, A. N. Butcher, and O. Appeldoorn, "Ultra-fast DC-charge infrastructures for EV-mobility and future smart grids," in *2010 IEEE PES ISGT Eur.*, 2010, pp. 1-8.

[300] N. Machiels, N. Leemput, F. Geth, J. Van Roy, J. Büscher, and J. Driesen, "Design criteria for electric vehicle fast charge infrastructure based on Flemish mobility behavior," *IEEE Trans. Smart Grid*, vol. 5, no. 1, pp. 320-327, Jan. 2014.

[301] C. Gonzalez, S. Weckx, N. Efkarpidis, P. Vingerhoets, T. De Rybel, and J. Driesen, "Constrained PV penetration level in LV distribution networks based on the voltage operational margin," in *CIRED 22*, 2013; pp. 1-4.

[302] C. Gonzalez-de Miguel, T: De Rybel, and J. Driesen, "Enhancing reliability in medium voltage distribution networks with directional fault passage indicators without voltage sensors," *Acta Electrotechnica*, vol. 54, no. 1, pp. 73-80, Oct. 2013.

[303] "6-36 kV Medium Voltage Underground Power Cables: XLPE insulated cables," Nexans S.A, 2014. [Online]. Available: http://www.nexans.be/Belgium/2013/Medium%20Voltage%20Underground%20Power%20Cables%20Catalogue.pdf

[304] "Evolutie van het aantal tankstations," Petrolfed, 2014. [Online]. Available: http://www.petrolfed.be/nl/petroleumindustrie/economie/evolutie-van-het-aantal-tankstations

[305] "Users's Manual – Model HCS," ClipperCreek, 2015. [Online]. Available: http://www.clippercreek.com/store/wp-content/uploads/2015/08/HCS-User-Manual-080520151.pdf

[306] J. Van Roy, "Electric vehicle charging integration in buildings," Ph.D. dissertation, ESAT, KU Leuven, Leuven, Belgium, 2015.

[307] E. De Caluwé, "Potentieel van demand side management, piekvermogen en netondersteunende diensten geleverd door plug-in hybride elektrische voertuigen op basis van een beschikbaarheidsanalyse," M.S. thesis, ESAT, KU Leuven, Leuven, Belgium, 2008.

Curriculum Vitae

Personal

Niels Leemput niels.leemput@gmail.com
Born November 12, 1987
Belgian

Education

2013 - 2015 KIC InnoEnergy PhD School: education in innovation and entrepreneurship for PhD candidates.

2010 - 2015 Doctoral Program in Engineering Science, KU Leuven.

09/2014 Energy Economics, Grenoble École de Management, Grenoble, France, 8-12 September 2014. *3 ECTS credits*

01/2014 E-mobility in Smart Cities, KU Leuven, Leuven, Belgium, 27-31 January 2014. *2 ECTS credits*

12/2013 - 01/2014 Economic, Scientific & Technological Intelligence, INSA Lyon, France, 13-15 November 2013, and 15-22 January 2014. *6 ECTS credits*

09/2013 Introductory Crash Course on Entrepreneurship, ESADE, Barcelona, Spain, 23-27 September 2013. *3 ECTS credits*

2008 - 2010 Master in Science and Engineering: Energy Engineering, KU Leuven. *Magna Cum Laude*

2005 - 2008 Bachelor in Electrical Engineering, minor in Mechanical Engineering, KU Leuven. *Cum Laude*

Academic

2012 - 2015 Doctoral scholarship IWT-Vlaanderen (IWT 111526): *grid integrated charging infrastructure for electric vehicles*.

2010 - 2015 PhD research assistant at dept. of electric engineering (ESAT), div. electric energy and computer architectures (ELECTA), KU Leuven

03 - 09/2014 Universitat Politècnica de Catalunya (UPC): 7-month research visit within the KIC InnoEnergy project.

List of publications

Internationally reviewed academic journals

- **N. Leemput**, F. Geth, J. Van Roy, J. Büscher, and J. Driesen, "Reactive power support in residential LV distribution grids through electric vehicle charging," *Sust. Energy, Grids and Networks*, vol. 3, pp. 24-35, Sept. 2015.
- **N. Leemput**, F. Geth, J. Van Roy, P. Olivella-Rosell, J. Driesen, and A. Sumper, "MV and LV residential grid impact of combined slow and fast charging of electric vehicles," *Energies (Special Section on "Electrical Power and Energy Systems for Transportation Applications")*, vol. 8, no. 3, pp. 1815-1822, March 2015.
- J. Van Roy, **N. Leemput**, F. Geth, J. Büscher, R. Salenbien, and J. Driesen, "Electric vehicle charging in an office building microgrid with distributed energy resources," *IEEE Trans. Sustain. Energy (Special Section on "Microgrids for Sustainable Energy Systems")*, vol. 5, no. 4, pp. 1389-1396, Oct. 2014.
- B. S. N. Alzand, **N. Leemput**, R. Willems, "Inappropriate implantable cardioverter-defibrillator shocks in a public swimming pool," *Europace*, vol. 16, no. 8, pp. 1124, Aug. 2014.
- **N. Leemput**, F. Geth, J. Van Roy, A. Delnooz, J. Büscher, and J. Driesen, "Impact of electric vehicle on-board single-phase charging strategies on a Flemish residential grid," *IEEE Trans. Smart Grid*, vol. 5, no. 4, pp. 1815-1822, Jul. 2014.
- J. Van Roy, **N. Leemput**, F. Geth, R. Salenbien, J. Büscher, and J. Driesen, "Apartment building electricity system impact of operational electric vehicle charging strategies," *IEEE Trans. Sustain. Energy)*, vol. 5, no. 1, pp. 264-272, Jan. 2014.
- N. Machiels, **N. Leemput**, F. Geth, J. Van Roy, J. Büscher, and J. Driesen, "Design criteria for electric vehicle fast charge infrastructure based on Flemish mobility behavior," *IEEE Trans. Smart Grid*, vol. 5, no. 1, pp. 320-327, Jan. 2014.

Book contributions

- **N. Leemput**, J. Van Roy, F. Geth, J. Driesen, and S. De Breucker, "Grid and fleet impact mapping of EV charge opportunities," in *Data Science and Simulation in Transportation Research*, Hershey, PA: IGI Global, 2014, ch. 17, pp. 364-390.
- K. Coninckx, R. Claes, S. Vandael, **N. Leemput**, T. Holvoet, and G. Deconinckx, "Anticipatory coordination of electric vehicle allocation to fast charging infrastructure," in *Advances in Practical Applications of Heterogeneous Multi-Agent Systems - The PAAMS Collection*, Cham, Switzerland: Springer International Publishing AG, 2014, pp. 74-85.
- J. Van Roy, **N. Leemput**, and J. Driesen, "Invloed van elektrische wagens op het elektriciteitsnet," in *Technologische verkenning – Elektrische voertuigen*, Geel, Belgium: VEI, 2011, ch. 9, pp. 100-121.

International conferences

- P. Olivella-Rosell, G. Bosch-Llufriu, R. Villafafila-Robles, D. Heredero-Peris, M. Kovacevic, and **N. Leemput**, "Assessment of the impact of electric vehicles on Iberian day-ahead electricity market," in *IEEE IEVC*, 2014, pp. 1-8.
- S. Iacovella, F. Geth, F. Ruelens, **N. Leemput**, P. Vingerhoets, G. Deconinck, and B. Claessens, "Double-layered control methodology combining price objective and grid constraints," in *IEEE Int. Conf. Smart Grid Commun.*, 2013, pp. 25-30.
- J. Verveckken, F. Geth, B. Hunyadi, J. Beerten, **N. Leemput**, J. Van Roy, P. Tielens, V. De Smedt, S. Iacovella, N. Koolen, H. De Clercq, G. Gielen, R. Puers, J. Vandewalle, S. Van Huffel, R. Belmans, G. Deconinck, and W. Dehaene, "Developing engineering-oriented educational workshops within a student branch," in *Proc. SEFI*, 2013, pp. 1-7.
- J. Verveckken, F. Geth, J. Beerten, B. Hunyadi, **N. Leemput**, J. Van Roy, P. Tielens, V. De Smedt, S. Iacovella, H. Höschle, N. Koolen, H. De Clercq, J. Driesen, G. Gielen, R. Puers, J. Vandewalle, S. Van Huffel, R. Belmans, G. Deconinck, and W. Dehaene "Development of open-source interactive smart energy house for K12 engineering education on residential energy efficiency," in *Eur. Soc. Eng. Edu. Annu. Conf.*, 2013, pp. 1-12.

- F. Geth, J. Verveckken, **N. Leemput**, J. Van Roy, J. Beerten, P. Tielens, V. De Smedt, S. Iacovella, B. Hunyadi, N. Koolen, H. De Clercq, G. Gielen, R. Puers, S. Van Huffel, R. Belmans, G. Deconinck, W. Dehaene, and J. Driesen, "Development of an open-source smart energy house for K-12 education," in *IEEE PES General Meeting*, 2013, pp. 1-5.
- J. Verveckken, F. Geth, B. Hunyadi, J. Beerten, **N. Leemput**, J. Van Roy, P. Tielens, V. De Smedt, S. Iacovella, N. Koolen, H. De Clercq, G. Gielen, R. Puers, J. Vandewalle, S. Van Huffel, R. Belmans, G. Deconinck, and W. Dehaene, "Developing engineering-oriented educational workshops within a student branch," in *Proc. IEEE EUROCON*, 2013, pp. 933-939.
- T. Devloo, **N. Leemput**, J. Van Roy, F. Geth, and J. Driesen, "Component improvements in the electrification of passenger vehicles drivetrains," in *IEEE Transportation Electrification Conf. Expo*, 2013, pp. 1-6.
- S. Luyten, **N. Leemput**, F. Geth, J. Van Roy, J. Büscher , and J. Driesen, "Standardization of conductive AC charging infrastructure for electric vehicles," in *CIRED*, 2013, pp. 1-4.
- F. Geth, **N. Leemput**, J. Van Roy, J. Büscher, R. Ponnette, and J. Driesen, "Voltage droop charging of electric vehicles in a residential distribution feeder," in *IEEE PES ISGT Eur.*, 2012, pp. 1–8.
- **N. Leemput**, F. Geth, B. Claessens, J. Van Roy, R. Ponnette, and J. Driesen, "A case study of coordinated electric vehicle charging for peak shaving on a low voltage grid," in *IEEE PES ISGT Eur.*, 2012, pp. 1–8.
- J. Tant, J. Zwysen, K. Engelen, **N. Leemput**, J. Van Roy, S. Weckx, and J. Driesen, "Power electronics for electric vehicles: A student laboratory platform," in *IEEE 13th Workshop on Control and Modeling for Power Electron.*, 2012, pp. 1-7.
- **N. Leemput**, S. De Breucker, K. Engelen, J. Van Roy, F. Geth, and J. Driesen, "Electrification of trucks and buses in an urban environment through continuous charging," in *IEEE IEVC*, 2012, pp. 1-8.
- **N. Leemput**, J. Van Roy, F. Geth, P Tant, B. Claessens, and J: Driesen, "Comparative analysis of coordination strategies for electric vehicles," in *IEEE PES ISGT Eur.*, 2011, pp. 1-8.
- J. Van Roy, **N. Leemput**, S. De Breucker, F. Geth, P. Tant, and J. Driesen, "An availability analysis and energy consumption model for a Flemish fleet of electric vehicles," in *EEVC*, 2011, pp. 1-12.